TO MY MOTHER

SPONTANEOUS ACTION POTENTIAL INITIATION

AND PROPAGATION IN

DEVELOPING CELL SEGMENTS OF

ACETABULARIA MEDITERRANEA

A thesis

submitted in fulfilment

of the requirements of the Degree

of

Doctor of Philosophy in Physics

at the

University of Waikato

by

PANOTE THAVARUNGKUL

University of Waikato

Hamilton, New Zealand

1985

ABSTRACT

The spontaneous action potentials which occur during the redevelopment of anucleate isolated stalk segments (ISS's) of the unicellular alga *Acetabularia mediterranea* have been studied using a novel non-invasive technique. This involved measurement of spatial samples of the time dependent potential in the external medium (sea water) and an inverse transformation to give the current distribution at the cell surface. A detailed description of the method of regularization needed to handle this ill-conditioned inversion problem is presented, along with the results of test experiments to demonstrate its validity.

The initiation region and subsequent propagation (if any) of each action potential was then analysed from the computed transmembrane currents. The results showed that the occurrences of the spontaneous action potentials followed a rhythm which had a period of ~24-30 hours. These action potentials initiated more frequently at the ends of the ISS's than in the middle region. Contrary to the findings of Novak and Bentrup (1972) in which the cell segments had been maintained in unnatural conditions (a partitioned cuvette with electrical isolation between partitions) which could very well have resulted in perturbation of the cell environment, our results show no firm correlation between the regions of action potential initiation and the site of the redeveloping apex. Generally both propagating and non-propagating action potentials were observed in the same ISS, the ratio of which seems to depend on the length of the cell. The analysed initiation sites and the propagation behaviour of the spontaneous action potentials generated by the ISS's during the redevelopmental process do not provide any support to the symmetry-breaking role of the propagating action potentials as proposed by Novak and Bentrup.

ACKNOWLEDGEMENTS

I express my sincere thanks to Dr R.A. Sherlock for his suggestions, advice and discussions throughout the course of this work. Without his help and support the task of completing this thesis would have been quite impossible.

I am also grateful to Dr I.J.D. Craig who suggested the application of the method of regularization to the ill-conditioned inversion problem, and for his discussions.

I would also like to thank:

Mr D.G. Kennett who helped in many ways;

Dr M.J. Collett, Dr D.L. Drysdall and his students of the French translation course, for translating the French papers;

Dr H.W. Morgan and Dr C.G. Harfoot for their advice about decontamination of the *Acetabularia* cultures;

Mrs E.J. Miller who proof-read this thesis;

Miss D.D. Bovill for her skilful typing;

The Ministry of Foreign Affairs of New Zealand for the Colombo Plan Scholarship,

and finally,

My family whose support has enabled me to "keep going" throughout my study years.

CONTENTS

ABSTRACT ii

ACKNOWLEDGEMENTS iii

CONTENTS iv

LIST OF TABLES vii

CHAPTER 1: INTRODUCTION 1

1.1 Perspective 1

1.2 Morphogenesis in *Acetabularia* 3

1.2.1 The Life Cycle 3
1.2.2 Morphogenetic Substances 4
1.2.3 Nucleocytoplasmic Interactions 5
1.2.4 Intracellular Communication and Control 7

1.3 Electrical Activities Associated with Development and Proposed Models 9

1.3.1 Transcellular Current and Self-Electrophoresis 9
1.3.2 The Role of Action Potentials 16

1.4 Objectives of Present Work 18

Figures 22

CHAPTER 2: THE CELL MEMBRANE AND ACTION POTENTIAL 29

2.1 The Cell Membrane 29

2.2 The Membrane Potential 31

2.2.1 The Electrochemical Gradient and the Nernst Equation 31
2.2.2 Ionic Relations and the Membrane Potential 34

2.3 The Action Potential 36

2.3.1 General Features of an Action Potential 36
2.3.2 Action Potential in *Acetabularia* 38

2.4 Analog Electrical Circuits 42

2.5 The Core Conductor Model 43

2.5.1 Nonlinear Properties of Excitable Membranes 43
2.5.2 Core Conductor Theory 45
2.5.3 Propagation of Action Potentials 46

Table and Figures 48

CHAPTER 3: THE MULTIPLE EXTRACELLULAR RECORDING TECHNIQUE 62

3.1 Intracellular and Extracellular Recordings 62

3.2 Theories of Analysis of Initiation Point 64

3.2.1 Method to Identify the Depolarized Region Using Differential Voltage 65
3.2.2 Successive Over-Relaxation Method 69
3.2.3 Method of Regularization 73
3.2.4 Simplified Equation 82

3.3 Experimental Verification of Methods of Analysis 84

3.3.1 Materials and Methods 85
3.3.2 Results 88
3.3.3 Discussion 92

Figures 95

CHAPTER 4: MEASUREMENT OF SPONTANEOUS ACTION POTENTIALS IN DEVELOPING ANUCLEATE ISOLATED STALK SEGMENTS 132

4.1 Culture Conditions and Preparation of Anucleate Isolated Stalk Segments 132

4.2 Electrodes 133

4.3 Cell Holder Assembly and Medium Feed System 135

4.4 Signal Processing Electronics 138

4.5 Computer Programs 139

4.5.1 The Transient Recorder Program - TR363E 139
4.5.2 The Transient Data Display Program - TDDP2E 141

4.6 Experimental Procedure and Data Analysis 142

Figures 149

CHAPTER 5: EXPERIMENTAL RESULTS 167

5.1 Redevelopments of ISS's 167

5.2 The Spontaneous Action Potentials During the Redevelopment 170

5.2.1 Action Potential Activity 170
5.2.2 Initiation Sites of the Action Potentials 172
5.2.3 Propagating and Non-Propagating Action Potentials 178
5.2.4 Sharp and Slow Take-Off Action Potentials 181

5.3 Other Observations 183

5.3.1 Mottled and Even Colour Appearances 183
5.3.2 The Action Potential Rhythm 184

Tables and Figures 185

CHAPTER 6: DISCUSSION 246

6.1 Validity of the Technique 246

6.2 Conclusions and Comparisons with Other Work 247

6.2.1 General Features 249
6.2.2 Initiation Sites of the Action Potentials 252
6.2.3 Action Potential Propagation 254

6.3 Future Work 255

APPENDIX 1: DERIVATION OF EQUATIONS OF VOLTAGES AND CURRENTS IN CHAPTER 3 257

APPENDIX 2: EXAMPLES OF PROPAGATION BEHAVIOUR OF SPONTANEOUS ACTION POTENTIALS ANALYSED BY USING DIFFERENTIAL VOLTAGE DISTRIBUTIONS 267

APPENDIX 3: COMPOSITION OF AE50 MEDIUM 271

APPENDIX 4: COMMANDS EXECUTED BY THE TRANSIENT DATA DISPLAY PROGRAM - TDDP2E 274

REFERENCES 278

LIST OF TABLES

2.1 Ionic concentrations of major ions in the cytoplasm and the external medium, the equilibrium potential, and the experimental membrane potential of *Acetabularia* and Squid axon. 48

5.1 SUMMARY OF EXPERIMENTAL RESULTS I. 186

5.2 SUMMARY OF EXPERIMENTAL RESULTS II. 187

CHAPTER 1

INTRODUCTION

1.1 Perspective

For over a century the subject of morphogenesis has been widely studied in both plants and animals. Although the temporal aspect of development has been well described, very little is known about the mechanism of spatial control.

To begin with, plants and animals develop from one celled zygotes which are approximately spherical and macroscopically featureless. The question is, how do these featureless cells generate their spatial patterns? A general hypothesis is that, in the simplest organism, spatial development will start once the zygote has acquired its polarity (a reference direction or coordinate system). This polarity is usually thought of as a gradient of some existing substance(s) inside the cell. The next question which arises is, how does the zygote acquire its polarity; in other words, how does asymmetry arise from symmetry? Numerous models of various concepts were suggested (for models of symmetry-breaking and/or pattern formation see e.g. Babloyantz and Hiernaux, 1975; Goodwin, 1975; Turing, 1952; Wolpert, 1969, 1975). However, firm biological and biochemical supports for these models are still lacking.

It is only relatively recently that developmentalists turned their attention to bioelectricity as a possible mechanism for induction of polarity. This followed the finding of transcellular ionic currents in developing organisms ranging from a small *Fucus* egg (approximately 70 μm in diameter) (Jaffe, 1966, 1968, 1969) to the

redevelopment of a new limb of a newt (Borgens *et al.*, 1977b) (Fig. 1.1). These currents are most likely not a mere by-product of differentiations and growths as they were observed before any growth could be seen. They may indicate the future site of growth, for example the *Fucus* rhizoid grows at the site where the current enters the cell (Jaffe, 1966). Also the suppression of transcellular current in redeveloping *Acetabularia* stops growth and differentiation (Novak and Sironval, 1975).

However, transcellular currents were also found in non-growing systems such as pollen tubes of *Lilium* which had been treated with cytochalasin B (Weisenseel *et al.*, 1975). (Note: cytochalasin B is an inhibitor of cytoplasmic streaming which involves microfilaments, e.g. see review by Wessells *et al.*, 1971). These results seem to indicate that the natural transcellular current is a necessary component of development but not the only control mechanism. In addition to this current some plants such as the green alga *Acetabularia* also generate electrical pulses (e.g. Gradmann, 1976; Saddler, 1971) which are somewhat analogous to nerve impulses. Although the purpose of these pulses is still unclear there is some evidence to suggest that they may also be linked to the developmental process (e.g. Novak and Bentrup, 1972). Suppression of some of these pulses leads to a delay in regeneration (Rogatykh *et al.*, 1979).

The roles which these electrical activities (transcellular current and electrical pulses) may play in polarization and development are described in section 1.3. The studies presented in this thesis are concentrated on the electrical pulses and their correlation (if any) to growth in *Acetabularia*. A cell of *A. mediterranea* is shown in Fig. 1.2. In its mature stage (Fig. 1.2b) it consists of three distinct features

(i) a rhizoid which contains the single nucleus

(ii) a cylindrical stalk

(iii) a cap in which reproductive cysts are formed.

The shape of the cap varies from species to species. For example, *A. mediterranea* has an umbrella-like cap (Fig. 1.2c) while the cap of *A. peniculus* consists of several separate sack-like chambers attached to the tip of the stalk (Fig. 1.2d). The species used in the present work was *A. mediterranea*.

1.2 Morphogenesis in *Acetabularia*

Although much progress has been made in the last decade in explaining the phenomenon of polarization in developmental processes, our knowledge is still very limited. Further investigation of individual organisms is possibly the best way to further this knowledge. In plants one of the most useful systems is the uninucleate unicellular green alga *Acetabularia* (Fig. 1.2). The large size of *Acetabularia* (2-5 cm long) makes it possible to measure easily the electrophysiological properties of a single cell. The location of the single, well defined nucleus, which is always at the bottom part of the cell (the rhizoid), makes it easy to separate out the nucleus and so investigate its influence. The capability of regeneration of parts of the cell together with the clear differentiation of the cell into cap, stalk and rhizoid are very useful for the investigation of morphogenesis.

1.2.1 The Life Cycle

The life cycle of *Acetabularia* (Fig. 1.3) starts when two gametes fuse to form a zygote which then germinates to form a

differentiated structure consisting of a stalk and a rhizoid which contains the single nucleus. After a period of stalk elongation, sterile whorls are formed at the apical end followed later by a cap. Once the cap reaches its maximum size and the cell reaches maturity the nucleus divides to form several secondary nuclei. These nuclei are then transported by cytoplasmic streaming into the rays of the cap where cysts are formed. Inside each cyst further nuclear divisions take place to form the gametes. Under laboratory conditions the whole cycle would take place in 5-6 months (Bonotto *et al.*, 1972; Shephard, 1970).

1.2.2 Morphogenetic Substances

Early studies on morphogenesis in *Acetabularia* were done by J. Hämmerling about 50 years ago (for reviews of basic experiments performed by Hämmerling referred to in this chapter, see Hämmerling, 1963). These experiments demonstrated that there have to be materials in the cytoplasm with nuclear origin which induce morphogenesis. He called these materials *morphogenetic substances (MS)*. Some of the experiments which led to this conclusion can be summarized as follows. If a cell was subdivided into three segments (Fig. 1.4) the apical segment and the rhizoid (with nucleus) were capable of forming caps while the anucleate stalk segment lacked the ability to increase in length or generate a cap. However, if,after the apical segment was removed, the *nucleate stalk segment* was kept in the dark for a few days before an *anucleate stalk segment* was separated from the rhizoid it was found that the anucleate stalk segment had acquired the ability to form cap i.e. the MS must have been transferred from the nucleus to the stalk during the period in the dark. The ability of the apical segment to form a cap after the

segment containing the nucleus was removed also indicated that these MS were released from the nucleus into the cytoplasm long before they became manifest. The distribution of these MS increases from basal end to apex. Experiments performed on anucleate stalk segments by Sandakhchiev *et al.* (1972) also showed that during illumination MS which were originally in the cytoplasm migrated into the cortex (a plasma layer adjacent to the plasma membrane).

Although direct proof is still lacking it is generally accepted that these MS are a type of *messenger ribonucleic acid (mRNA)*. After removal of the nucleus the MS still exist in the cytoplasm for quite a long time, which is a surprising result considering the high levels of ribonuclease in the cytoplasm of an *Acetabularia* cell (Schweiger, 1966). The long term stability of these MS or mRNA was postulated to be achieved by the combination of mRNA with protein to form *ribonucleo-protein particles (RNP's)*. Several classes of such particles exist in *Acetabularia*. They sediment at about 20S, 40S and 110-120S (Kloppstech and Schweiger, 1975). The 40S particles have been isolated and injected into basal fragments of anucleate stalk segments by Alexeev *et al.* (1974). They found that in 10 percent of the cases some limited morphogenesis took place (formation of whorl and rudimentary cap). However, more convincing results are still needed to draw any conclusion that these 40S RNP's are in fact MS.

1.2.3 Nucleocytoplasmic Interactions

The studies on nucleocytoplasmic interactions are mainly concerned with the influence of the nucleus on the cytoplasm and vice versa. The interrelationship between the nucleus and the cytoplasm is of special interest as it contains information as to how the expression of the genes is controlled.

The knowledge of the way in which a nucleus can affect the cytoplasm arises from Hämmerling's experiments on grafting two different species of *Acetabularia*, *A. mediterranea* and *A. crenulata*, having morphologically distinct caps. The rhizoid including the nucleus of one species was grafted on an anucleate stalk of the other. The cap formed was that of the species of the nucleus, whereas the anucleate stalk alone would (at least partly) form the cap characteristic of its own species. That is, the MS which was originally present in the anucleate stalk was overriden and changed into the species-specific MS appropriate to the species of the nucleus. A better understanding of how a nucleus can influence cytoplasm will hopefully be obtained by identifying these MS and hence their function(s).

In *Acetabularia* the cytoplasm can also influence the nucleus as demonstrated by Hämmerling (1963). In a normal cell of *Acetabularia* the division of the nucleus occurred after cap maturation. However, nuclear division can be inhibited by continuous removal of the initial full grown cap and the subsequent regenerated ones. Normal divisions and cyst formations take place only when a cap is allowed to mature. Inhibition of nuclear division can also occur by transplanting a young stalk onto an old rhizoid with a mature nucleus. On the other hand transplantation of the mature cap-bearing stalk onto a rhizoid with a young nucleus leads to an early division of the nucleus. This influence of the cytoplasm on the nucleus is a subject still under investigation (see e.g. Clérin *et al.*, 1975; Schweiger *et al.*, 1975).

1.2.4 Intracellular Communication and Control

Investigations of the morphogenesis in *Acetabularia* described so far indicate definite interrelationships between cytoplasm and nucleus. However, the mechanisms of transfer of information and materials between nucleus and cytoplasm are still unclear. The simplest method would be diffusion, which may be adequate for cells a few micrometers in size, but would hardly be sufficient for *Acetabularia* which has a length up to a few centimeters. The observations of the transport systems for intracellular materials are made easier by the help of an electron microscope (e.g. as used by Koop and Kiermayer, 1980a, 1980b) and time-lapse photography (as used by e.g. Schmid and Koop, 1983) in which two systems of intracellular transport (cytoplasmic streaming) in *Acetabularia* have been observed. These systems were found to run at velocities 1-2 $\mu m\ s^{-1}$ and 3-11 $\mu m\ s^{-1}$ respectively (Koop, 1981). Inhibition of both systems by cytochalasin B (Koop, 1981; Puiseux-Dao, 1979) indicates involvements of microfilaments (fine protein filaments resembling the actin-containing filaments of muscle). The inhibition of the faster system by colchicine (Koop, 1981) also indicates possible microtubules' (minute unbranched tubules occurring in groups and composed of globular protein subunits) involvement in the system. Both microtubules and microfilaments are found to be involved in a wide variety of transporting and developing processes (e.g. Hepler and Palevitz, 1974; Wessells *et al.*, 1971). Observations indicate the possibility of the slower system being responsible for the transportation of chloroplasts (Koop and Kiermayer, 1980a; Schmid and Koop, 1983) and for the rapid condensation of cytoplasm (Puiseux-Dao, 1979). It was suggested that the faster process which carries

small vesicles, chloroplasts (in adult cells), and secondary nuclei (Koop and Kiermayer, 1980a), might be involved in growth and communication activities due to its ability to link rapidly between the apex and the nucleus (Puiseux-Dao, 1979). The slowing down of the cytoplasmic streaming in the dark (Borghi *et al.*, 1983; Dazy *et al.*, 1981) suggests the presence of at least one photoreceptor mechanism. The decrease in the movements of cytoplasm in the dark are also found to be parallel with the decrease in growth (Borghi *et al.*, 1983). Puiseux-Dao (1979) has suggested a possible role of cytoplasmic ionic composition in the regulation of cytoplasmic streaming and morphogenesis in *Acetabularia*. The proposal was that the changes in the cell membrane permeability (by photoreceptors or some other means) would alter the cytoplasmic ionic composition which in turn would alter the building up and function of microtubules and microfilaments since these processes are sensitive to ionic composition (see e.g. Hepler and Palevitz, 1974). This would affect the cytoplasmic streaming and hence the transport of growth materials such as Golgi vesicles to the growing site as well as the assembly of microtubules which may be necessary for cell wall construction. This suggestion was supported by several observations of cessation of tip growth in various plant systems, including *Acetabularia*, when cytoplasmic streaming was inhibited by cytochalasin B (Herth *et al.*, 1972; Weisenseel *et al.*, 1975).

Cytoplasmic streaming, however, does not give a complete explanation for transport processes in *Acetabularia*. For example, during the outgrowth of a cap the stalk acquires a pale green appearance due to the flow of part of the cytoplasm from the stalk into the cap (Lüttke, 1983). This translocation process is a unidirectional movement while cytoplasmic streaming is a

bidirectional process. Hence, there has to be an additional mechanism which moves chloroplasts and other particles transported by cytoplasm into the growing cap (Lüttke, 1983).

1.3 Electrical Activities Associated with Development and Proposed Models

The role of electrical phenomena in development in plants has only recently become a major topic of study (e.g. Jaffe and Nuccitelli, 1977; Weisenseel, 1983). Favourable subjects are those which are initially apolar and can be induced to grow during the course of experiments, for examples eggs of the brown algae *Fucus* and *Pelvetia*, pollen grains of *Lilium* and the anucleate stalk segments of *Acetabularia* which have lost their original polarity after having been kept in the dark. In this section the possible link(s) between electrical activities, developmental polarization and morphogenesis will be discussed.

1.3.1 Transcellular Current and Self-Electrophoresis

The self-electrophoresis hypothesis proposed by Jaffe (1966, 1968, 1969) to explain how an apolar cell can become polar arose from the study of electrophysiological activities in *Fucus* eggs. This egg has a size of 60-100 μm in diameter and is densely filled with cytoplasm. Once fertilized visible growth follows in 10-12 hours. Until shortly before visible growth, a polar axis can be induced by a number of physical and chemical factors such as light, chemical gradients and imposed current (see e.g. Weisenseel, 1979, 1983 for general review). In the absence of these inducing factors, growth occurred at the site of sperm entry (Knapp, 1931).

During the early hours of development many cells have shown changes in the properties of their membranes. Generally the membranes become hyperpolarized (i.e. cytoplasm becomes more negative with respect to surrounding medium (Weisenseel, 1977)) and become more selective to ions. The mechanism which triggers these changes is still unknown. Jaffe suggested that the changes in membrane properties may lead to spatial development. The hypothesis, which is known as *self-electrophoresis*, assumes that the asymmetric perception of a signal (e.g. unilateral light) by specific receptors causes the original random distribution of ion pumps (active transport, see chapter 2) and ion leaks (passive transport) within the membrane to become asymmetrical. In effect, this causes the transcellular current to flow, entering the cell at the leak end and leaving at the pump end. This transcellular current can induce an electric field in the cytoplasm which it traverses. The relationship between the current and the induced electric field is given by

$$\underline{J} = \sigma \underline{E} \tag{1.1}$$

where $\underline{J}$ is the current density (A m^{-2}), $\underline{E}$ is the electric field (V m^{-1}), and σ is the conductivity (Ω^{-1} m^{-1}) of the charge carriers. If the charge carriers are of a single type ion then

$$\sigma = CzFu$$

where C is the molar concentration of the ion (mol m^{-3}), z is the charge number (positive or negative integer), F is the Faraday constant (9.6487×10^4 C mol^{-1}), and u is the electrophoretic mobility (m^2 s^{-1} V^{-1}). Equation (1.1) can be generalized to include the case where there are more than one type of mobile charge carriers i.e.

$$\underline{J} = \sum_{i=1}^{n} \underline{J}_i$$

thus

$$\underline{J} = (\sigma_1 + ... + \sigma_n)\ \underline{E} \qquad (1.2)$$

In some cases it is convenient to express the electric field in equation (1.1) as

$$\underline{E} = \rho \underline{J} \qquad (1.3)$$

where ρ is the resistivity = $1/\sigma$ (Ω m).

Such an electric field can move negatively charged entities to one end and positively charged entities to the other resulting in a concentration gradient of charged cytoplasmic and membrane components. This concentration gradient is the result of an electrophoretic movement of the particles in one direction and their back-diffusion in the opposite direction and in the steady state can be obtained through the relation

electrophoretic flow = diffusion flow

$$C u \underline{E} = D \underline{\nabla} C$$

i.e.
$$\underline{G} = \frac{\underline{\nabla} C}{C} = \frac{u}{D}\ \underline{E} \qquad (1.4)$$

where $\underline{G}$ is the concentration gradient (expressed in fraction change per metre, m^{-1}), $\underline{\nabla} C = \Delta C / \Delta X$, ΔC is the concentration difference (mol m^{-3}) within the distance ΔX (m), C is the average concentration (mol m^{-3}), u is the electrophoretic mobility ($m^2\ s^{-1}\ V^{-1}$), D is the diffusion coefficient ($m^2\ s^{-1}$), and $\underline{E}$ is the electric field ($V\ m^{-1}$). This concentration gradient $\underline{G}$ may then act back to amplify and

stabilize the original small concentration gradient by means of positive feedback. This hypothesis is summarized in Fig. 1.5.

It is also possible that this current can create voltage gradients along the membrane, i.e. an electric field along the membrane. This field can then cause movements of charged and mobile membrane components within the membrane, a phenomenon called *lateral electrophoresis* (Jaffe, 1977). This idea is supported by the observations of movements of membrane components in response to the voltage gradient (Poo and Robinson, 1977).

Considerable evidence indicates that calcium ion, Ca^{2+}, and its gradient may in fact play an important role in polarization and/or development. Some of this evidence is

(i) rhizoids of Fucoid eggs tend to grow at the pole that has the higher concentration of Ca^{2+} (Robinson and Cone, 1980).

(ii) Ca^{2+} gradients were found in tip growing plant cells such as *Acetabularia* and the pollen tube of *Lilium* with the highest concentration at the growing tips (Jaffe, L.A. *et al.*, 1975; Reiss and Herth, 1978, 1979b).

(iii) perturbation of intracellular ionic composition caused by the application of Ca^{2+}, Mg^{2+} ionophore (A23187) (possibly resulting in disturbance of the existing Ca^{2+} gradient (Reiss and Herth, 1979a)) led to cessation of tip growth in pollen tube of *Lilium* (Herth, 1978; Reiss and Herth, 1979a)) and inhibition of whorl and cap formations in *Acetabularia* (Goodwin and Pateromichelakis, 1979). This latter event was also observed when there was a change in concentration of Ca^{2+} in the external medium or when Ca^{2+} passages into the cell were blocked or interfered with (Goodwin *et al.*, 1983).

(iv) calcium was a substantial component of the pregerminated transcellular current in Fucoid egg (Robinson and Jaffe, 1975).

Some of the observations given above (i, iv) provided the main evidence which led Jaffe and coworkers (e.g. Jaffe, L.F. *et al.*, 1975; Robinson and Jaffe, 1975) to make a further hypothesis for the self-electrophoresis model. This is that the asymmetry in the distribution of ion pumps and leaks leads to the creation of a Ca^{2+} gradient and that this gradient is an essential step in the polarization process, either by electrophoresis or other means, with growth occurring in the region of highest Ca^{2+} concentration. The evidence in (i)-(iv) seems to support this suggestion.

The possibility that a Ca^{2+} gradient is involved in the self-electrophoresis process as a current carrying ions (as found in Fucoid eggs (iv) above) is an attractive idea. This is because Ca^{2+} is strongly bound to cytoplasm (Hodgkin and Keynes, 1957; Kushmerick and Podolsky,1969) and hence the effective conductivity associated with the Ca^{2+} gradient in the cytoplasm (σ in equation (1.1)) (see Jaffe *et al.*, 1974) would be lower than for non-binding ions such as K^+ or Cl^-. For the same current density ($\underline{J}$ in equation (1.1)) it was estimated in Fucoid eggs that current carried by Ca^{2+} would give rise to a 1,000 times larger electric field ($\underline{E}$) than if carried by K^+ (Jaffe *et al.*, 1974). This larger electric field would in turn create a larger concentration gradient of charged cytoplasmic components (see equation (1.4)).

In some systems however, other ions are found to be the major current carrying ions, but there are indications that Ca^{2+} may still play some important roles. For example, it was found that the major

current carrying ion in the transcellular current of *Xenopus* oocytes was Cl^- and that the Cl^- permeability was controlled by Ca^{2+} (Robinson, 1979).

The hypothesis of self-electrophoresis is mainly supported by the observations that polarity can be induced by imposed current (e.g. Peng and Jaffe, 1976) and that polarizing cells drive current through themselves. In view of this hypothesis and the fact that secretory vesicles, which are normally involved in cell growth, are negatively charged (Matthews, *et al.*, 1972; Vos *et al.*, 1968) there should be an accumulation of these vesicles at the positive pole. Microscopic observations support this conclusion. Negatively charged vesicles and RNA are found accumulated at the *positive* growing pole (Jaffe, 1968). In a tip growing green alga such as *Acetabularia*, vesicles which contain cell wall precursor materials are also found accumulated in the stalk tip of growing cells (Werz, 1970). However, the transcellular current in this plant flows in the opposite direction to that of Fucoid eggs i.e. the current is *leaving* the cell at the site of growth (considered from the measuring external potential e.g. Broda and Schweiger, 1981; Borghi *et al.*, 1983) and hence growth occurs at the *negative* pole. However, current evidence does not enable us to confirm (or contradict) the above hypothesis since the charges on the vesicles in *Acetabularia* have not (to our knowledge) been identified. In anucleate stalk segments of *Acetabularia* contradictory results have been obtained. Some workers have reported that transcellular current, as in nucleate cells, leaves the growing end and enters the non-growing end (Novak and Bentrup, 1972; Novak and Sironval, 1975; Goodwin and Pateromichelakis, 1979) while others reported the opposite (Christ-Adler and Bentrup, 1976). Since the direction of the transcellular current seems to play an important role in development of some

systems (see later), we feel that further research to identify the direction of this current is necessary. A separate project in our laboratory is to develop a technique such that the transcellular current can be obtained from the measurement of the small extracellular potentials (Williams, 1984) in the external medium surrounding an *Acetabularia* cell.

Some animals, such as newts, have the ability to generate lost limbs. In regenerating limbs of newts, transcellular current is leaving the amputated part and entering the stump behind it (Borgens *et al.*, 1977b). Such currents have also been induced in the amputated limbs of frogs (frogs have no natural ability to generate lost parts). This led to considerable growth of bone, muscle, and nerves compared to a normal stump. Reversal of the direction of current did not only stop growth; it led to degeneration of the existing components in the stump particularly of the bone and muscle (Borgens *et al.*, 1977a). This seems to indicate the importance of the direction of the transcellular current in developmental process.

Although much evidence indicates the necessity of transcellular current (and associated electric field) for developmental process the fact that similar currents are also found in non-growing systems (Weisenseel *et al.*, 1975) indicates involvement of the current in processes other than growth. On the other hand incomplete growth of frog limbs induced by applied transcellular current described above seems to indicate involvement of other factors in developmental process. Overall these results suggest that the relationship between transcellular current, electric field and development is a complicated one. However, the fact that electric fields and transcellular currents are relatively easy to measure make them useful experimental observables.

1.3.2 The Role of Action Potentials

Steady transcellular current is not the only electrical activity observed in developing systems. In *Acetabularia*, the pollen tube of *Lilium*, and Fucoid eggs spontaneous electrical pulses have also been observed (e.g. Novak and Bentrup, 1972; Weisenseel *et al.*, 1975; Nuccitelli and Jaffe, 1974). Among these systems such activities have been most studied in *Acetabularia* where the size of the cell makes measurement much easier.

The appearance of these pulses or action potentials in *Acetabularia* has a similarity to nerve and muscle impulses in animals. They are generally caused by the transient depolarization of the cell membrane (see chapter 2) and, like nerve impulse, can propagate along the cell membrane. In some cases, however, no propagation is observed (Lertsithichai, 1980; Thavarungkul, 1980) i.e. there are also non-propagating action potentials. It may be helpful to note here that the term action potential was defined by Gradmann (1976) and later by Gradmann and Mummert (1980) as a temporary, regenerative change of the membrane potential which includes all features of the nerve impulse (see chapter 2), one of which is the ability to propagate. However, in this thesis *all* spontaneous depolarizations of the membrane potential will be referred to as action potentials, i.e. including *both* propagating action potentials (as defined by Gradmann) and non-propagating depolarizations.

The purpose of the occurrence of action potentials in animals is quite well understood. In nerve cells the action potential or nerve impulse is the mechanism used to transmit information. In muscle cells the action potential stimulates the contraction of muscle

fibres. In *Acetabularia*, however, the purpose (if any) of the spontaneous action potentials is still unknown.

In addition to their occurrence in normal cells action potentials have also been observed in regenerating anucleate stalk segments of *Acetabularia* (Novak and Bentrup, 1972; Christ-Adler and Bentrup, 1976; Goodwin and Pateromichelakis, 1979; Lertsithichai, 1980). Novak and Bentrup (1972) reported that spontaneous action potentials observed in the regenerating cell initiated at the new tip-growing region. They also suggested that these action potentials might be a mode of transmitting information and triggering growth at the initiation site. This would fit in well with Goodwin's (1975, 1976) proposed membrane model which generates a wave of activation of a certain enzyme. This wave spreads along the membrane in all directions and generates a stable gradient in the nonlinear system. It also gives rise to periodic reinitiation of the wave from the point where it first occurred. In this way symmetry can be broken and an initially uniform system (in this case an anucleate stalk segment which has lost its original polarity) may become spatially organized and hence result in differentiated regeneration. However, later works indicate that action potentials can also initiate at the other end which is not the tip growing site (Christ-Adler and Bentrup, 1976; Lertsithichai, 1980).

Zubarev and Rogatykh (1979) proposed another role for action potentials (spontaneous and/or induced) in *Acetabularia*. In their model (Fig. 1.6) action potentials act as communication signals from the growing apex to the perinuclear layer. On receiving the action potential signal this layer will respond by initiating some mechanism capable of inducing mRNA synthesis (transcription) in the nucleus. This would then be transported to the cytoplasm in the form of RNP, considered to be the MS proposed by Hämmerling (Yasinovsky *et al.*,

1979; Alexeev *et al.*, 1974). The rate of synthesis and/or transport depends on the frequency of the series of action potentials. This model was supported by the experiments in which cap formation was stimulated by a series of induced action potentials (Zubarev and Rogatykh, 1979).

Another possible role of action potentials was suggested by Goldsworthy (1983). The hypothesis is that the action potential is used as a response mechanism for injury in which it rapidly switches off the membrane potential while the cell is being repaired, the signal for it to occur being the partial depolarization brought about by ions leaking through the injured region. This injury also includes the localized tearing of plasmalemma due to the movement of the expanding cell wall during growth. Experimental confirmation of this hypothesis is difficult since any injury to the cell will generally lead to depolarizations of the membrane potential (due to leakage in the cell membrane) which will then invoke action potentials.

1.4 Objectives of Present Work

Of the hypotheses described in section 1.3.2, all were based on the idea that spontaneous action potentials initiate in the growing region. Two of the hypotheses also required the ability of these action potentials to propagate. To confirm any of these hypotheses, data on the point of initiation, the direction of propagation (if any) of the action potentials and the point of regeneration is needed. Although Novak and Bentrup (1972) provided some such data, their measurements have a number of ambiguities and unsatisfactory features. The present work aims to improve and extend these measurements.

Novak and Bentrup used adult cells of *Acetabularia* with a cap diameter of 2-4 mm. The apical (cap) part was cut off and the remaining nucleate stalk segment was kept in the dark for 5-7 days. The rhizoid containing the nucleus was then cut off and the resulting anucleate stalk segment kept in the dark for another day during which time the cell lost its original polarity (Hämmerling, 1963). Development leading to polar regeneration was then elicited by continuous white light. Spontaneous action potentials were found to initiate at the regenerating end which occurred at the cell pole where the membrane potential was highest, that is, where the cytoplasm was most negative. This is a rather surprising result in that for any mechanism where action potentials arise from spontaneous fluctuations, one would expect to find more action potentials initiating in the region where the magnitude of the membrane potential was lower (i.e. less negative and hence closer to the threshold potential, see chapter 2). In the Novak and Bentrup experiments the cell was placed in a narrow groove which ran through a cuvette containing several separate compartments. Silicone grease was applied onto the surface of the cell at the separation between the compartments to insulate one compartment from another. Fig. 1.7 shows the apparatus used in the experiments (and the electrical circuit). The insulation between compartments gave rise to a very high extracellular resistance R_L between the ends of the cell segment compared to the natural condition when the cell was surrounded by sea water. This was very unnatural and could create a serious perturbation in the cell environment. In fact the current in the extracellular medium during the experiment was estimated to be 1,000 times smaller than what it was supposed to be in a natural environment (Bentrup, 1977; Novak and Bentrup, 1972).

Despite the unnatural conditions new growth was still observed. However, the electrophysiological results were rather ambiguous. Initially steady current was found to leave the cell at the growing end. Later in the voltage clamp experiments it was found to enter the growing end. From these observations and the fact that very small currents flowed (as described above) through the cell Novak and Bentrup concluded that this transcellular current was not necessary for growth in anucleate stalk segment of *Acetabularia*. However, later works by Novak and Sironval (1975) indicated the opposite (i.e. growth required transcellular current-flows).

The insulation between compartments in Novak and Bentrup experiments also limited the propagation of any action potential that might occur. Because of this limitation, Novak and Bentrup could only identify the initiation site of an action potential as predominantly at one end or another, and assume that it propagated to the other end. This in fact may not be true since non-propagating action potentials have also been observed (Lertsithichai, 1980; Thavarungkul, 1980).

These limitations lead to the need for a technique to pin-point the initiation site of an action potential and the direction of propagation (if any) for a cell in its natural environment. Part of this thesis deals with the development of such a technique which will be described in detail in chapter 3. This is then applied to the measurement of spontaneous action potentials during the redevelopment of anucleate stalk segments of *Acetabularia*.

This technique is based on the identification of the depolarized region(s) of the cell and subsequent propagation (if any) from the calculated time and space dependent *action currents*. The action currents are calculated from the time dependent electrical potentials

measured by an array of evenly spaced Ag-AgCl electrodes. A sophisticated procedure, the method of regularization, is necessary to handle the ill-conditioned inversion problem (see chapter 3). The potential at the electrodes is continuously monitored by a computer-based data acquisition system. Time sequences of interest (i.e. those containing action potentials) are displayed on the cathode ray tube (CRT) screen and stored on magnetic disc (floppy disc) for subsequent processing and analysis if desired.

It is hoped that further knowledge of the initiation region and subsequent propagation of the action potentials gained by this research, and their correlation with other factors, will lead to a better understanding of the significance of the action potential in *Acetabularia*.

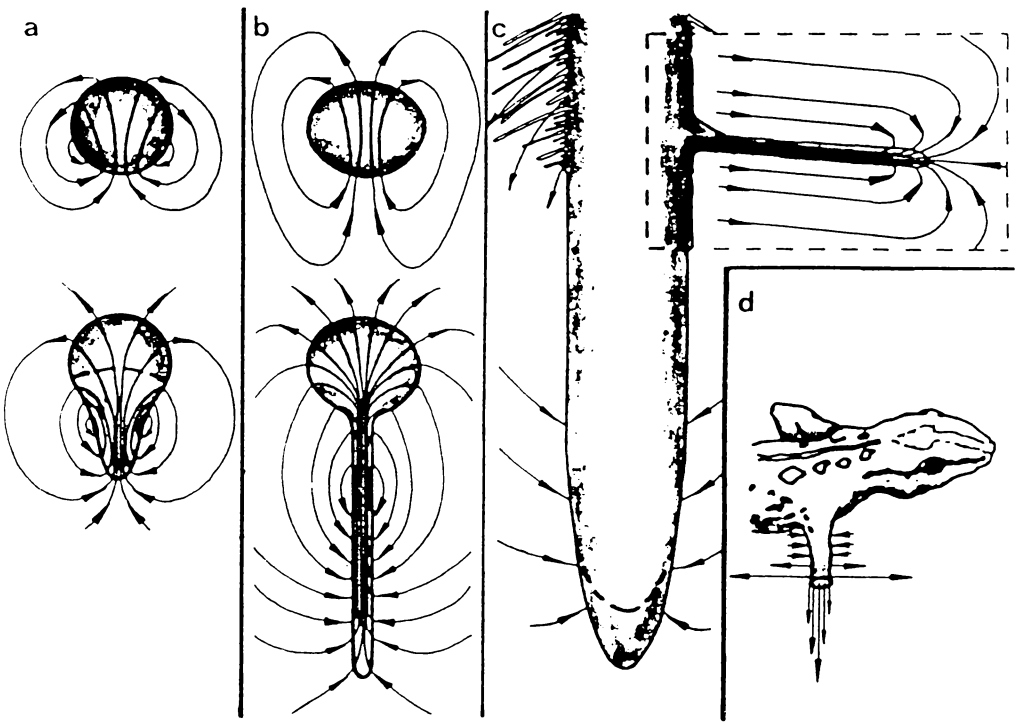

Fig. 1.1 Schematic representation of some typical examples of the pattern of endogeneous electric currents that traverse cells and tissues of plants and animals.

a Zygotes of brown algae before and after the formation of a rhizoid.

b Lily pollen before and after germination.

c Barley root and root hairs.

d Amputated arm of a newt.

(From Weisenseel,1983. The various objects are not drawn to the same scale)

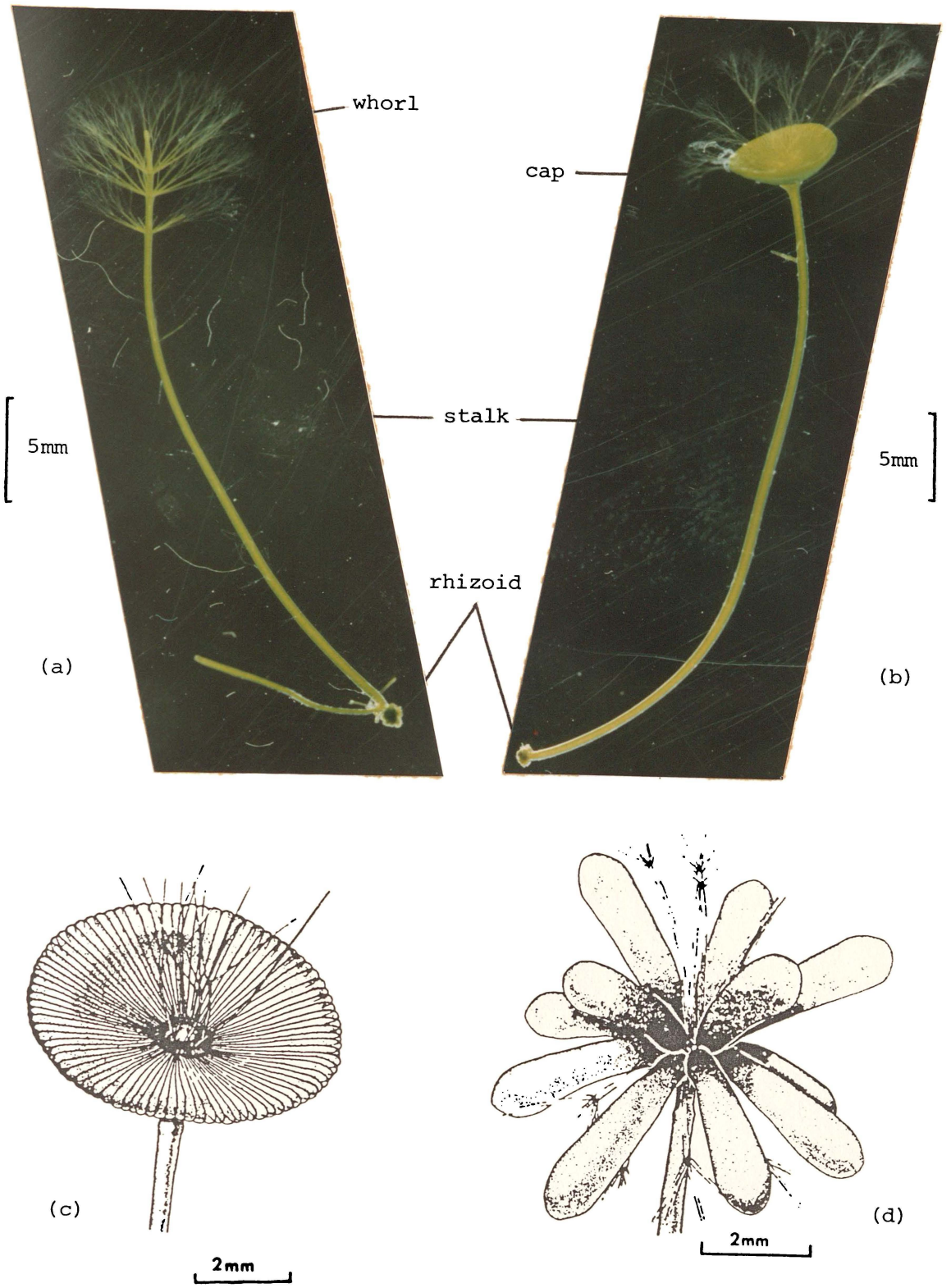

Fig. 1.2 (a) Young plant of *A. mediterranea* with whorls.

(b) *A. mediterranea* with reproductive cap.

Adult caps of (c) *A. mediterranea* and

(d) *A. peniculus (cliftonii)*

((c) and (d) from Puiseux-Dao,1970).

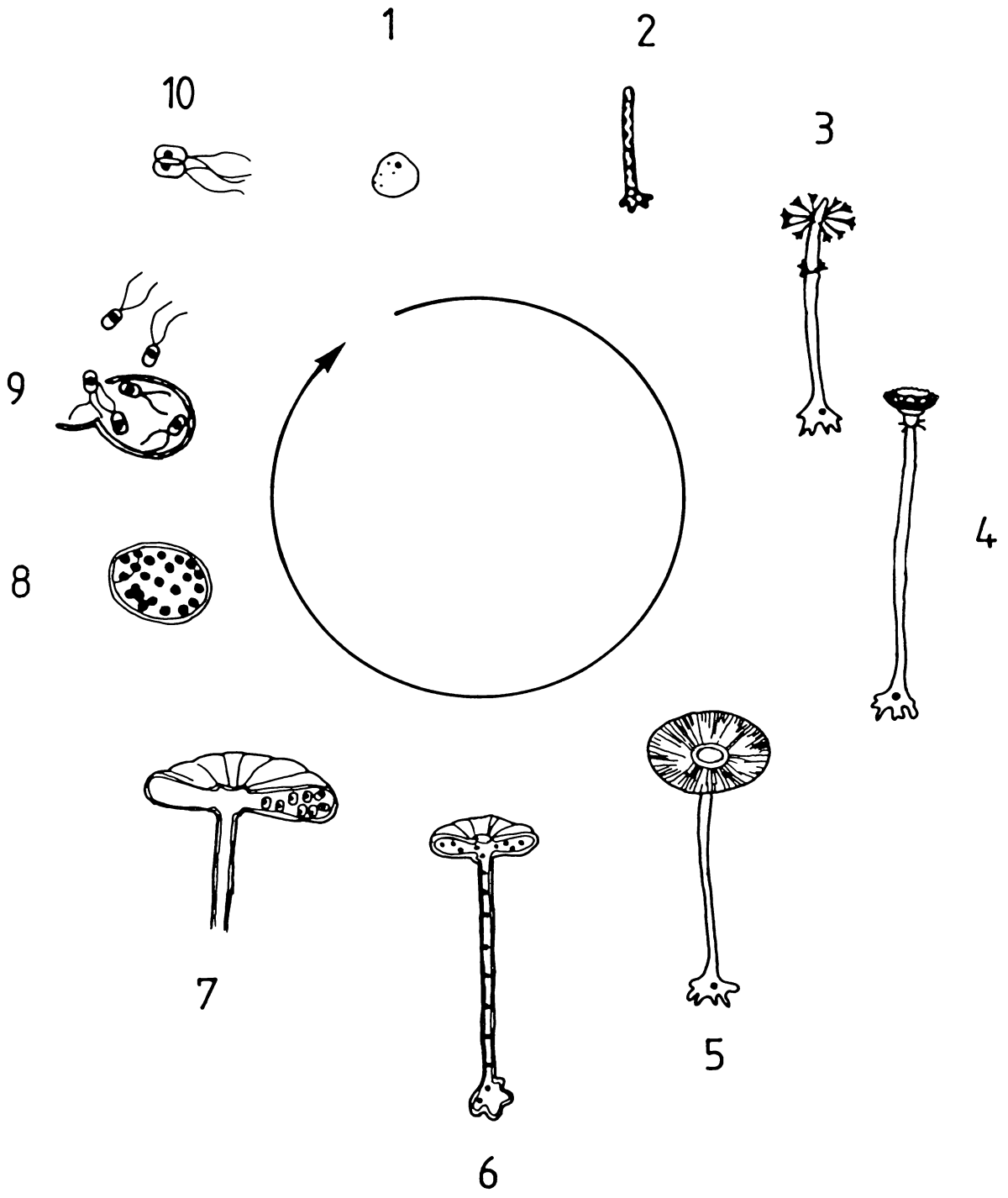

Fig. 1.3 Life cycle of *Acetabularia mediterranea* (modified from Bonotto *et al.*, 1972, Koop, 1977)
1. Zygote; 2. Stalk and rhizoid development; 3. Whorl formation; 4. Cap growth; 5. Maximum cap and cell size; 6. Secondary nuclei formation and their migration into the cap's rays; 7. Cyst formation; 8. Cyst with nuclei and cytoplasmic organelles; 9. Release of gametes; 10. Fusion of gametes (the various stages are not drawn to the same scale).

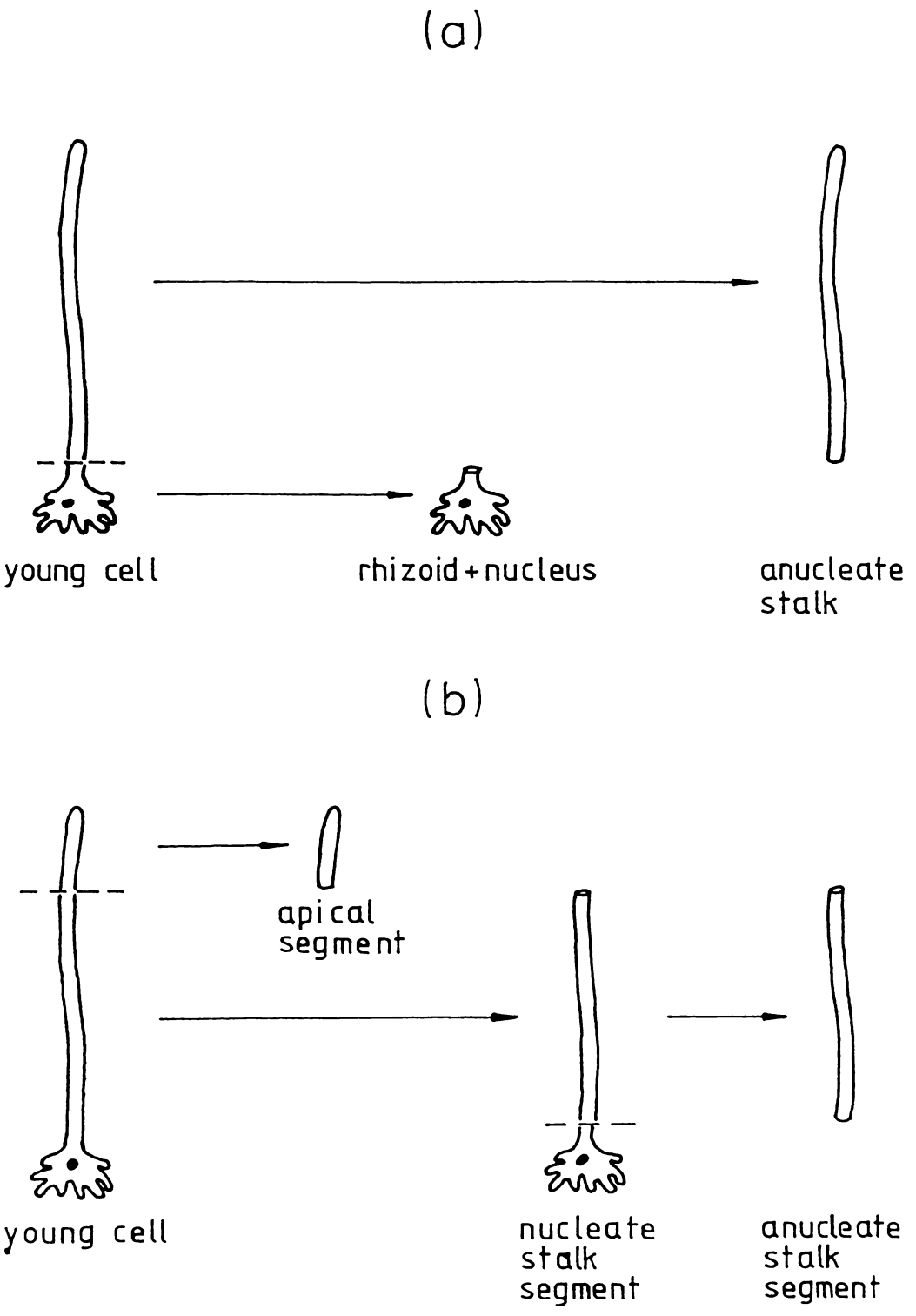

Fig. 1.4 Illustration of some typical cell segments used in the study of morphogenesis in *Acetabularia*.

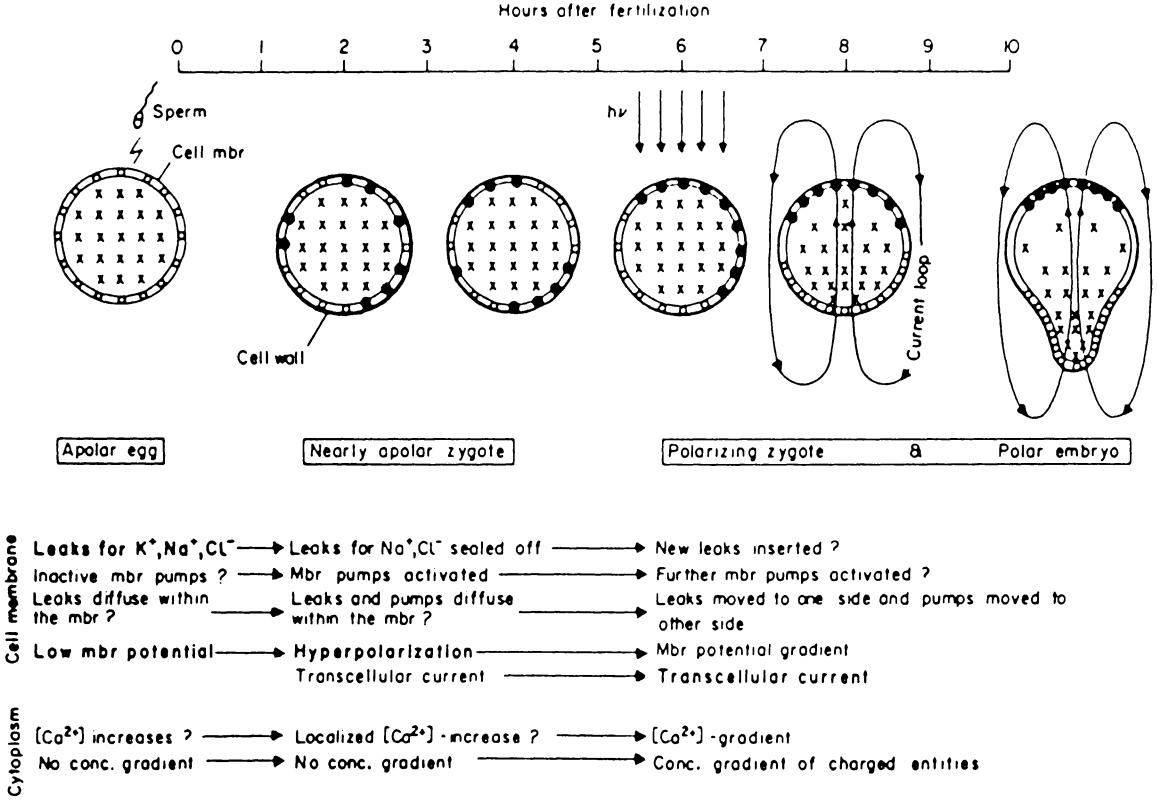

Fig. 1.5 Hypothetical model of the major events in the membrane and in the cytoplasm during early development of a fucoid egg that becomes polarized by unilateral light. Properties and events that have already been established experimentally are written with *bold letters;* those that seem to need more experimental support are written in *normal letters;* and properties and events that are speculative are labeled with a *question mark*. o, membrane leaky site; ●, active membrane pump. (The size of the cell membrane is drawn grossly exaggerated) (from Weisenseel,1979).

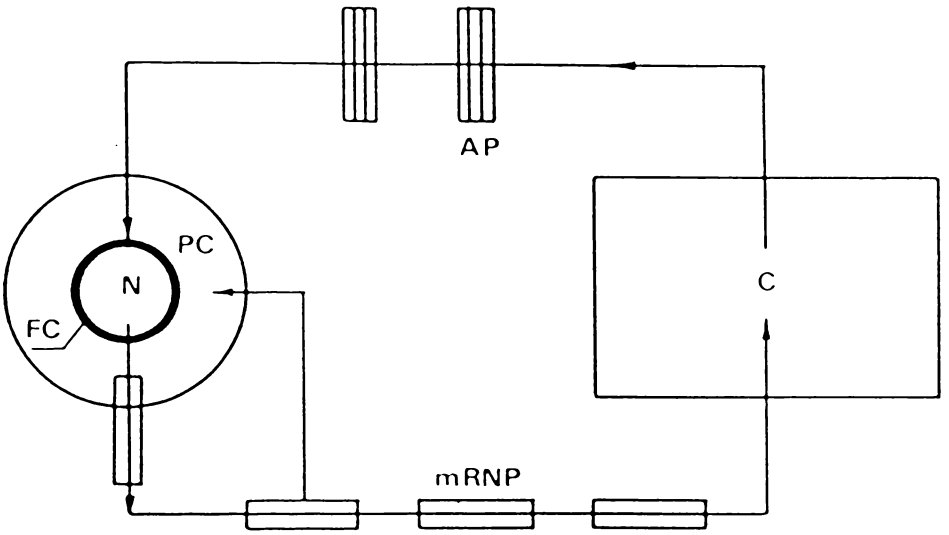

Fig. 1.6 Model for the regulation of morphogenesis in *Acetabularia*.

N: nucleus; PC: perinuclear layer; mRNP: messenger ribonucleoprotein particles; C: cytoplasm; AP: series of action potentials; FC: frontier complex (from Zubarev and Rogatykh,1979).

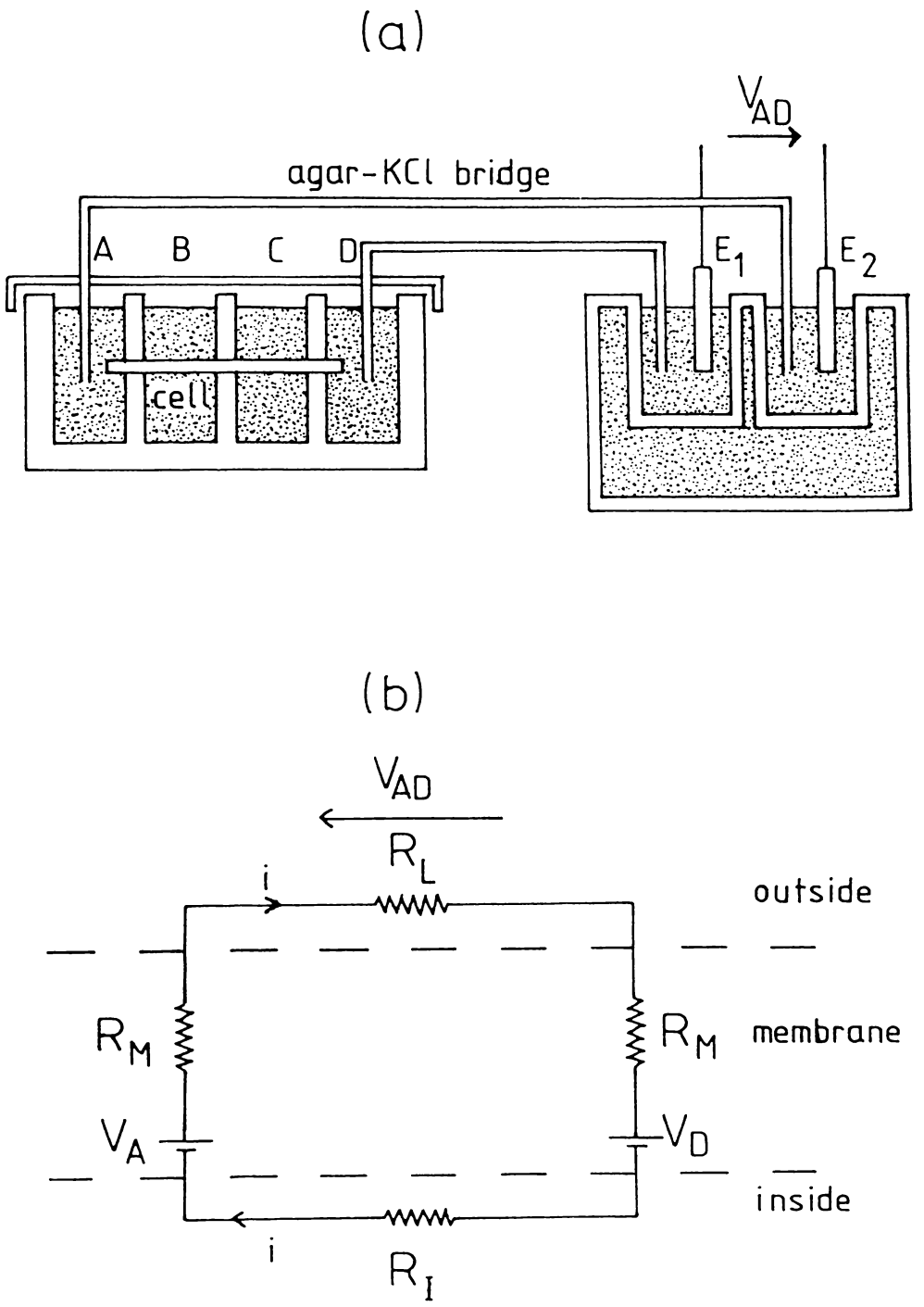

Fig. 1.7 (a) Special cuvette used in Novak and Bentrup's experiments (from Novak and Bentrup, 1972) showing the electrical isolated compartments A,B,C, and D. V_{AD} was measured by electrodes E_1 and E_2.

(b) The equivalent circuit of the cell fragment in the cuvette.

CHAPTER 2

THE CELL MEMBRANE AND ACTION POTENTIAL

2.1 The Cell Membrane

All large organisms are comprised of a number of basic units called cells. Every cell is bounded by a cell membrane of approximately 5-10 nm thick. This membrane acts as a phase boundary between the cytoplasm and the external environment. The membrane has several important properties (see e.g. Robertson, 1983), two of which are of particular interest here. First, its *selective permeability* which allows only certain substances to move in and out of the cell. Second, its ability to move substances against their electrochemical gradients by way of active transport mechanisms or *pumps*. These two properties make it possible for the membrane to maintain the difference between the composition of the solution inside and outside the cell to suit the biochemical processes of cellular function.

The cell membrane consists mainly of lipids and proteins, the proportion of which varies with the type of the membrane (see e.g. Robertson, 1983). The lipids consist mostly of phospholipids with some sphingolipids and cholesterol. The distribution of these lipids also depends on the type of membrane (see e.g. Frömter, 1983). The proteins, however, have not been so thoroughly characterised. Several models for the structure of cell membranes have been proposed (see e.g. Fisher and Stoeckenius, 1983). Currently the most accepted model is the *fluid mosaic model* proposed by Singer and Nicolson (1972). In this model (Fig. 2.1) the membrane consists of two layers of lipids oriented with their polar headgroups exposed at the upper

and lower surfaces of the bilayer in contact with the aqueous solution. This lipid bilayer is impermeable to ions and is generally a very good insulator. Buried within the lipid bilayer are several proteins some of which penetrate right through the lipid layers. Furthermore, both protein and lipid molecules are able to diffuse freely in the *fluid* lipid bilayer.

Membrane proteins are believed to have several different functions, some of which appear to be involved in the transport of ions across the membrane (e.g. Hendry, 1981). Proteins which use chemical energy to transport ions across the membrane against their electrical and chemical gradients constitute *ion pumps*. This ionic movement is termed *active transport* as distinct from *passive transport* down a gradient. For the latter process, a protein may regulate the selective ionic permeability by two mechanisms (Fig. 2.2).

(i) it can act as a carrier which binds an ion at one side, diffuses across the bilayer, and releases it at the other side.

(ii) it can span the bilayer and form a pore structure through which the ion can pass from one side to the other.

Ion permeabilities of the membrane can also be induced by ionophores. These ionophores consist of a wide range of small molecules some of which are synthetic compounds, others are synthesized by micro-organisms. The term ionophore was originally assigned to the compounds which act as mobile ion carriers. However, currently it has been extended to cover substances which induce ion permeability by forming pores in the membrane. There are several types of ionophore each of which induces permeability to a different ion(s) (see e.g. Gomperts, 1977). For example, ionophore A23187 is a carrier substance for divalent cations Ca^{2+} and Mg^{2+} (Reed and Lardy,

1972) and has been widely used as a probe of Ca^{2+} function in cellular activities (e.g. Goodwin and Pateromichelakis, 1979; Reiss and Herth, 1979a).

The ability of the membrane to maintain the ionic concentrations inside the cell (by selective permeability and active transport) so that they differ from the outside gives rise to an electrical potential difference between the interior and the environment. This potential difference is known as the *membrane potential* and its sign is such that the cytoplasm is normally negative with respect to the external environment. Different types of cell have different membrane potentials, value typically lying in the range -20 to -200 millivolts.

Some cells have the special characteristic that their membrane potentials may change quite rapidly in response to suitable stimuli such as electric current injection or changes in the chemical environment. These cells are called *excitable cells* and we sometimes call the membranes of these cells *excitable membranes*. Excitable cells include, for example, nerve cells, muscle cells, sensory cells, and also some plant cells such as the giant alga *Acetabularia mediterranea* studied in this work.

2.2 The Membrane Potential

2.2.1 The Electrochemical Gradient and The Nernst Equation

As already described, the membrane potential of a biological cell arises from the differences in ionic concentrations inside and outside the cell. The circumstances under which the membrane potential is established is quite complex and still not completely understood (see e.g. Neumcke, 1983; Ohki, 1979). However, some

explanation of the membrane potential can be obtained by considering the diffusion potentials of the major ions of the cytoplasm and external medium.

Let us consider the system shown in Fig. 2.3 where there are two compartments containing different concentrations of an electrolyte AB in aqueous solution separated by a membrane permeable to A^+ but not B^- i.e. it is selectively permeable. Assuming that the concentration in compartment 1 is higher than that in compartment 2, A^+ ions will then tend to move from compartment 1 to 2 down its chemical or concentration gradient. Since B^- cannot diffuse across the membrane there is soon an excess of A^+ ions in compartment 2 and an excess of B^- ions in compartment 1. This produces a potential difference across the membrane and an electric field that retards the flow of A^+ ions from compartment 1 to 2 and accelerates their flow from compartment 2 to 1. A dynamic equilibrium is established when the *driving forces* of the concentration and electrical potential gradients are equal and opposite.

From elementary thermodynamic considerations, the work required to move δn molecules of A^+ across the membrane against the concentration gradient from compartment 2 to 1 is

$$\delta W_c = \delta n \, RT \, \ell n \left[\frac{A_1}{A_2}\right]$$

where R = gas constant = 8.3143 J K^{-1} mol^{-1}

T = absolute temperature

A_1, A_2 = molar concentration of A^+ in compartment 1 and 2 respectively.

And the work required to move δn molecules of A^+ against the electrical gradient is

$$\delta W_e = \delta n \, zFE_{21}$$

where z = the charge on the ion

F = Faraday constant = 96,487 C mol^{-1}

E_{21} = the potential of compartment 2 with respect to compartment 1 (V)

In the dynamic equilibrium state

$$\delta w_c = \delta w_e$$

and hence

$$E_{21} = \frac{RT}{zF} \ln \left[\frac{A_1}{A_2}\right] \qquad (2.1)$$

Equation (2.1) is known as the *Nernst Equation*, and E_{21} is called the *Nernst* or *equilibrium potential*.

In order to calculate the equilibrium potential of a particular ion inside the cell with respect to the surrounding medium we substitute A_2 with the value of the internal ionic concentration (i.e. in cytoplasm) and A_1 with the value of the external ionic concentration. The equilibrium potentials of the major ions of *Acetabularia mediterranea* are shown in Table 2.1 along with those for squid axon as an example of a much-studied nerve cell system. We see that unlike the squid axon the membrane potential of *Acetabularia* lies outside the range of the equilibrium potentials. To date, the most likely explanation for the deviation concerns the electrogenic pump of the Cl^- ion and this will be discussed later in this chapter. Another possible explanation is that the membrane potential is the result of the difference in surface potentials on both sides of the membrane due to fixed surface charges as well as the Nernst diffusion potentials (see Ohki, 1979).

In spite of these considerations the Nernst equilibrium potential of an ion is still a useful parameter since it gives the net driving force across the membrane for the various ions. This arises from the electrochemical potential difference V_m-E_i (membrane potential - equilibrium potential of ion i) i.e. if $V_m-E_i \neq 0$ a passive flux of ionic species i between the cell and the external medium will arise, provided that there is a conductive channel. The direction of this flux will depend on the value of V_m-E_i and the charge of the ion, i.e. $V_m-E_i > 0$ indicates gradient favouring positive ion efflux and negative ion influx and vice versa for $V_m-E_i < 0$ (see Fig. 2.4). Thus from the value of the membrane potential, V_m, and the equilibrium potentials, E_i, of the various ions we have some indication of the passive ionic fluxes (leakages). The equilibrium potentials, electrochemical potential differences, and the potential driving passive leakage pathways of both *Acetabularia* and squid axon are shown in Fig. 2.4.

2.2.2 Ionic Relations and the Membrane Potential

(a) In *Acetabularia*

At present the details of the ionic pathways of the major ions in *Acetabularia* are not fully understood. The diagram in Fig. 2.4 suggests the passive (diffusion) pathway of Na^+, K^+ influxes and Cl^- efflux, and active pathway for Na^+, K^+ effluxes and Cl^- influx. So far there is only evidence to confirm that Na^+ influx and efflux are passive and active processes respectively (Saddler, 1970a, 1970c), and that Cl^- influx is an active process (e.g. Saddler 1970b). As for K^+ influx and efflux, and Cl^- efflux, the mechanisms are still unclear. Regarding the contribution of these ions to the membrane

potential it was found that among the cations of the external medium, only K^+ affects the membrane potential (e.g. Apostolova and Ksenzhek, 1977; Gradmann and Bentrup, 1970;Saddler, 1970b). As for the anion i.e. Cl^- it was found that if the cell is subjected to conditions which inhibit the operation of the Cl^- influx electrogenic pump (see Saddler, 1970b) the membrane potential will depolarize to a new steady level of approximately -80 to -90 mV, the K^+ equilibrium potential. Following this it has been suggested that the Cl^- influx electrogenic pump which is located in the outer plasma membrane or plasmalemma (Freudling and Gradmann, 1979) is the only possible active process which contributes the highly negative value of the membrane potential (Saddler, 1970b). From these results it appears that Cl^- and K^+ are the only two ions that affect the resting membrane potential (see also Apostolova and Ksenzhek, 1977). This implies that the conductance of the Na^+ channel is small in comparison with that of the other ions.

Recent work by Gradmann *et al.* (1982) indicated that the electrogenic Cl^- pump may be an ATPase (Adenosine triphosphatase), an enzyme which is also involved in other ion transport mechanisms (Hodges, 1976).

(b) <u>In the Squid Axon</u>

In the case of the squid axon we see in Fig. 2.4 that passive diffusion will give K^+ and Cl^- effluxes and an Na^+ influx. To maintain this non-equilibrium state, there must be some active process which imports K^+, Cl^- and exports Na^+ against the electrochemical gradients. In fact, there is evidence that Na^+ efflux is an active process and probably coupled by the K^+ influx pump (Hodgkin and Keynes, 1955a), and that Cl^- influx is an active

process as well (Keynes, 1963). Fig. 2.4 also shows that in this case the membrane potential lies within the range of equilibrium potentials, and it has been shown that the membrane potential is mainly due to the diffusion potential of K^+ (Hodgkin and Keynes, 1955b), probably with small contributions from Na^+ and Cl^-.

2.3 The Action Potential

2.3.1 General Features of an Action Potential

Originally the term *action potential* applied to the rapid electrical changes in living cells which cause some kind of action, such as contraction of a muscle fibre. The properties of such action potentials have been studied in detail (see e.g. Katz, 1966). At present the term action potential is also applied to similar phenomena in a wide variety of organisms in some of which no obvious *action* is known (see e.g. Hope and Walker, 1975). Hence, the actual meaning of an action potential has shifted and is now defined as *a temporary regenerative change of the membrane potential* (Gradmann and Mummert, 1980). The following list of criteria were given by Gradmann (1976) in order to provide a reasonable definition for an action potential.

(i) large transient change of transmembrane potential difference

(ii) all-or-none characteristic (i.e. highly nonlinear response to external stimuli)

(iii) endogeneous energy supply

(iv) propagation

An example of an action potential is shown in Fig. 2.5 (trace c) which can be described as follows: when a cell is subjected to a

suitable stimulus the membrane potential will become less negative (i.e. depolarize) with respect to the resting membrane potential. The amount of depolarization depends on the strength of the stimulus. If the stimulus is not strong enough, the membrane potential will decay back to the resting value after a slight depolarization (trace a, Fig. 2.5). If the stimulus is strong enough for the change in membrane potential to reach a point of electrical instability known as the *threshold*, two things can happen:

(i) the depolarization may decline after a small variable delay; this is *local* or *subthreshold response* (trace b, Fig. 2.5);

(ii) it may suddenly depolarize into a much larger signal; this is the *action potential* (trace c, Fig. 2.5), which is no longer linearly proportional to the stimulus.

A stimulus which has just sufficient strength to depolarize the membrane potential to the threshold value and initiate an action potential is sometimes called a *threshold stimulus*. After the depolarization phase reaches the peak it is followed by a repolarization phase which brings the membrane potential back to the resting value. Once the stimulus is strong enough to create an action potential, further increases in the strength of the stimulus will only produce an action potential of the same amplitude i.e. an *all-or-none* response. The energy of the action potential is provided locally along the cell, and not by the stimulus which sets up the action potential. This action potential is then propagated along the cell membrane.

After the occurrence of an action potential there is an interval during which the cell is unable to undergo another depolarization. This time lapse is known as the *refractory period*.

If a nerve cell is stimulated with rectangular current pulses it is found that the threshold stimulus intensity rises as the pulse length is lessened. This effect is known as the *strength-duration* relation (Fig. 2.6).

In *Acetabularia* such transient changes of membrane potential with the above properties are also found (i.e. properties i to iv, refractory period, strength-duration relation and regenerative (Gradmann, 1976)), so we can regard such events as action potentials. For *Acetabularia*, in addition to the induced action potential, spontaneous action potentials which occur without applying any obvious stimulus are found (e.g. Saddler, 1971). The purpose (if any) of these two types of action potential in *Acetabularia* is still unclear.

As previously mentioned (see section 1.3.2) some of the spontaneous transient depolarization signals, which resemble action potentials, observed in *Acetabularia* do not show any true propagation (Lertsithichai, 1980; Thavarungkul, 1980). This behaviour has also been observed in some higher plants (Pickard, 1973). Following these observations it has been suggested that propagation may not be a necessary property in plant (spontaneous) action potentials (Goldsworthy, 1983). Hence, in this work we shall use the term *spontaneous action potential* for *all spontaneous large transient changes of membrane potential* (i.e. it includes both the propagating and the non-propagating spontaneous action potentials).

2.3.2 Action Potential in *Acetabularia*

Previously we discussed the general features of action potentials. In this section we shall consider more specifically the

action potentials in *Acetabularia* (Fig. 2.7) and the ionic movements which give rise to the membrane potential changes during an action potential.

In *Acetabularia* it has been reported that Cl^- efflux (Saddler, 1971; Gradmann, 1976; Gradmann and Mummert, 1980) and K^+ efflux (Gradmann and Mummert, 1980; Mummert and Gradmann, 1976) increase during an action potential. Cl^- efflux was suggested to be responsible for the depolarization phase of the action potential and K^+ efflux, the repolarization phase (Gradmann, 1976; Gradmann and Mummert, 1980). Early study of Cl^- efflux (Gradmann, 1976) during an action potential led to the initial conclusion that the whole depolarization phase of an action potential is a result of a net Cl^- efflux caused by the blockage of the electrogenic Cl^- import pump which is closely related to energy metabolism (Gradmann, 1975). Hence, it has been called *metabolic* action potential (Gradmann, 1976). However, further study indicated that this is not the case. Cl^- efflux was also found to be caused by the change in membrane permeability, that is, a *passive* event (Gradmann and Mummert, 1980). From the evidence obtained so far a mechanism of the action potential was proposed (Gradmann, 1976; Gradmann and Mummert, 1980), which can be summarized as follows.

In a resting state, the membrane potential of *Acetabularia* is approximately -170 mV (e.g. Saddler, 1970b). If during a depolarization the membrane potential reaches the threshold value of approximately -160 to -150 mV (Gradmann, 1976; Gradmann and Mummert, 1980) the shut down of the electrogenic Cl^- pump, which is associated with the energy metabolism (Gradmann, 1975), will occur. This will cause a further depolarization in membrane potential. This is known as the *metabolic* part. When the depolarized membrane potential reaches approximately -100 mV the *passive* part starts. At this point

an extra Cl^- efflux pathway is triggered (i.e. increases in Cl^- conductance) yielding a final peak depolarization of approximately -50 mV. For membrane potential more positive than the equilibrium potential of K^+ ($E_k \simeq -90$ mV), there is a large K^+ conductance and K^+ will leave the cell via its electrochemical gradient (e.g. Mummert and Gradmann, 1976). This K^+ efflux balances Cl^- efflux and thus brings the membrane potential back towards E_k. During the repolarization the Cl^- conductance, which initiates the passive part of the action potential, also decreases. This indicates that it is dependent not only on voltage but also on time. At this point near E_k the plateau (of membrane potential) may be prolonged if the cell is in a lower energy state. If the Cl^- pump does operate the rest of the repolarization takes place relatively quickly at first and slows down after a while (Gradmann, 1976, see Fig. 2.7). Thus the major features of the action potential can be understood in terms of the dependence of the Cl^- import pump and the Cl^- and K^+ conductances on the membrane potential (Cl^- conductance also depends on time).

For completeness, we should mention here that during an action potential a large Cl^- efflux *burst* (much larger than the passive Cl^- efflux described above) was sometimes observed (Gradmann *et al.*, 1973; Gradmann and Mummert, 1980; Mummert and Gradmann, 1980; Wendler *et al.*, 1983). This Cl^- burst was originally thought to be responsible for the depolarization during an action potential (Gradmann *et al.*, 1973). However, it was observed that this Cl^- efflux burst could occur without the occurrence of an action potential (Wendler *et al.*, 1983), and in addition many action potentials occur without these Cl^- bursts (Mummert and Gradmann, 1980). Thus there was no strict correlation between these two phenomena. Recent experiments by Wendler *et al.* (1983) indicated a

strong correlation between this Cl^- burst and the regulation of the turgor pressure in *Acetabularia*. As for the mechanism(s) by which the Cl^- efflux is transported, these are still unclear (see Gradmann and Mummert, 1984; Mummert and Gradmann, 1980; Wendler *et al.*, 1983, 1984).

It is interesting to compare the situation to that in the squid axon where qualitalively similar behaviour is produced by quite different detailed mechanism. Hodgkin and Huxley (e.g. 1952a); Hodgkin and Katz (e.g. 1949); and Keynes (e.g. 1951) have shown that the depolarization phase of an action potential is caused by the increase in permeability to the inward Na^+ ions and the repolarization phase due to the increase in permeability to the outward flow of K^+ ions (see Fig. 2.8). Thus, the main differences are

(i) the ions involved; Na^+/K^+ in the axon and Cl^-/K^+ in *Acetabularia*

(ii) the action potential in the squid axon is due solely to voltage dependent changes in the permeabilities of the passive pathways, while in *Acetabularia* it is due to the blockage of the Cl^- electrogenic pump in addition to voltage dependent changes of the Cl^- and K^+ permeabilities

(iii) the time scale of the action potential in *Acetabularia* is ~10-100 seconds as compared with ~ milliseconds for the squid axon, and the propagation speed is correspondingly slower (~mm s^{-1} instead of m s^{-1}). This difference is undoubtedly due to the longer time constant associated with the turning on or off of the metabolically driven Cl^- pump.

It is perhaps appropriate to mention here that, following the observations of a large K^+ efflux during an action potential, Mummert and Gradmann (1976) proposed that action potentials could play an important role in regulating the intracellular K^+ concentration (see chapter 1 for other proposals for the function of an action potential). According to the diagram in Fig. 2.4 during the steady state (no action potential) there must be a passive K^+ influx due to the difference between V_m and E_k. Without a regulatory mechanism the K^+ influx would continue until $V_m = E_k$ i.e. when the intracellular K^+ concentration is about 10 M/l. However, this is not the case for it was found that K^+ in the cytoplasm is only ~400 mM/l (Saddler, 1970a). From the amount of K^+ efflux measured during an action potential it was calculated that an average of 0.5 spontaneous action potential per hour would be enough to keep the the cytoplasmic content of K^+ at this level (Gradmann and Mummert, 1980). However, it has been observed that sometimes the period between two successive spontaneous action potentials could be as long as 4-10 hours (Lertsithichai, 1980). Although spontaneous action potentials seem to arise at the part of the cell subjected to higher K^+ concentration (Christ-Adler and Bentrup, 1976), there is no direct evidence to indicate that the internal K^+ concentration directly triggers an action potential when it exceeds a fixed level.

2.4 Analog Electrical Circuits

Studies of the steady state electrophysiological properties of the membrane of *Acetabularia*, which include flux measurements (Gläsel and Zetsche, 1975; Saddler, 1970a), electrical properties (Gradmann, 1975; Gradmann and Klemke, 1974), and ATP measurements (Gradmann,

1975; Gradmann and Bokeloh, 1975) enable an analog circuit of the *Acetabularia* cell membrane to be constructed (Gradmann, 1975). Although this circuit (Fig. 2.9) was devised to represent the steady state condition it also proved useful for the analysis for dynamic events, such as action potentials (Gradmann, 1976; Gradmann and Mummert, 1980), and the analysis of fast light-induced depolarization of the *Acetabularia* membrane potential (Gradmann, 1978). However, the detailed arguments for the inclusion of the various elements are complex and not of direct relevance to the present work. The important point is just that the electrical behaviour of the membrane can be represented quite well by such a circuit model.

For comparison, an analog circuit for the squid axon derived by Hodgkin and Huxley (1952b) is shown in Fig. 2.10.

2.5 The Core Conductor Model

As discussed in the previous section (2.4) the cell membrane's electrical behaviour can be represented by equivalent elements as shown in Figs. 2.9, 2.10. We can see that the circuits are complex and involve many factors, and we are faced with a great problem if we want to obtain any calculated result from such circuits. However, certain simplifications are possible as will be discussed later in this section.

2.5.1 Nonlinear Properties of Excitable Membranes

In excitable cells, under certain circumstances (e.g. small changes of membrane potential V_m) membrane properties can be considered as *linear*, i.e. the relationship between the membrane

voltages and currents obeys the principle of superposition (see e.g. Jack *et al.*, 1975). In other words, the parameter values in the membrane equivalent circuit are voltage independent. However, the range of potentials over which the membrane may be assumed to be linear is restricted (~10 mV in *Acetabularia* - Gradmann, 1976). Thus outside the range of such potentials (i.e. between the resting membrane potential and the threshold value) the membrane properties are *nonlinear.*

The most important nonlinearity concerns the *membrane conductance*, G_m (the reciprocal of the membrane resistance R_m). In a linear membrane, a linear relationship exists between membrane ionic current ΔI_i and the membrane potential i.e.

$$\Delta I_i = G_m \Delta V \qquad (2.2)$$

ΔV is the potential expressed as a deviation from the resting potential and G_m is a constant. Nonlinearity arises when the conductance G_m is not constant i.e. it changes when the voltage changes. In this case G_m depends on the current-voltage relationship of the system. Examples of such a nonlinearity is the sudden change of Na^+ and K^+ channel conductivities in squid axon and an increase in Cl^- conductance in *Acetabularia* when the membrane potential passes through these values in the course of an action potential.

In some cases the change in conductance of the membrane to certain ion(s) gives rise to a current-voltage relationship similar to that found in a diode. The terminology used to describe such behaviour is *membrane rectification.* By this we mean that the membrane passes current more easily in one direction than the other. A membrane which passes outward current more easily than inward

current is said to show *outward-going rectification*, whereas a membrane which passes inward current more easily than outward current is said to show *inward-going rectification*. Fig. 2.11 shows the symbols frequently used in electrical equivalent circuit to represent these forms of rectification. An example is the *Acetabularia* membrane which shows an outward-going rectification in the pathway of potassium ionic current (see Fig. 2.9 also Gradmann and Bentrup, 1970).

2.5.2 Core Conductor Theory

If we consider the total electrical current that passes through the membrane rather than the individual ionic contributions, then the equilvalent circuit of the membrane can be represented by a simpler circuit. This circuit contains only a resistance in series with a battery (Fig. 2.12a). We also assume that the system has regular geometry, in this case cylindrical, and therefore the resistance and capacitance (of a unit length) do not change along the length of the system. The resistance is normally represented by the membrane resistance of a unit length r_m (Ω cm, which is nonlinear in general), and the battery assumes the value of the membrane potential V_m as measured experimentally. Also, in order to represent the time dependent changes observed in the membrane potential (e.g. the decay of the voltage response after removing the stimulating pulse with the value less than the threshold stimulus trace a, b, Fig. 2.5) we need to incorporate a capacitance (Fig. 2.12b) normally denoted by c_m, the capacitance per unit length ($\mu F\ cm^{-1}$). If we now consider the propagation of an action potential we need to take account of the distributed nature of the system i.e. we must also include two other

components, the longitudinal resistance per unit length of the extracellular fluid (i.e. external medium) (r_e, Ω cm^{-1}) and the longitudinal resistance per unit length of the intracellular material (cytoplasm) (r_i, Ω cm^{-1}). The complete network is shown in Fig. 2.12c. The representation of membrane in this way is known as the *lumped element core conductor model*, since it implies that the cell behaves as a poorly insulated cable. For this reason we sometimes refer to it as *cable theory* (see e.g. Jack *et al.*, 1975). Normally the representation of such cells as cable networks has been simplified by the following assumption.

(i) The radius of the cell is small enough, so that we can omit the radial resistances of the external and the intracellular materials;

(ii) the intracellular impedance to axial current flow is a simple resistance.

This representation can be easily applied to any similar system; we only need to determine the value of the cable constants (i.e. r_m, c_m, r_i, r_e). For *Acetabularia* the representation of the membrane is shown in Fig. 2.13.

The elements of this circuit are nonlinear, but for small changes in the membrane potential it can be approximated by a linear network (see e.g. Jack *et al.*, 1975).

2.5.3 Propagation of Action Potentials

From the core conductor model discussed previously we can now consider how the action potential is propagated (for more detail see e.g. Aidley, 1978).

When any region of the cell is stimulated so that an action potential occurs then in this *depolarized* or *active region* the membrane potential is positive with respect to the adjacent regions (Fig. 2.14). The difference of the potentials between the depolarized region A and the adjacent regions B and C leads to the current-flows as shown in Fig. 2.14. The current-flows (leaving the cell) in regions B and C will reduce the membrane potential in these regions. When the potential has been reduced so that it reaches a threshold value, the action potentials occur at regions B and C. Now regions B and C are active and can stimulate the regions on their right and left respectively. In this way the action potential is propagated. This hypothesis of the mechanism of conduction is known as the *local circuit theory*, i.e. propagation is brought about by the flow of current between the active region and the adjacent resting regions. Fig. 2.15 shows the propagation of an action potential. In this case the outward current on the right of the depolarized region will induce the action potential in that region which enables the action potential to propagate from left to right. Subsequently the initial depolarized region will repolarize and as a result the current will leave the cell from this region (Fig. 2.15 at time $t_o+\Delta t$ and $t_o+2\Delta t$). This current should reduce the membrane potential and generate another action potential in this region. However, this is not the case due to the fact that each time a region undergoes an action potential depolarization it is left in a refractory state (indicated by non-active region in Fig. 2.15) for a period of time (i.e. refractory period). This period differs from one system to another, for example the refractory period in a nerve axon is ~2 ms (Katz, 1966) and is ~3 minutes in *Acetabularia* (Gradmann, 1976). It is this property that enables the action potential to propagate as a well defined pulse along the length of the cell.

TABLE 2.1 Ionic concentrations (mM/l) of major ions in the cytoplasm and the external medium, the equilibrium potential E_i (mV), and the experimental membrane potential V_m (mV) of *Acetabularia* and Squid Axon (modified from Saddler, 1970a and Katz, 1966).

Ion	*Acetabularia*			Squid Axon		
	External medium	Cytoplasm	E_i	External medium	Cytoplasm	E_i
Na^+	470	60	+51	460	50	+55
K^+	10	400	-92	10	400	-92
Cl^-	550	490	- 3	540	70	-51
V_m	-170			-60		

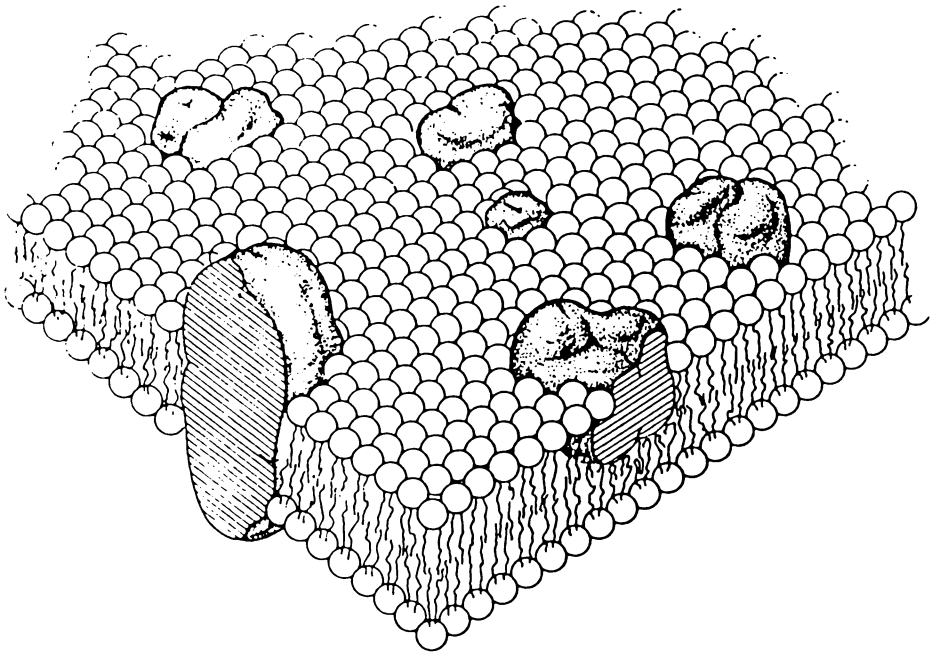

The lipid-globular protein mosaic model with a lipid matrix (the fluid mosaic model); schematic three-dimensional and cross-sectional views. The solid bodies with stippled surfaces represent the globular integral proteins, which at long range are randomly distributed in the plane of the membrane. At short range, some may form specific aggregates, as shown.

Fig. 2.1 The Fluid Mosaic Model (from Singer and Nicolson, 1972).

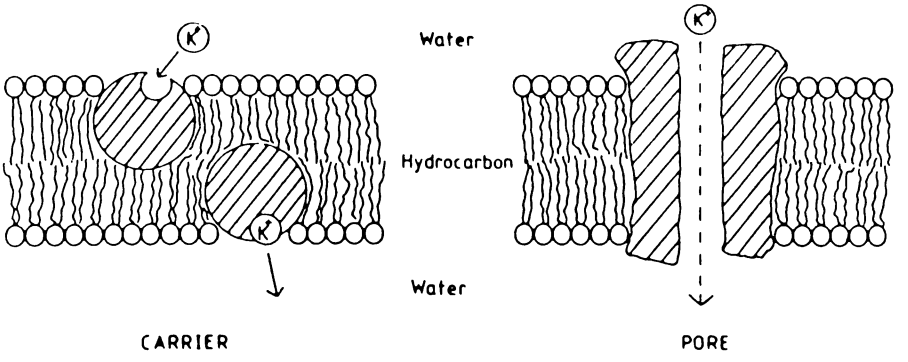

Fig. 2.2 The Carrier and Pore Mechanisms by which a Protein May Allow Ions to Cross the Bilayer.
(from Hendry, 1981).

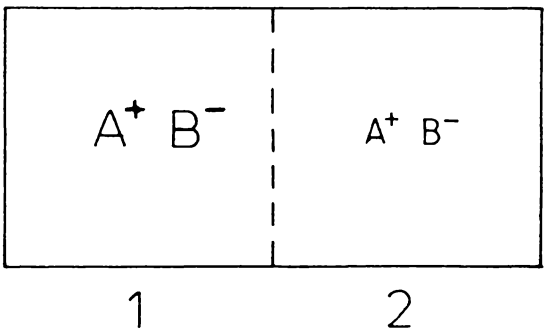

Fig. 2.3 Concentration cell.

Fig. 2.4 Equilibrium potentials, E_i (———), electrochemical potential differences, $V_m - E_i$ (-----) and the membrane potentials (V_m) of *Acetabularia* and squid axon (values from Table 2.1).

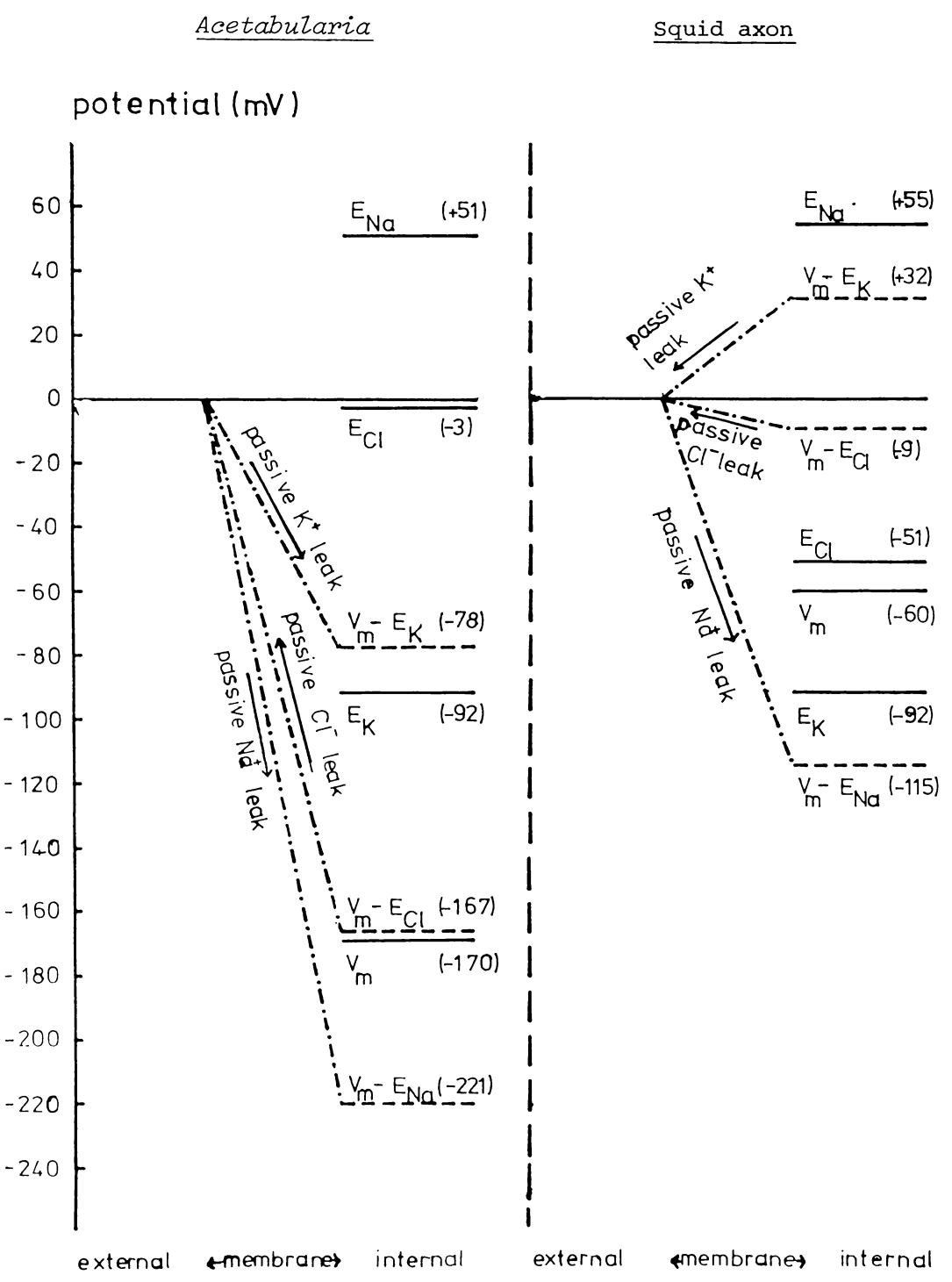

Fig. 2.5 Variations of membrane potential in squid axon caused by current pulses of fixed duration (2 ms), but various size (modified from Katz, 1966).

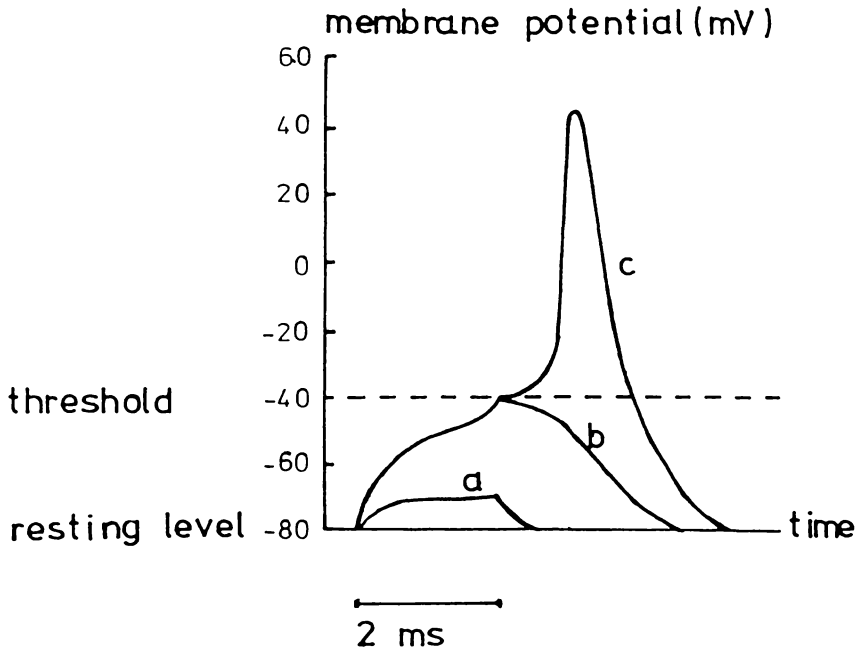

a depolarization caused by weak stimulus

b subthreshold response

c action potential

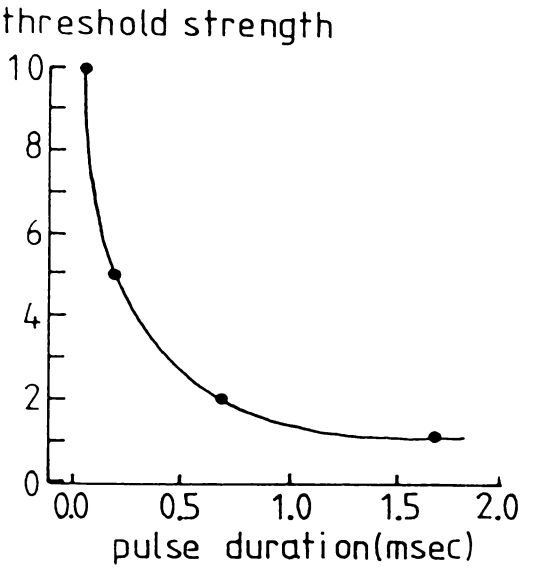

Fig. 2.6 Strength-duration curve, showing the relation between the duration of a stimulating current (square wave) and the current strength needed to produce a nerve impulse (modified from Katz, 1966).

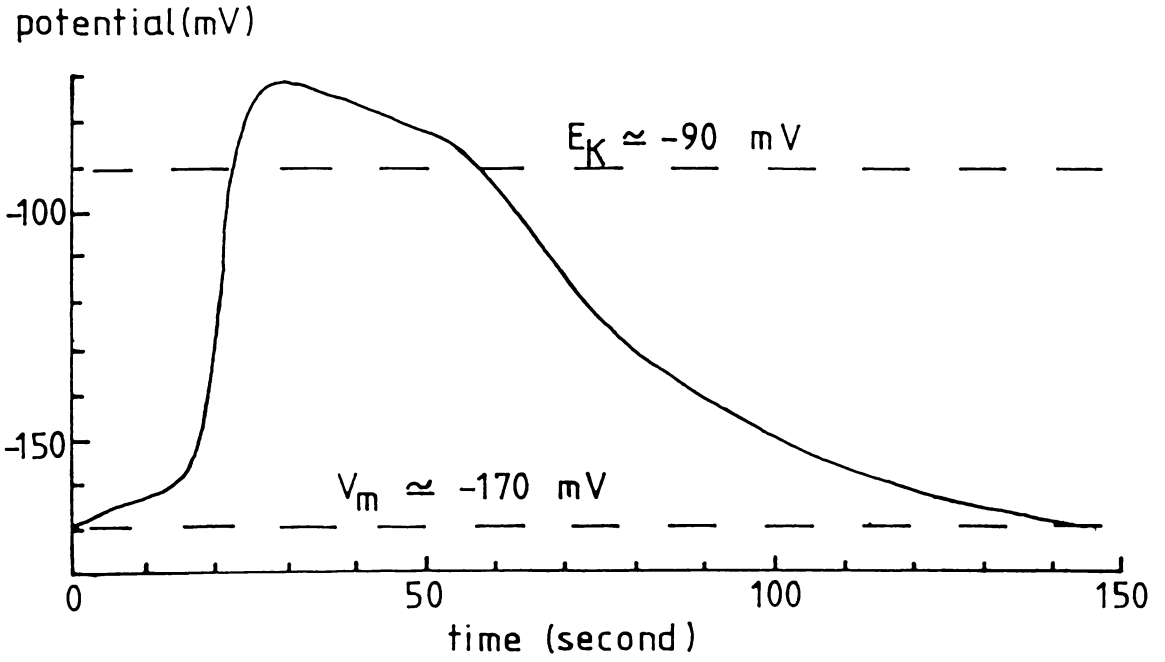

Fig. 2.7 Intracellular recording of an action potential in an *Acetabularia* cell (modified from Lertsithichai, 1980).

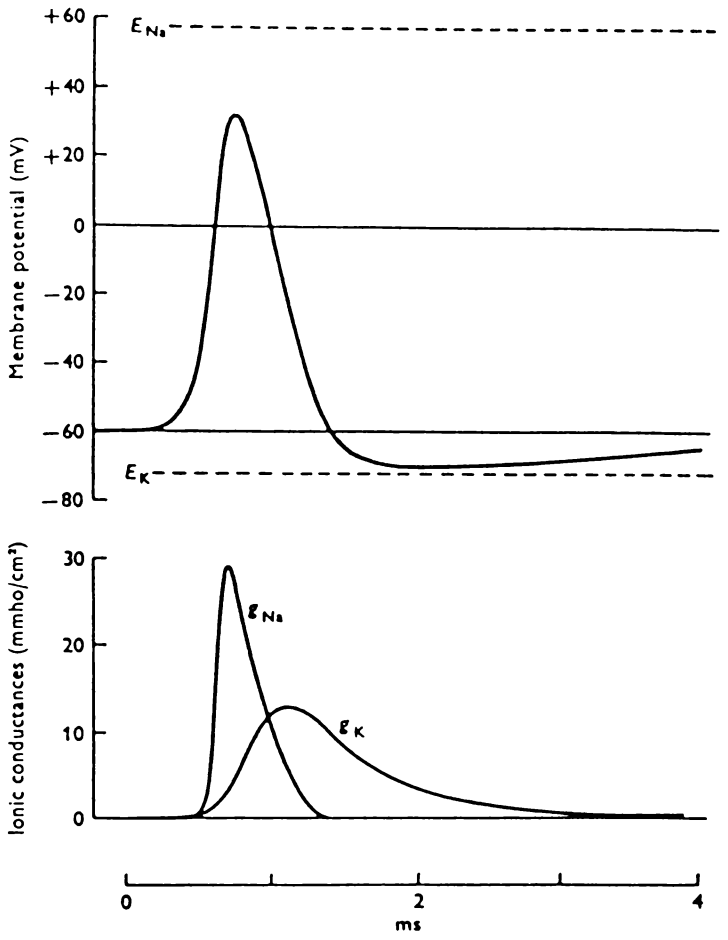

Fig. 2.8 Calculated changes in membrane potential (upper curve) and sodium and potassium conductances (lower curve) during a propagated action potential in a squid giant axon (from Aidley, 1978).

Fig. 2.9 Electrical analog circuit of *Acetabularia* membrane (from Gradmann, 1975).

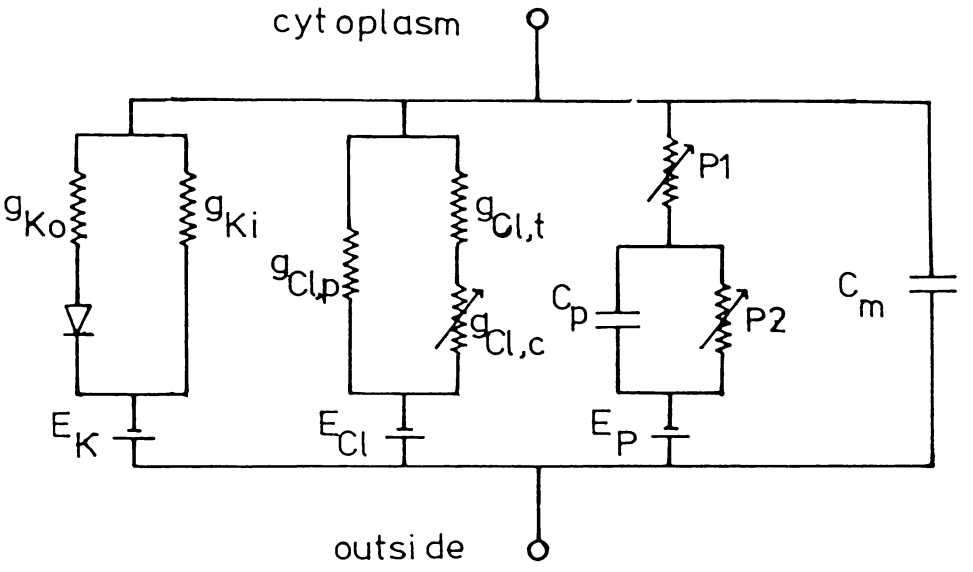

g_{Ki}	=	inward K^+ conductance	15	$\mu mho cm^{-2}$
g_{Ko}	=	outward K^+ conductance	600	$\mu mho cm^{-2}$
$g_{Cl,p}$	=	Cl^- conductance of plasmalemma	12	$\mu mho cm^{-2}$
$g_{Cl,t}$	=	Cl^- conductance of tonoplast	1	$\mu mho cm^{-2}$
$g_{Cl,c}$	=	Cl^- conductance of cytoplasm	500	$\mu mho cm^{-2}$
E_K	=	K^+ equilibrium potential	-90	mV
E_{Cl}	=	Cl^- equilibrium potential	±0	mV
E_p	=	e.m.f. of the active pump	-190	mV
C_m	=	membrane capacitance	5	$\mu F cm^{-2}$
C_p	=	a quasi-capasitor	3000	$\mu F cm^{-2}$

Fig. 2.10 Electrical analog circuit of squid axon membrane (modified from Hodgkin and Huxley, 1952b).

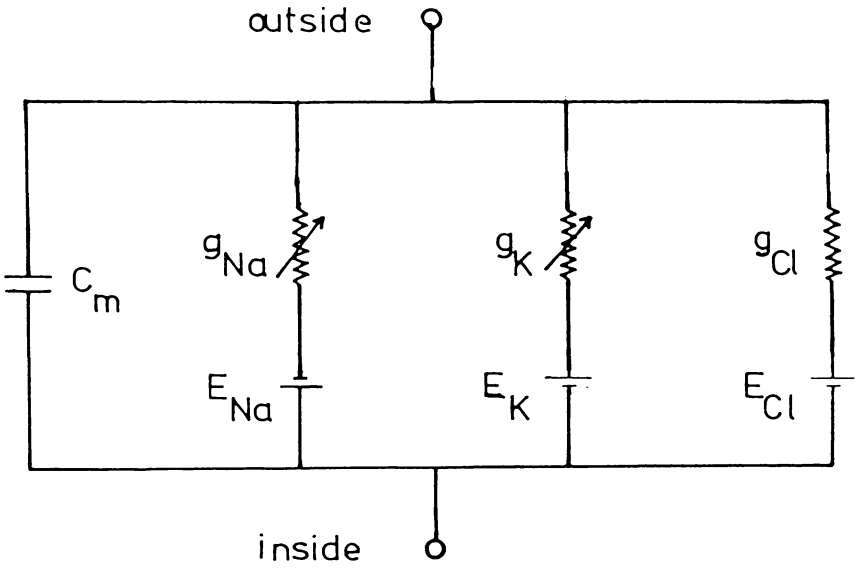

E_{Na} = Na^+ equilibrium potential

E_K = K^+ equilibrium potential

E_{Cl} = Cl^- equilibrium potential

g_{Na} = Na^+ conductance

g_K = K^+ conductance

g_{Cl} = Cl^- conductance

C_m = membrane capacitance

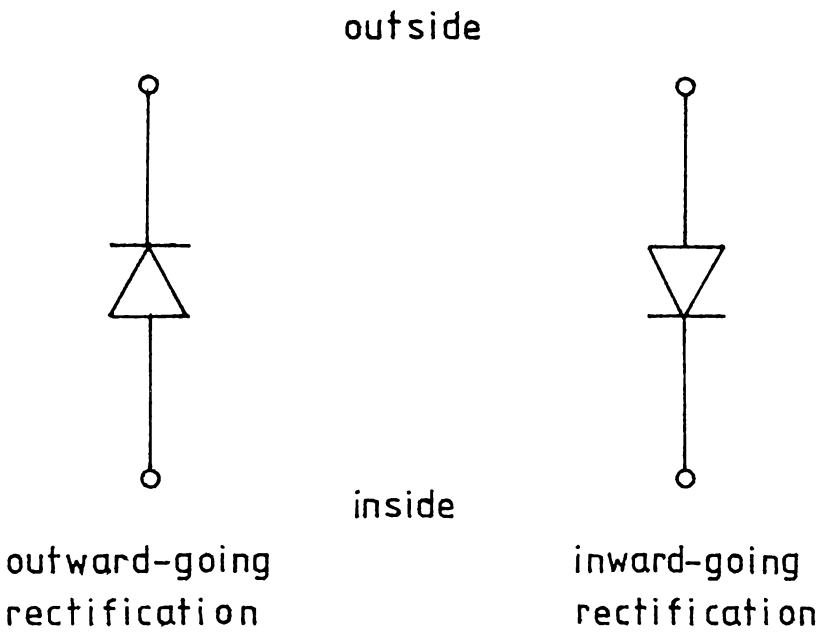

Fig. 2.11 Electrical equivalent circuit symbols for membrane rectifications.

Fig. 2.12 Circuit representing the membrane.

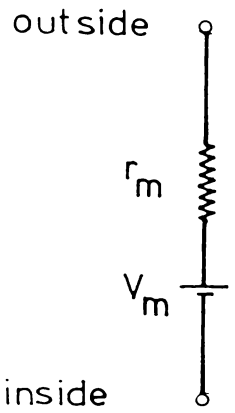

(a) membrane represented by r_m and V_m

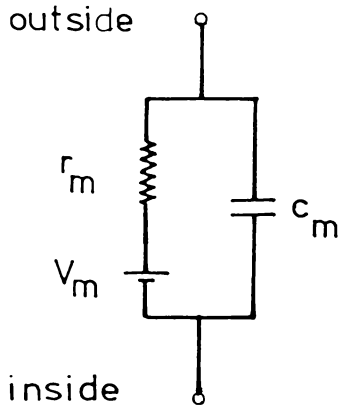

(b) membrane represented by r_m, V_m and C_m

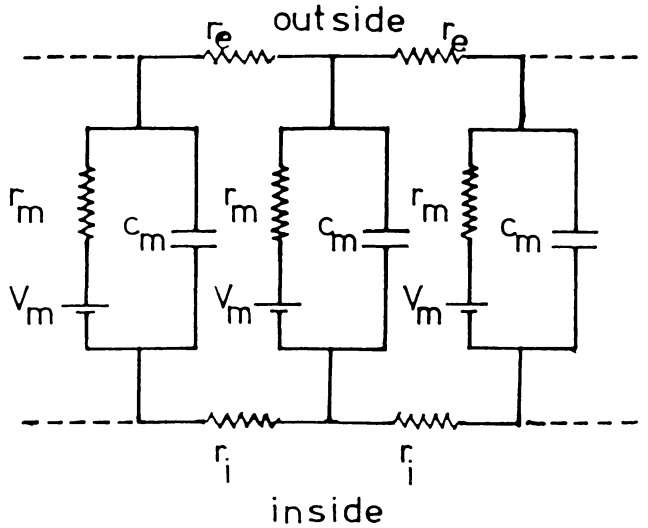

(c) core conductor model

Fig. 2.13 Representation of an extended region of *Acetabularia* membrane (a) by the core conductor model (b).

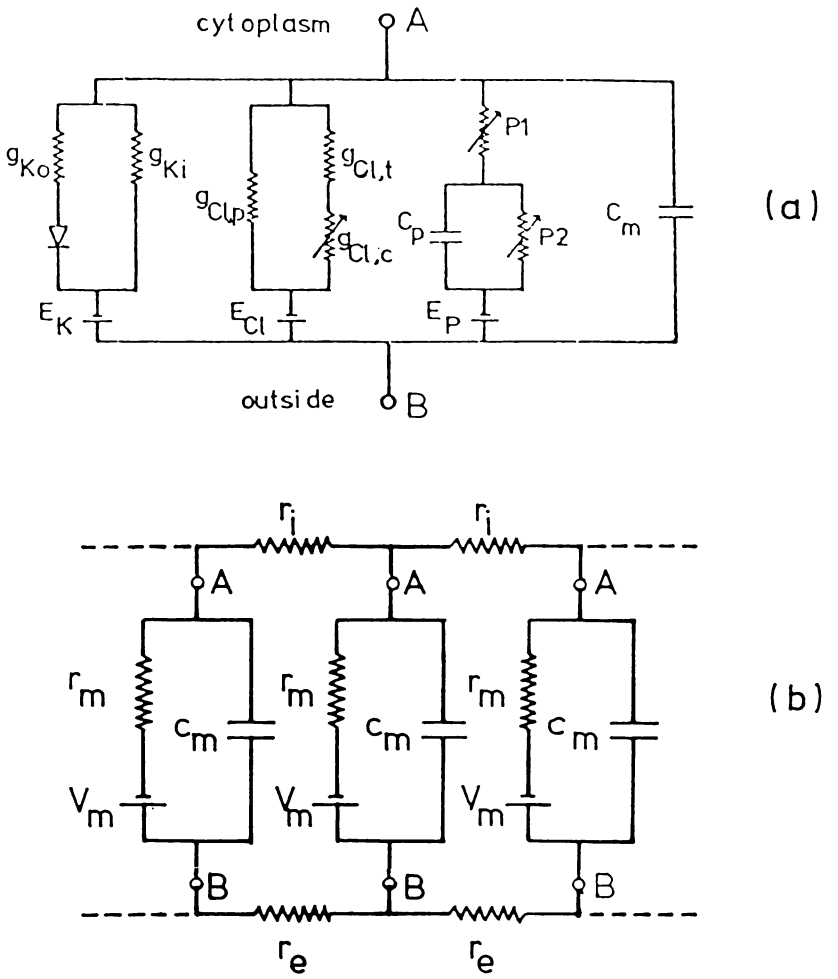

r_e	= external medium resistance per unit length	=	.24 ± .01	$k\Omega cm^{-1}$
r_i	= intracellular fluid " " " "	=	53 ± 12	$k\Omega cm^{-1}$
r_m	= membrane resistance per unit length	=	8.7 ± 2.2	$k\Omega cm$
c_m	= membrane capacitance per unit length	=	330 ± 57	μFcm^{-1}

(modified from Freudling and Gradmann, 1979; Gradmann and Klemke, 1974 ; r_e from experimental measurement in this work).

Fig. 2.14 Diagrams illustrating (a) the local circuit current flow due to a depolarized region and (b) the equivalent core conductor model representation.

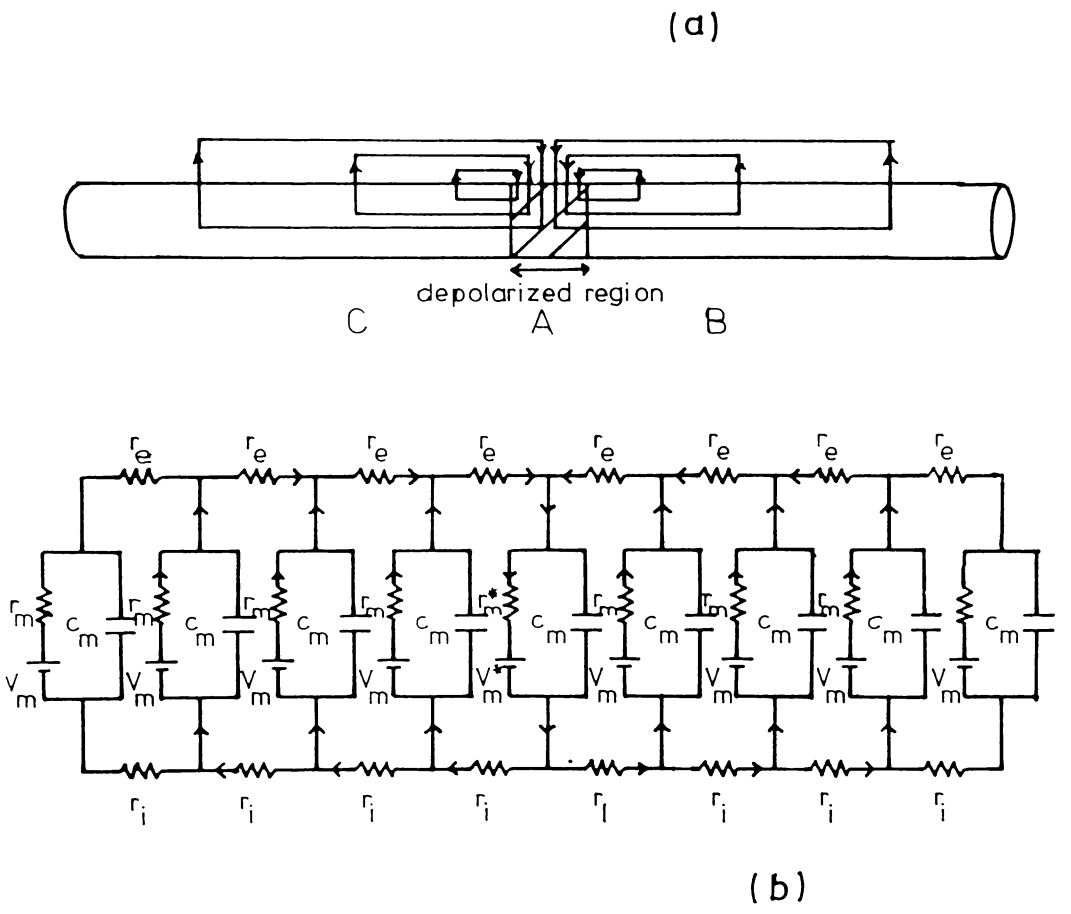

$r_m^* < r_m$ and $| V_m^* | < | V_m |$, the arrows indicate the direction of conventional current flow.

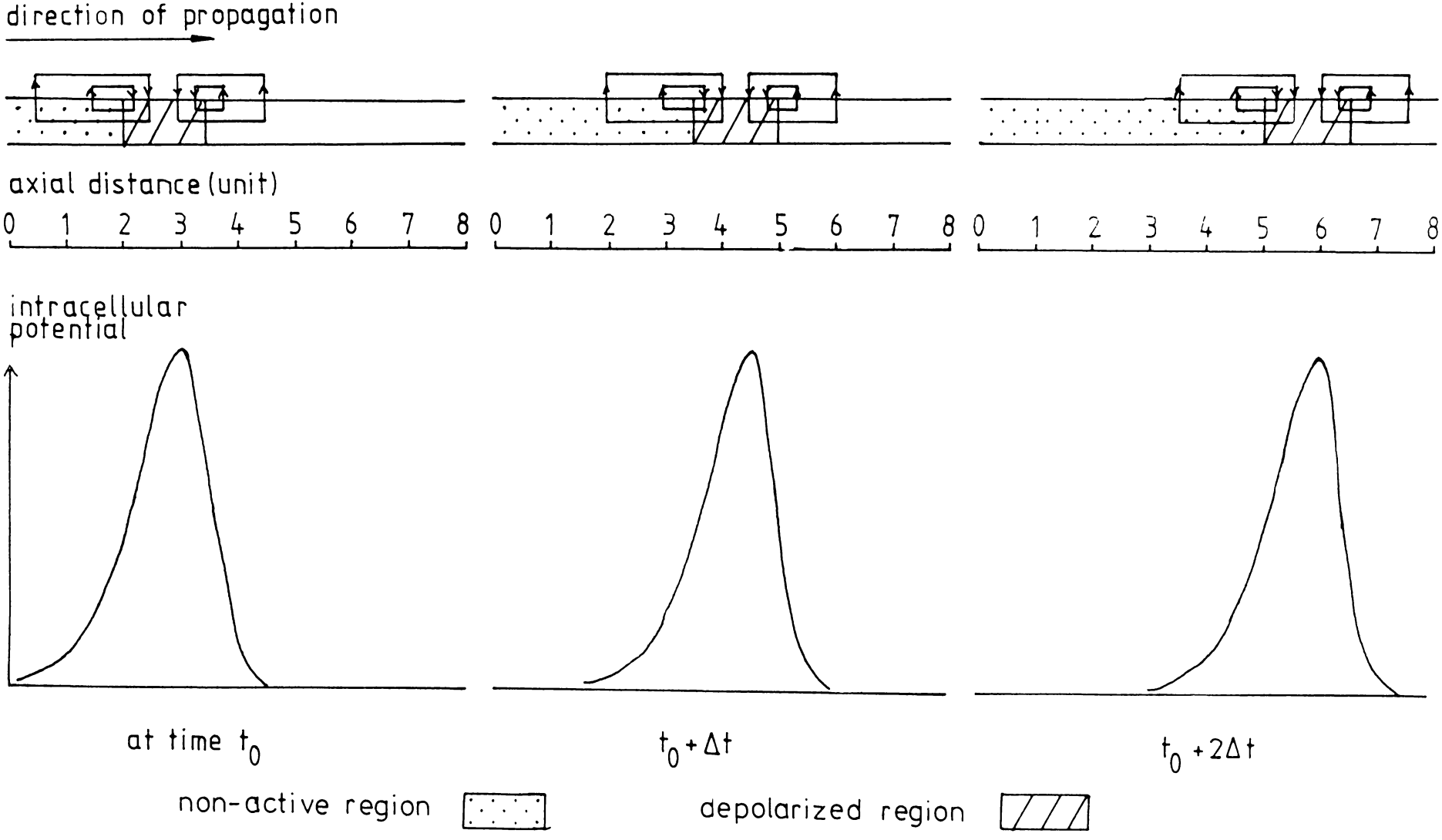

Fig. 2.15 Schematic representation of a propagating action potential.

CHAPTER 3

THE MULTIPLE EXTRACELLULAR RECORDING TECHNIQUE

3.1 Intracellular and Extracellular Recordings

As described in the previous chapter, the membrane potential goes through a transient change during an action potential. This change causes the current to flow inside the cell, in the cytoplasm, and also in the external conducting medium. Thus cell electrical activities can be investigated by recording the potentials inside the cell or in the external medium.

The general form of the potential distribution in a conducting medium outside the region containing sources can be derived as follows. The relationship between the current density and the electric field in a conducting medium is

$$\underline{J} = \sigma \underline{E} \tag{3.1}$$

(see chapter 1, equation (1.1)) where σ is the electrical conductivity. Since there are no other sources, the current density J flows in such a way that

$$\underline{\nabla}\cdot\underline{J} = \sigma \underline{\nabla}\cdot\underline{E} = 0 \tag{3.2}$$

Since $$\underline{E} = -\underline{\nabla}V \tag{3.3}$$

where V is the electrical potential, we have

$$\sigma \underline{\nabla}\cdot\underline{E} = -\sigma \underline{\nabla}\cdot\underline{\nabla} V = 0$$

which is in fact Laplace's equation

$$\nabla^2 V = 0 \qquad (3.4)$$

Thus the potential distribution in the external medium during an action potential for an isolated cylindrical cell (e.g. nerve cell) can be calculated by solving Laplace's equation with appropriate boundary conditions. This problem has been studied by several workers using different approaches. For example, Lorente de Nó (1947) obtained the solution (i.e. the potential distribution in the volume conductor) by considering an electrostatic analogy. That is, the active fibre transmembrane current was represented by a line of point charges and the potential of interest was calculated by summing the potentials at that point due to each charge considered alone. Another approach was used by Clark and Plonsey (1968). Assuming that the transmembrane potential was a propagating action potential with a known waveshape and conduction velocity, the necessary transmembrane potential data were then modified from various existing experimental data. The solutions were then numerically calculated from the equation. More recently Barker *et al.* (1979) introduced another alternative approach using a finite-difference numerical relaxation model. In this case the potential distribution in the conducting medium was calculated from the transmembrane current data using a numerical iterative method (for more detail see section 3.2.2).

In all cases similar features of the potential distribution were obtained. Fig. 3.1a shows the intracellular and the calculated

extracellular potential distributions obtained by Clark and Plonsey (1968). While the intracellular potential is a monophasic waveform the extracellular potential is a triphasic waveform. The external potential field plot is given in Fig. 3.1b and is composed of three distinctive zones that are delineated by two zero isopotential lines.

The choice of extracellular or intracellular recording of the potential depends on the object of the experiments, since each method has its own advantages and disadvantages. For example intracellular recording technique will give much larger potential, but the cell will be perturbed by the insertion of the microelectrode, which may even lead to the death of the cell (Novak and Bentrup, 1972). In general intracellular recording is only suitable for short term experiments.

3.2 Theories of Analysis of Initiation Point

In this section the details of methods of analysis of the initiation point (and subsequent propagation) of the depolarized region from measurements of the external potential distribution are described. This multicellular recording technique (see chapter 4 for practical details) was developed to overcome the limitation of the technique used by Novak and Bentrup (1972) which placed the cell in a highly unnatural environment and gave very limited information (as described in chapter 1). Extracellular electrodes were necessary because regenerating cells need about 30-50 hours before any development can be observed (Lertsithichai, 1980; Novak and Bentrup, 1972) while the cell can only survive for approximately 12 hours after penetration by intracellular electrodes (Novak and Bentrup, 1972). By placing as many extracellular electrodes as possible along

the cell we can sample the external potential at these points simultaneously and hence improve the accuracy of location of the action potential occurrence.

3.2.1 Method to Identify the Depolarized Region Using Differential Voltage

The method described here was first developed (Thavarungkul, 1980) to identify the depolarized regions due to action potentials generated by normal cells and cell fragments of *Acetabularia* (Lertsithichai, 1980). In these experiments eight electrodes (0 to 7) together with a reference electrode (R) were used to record the extracellular potential distribution along the cell as shown in Fig. 3.2a. These electrodes were evenly spaced and placed at approximately the same distance from the cell. From this arrangement we could then calculate the approximate potential distribution generated along the cell by the current-flow in the external surrounding medium using the lumped element equivalent circuit model of Fig. 3.2b. In this circuit R_e represents the resistance of the sheath of external medium between two electrodes, i_0 to i_7 are the transmembrane current-flows in the region between electrode pairs (0,1) to (7,R), and v_0 to v_7 are the potential differences between electrodes 0 to 7 and R respectively.

The voltages v_0 to v_7 can be obtained from the circuit in Fig. 3.2b as a function of the currents and these can be represented in matrix form as

$$\underline{v} = A\,\underline{i} \tag{3.5}$$

where $$A = \frac{R_e}{2}\begin{bmatrix} 1 & 3 & 5 & 7 & 9 & 11 & 13 & 15 \\ 0 & 1 & 3 & 5 & 7 & 9 & 11 & 13 \\ 0 & 0 & 1 & 3 & 5 & 7 & 9 & 11 \\ 0 & 0 & 0 & 1 & 3 & 5 & 7 & 9 \\ 0 & 0 & 0 & 0 & 1 & 3 & 5 & 7 \\ 0 & 0 & 0 & 0 & 0 & 1 & 3 & 5 \\ 0 & 0 & 0 & 0 & 0 & 0 & 1 & 3 \\ 0 & 0 & 0 & 0 & 0 & 0 & 0 & 1 \end{bmatrix}$$

(for derivation see Appendix 1). From this relationship we can in turn find the solution for the currents as a function of voltages. These solutions can be expressed as (see Appendix 1)

$$\underline{i} = A^{-1}\,\underline{v} \tag{3.6}$$

where A^{-1} is the inverse of matrix A i.e.

$$A^{-1} = \frac{2}{R_e}\begin{bmatrix} 1 & -3 & 4 & -4 & 4 & -4 & 4 & -4 \\ 0 & 1 & -3 & 4 & -4 & 4 & -4 & 4 \\ 0 & 0 & 1 & -3 & 4 & -4 & 4 & -4 \\ 0 & 0 & 0 & 1 & -3 & 4 & -4 & 4 \\ 0 & 0 & 0 & 0 & 1 & -3 & 4 & -4 \\ 0 & 0 & 0 & 0 & 0 & 1 & -3 & 4 \\ 0 & 0 & 0 & 0 & 0 & 0 & 1 & -3 \\ 0 & 0 & 0 & 0 & 0 & 0 & 0 & 1 \end{bmatrix}$$

In principle the measurement of a vector $\underline{v} = (v_0, \ldots\ldots, v_7)$ enables $\underline{i} = (i_0, \ldots\ldots, i_7)$ to be calculated from equation (3.6). Knowing the values of current $\underline{i}$ we could then immediately identify

the depolarized region of the cell by using the fact that the current flows from the external medium into the cell at the depolarized region and from the cell into the external medium outside this region. From the experimental measurement of $\underline{v}$ as a function of time we could calculate $\underline{i}$ as a function of time, which would enable us to find out the nature of propagation (if any) of the depolarized region. Unfortunately, severe problems arose when we applied equation (3.6) to experimental data; a small percentage error in $\underline{v}$ (as small as 1%) can cause a large error in $\underline{i}$ due to the large alternating values of the elements in the matrix A^{-1}.

Although calculation of $\underline{i}$ was not possible, we found that the values of differential voltages were quite sufficient to identify the depolarized region. The method depends on the identification of the boundaries between the depolarized and the normal polarized regions during an action potential using the turning point(s) of the differential voltage. The following arguments describe how these boundaries can be identified.

Consider Fig. 3.3a in which a depolarized region is situated between electrode pair (n, n+1). The directions of the current-flow due to the depolarized region are indicated in Fig. 3.3b. If we take inward current as positive transmembrane current, i_n is the only positive current while i_{n-1} and i_{n+1} are maximum negative currents. The differential voltage d_n can be expressed as

$$d_n = v_n - v_{n+1} = (j_n + j_{n+1}) \frac{R_e}{2}$$

or

$$d_n = (j_n - \frac{i_n}{2}) R_e = (j_{n+1} + \frac{i_n}{2}) R_e \qquad (3.7)$$

Therefore in this situation (Fig. 3.3a), since j_{n-1} and j_{n+2} are positive and negative respectively, we have

$$d_{n-1} = (j_{n-1} - \frac{i_{n-1}}{2}) R_e = \text{maximum positive}$$

and $$d_{n+1} = (j_{n+2} + \frac{i_{n+1}}{2}) R_e = \text{maximum negative}$$

Fig. 3.3c indicates the values of d_n's. From Figs. 3.3 a, b and c we see that the left boundary of the depolarized region is at the second electrode of electrode pair (n-1, n) which gives maximum differential voltage d_{n-1} and the right boundary is at the first electrode of the electrode pair (n+1, n+2) which gives minimum (maximum negative) differential voltage d_{n+1}. In a more general description, if the extremum of a particular d_n is positive the depolarized region is approaching it from the right while a negative extremum indicates that the depolarized region is approaching from the left. Examples of some differential voltage distributions (obtained experimentally) and the corresponding depolarized regions are shown in Fig. 3.4.

For a propagating action potential the position of the depolarized region will change as a function of time. Thus the extremum of the differential voltages $\underline{d} = (d_o, \ldots\ldots, d_n)$ will also change with time. Fig. 3.5a shows some typical time dependent differential voltages which have been obtained experimentally. In order to analyse this form of data the time at which the first extremum occurred in each d_n is noted and the boundary of the depolarized region associated with each extemum is analysed using the method described above. These boundaries are then plotted as a function of time as shown in Fig. 3.5b. From this diagram the initiation point of the depolarized region can be found i.e. the

position corresponded to the earliest point in time (the left most point) and is indicated by an arrow in Fig. 3.5b.

This method of analysis was tested experimentally by inserting a micropipette into the cell of *Acetabularia* to cause a slight injury so that depolarizations and action potentials would be induced. The point of initiation of an action potential analysed by the above method always coincided with the point of insertion as shown in Fig. 3.6 (taken from Thavarungkul, 1980).

Although this method of analysis proved to be satisfactory in analysing the initiation point of an action potential, the investigation of the propagation of the depolarized region is a tedious process. That is, for each point in time (or some interval of time) the maximum (positive) and minimum (negative) of the components of $\underline{d}$ have to be found and the depolarized region is then located as described above (for examples see Appendix 2). However, this task would be made much easier if we could find a method in which the current $\underline{i}$ could be obtained from the voltage measurements since positive value of i_n('s) would immediately indicate depolarization in that region. Clearly higher precision measurement of the voltage distribution were needed and more sophisticated analysis methods were pursued.

3.2.2 Successive Over-Relaxation Method

The next attempt to calculate the transmembrane current distribution made use of the model of Barker *et al.* (1979). In this model a numerical iterative technique known as successive over-relaxation (SOR) method was used to solve Laplace's equation and obtain the potential values at various distances from the active

nerve fibre, assuming the surface current distribution was known. It was hoped that perhaps the inverse calculation could also be obtained (i.e. calculated current distribution from a known potential distribution).

Assuming radial symmetry, Laplace's equation in cylindrical co-ordinates becomes

$$\frac{\partial^2 V}{\partial r^2} + \frac{1}{r}\frac{\partial V}{\partial r} + \frac{\partial^2 V}{\partial z^2} = 0 \qquad (3.8)$$

If the interior of the model is divided by a series of mesh lines running parallel to the radial (r) and longitudinal (z) axes as shown in Fig. 3.7, then finite-difference expressions for the partial derivative of the potential V at point (i,j) ($=V_{i,j}$) in terms of the potentials at surrounding points may be derived from Taylor series expansion (see e.g. Burden *et al.* 1978). Neglecting higher order terms we have

$$\frac{\partial^2 V}{\partial r^2} = \frac{V_{i,j+1} - 2V_{j,j} + V_{i,j-1}}{h_1^2}$$

$$\frac{\partial V}{\partial r} = \frac{V_{i,j+1} - V_{i,j-1}}{2h_1}$$

and

$$\frac{\partial^2 V}{\partial z^2} = \frac{V_{i-1,j} - 2V_{i,j} + V_{i+1,i}}{h_2^2}$$

Thus equation (3.8) becomes

$$(V_{i,j+1} + V_{i,j-1})h_2^2 + (V_{i,j+1} - V_{i,j-1})\frac{h_1 h_2^2}{2r_j}$$

$$+ (V_{i-1,j} + V_{i+1,j})h_1^2 - (2h_1^2 + 2h_2^2)V_{i,j} = 0 \qquad (3.9)$$

Equation (3.9) enables $V_{i,j}$ to be calculated from the potentials at adjacent points. This equation is used for all interior points.

At the outer boundary where the conducting medium ends, the current density in the r direction is = 0 i.e.

$$J_r = \sigma E_r = -\sigma \frac{\partial V}{\partial r} = 0$$

This gives

$$\frac{\partial V}{\partial r} = \frac{V_{i,j+1} - V_{i,j-1}}{2h_1} = 0$$

and therefore

$$V_{i,j+1} = V_{i,j-1}$$

and equation (3.9) reduces to

$$2V_{i,j-1}h_2^2 + (V_{i-1,j} + V_{i+1,j})\, h_1^2 - (2h_1^2 + 2h_2^2)V_{i,j} = 0 \qquad (3.10)$$

This equation is therefore used to calculate the potential of points at the conductor-insulator boundary.

A current waveform (Fig. 3.8) modified from Lorente de Nó (1947) by Barker *et al.* (1979) was placed on the r=0 line. Barker *et al.* did not specify how the potential along this line was calculated from the current. In our case we applied the cable equation

$$\frac{\partial^2 V}{\partial z^2} = -\frac{I_m}{\sigma}$$

where I_m is the transmembrane current and σ is the conductivity of the external medium (see e.g. Clark and Plonsey, 1966; Taylor, 1963)

i.e.

$$\sigma(V_{i-1,j} - 2V_{i,j} + V_{i+1,j}) + I_m(i)\, h_2^2 = 0 \qquad (3.11)$$

This equation is used to calculate the potential of points along the r=0 line, where $I_m(i)$ is the value at the (i,0) mesh point of the current shown in Fig. 3.8 (the transmembrane current waveform used in our calculation is in arbitrary unit and thus the calculated surface potential is also in arbitrary unit).

The potential at the mesh points is calculated by using the SOR method

$$V_{i,j}^{(n)} = V_{i,j}^{(n-1)} + \omega\,(V_{i,j(cal)} - V_{i,j}^{(n-1)}) \qquad (3.12)$$

where the top bracket indicates the number of iteration, ω is the over-relaxation constant, and $V_{i,j(cal)}$ is the potential calculated by equation (3.9), (3.10) or (3.11). In the SOR method ω normally lies between 1 and 2 (e.g. Barker *et al.*, 1979; Darby, 1980) which leads to a faster convergence of a system than when $\omega = 1$, which is known as the Gauss-Seidel iterative method. The iterative process is stopped when a chosen accuracy criteria is met (see Barker *et al.*, 1979; Burden *et al.*, 1978; Darby, 1980 for computational detail).

The surface potential (potential at the outer boundary) in our calculation (Fig. 3.8) was similar to that obtained by Barker *et al.*, thus confirming the numerical procedure. From this potential distribution we then tried to obtain the current waveform from the inverse process. However, the attempts were unsuccessful in that the inverse calculations failed to converge to a solution. It was later

found that the failure in obtaining the current distribution was due to the fact that the potential distribution, which was originally obtained in the direct process, contained some errors (e.g. error due to discretisation) which arose during the iterative process. Insufficient information makes it impossible to separate the errors from the values needed to obtain the inverse solution. Also the narrow current waveform (which may be considered as high information content data) could not be easily calculated from the more spread (lower information content data) potential waveform (Dr I.J.D. Craig, private communication). In the following section it will be shown that under certain conditions it is possible for the solution of the current to be obtained.

3.2.3 Method of Regularization

The failure in the attempt to solve the inverse problem using the SOR method led us to reconsider solving the equations (3.5, 3.6). As previously indicated the main problem is the oscillation of the solution due to the large alternative elements in the matrix A^{-1}. Hence, an improvement of the solution should be obtained if we could find an equation in which $\underline{i}$ could be calculated from a matrix containing smaller elements than A^{-1}. This can be achieved by considering the relationship between $\underline{i}$ and $\underline{d}$ as indicated in the equivalent circuit model in Fig. 3.9. The differential voltage $\underline{d}$ is now related to $\underline{i}$ by the equation (for derivation see Appendix 1)

$$\underline{d} = G\,\underline{i} \tag{3.13}$$

where

$$G = \frac{R_e}{2}\begin{bmatrix} 1 & 2 & 2 & 2 & 2 & 2 & 2 & 2 & 2 & 2 & 2 & 2 \\ 0 & 1 & 2 & 2 & 2 & 2 & 2 & 2 & 2 & 2 & 2 & 2 \\ 0 & 0 & 1 & 2 & 2 & 2 & 2 & 2 & 2 & 2 & 2 & 2 \\ 0 & 0 & 0 & 1 & 2 & 2 & 2 & 2 & 2 & 2 & 2 & 2 \\ 0 & 0 & 0 & 0 & 1 & 2 & 2 & 2 & 2 & 2 & 2 & 2 \\ 0 & 0 & 0 & 0 & 0 & 1 & 2 & 2 & 2 & 2 & 2 & 2 \\ 0 & 0 & 0 & 0 & 0 & 0 & 1 & 2 & 2 & 2 & 2 & 2 \\ 0 & 0 & 0 & 0 & 0 & 0 & 0 & 1 & 2 & 2 & 2 & 2 \\ 0 & 0 & 0 & 0 & 0 & 0 & 0 & 0 & 1 & 2 & 2 & 2 \\ 0 & 0 & 0 & 0 & 0 & 0 & 0 & 0 & 0 & 1 & 2 & 2 \\ 0 & 0 & 0 & 0 & 0 & 0 & 0 & 0 & 0 & 0 & 1 & 2 \\ 0 & 0 & 0 & 0 & 0 & 0 & 0 & 0 & 0 & 0 & 0 & 1 \end{bmatrix}$$

and $$\underline{i} = G^{-1}\,\underline{d} \qquad (3.14)$$

where G^{-1} is the inverse of the matrix G i.e.

$$G^{-1} = \frac{2}{R_e}\begin{bmatrix} 1 & -2 & 2 & -2 & 2 & -2 & 2 & -2 & 2 & -2 & 2 & -2 \\ 0 & 1 & -2 & 2 & -2 & 2 & -2 & 2 & -2 & 2 & -2 & 2 \\ 0 & 0 & 1 & -2 & 2 & -2 & 2 & -2 & 2 & -2 & 2 & -2 \\ 0 & 0 & 0 & 1 & -2 & 2 & -2 & 2 & -2 & 2 & -2 & 2 \\ 0 & 0 & 0 & 0 & 1 & -2 & 2 & -2 & 2 & -2 & 2 & -2 \\ 0 & 0 & 0 & 0 & 0 & 1 & -2 & 2 & -2 & 2 & -2 & 2 \\ 0 & 0 & 0 & 0 & 0 & 0 & 1 & -2 & 2 & -2 & 2 & -2 \\ 0 & 0 & 0 & 0 & 0 & 0 & 0 & 1 & -2 & 2 & -2 & 2 \\ 0 & 0 & 0 & 0 & 0 & 0 & 0 & 0 & 1 & -2 & 2 & -2 \\ 0 & 0 & 0 & 0 & 0 & 0 & 0 & 0 & 0 & 1 & -2 & 2 \\ 0 & 0 & 0 & 0 & 0 & 0 & 0 & 0 & 0 & 0 & 1 & -2 \\ 0 & 0 & 0 & 0 & 0 & 0 & 0 & 0 & 0 & 0 & 0 & 1 \end{bmatrix}$$

The elements of matrix G^{-1} are smaller than the elements of the matrix A^{-1} (equation (3.6)) and therefore may allow $\underline{i}$ to be calculated using equation (3.14).

This potential improvement is of course only achieved if the differential voltage $\underline{d}$ is measured directly with at least the same accuracy as the voltage $\underline{v}$, obtained in the previous experiments (see section 3.2.1). In fact the measurements were made with improved accuracy and stability (see chapter 4) when the need for this was recognised.

Despite the above improvements the solution obtained from equation (3.14) is almost always poor in the sense that the solution is still oscillatory or displays some other feature which conflicts with our knowledge of its essential form. An example is given in Fig. 3.10 where the values of the current $\underline{i}_{I/P}$ (I/P = input) were known while the differential voltage $\underline{d}$ was measured experimentally (for more detail see section 3.3). Equation (3.14) was used to obtain $\underline{i}_{CAL}$ (calculated) which clearly indicates the oscillatory feature.

The basic difficulty in solving equation (3.13) arises from the fact that the matrix G is *ill-conditioned* owing to the near linear dependence of its adjacent rows (Dr I.J.D. Craig, private communication). This causes an instability on inversion (i.e. a small error could give a large oscillation) and hence direct inversion (equation (3.14)) is not practical with noisy experimental data. This situation arises in other areas of experimental science and has been considered in detail by a number of authors (e.g. see Twomey, 1977).

(a) Theoretical Consideration

One method to attack such a problem is the *method of regularization* or *constrained linear inversion.* It was proposed independently by Phillips (1962) and Tihonov (1963, 1964), and has been subsequently developed and extended by Twomey (1963, 1965), Ribiere (1967) and many others (for review see e.g. Baker, 1977; Miller, 1974).

The method is to replace the ill-conditioned problem, in our case $G\underline{i} = \underline{d}$, by a stable minimization problem involving a small positive parameter γ i.e. instead of solving equation (3.13) directly we sought to obtain the solution which minimizes the quantity

$$\|G\underline{i} - \underline{\tilde{d}}\|^2 + \gamma \|L\underline{i}\|^2 \tag{3.15}$$

where L is some linear operator, $\underline{\tilde{d}} = \underline{d} + \underline{\text{error}}$ (in our case from experimental measurements), and $\|\cdot\|$ represent the Euclidean or square norm ($\| \underline{x} \| = (\underline{x}\cdot\underline{x})^{1/2}$). If L is suitably chosen, the second term has a *smoothing* or *stabilizing* effect on the solution (see e.g. Twomey 1963, 1965, 1977).

The quantity $\|L\underline{i}\|^2$ is referred to by Twomey (1965, 1977) as the measure of deviations from smoothness in the solution $\underline{i}$. The measure of non-smoothness, $\|L\underline{i}\|^2 = \underline{i}^T L^T L \underline{i} = \underline{i}^T H \underline{i}$, can have many forms. For example if $L\underline{i}$ is the second derivative of $\underline{i}$, then the process is termed second order regularization (i.e. if the k'th derivative is selected the process is termed k'th order regularization - see Twomey, 1963, 1965, 1977 for other measures of non-smoothness). Thus

$$\|L\underline{i}\|^2 = \sum_{j=0}^{n} \left[i_{j-1} - 2i_j + i_{j+1} \right]^2$$

$$= \underline{i}^T H \underline{i}$$

If the boundary conditions are such that i_{-1} and $i_{n+1} = 0$ we then have

$$H = L^T L = \begin{bmatrix} 5 & -4 & 1 & 0 & 0 & 0 & 0 & 0 & 0 & 0 & 0 & 0 \\ -4 & 6 & -4 & 1 & 0 & 0 & 0 & 0 & 0 & 0 & 0 & 0 \\ 1 & -4 & 6 & -4 & 1 & 0 & 0 & 0 & 0 & 0 & 0 & 0 \\ 0 & 1 & -4 & 6 & -4 & 1 & 0 & 0 & 0 & 0 & 0 & 0 \\ 0 & 0 & 1 & -4 & 6 & -4 & 1 & 0 & 0 & 0 & 0 & 0 \\ 0 & 0 & 0 & 1 & -4 & 6 & -4 & 1 & 0 & 0 & 0 & 0 \\ 0 & 0 & 0 & 0 & 1 & -4 & 6 & -4 & 1 & 0 & 0 & 0 \\ 0 & 0 & 0 & 0 & 0 & 1 & -4 & 6 & -4 & 1 & 0 & 0 \\ 0 & 0 & 0 & 0 & 0 & 0 & 1 & -4 & 6 & -4 & 1 & 0 \\ 0 & 0 & 0 & 0 & 0 & 0 & 0 & 1 & -4 & 6 & -4 & 1 \\ 0 & 0 & 0 & 0 & 0 & 0 & 0 & 0 & 1 & -4 & 6 & -4 \\ 0 & 0 & 0 & 0 & 0 & 0 & 0 & 0 & 0 & 1 & -4 & 5 \end{bmatrix}$$

where $L =$

$$\begin{bmatrix} -2 & 1 & 0 & 0 & 0 & 0 & 0 & 0 & 0 & 0 & 0 & 0 \\ 1 & -2 & 1 & 0 & 0 & 0 & 0 & 0 & 0 & 0 & 0 & 0 \\ 0 & 1 & -2 & 1 & 0 & 0 & 0 & 0 & 0 & 0 & 0 & 0 \\ 0 & 0 & 1 & -2 & 1 & 1 & 0 & 0 & 0 & 0 & 0 & 0 \\ 0 & 0 & 0 & 1 & -2 & 1 & 0 & 0 & 0 & 0 & 0 & 0 \\ 0 & 0 & 0 & 0 & 1 & -2 & 1 & 0 & 0 & 0 & 0 & 0 \\ 0 & 0 & 0 & 0 & 0 & 1 & -2 & 1 & 0 & 0 & 0 & 0 \\ 0 & 0 & 0 & 0 & 0 & 0 & 1 & -2 & 1 & 0 & 0 & 0 \\ 0 & 0 & 0 & 0 & 0 & 0 & 0 & 1 & -2 & 1 & 0 & 0 \\ 0 & 0 & 0 & 0 & 0 & 0 & 0 & 0 & 1 & -2 & 1 & 0 \\ 0 & 0 & 0 & 0 & 0 & 0 & 0 & 0 & 0 & 1 & -2 & 1 \\ 0 & 0 & 0 & 0 & 0 & 0 & 0 & 0 & 0 & 0 & 1 & -2 \end{bmatrix}$$

(Baker, 1977).

It is interesting to note here that there are two distinct ways in which we can arrive at the above formulation (3.15):

(i) it is practical to write equation (3.13) as $G\underline{i} = \underline{\tilde{d}} = \underline{d} + \underline{\epsilon}$ where $\underline{\epsilon}$ is chosen to correspond to the error in $\underline{d}$. Since $\underline{d}$ is subjected to error some criteria must be invoked to select a stable unique solution from the set of all solutions $\underline{i}$'s which are associated with $\underline{d}$'s (through equation (3.13)) lying within the prescribed error $\underline{\epsilon}$. This is equivalent to the application of one or more constraints to the solution $\underline{i}$. Therefore, let us consider the case where $\|G\underline{i} - \underline{\tilde{d}}\|^2 = \|\underline{\epsilon}\|^2$ = constant and let us minimize the deviation from smoothness of the solution $\underline{i}$ which is represented by $\|L\underline{i}\|^2$. We now have a problem of conditional extremum, which can be solved by the method of Lagrangian multipliers. The solution is obtained by minimizing

$$\|L\underline{i}\|^2 + \gamma^{-1}\|G\underline{i} - \underline{\tilde{d}}\|^2$$

where γ^{-1} is the Lagrangian multiplier. This is equivalent to minimizing

$$\|G\underline{i} - \underline{\tilde{d}}\|^2 + \gamma\|L\underline{i}\|^2$$

which is the formula in (3.15)

alternatively

(ii) we would like our solution to have the property $\|L\underline{i}\|^2$ = constant and the quantity to be minimized is $\|G\underline{i} - \underline{\tilde{d}}\|^2$. In this case we minimize (3.15) where γ is the Lagrangian multiplier.

The only difference in these two cases is that γ must be determined to correspond with the assigned constant associated with each case. Following Twomey (1963) in which (i) was considered, the solution $\underline{i}$ is obtained by solving for the extremum of equation (3.15) i.e. for all n

$$\frac{\partial}{\partial i_n}\left[(G\underline{i} - \underline{d})^T (G\underline{i} - \underline{d}) + \gamma\, \underline{i}^T H\, \underline{i}\right] = 0 \quad (H=L^TL)$$

$$\frac{\partial}{\partial i_n}\left[\underline{i}^T G^T G\underline{i} - \underline{d}^T G\underline{i} - \underline{i}^T G^T \underline{d} + \gamma\, \underline{i}^T H\, \underline{i}\right] = 0$$

The differentiation of $\underline{i}$ w.r.t. i_n gives a vector with zeros in all but the n^{th} element, denoted by $\underline{e}_n$, so we obtain

$$\underline{e}^T_n(G^TG\underline{i} - G^T\underline{d} + \gamma\, H\underline{i}) + (\underline{i}^TG^TG - \underline{d}^TG + \gamma\, \underline{i}^TH)\underline{e}_n = 0$$

The second term is the transpose of the first so if the sum vanishes the terms must vanish separately and hence

$$G^TG\underline{i} - G^T\underline{d} + \gamma H\underline{i} = 0$$

or $$(G^TG + \gamma H)\underline{i} = G^T\underline{d}$$

and $\underline{i}$ is given by

$$\underline{i} = (G^TG + \gamma H)^{-1}G^T\, \underline{d} \qquad (3.16)$$

This is the equation for the constrained linear inversion (the name used by Twomey, 1977) or the method of regularization (the term used by Miller, 1974; Ribiere, 1967). We can see that if $\gamma = 0$ equation (3.16) reduces to obtaining $\underline{i}$ by direct inversion (equation (3.14)).

In practice the exact value of the constant ($=\|G\underline{i} - \underline{\bar{d}}\|^2 = \|\underline{\epsilon}\|^2$) is not known and the general procedure for applying this equation (3.16) is to choose several values of γ and obtain the residual $\underline{r} = G\underline{i} - \underline{\bar{d}}$. An increase in γ produces an increase in the quantity $\|\underline{r}\| = \|G\underline{i} - \underline{\bar{d}}\|$ and a decrease in $\|L\underline{i}\|$ (i.e. the solution becomes less oscillatory), and conversely. It is a question of balancing the magnitude of the residual $\|\underline{r}\|$ against the smoothness of the solution as measured by $\|L\underline{i}\|$. Generally γ is chosen to give the smoothest solution $\underline{i}$ in which the value $\|\underline{r}\| = \|G\underline{i} - \underline{\bar{d}}\|$ is less than some estimated value $\|\underline{\epsilon}\|$ i.e. the magnitude of the residual which arises from the smoothing of the solution is less than (or equal to) the estimated error in $\underline{\bar{d}}$ (Phillips, 1962; Twomey, 1963, 1965). This method has been demonstrated by Phillips (1962, who used second order regularization), Twomey (1965, 1977) and several others (e.g. Ribiere, 1967) to be a very useful tool in solving ill-conditioned problems.

(b) Application

In the demonstrations of the usefulness of this method Phillips (1962) and Twomey (1963, 1977) considered cases where the solutions of the problems were known. The solutions obtained by equation (3.16) using various γ were then compared to the known solutions. However, in a more general situation the solution to an equation is not normally known. Therefore it was necessary to test whether this method could be applied to a problem like ours by assuming a known solution and we proceeded as follows:

(i) assumed values of current $\underline{i} = (i_0, \ldots\ldots, i_B) = \underline{i}_{I/P}$ (I/P = input)

(ii) calculated the differential voltage $\underline{d} = (d_0, \ldots\ldots, d_B)$ using equation (3.13)

(iii) generated random number $\underline{y}$ from a uniform distribution [0,1] in which the noise $\underline{x}$ was calculated i.e. $x_n = (0.5 - y_n)\times 2$

(iv) added error on to $\underline{d}$ and we have $\tilde{\underline{d}}$ where

$$\tilde{d}_n = d_n + \left[x_n + \frac{\text{percentage error} \times d_n}{100}\right]$$

(v) calculated the solution

$$\underline{i}_{cal} = \underline{i} = (G^T G + \gamma H)^{-1} G^T \tilde{\underline{d}}$$

(vi) repeated (i) to (v) for other $\underline{i}$'s.

Figs. 3.11 to 3.13 show the results of the above process for a second order regularization with 5% error (in step (iv)). Although $\tilde{\underline{d}}$'s do not differ from $\underline{d}$'s by much (Figs. 3.11a-3.13a) large oscillations still exist in the direct inversion solutions (Fig. 3.11b-3.13b). The oscillations, however, decrease when regularizations are applied (Figs. 3.11c-3.13c). Generally $\underline{i}$'s were chosen at the value of γ which gave

$$\|\underline{r}\| = \|G\underline{i} - \tilde{\underline{d}}\| < \|\tilde{\underline{d}} - \underline{d}\| = \|\underline{\epsilon}\|$$

Figs. 3.11d-3.13d show the differential voltage calculated from $G\underline{i}$'s (equation (3.13)). They do not show any great deviation from $\tilde{\underline{d}}$'s which give the oscillatory solutions, which is as expected because due to ill-conditioned matrix G the oscillations in the direct inversion are caused by only small errors.

Figs. 3.14 a and b show the results when γ is too small and too large respectively. When γ is too small the oscillation still exists (although it has been reduced), while the solution tends to have the *round off* effect around the peaks when γ is too large.

Figs. 3.15-3.17 show the results of the above process where 20 sets of error have been generated for each waveform. In (a) the solutions $\underline{i}$'s were obtained from equation (3.14) and in (b) $\underline{i}$'s were obtained from equation (3.16). The vertical bars indicate the standard deviations of the solutions at those points. These bars are large in (a) and reduce dramatically in (b) (where $\gamma = 1 \times 10^{-5}$). These results seem to indicate that the second order regularization can be used to solve our ill-conditioned problem.

3.2.4 Simplified Equation

As demonstrated in the previous section, the method of regularization was applied successfully to our ill-conditioned problem. However, the solution required several steps of calculation which were not possible to implement on the computer used in monitoring the experiments. Therefore, solutions of the current cannot be obtained from the measured action potentials generated by the anucleate isolated stalk segments (ISS's) of *Acetabularia* while the experiments are in progress. A method with a small amount of calculation is needed to give us an approximate indication of the current waveform associated with each action potential during the experiment.

We can get a better conditioned matrix by considering a different approximation model as shown in Fig. 3.18. Instead of assuming the current-flows enter the cell between the electrodes we now assume that they enter the cell at the position of each electrode. The voltage-current relationship becomes (see Appendix 1 for deviation)

$$\underline{d} = G' \underline{i}' \tag{3.17}$$

where $\underline{d} = (d_0, d_1, \ldots\ldots, d_9, d_A, d_B)$

$\underline{i}' = (i_0', i_1', \ldots\ldots, i_9', i_A', i_B')$

(note: i_c' is not included in the vector $\underline{i}'$, see Appendix 1).

where $G' = R_e$

$$\begin{bmatrix}
-1 & 0 & 0 & 0 & 0 & 0 & 0 & 0 & 0 & 0 & 0 & 0 \\
-1 & -1 & 0 & 0 & 0 & 0 & 0 & 0 & 0 & 0 & 0 & 0 \\
-1 & -1 & -1 & 0 & 0 & 0 & 0 & 0 & 0 & 0 & 0 & 0 \\
-1 & -1 & -1 & -1 & 0 & 0 & 0 & 0 & 0 & 0 & 0 & 0 \\
-1 & -1 & -1 & -1 & -1 & 0 & 0 & 0 & 0 & 0 & 0 & 0 \\
-1 & -1 & -1 & -1 & -1 & -1 & 0 & 0 & 0 & 0 & 0 & 0 \\
-1 & -1 & -1 & -1 & -1 & -1 & -1 & 0 & 0 & 0 & 0 & 0 \\
-1 & -1 & -1 & -1 & -1 & -1 & -1 & -1 & 0 & 0 & 0 & 0 \\
-1 & -1 & -1 & -1 & -1 & -1 & -1 & -1 & -1 & 0 & 0 & 0 \\
-1 & -1 & -1 & -1 & -1 & -1 & -1 & -1 & -1 & -1 & 0 & 0 \\
-1 & -1 & -1 & -1 & -1 & -1 & -1 & -1 & -1 & -1 & -1 & 0 \\
-1 & -1 & -1 & -1 & -1 & -1 & -1 & -1 & -1 & -1 & -1 & -1
\end{bmatrix}$$

From Appendix 1 we have

$$\underline{i}' = (G')^{-1} \underline{d} \quad \text{and} \quad i_c' = \frac{d_B}{R_e} \tag{3.18}$$

where $(G')^{-1} = \frac{1}{R_e}$

$$\begin{bmatrix} -1 & 0 & 0 & 0 & 0 & 0 & 0 & 0 & 0 & 0 & 0 & 0 \\ 1 & -1 & 0 & 0 & 0 & 0 & 0 & 0 & 0 & 0 & 0 & 0 \\ 0 & 1 & -1 & 0 & 0 & 0 & 0 & 0 & 0 & 0 & 0 & 0 \\ 0 & 0 & 1 & -1 & 0 & 0 & 0 & 0 & 0 & 0 & 0 & 0 \\ 0 & 0 & 0 & 1 & -1 & 0 & 0 & 0 & 0 & 0 & 0 & 0 \\ 0 & 0 & 0 & 0 & 1 & -1 & 0 & 0 & 0 & 0 & 0 & 0 \\ 0 & 0 & 0 & 0 & 0 & 1 & -1 & 0 & 0 & 0 & 0 & 0 \\ 0 & 0 & 0 & 0 & 0 & 0 & 1 & -1 & 0 & 0 & 0 & 0 \\ 0 & 0 & 0 & 0 & 0 & 0 & 0 & 1 & -1 & 0 & 0 & 0 \\ 0 & 0 & 0 & 0 & 0 & 0 & 0 & 0 & 1 & -1 & 0 & 0 \\ 0 & 0 & 0 & 0 & 0 & 0 & 0 & 0 & 0 & 1 & -1 & 0 \\ 0 & 0 & 0 & 0 & 0 & 0 & 0 & 0 & 0 & 0 & 1 & -1 \end{bmatrix}$$

Hence, $\underline{i}'$ and i_c' can easily be obtained by using equation (3.18) (although $\underline{i}'$ is easier to obtain than $\underline{i}$ (equation (3.16)), it will be shown in section 3.3 that $\underline{i}$ in fact gives a more accurate solution).

3.3 Experimental Verification of Methods of Analysis

The method of regularization has convincingly demonstrated its usefulness when applied to the simulated data as shown in section 3.2.3. Although the method seems to produce the correct solutions under this circumstance, one might ask whether it would behave the same way under experimental conditions. In other words, is the solution for the current $\underline{i}$ obtained in this way (using the method of regularization) from the experimental measurements of $\underline{\tilde{d}}$ the same as the current distribution in the conducting medium generated by the cell? To answer this question we have designed an experiment in which the voltage distribution in the conducting medium due to an

artificial cell giving a known current distribution was measured. These voltage values ($\underline{d}$) were then used to obtain the solution $\underline{i}$ (using equation (3.16)) which could be compared to the known input current distribution. This section describes the procedures and displays some of the results.

3.3.1 Materials and Methods

An *artificial cell system* was made which had some similarities to the experimental set up used with cell segments of *Acetabularia* (Fig. 3.19). This consisted of a perspex tube with ~11 mm inner diameter and ~250 mm in length with both ends sealed. Along the length of the tube a slot of ~3 mm wide was made for the electrodes to enter. On the opposite side a thin slit was made also along the length of the tube for the connections between the artificial cell and the current sources.

The artificial cell consisted of 25 *current element* units each of which was a brass cylinder (diameter = 3.0 ± 0.1 mm, length = 7.0 ± 0.3 mm - Fig. 3.19) with an electrical connection attached to one side. The cylinders were gold plated to minimize surface contamination. The two circular end surfaces and the side connection were painted to provide electrical insulation between current elements. After the paint was dried the current elements were arranged in the perspex tube with the side connections emerging through the slit as shown in Fig. 3.19. Epoxy resin was then applied on the outer surface of the tube along the slit to prevent any leakage of the conducting solution which filled the perspex tube during an experiment as well as to keep the current elements fixed in their places.

Each current element was connected to a corresponding current source (Fig. 3.20) except the last element on the right hand side which acted as a common unit (i.e. 24 current element units were connected to 24 current sources). The circuit diagram of the current sources is shown in Fig. 3.20. The variable resistance for each current was adjusted to give the assigned value which was monitored by the 1K resistor; 1 mV across this resistor corresponded to 1 μA generated by the source. These current sources were divided into three equal sections. The middle section was designed so that the current would leave the current elements and enter the common unit, and conversely for the two adjacent sections (Fig. 3.21). The current value assigned to each element is indicated in Fig. 3.21. The algebraic sum of all the current sources is zero so no current flows through the reference element (common unit). This was checked by the ammeter (A) (Figs. 3.20, 3.21). Usually each current source was adjusted to approximately 1-2% of the assigned value which would give a reading of $\simeq$0 μA at (A). A common switch was implemented to turn all the current sources on or off at the same time.

During the experiment the artificial cell was surrounded by AE50 solution, the solution used in the main experiments as growth medium for *Acetabularia* as well as the conducting medium for voltage measurements. The voltage distribution in the solution was measured by a set of 13 evenly spaced Ag-AgCl electrodes, (each space covered two current elements, ~14 mm). The measured differential voltage waveforms were displayed on a CRT and stored on floppy disc for further analysis (details of the electrodes, data processing electronics, and the computer program will be described in chapter 4). An example of the differential voltage waveforms measured during the experiment is shown in Fig. 3.22a.

The value of current in each current element was fixed throughout the experiment (except on a few occasions where a few values were changed, see later). However, the set of electrodes could be moved slightly towards the left or the right along the length of the artificial cell which enabled the values of current between electrode pairs to be changed. Hence, we were able to acquire a limited number of different voltage distributions. Some of these positions are shown in Figs. 3.21 as positions A, B1, and C (results are shown in Figs. 3.23-3.25 respectively). Positions A and C are identical, the difference being the values of current assigned to the current elements. The values for position C which differ from position A are shown in the brackets in Fig. 3.21 (i.e. A is the setting for the model used for simplified equation Fig. 3.18, and C is the setting for the original model Fig. 3.9). Two experiments were performed: one with the artificial cell lying at the bottom of the tube as shown in Fig. 3.19 and the other with the cell placed in the middle of the tube.

In order to calculate the current from the voltage we needed to know the resistances, R_e's, of the external medium between pairs of electrodes. Thus, after each experiment all the current sources were disconnected from the current elements and a 10 μA current source was connected to the first and last current elements. The voltage drops between different electrode pairs caused by the current-flows in the conducting medium were measured and R_e's were calculated i.e.

R_e = resistance of the sheath of conducting medium between 2 electrodes

$$= \frac{\text{differential voltage}}{10\ \mu A}$$

Since the electrodes were evenly spaced R_e's between all pairs of electrodes were approximately equal. The value of R_e in these experiments was found to be 14 ± 1 ohm. (Note: in the normal AE50 solution, due to the high values of current, the maximum voltage was > 2 mV which is the saturation level of the amplifier system, hence for these experiments extra NaCl was added to the AE50 solution to reduce the resistivity of the conducting medium).

3.3.2 Results

Fig. 3.22a shows an example of the differential voltage $\underline{\tilde{d}}$ along the cell ($\underline{\tilde{d}} = (\tilde{d}_0, \tilde{d}_1, \ldots\ldots, \tilde{d}_9, \tilde{d}_A, \tilde{d}_B)$ is a vector with 12 components) as a function of time when the sources are switched on for ~25 seconds. To avoid confusion, let us define $\tilde{\tilde{D}}$ as a (12 x k) matrix containing vectors $\underline{\tilde{d}}(t)$ at k points in time i.e.

$$\tilde{\tilde{D}} = \begin{bmatrix} \tilde{d}_0(t_1) & . & . & . & . & \tilde{d}_0(t_k) \\ \tilde{d}_1(t_1) & . & . & . & . & \tilde{d}_1(t_k) \\ . & . & . & . & . & . \\ . & . & . & . & . & . \\ \tilde{d}_9(t_1) & . & . & . & . & . \\ \tilde{d}_A(t_1) & . & . & . & . & . \\ \tilde{d}_B(t_1) & . & . & . & . & \tilde{d}_B(t_k) \end{bmatrix} \quad (= \underline{\tilde{d}}\,(t)) \qquad (3.19)$$

and similarly

$$I = \begin{bmatrix} i_0(t_1) & . & . & . & . & i_0(t_k) \\ i_1(t_1) & . & . & . & . & i_1(t_k) \\ . & . & . & . & . & . \\ . & . & . & . & . & . \\ i_9(t_1) & . & . & . & . & . \\ i_A(t_1) & . & . & . & . & . \\ i_B(t_1) & . & . & . & . & i_B(t_k) \end{bmatrix} \quad (= i\ (t)) \qquad (3.20)$$

According to the new definition Fig. 3.22a shows an example of $\tilde{D}$ (the ~ notation indicates that it contains some errors). Originally all the current sources were off, but they were turned on during the period between the 12th and the 37th seconds. Solutions for the current using direct inversion (equation (3.14)) and second order regularization (equation (3.16)) were shown in Figs. 3.22b and 3.22c respectively. Although Fig. 3.22b does not clearly show the oscillatory behaviour, Fig. 3.22c is definitely a better solution (i.e. more smooth).

This method of displaying the results cannot demonstrate clearly the difference in the solution by direct inversion and that by using the method of regularization. Hence, we chose to display the result at only one point in time during the period in which the current sources were operating i.e. $\underline{d}(t_j)$ and $\underline{i}(t_j)$ where j is any point between the 12th and the 37th seconds (normally it is the mid point that we have chosen).

Examples of the solutions obtained from the experimental measurements of $\underline{d}$'s when the cell was in the centre of the tube as compared to the input current data are shown in Figs. 3.23-3.25 (note: Figs. 3.23-3.25 corresponded to the electrode positions A, B1

and C in Fig. 3.21 respectively). In the diagrams positive current value indicates current flows into the cell and negative value indicates current flows out of the cell. The error in the measurement was estimated to be approximately 3% (except Fig. 3.25 which will be discussed later). Even at this low percentage, direct inversion solutions (equation (3.14)) still show oscillatory behaviours (Fig. 3.23b-3.25b show the values of $\Delta i_n = i_n(\text{calculated}) - i_n(\text{input})$). The solutions, however, improved when second order regularization was applied (equation (3.16)) (Fig. 3.23a,b-3.25a,b). In applying this method to $\tilde{D}$ (as in Fig. 3.22) a slightly different criterion (from that in section 3.2.3) of choosing γ was adopted. The reason for this is that in section 3.2.3 the differential voltage (and hence current) was just a vector $\underline{d}$ (and $\underline{i}$) while in this case we have a matrix $\tilde{D}$ (and I as defined by equations (3.19) and (3.20)). Here γ was chosen so that the average of the magnitude of the residual R (= $\underline{r}(t)$ defined the same way as equation (3.19)) over k points in time is less than or equal to the average of the magnitude of the estimated error E (=$\underline{\epsilon}(t)$) over k points in time i.e.

$$\text{average of } \|R\| = \frac{\sum_{j=1}^{k} \|\underline{r}(t_j)\|}{k}$$

$$= \frac{\sum_{j=1}^{k} \|G\underline{i}(t_j) - \underline{d}(t_j)\|}{k}$$

is less than or equal to the

$$\text{average of } \|E\| = \frac{\sum_{j=1}^{k} \|\underline{\epsilon}(t_j)\|}{k}$$

$$= \frac{\sum_{j=1}^{k} \left\| \frac{\text{estimated percentage error}}{100} \cdot \underline{\tilde{d}}\ (t) \right\|}{k} \qquad (3.21)$$

Using the above criterion I (=$\underline{i}(t)$) was then calculated from equation (3.16). In the case of Figs. 3.23-3.25 where one point in time (t_j) was considered (i.e. only $\underline{\tilde{d}}(t_j)$, and $\underline{i}\ (t_j)$) this reduces to choosing γ which gives the magnitude of the residual

$$\|\underline{r}(t_j)\| = \| G\ \underline{i}\ (t_j) - \underline{\tilde{d}}\ (t_j)\|$$

less than or equal to the magnitude of the estimated error

$$\|\underline{\epsilon}(t_j)\| = \left\| \frac{\text{estimated percentage error}}{100} \cdot \underline{\tilde{d}}\ (t_j) \right\| \qquad (3.22)$$

The calculated $\underline{i}$'s by the second order regularization with 3% estimated error show very good results (Figs. 3.23a,b-3.24a,b). However, over-estimation of error caused an *over-smooth* solution. In Figs. 3.23b-3.24b the calculated current when the error was estimated to be 5% was plotted. In most of these cases the peaks were rounded off.

For comparison the results obtained from the simplified equation (equation (3.18)) are also shown in Figs. 3.23c-3.25c. The values of the input current were slightly different from those of the method of regularization due to the different assumed positions of the transmembrane current-flows in each model (Fig. 3.9 c.f. Fig. 3.18). The solutions were quite well-behaved in the sense that no large oscillation was observed. However, in most cases they were not as accurate as those using second order regularization. In one case where the measurement was carried out when the electrodes had become

very noisy (i.e. larger error) the current obtained by direct inversion was oscillating very badly (Fig. 3.25b shows Δi_n) and the solution using simplified equation also did not compare well with the input. Here the method of regularization shows its power; γ was chosen to correspond to an estimated error of about 7.5% and the solution was very much improved (Fig. 3.25 a and b).

The results from the experiment when the cell was at the bottom of the tube were very similar to the ones described above. The comparisons of these two experiments are shown in Fig. 3.26.

In a few cases solutions were also obtained by using the first order regularization (i.e. $L\underline{i}$ = first derivative of $\underline{i}$) (Fig. 3.27). The results were very similar to those obtained by the second order regularization, the only difference being the rate at which the solution became smooth i.e. for the second order the solution became smooth faster than the first order (γ second order < γ first order).

3.3.3 Discussion

The results presented in section 3.3.2 demonstrated quite clearly the successful application of the method of regularization, particularly the second order regularization, to experimental measurements. The solutions obtained agreed very well with the input data except a slight error in the right hand end of Fig. 3.24a when the electrodes were at positions B1 (see Fig. 3.21). This was as expected since in this case the cell extended beyond the last electrode (C) and thus $j_c \neq 0$ (j_c = 8 + 9 = 17 μA) as assumed in the model (Fig. 3.9). When the electrodes were at position A (see Fig. 3.21) $j_c \neq 0$ also; however it was less than j_c in position B1 (i.e. 8 c.f. 17 μA) and a reasonable result was obtained at this

right hand end (Fig. 3.23a). In view of the result of position B1 (Fig. 3.24a) however, it is clearly better to position the cell according to the place assumed in the model i.e. the right hand end of the cell was placed midway between electrode B and C (see Fig. 3.9). This was in fact what we did for all the anucleate isolated stalk segments (ISS's) in the main experiments (see chapter 4).

These results together with those in section 3.2.3 confirmed the usefulness of such a method in solving our ill-conditioned problem. The only disadvantage is the many steps of calculation which make it impossible to obtain the solution I in *real time* during an experiment due to the limited capacity of our laboratory computer. In this case the simplified equation (3.18) becomes useful. Although it produces a less accurate solution, it can be implemented within the experimental monitoring program (see chaper 4). Therefore, we are able to obtain some indication of the initiation point and the propagation behaviour of the depolarized region from this approximate current solution while the experiment is in progress.

As already indicated in both sections 3.2.3 and 3.3.2, over-estimation of the error would lead to an over-smooth solution. In the experiments we do not have the original input values of I to compare to the calculated solution and therefore have to be very careful when estimating the errors. It is important to realize that our inversion problem (using second order regularization) does not possess a unique solution and the selection of a preferred solution (i.e. a smooth solution using a particular γ which gives an acceptable value of residual) from all the possible solutions ($\gamma \geq 0$) is an imposed additional condition. That is, we rely on the knowledge that the solution should be smooth to select from all the solutions a most acceptable candidate. This imposed condition is not

always clear. If for example a particular solution possesses an unexpected oscillatory behaviour, the application of a criterion designed to eliminate such features as much as possible would hardly be realistic. Fortunately, the shape of the solution could also be obtained from the simplified equation (equation (3.18)) in most cases to provide a sufficient indication of the behaviour. In chapters 4 and 5, examples of experimental results will be shown and as expected the solutions of current I are smooth functions.

Fig. 3.1 (a) Extracellular and intracellular potential distributions of an isolated cylindrical cell and (b) the extracellular potential fields (modified from Clark and Plonsey, 1968).

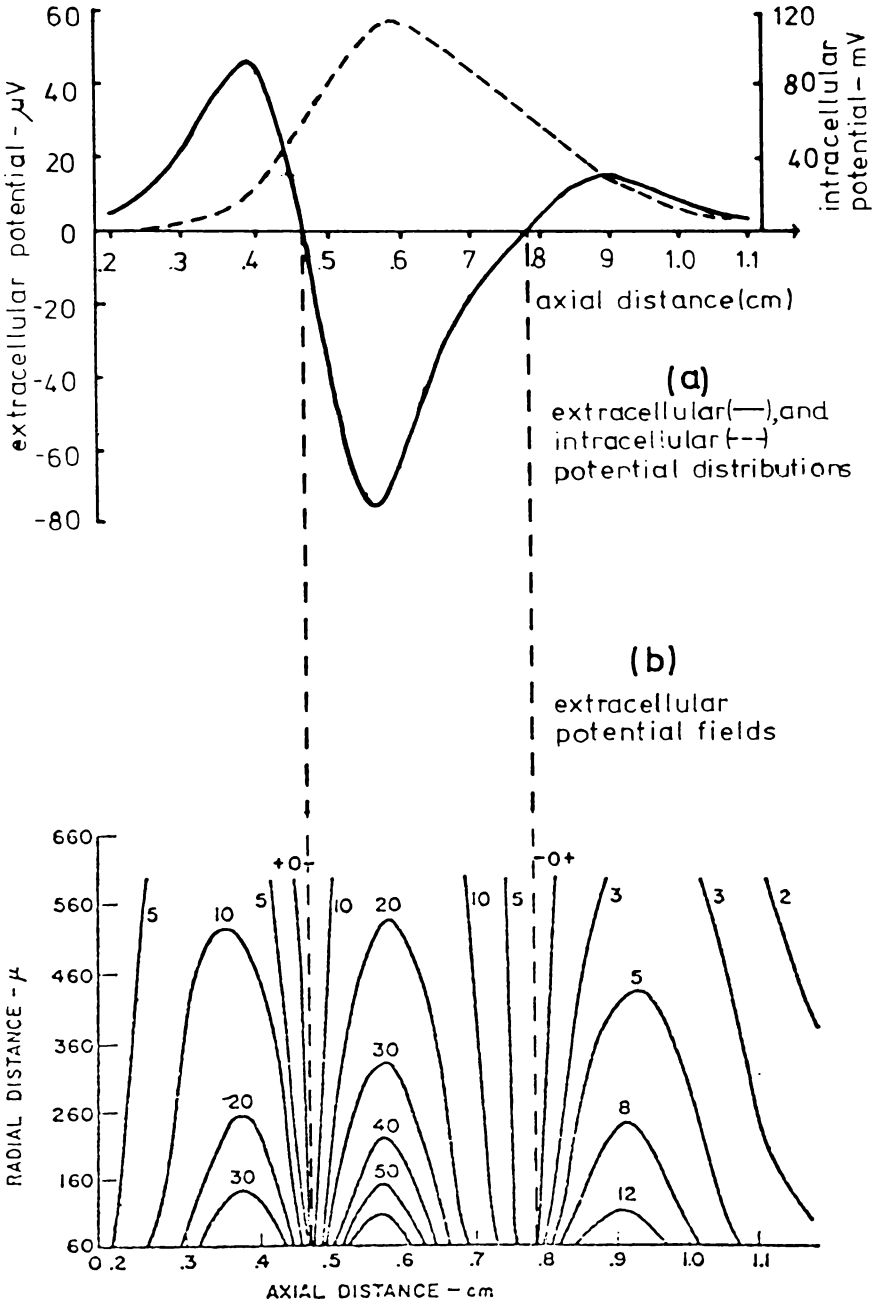

Calculated external potential field of 120 μ crayfish lateral giant axon immersed in an extensive volume of sea water for various values of radial distance (r) and axial distance (z). The values of the isopotential lines in this figure are in microvolts. Since the radius of the axon is 60 μ, the radial distance $r = 60\ \mu$ corresponds to the outer membrane surface of the axon.

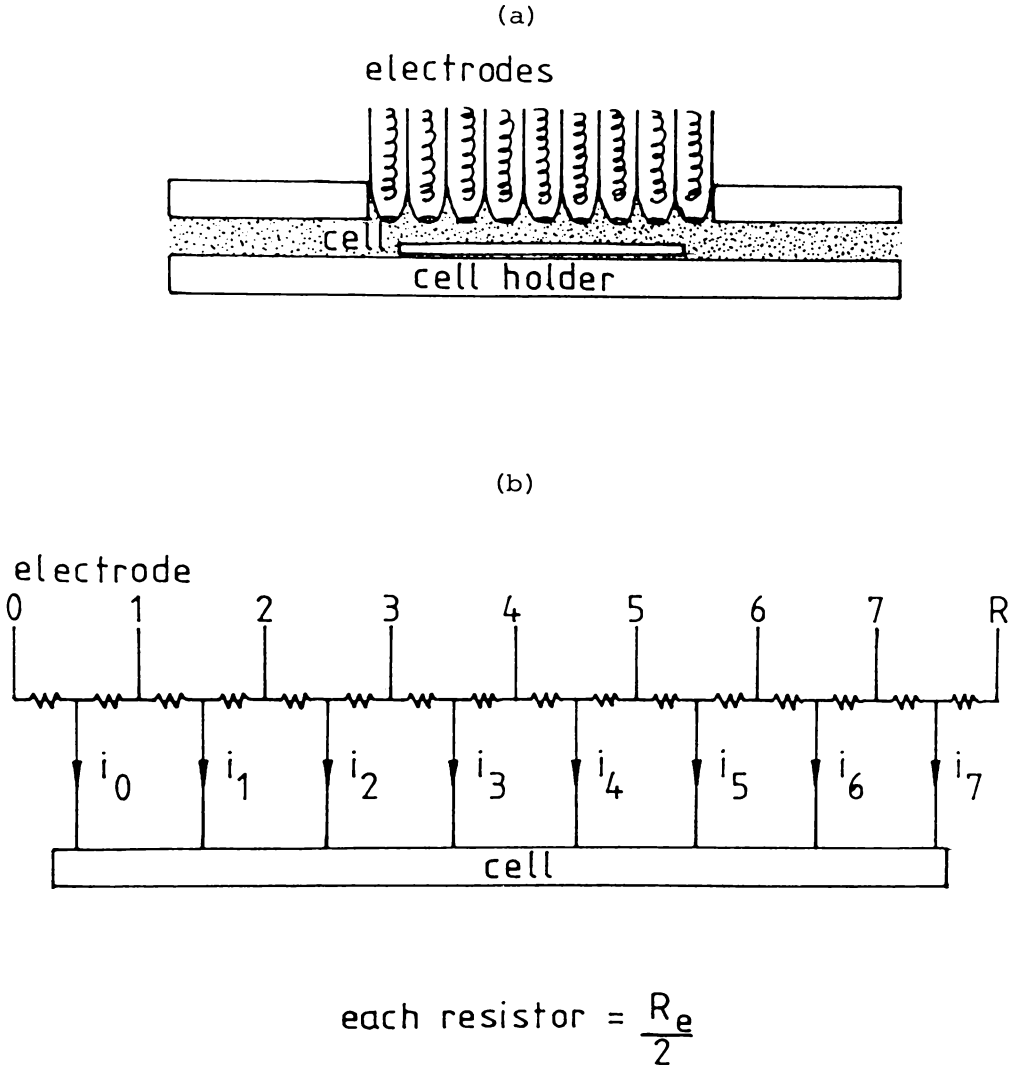

Fig. 3.2 Cell stem in a cylindrical holder (a) and its equivalent circuit model (b). R_e represents the resistance of the sheath of the external medium between two electrodes, and i_n the transmembrane current-flow between electrode (n,n+1) (n = 0,....,7).

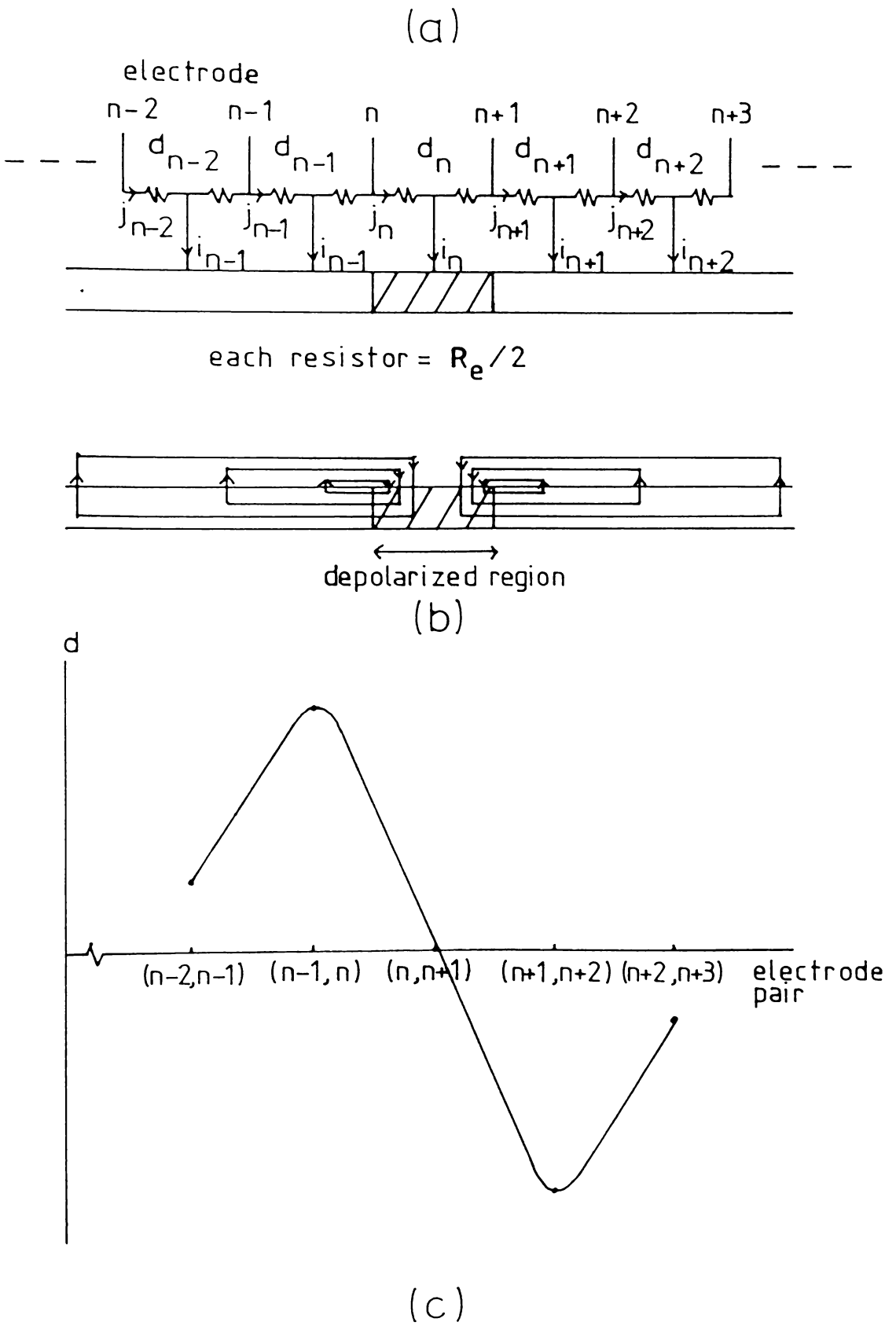

Fig. 3.3 Diagram showing (a) part of the equivalent circuit model with a depolarized region; (b) the current-flow due to the depolarized region and (c) the plot of differential voltages with respect to electrode pairs.

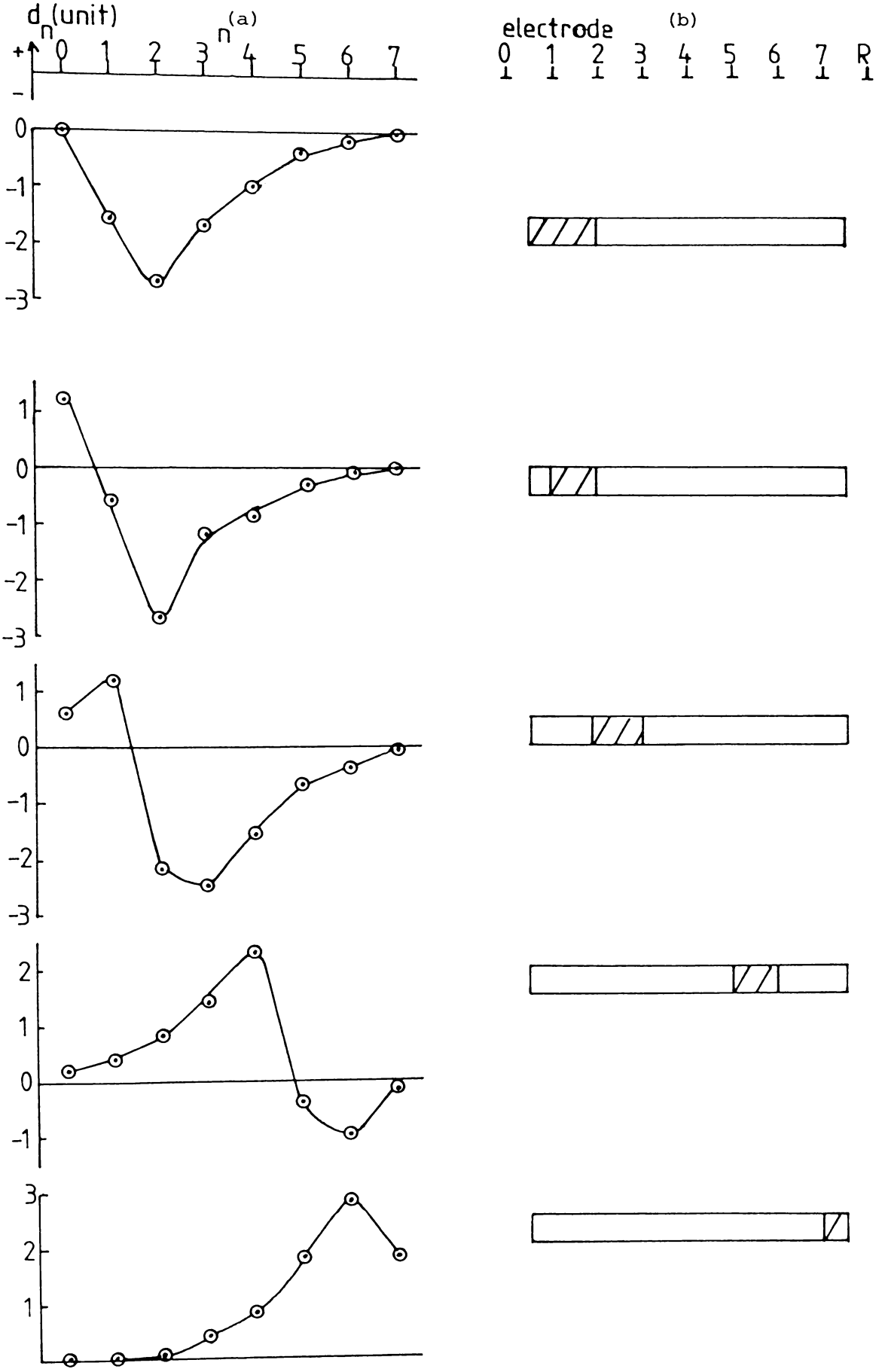

Fig. 3.4 Examples of differential voltage distributions (a) and the analysed depolarized regions (▨) (b).

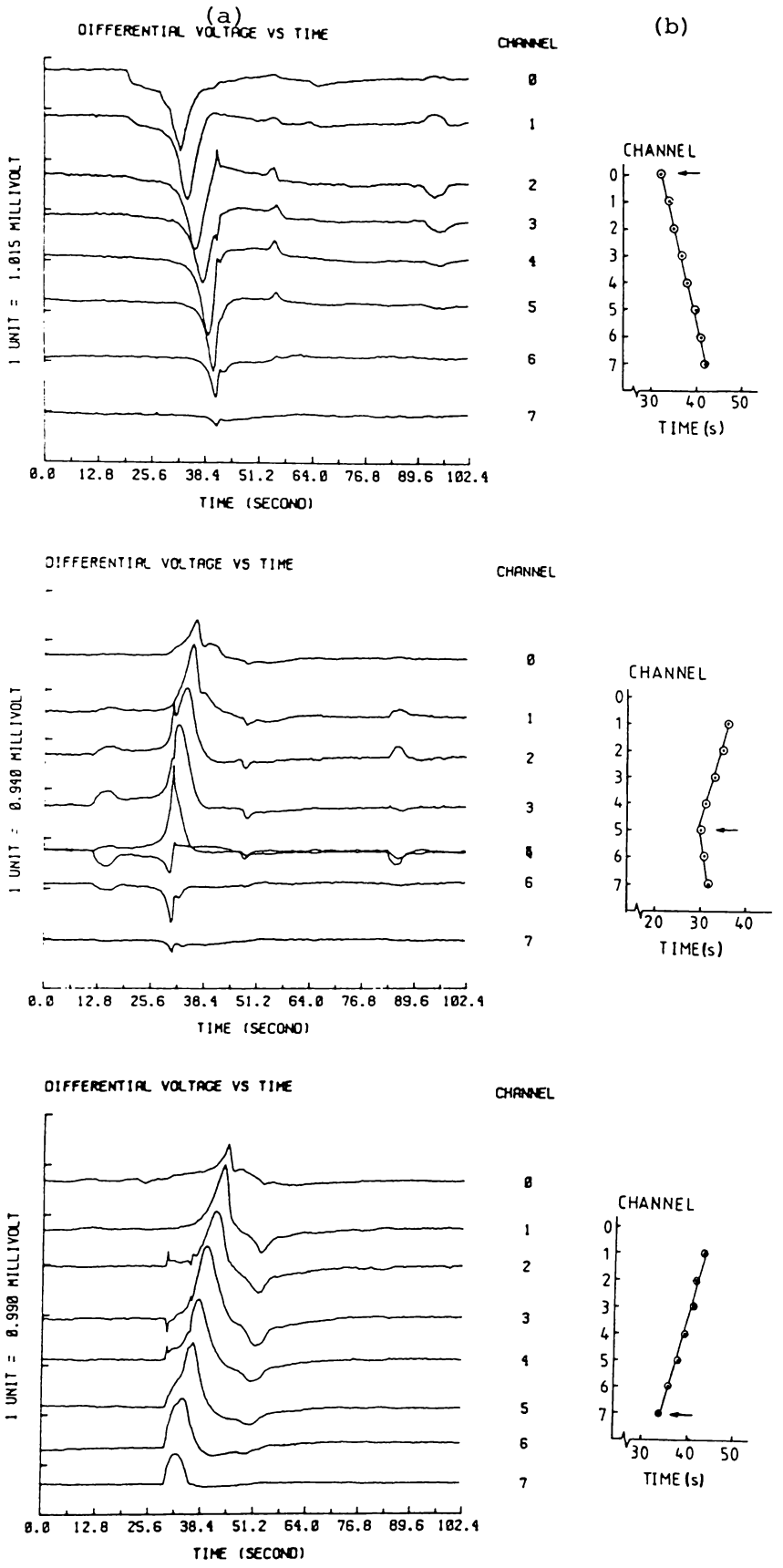

Fig. 3.5 Examples of spontaneous action potentials showing
(a) the differential voltage waveforms and
(b) the plot to analyse for the initiation point.

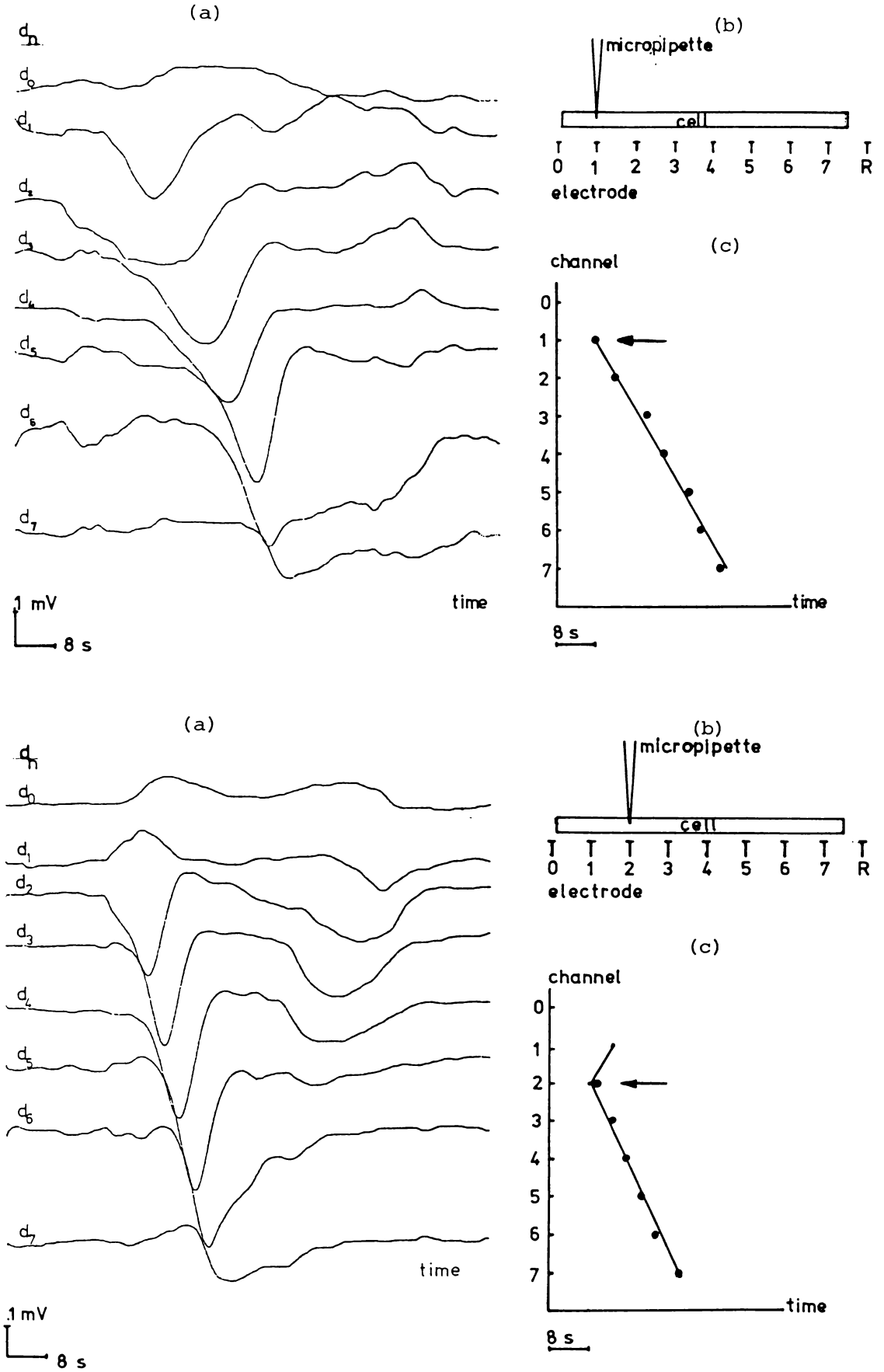

Fig. 3.6 Examples of stimulated action potentials showing (a) the differential voltage waveforms, (b) position of stimulation and (c) the plot to analyse the initiation point.

(a)

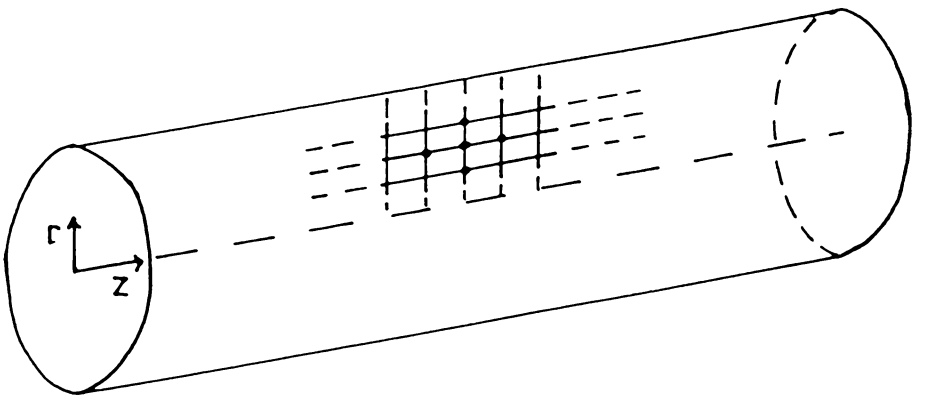

(b)

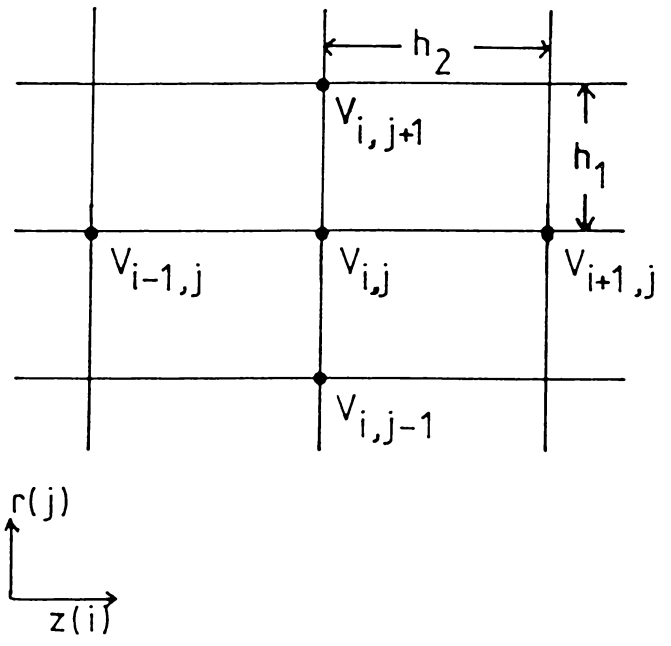

Fig. 3.7 (a) The cylindrical relaxation model and

(b) values required to approximate $\nabla^2 V$ at a general mesh point (i,j) with a mesh size $h_1 \times h_2$.

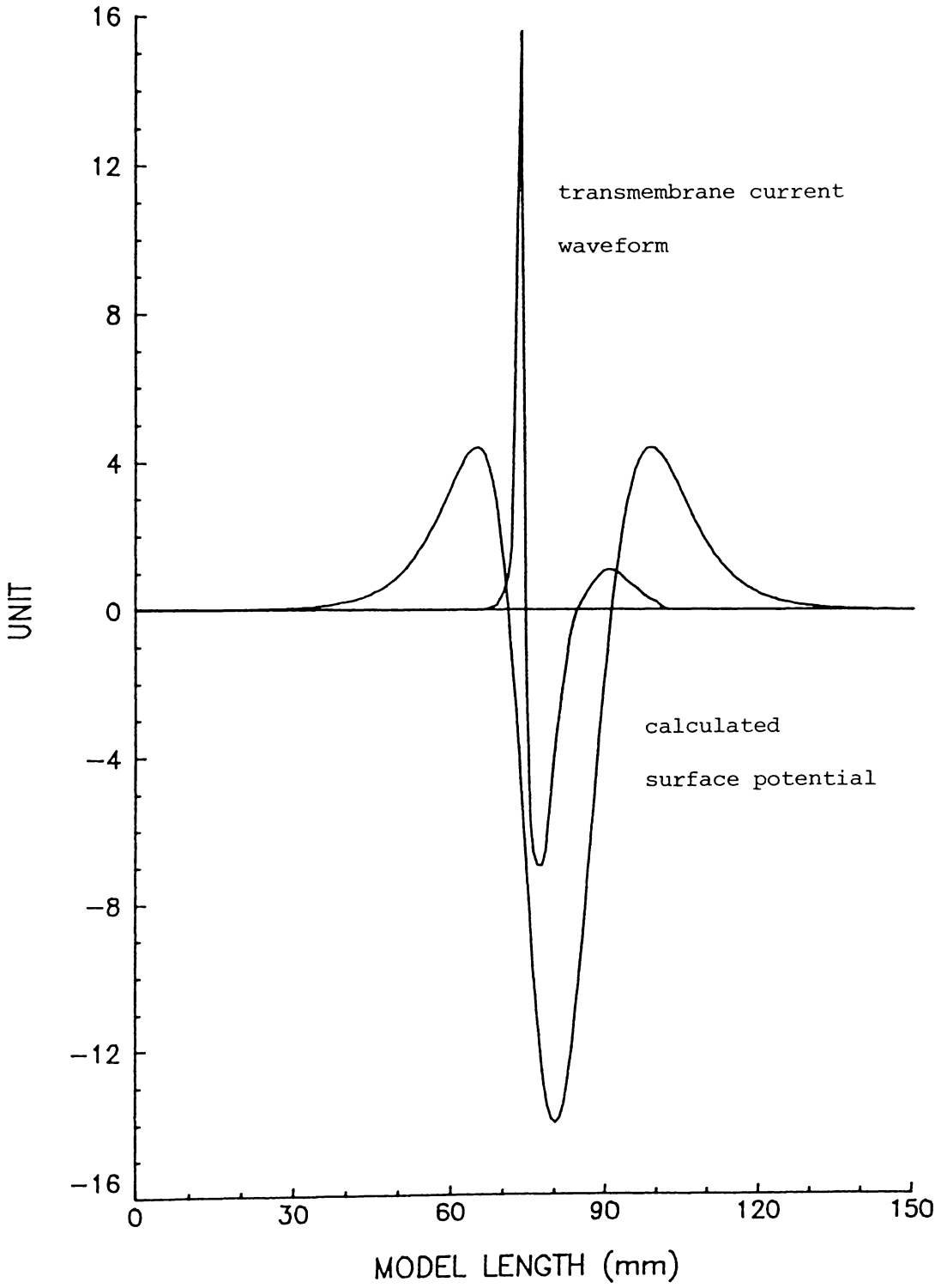

Fig. 3.8 Transmembrane current waveform and the surface potential calculated by successive over-relaxation method (see text).

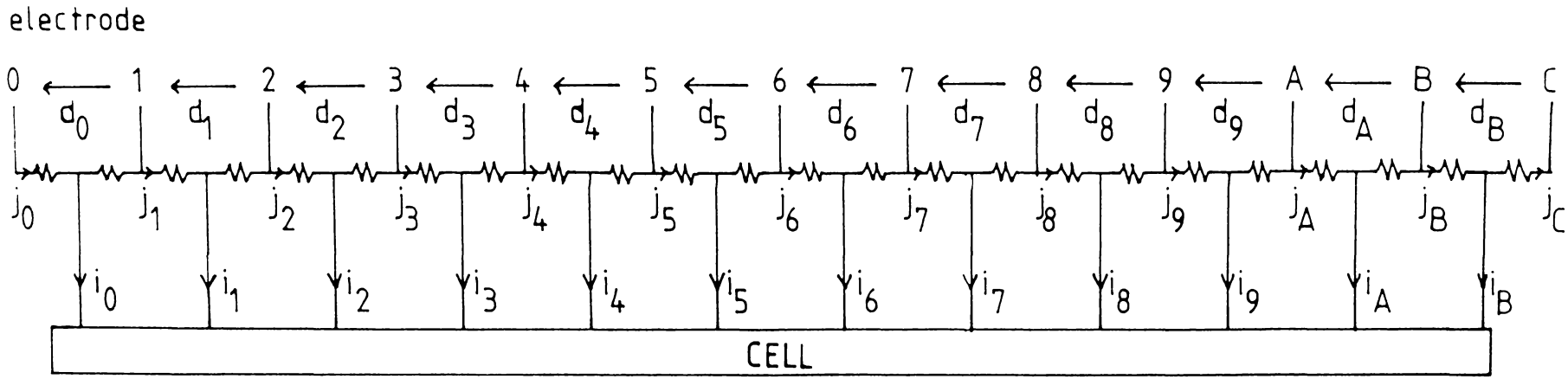

$$\text{each resistor} = \frac{R_e}{2}$$

Fig. 3.9 Equivalent circuit model of a cell stem in a cylindrical holder. R_e represents the resistance of the sheath of the external medium between two electrodes, d_n the differential voltage between electrode pair (n,n+1), and i_n the transmembrane current flow between electrode pair (n,n+1) where n = 0,1,.....,9,A,B.

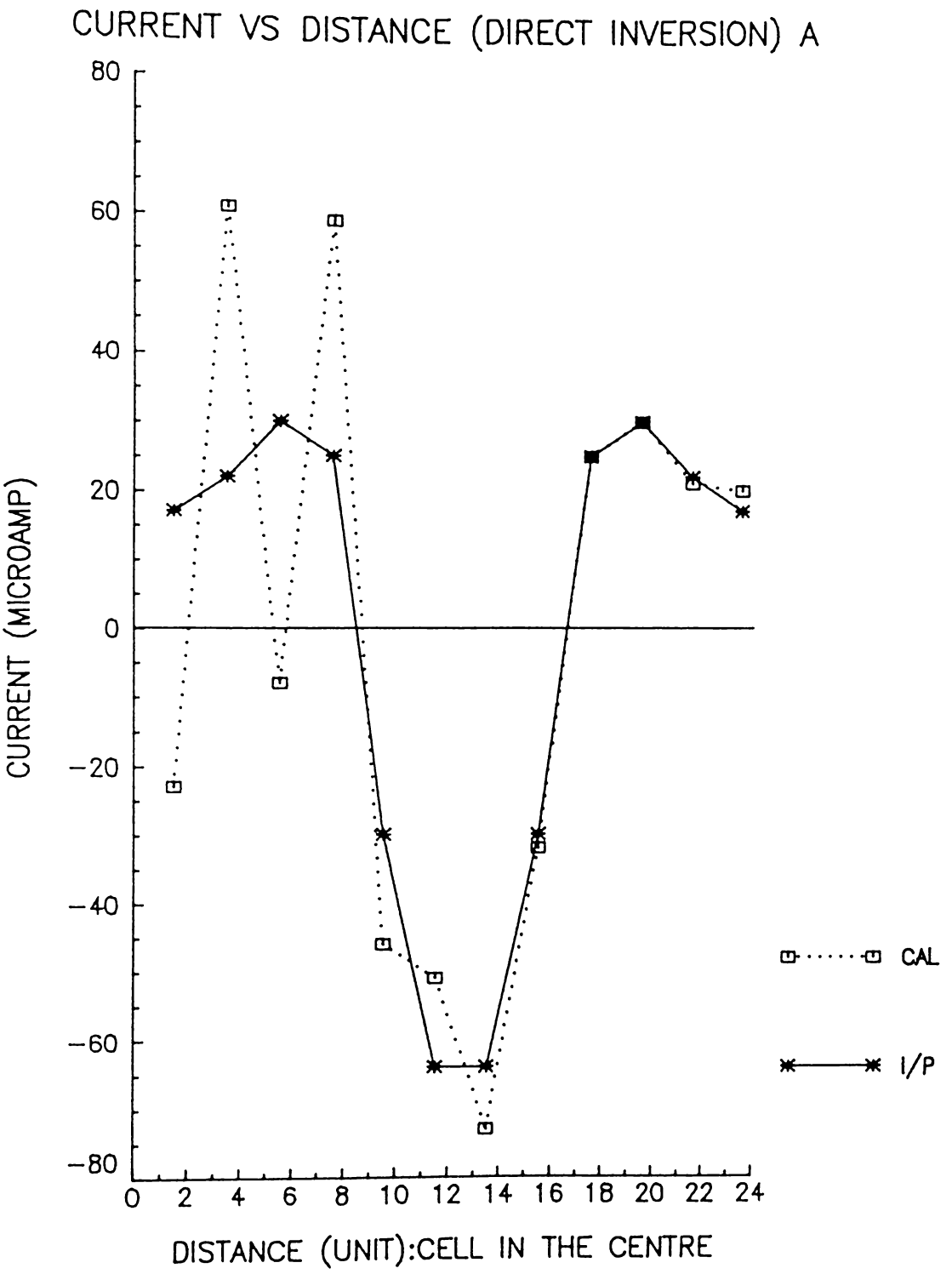

Fig. 3.10 Examples of current distributions showing

I/P input current distribution

CAL calculated current distribution obtained from experimental measurement of differential voltage by direct inversion (see text).

Fig. 3.11-3.13 Examples of simulated current and differential voltage distributions showing

(a) differential voltage $\underline{d}$ and $\underset{\sim}{\underline{d}} = \underline{d}$ + 5% error

(b) input current (I/P) and the calculated current (CAL) by direct inversion

(c) input current (I/P) and the calculated current (CAL) by second order regularization

(d) differential voltage $\underset{\sim}{\underline{d}}$ and the differential voltage calculated from calculated current in (c) (= matrix G × current $\underline{i}$ = G$\underline{i}$).

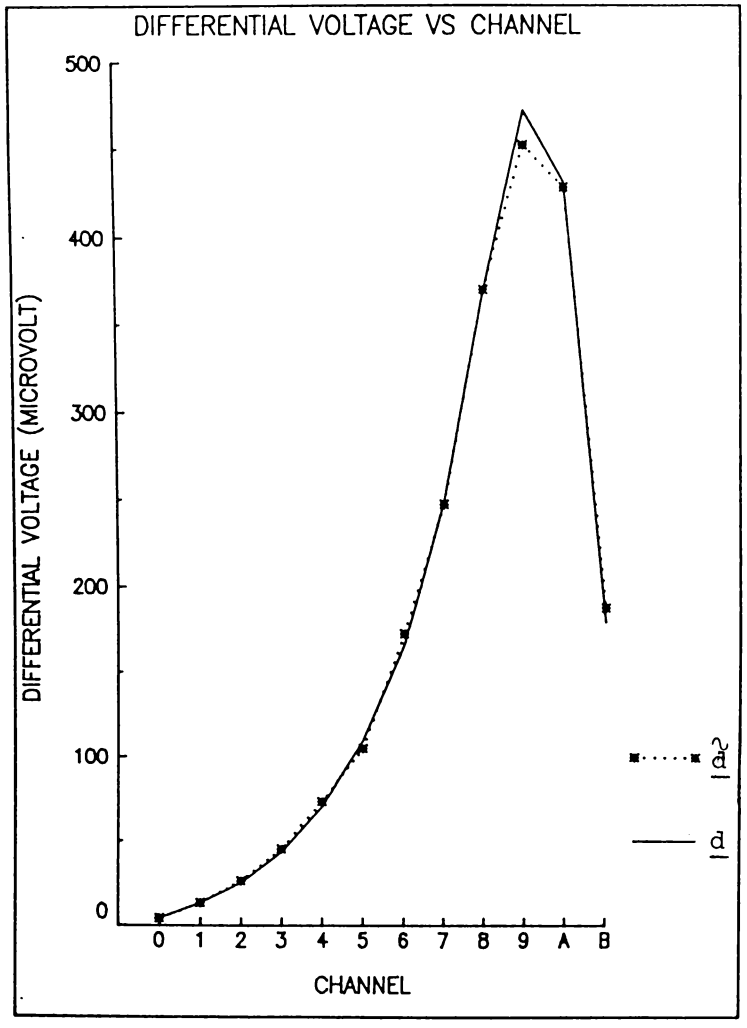
DIFFERENTIAL VOLTAGE VS CHANNEL
DIFFERENTIAL VOLTAGE (MICROVOLT)
500
400
300
200
100
0
0 1 2 3 4 5 6 7 8 9 A B
CHANNEL
|a2
|a

(a)

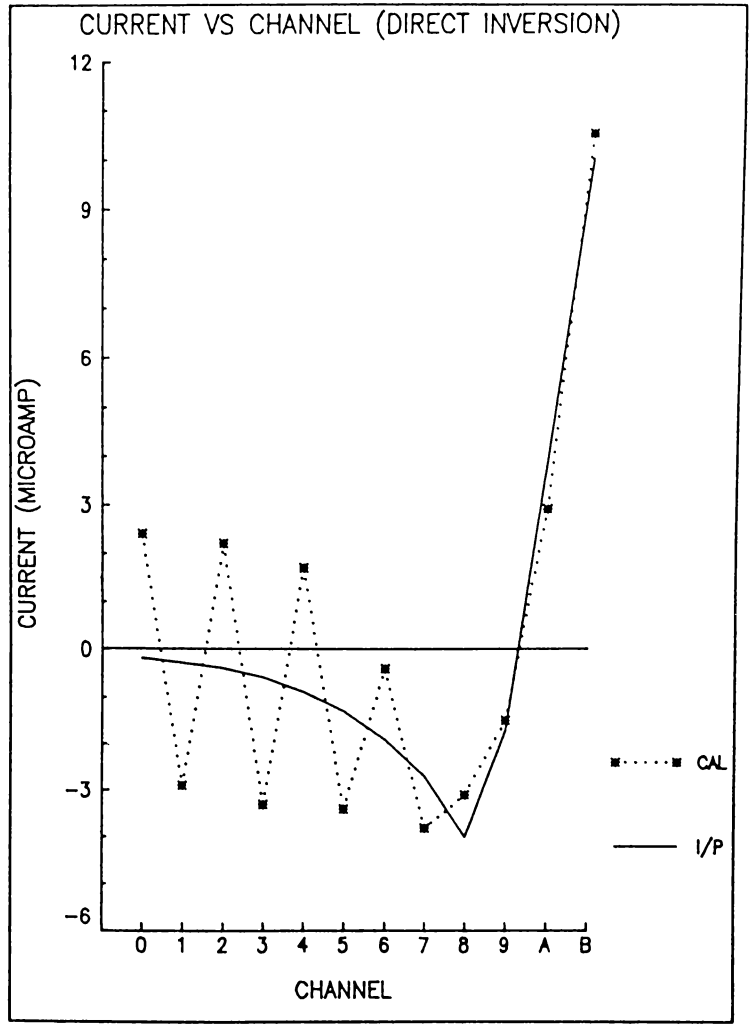
CURRENT VS CHANNEL (DIRECT INVERSION)
CURRENT (MICROAMP)
12
9
6
3
0
-3
-6
0 1 2 3 4 5 6 7 8 9 A B
CHANNEL
CAL
I/P

(b)

Fig. 3.11

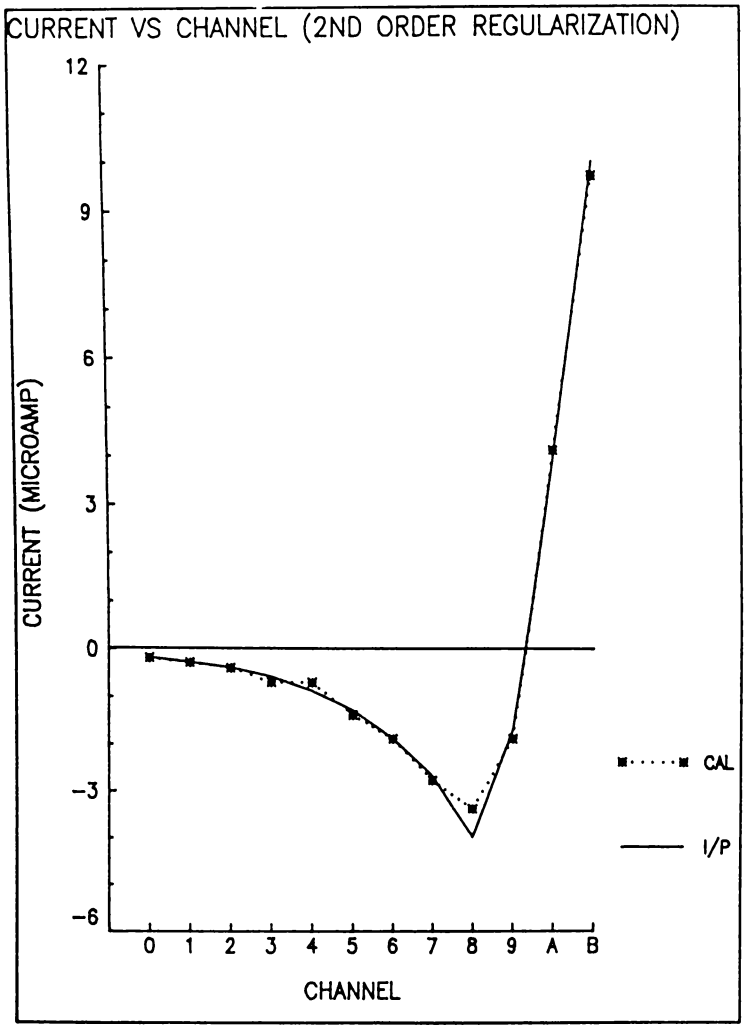
CURRENT VS CHANNEL (2ND ORDER REGULARIZATION)
CURRENT (MICROAMP)
12
9
6
3
0
-3
-6
0 1 2 3 4 5 6 7 8 9 A B
CHANNEL
CAL
I/P

(c)

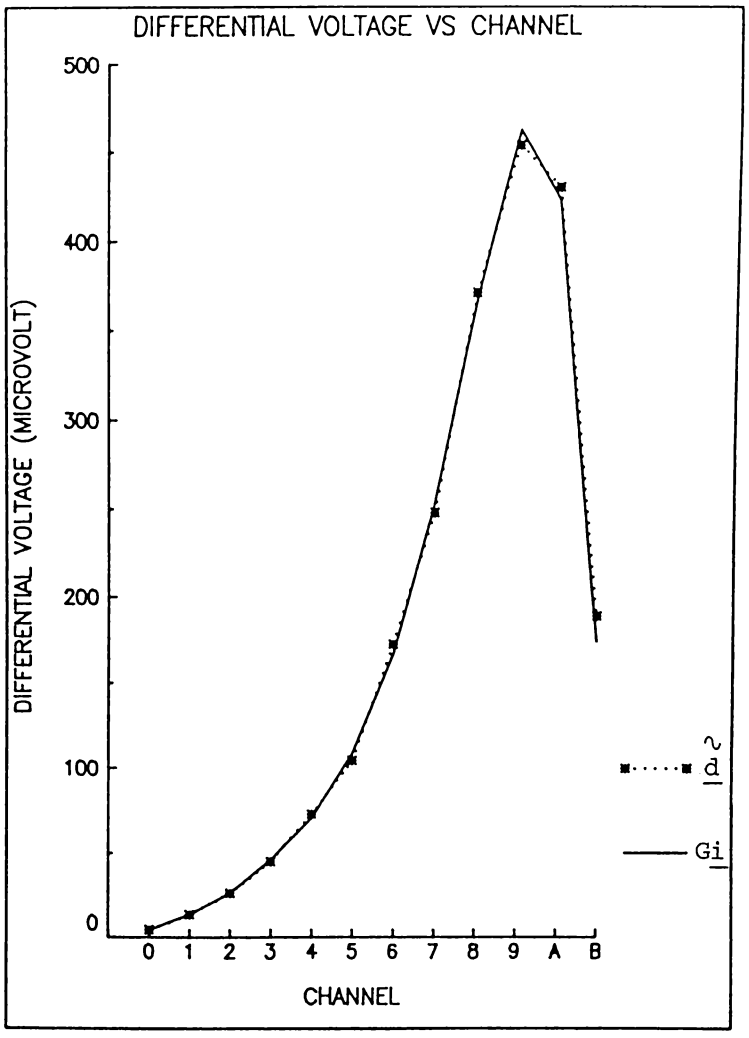
DIFFERENTIAL VOLTAGE VS CHANNEL
DIFFERENTIAL VOLTAGE (MICROVOLT)
500
400
300
200
100
0
0 1 2 3 4 5 6 7 8 9 A B
CHANNEL
Gi

(d)

Fig. 3.11

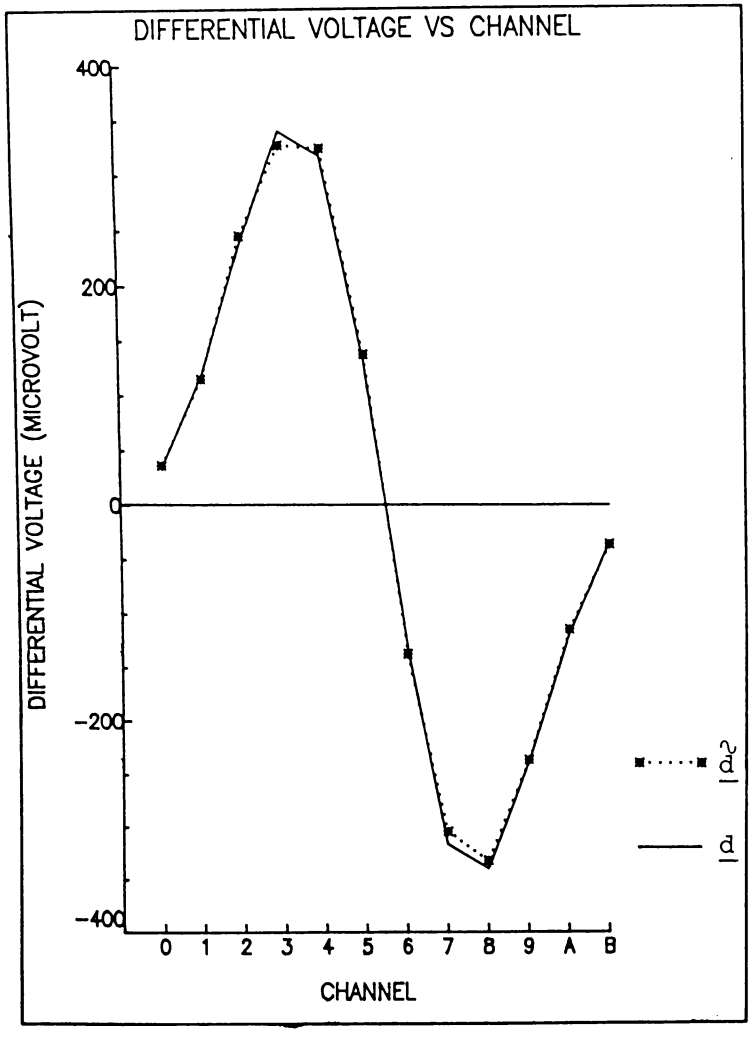
DIFFERENTIAL VOLTAGE VS CHANNEL
DIFFERENTIAL VOLTAGE (MICROVOLT)
400
200
0
-200
-400
0 1 2 3 4 5 6 7 8 9 A B
CHANNEL
2d
d

(a)

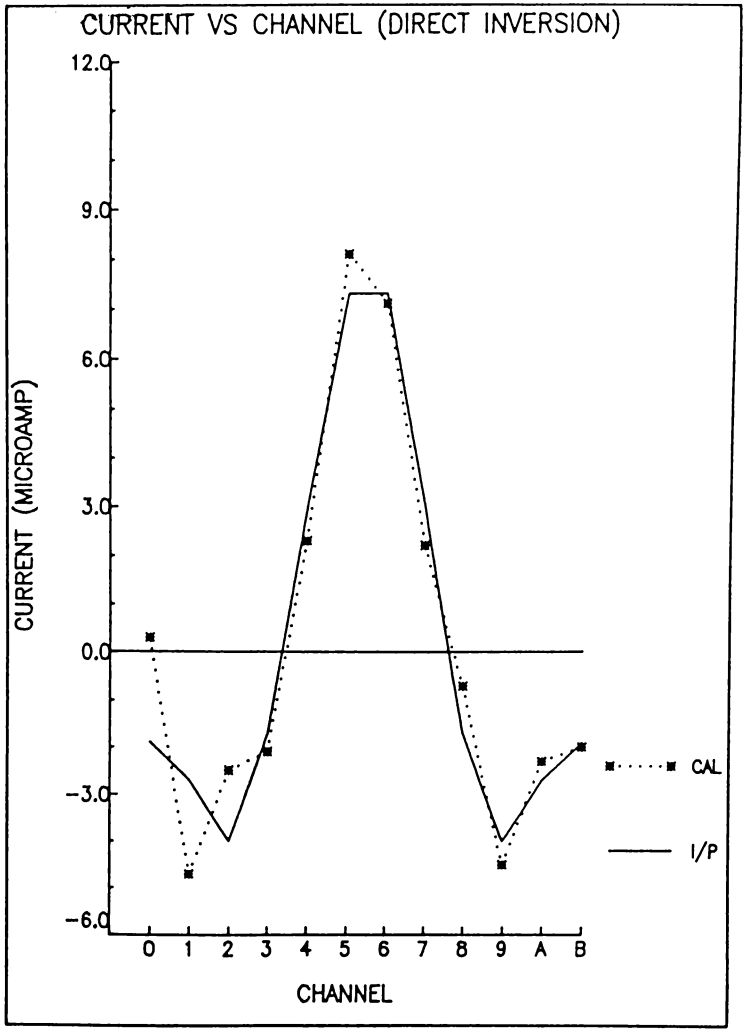
CURRENT VS CHANNEL (DIRECT INVERSION)
CURRENT (MICROAMP)
12.0
9.0
6.0
3.0
0.0
-3.0
-6.0
0 1 2 3 4 5 6 7 8 9 A B
CHANNEL
CAL
I/P

(b)

Fig. 3.12

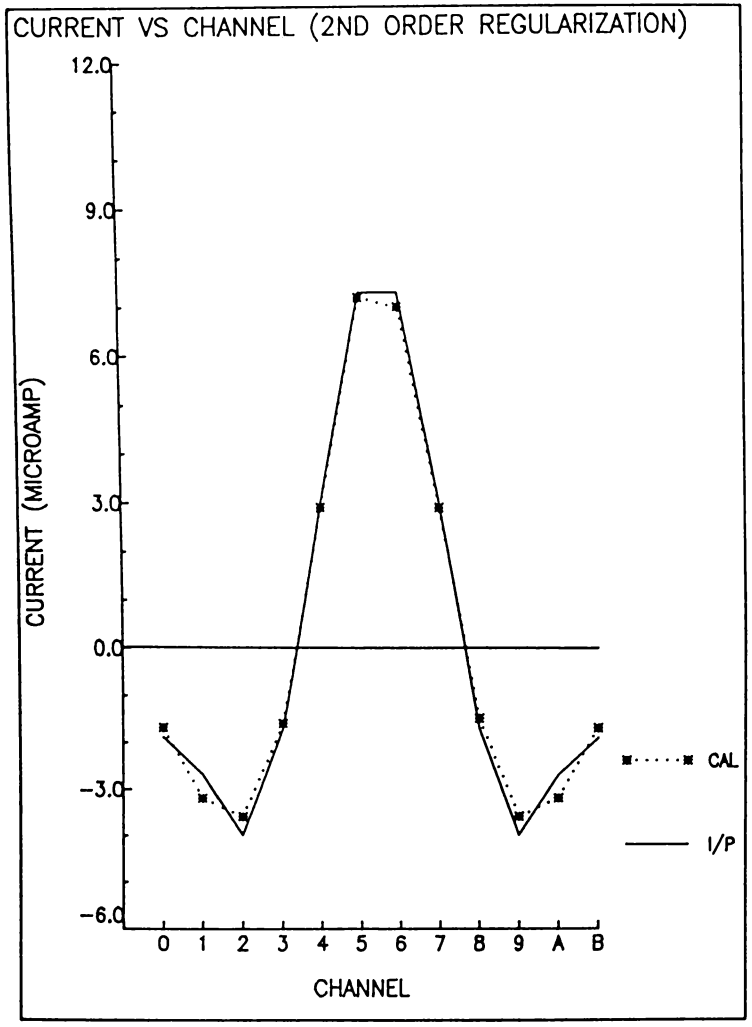
CURRENT VS CHANNEL (2ND ORDER REGULARIZATION)
CURRENT (MICROAMP)
12.0
9.0
6.0
3.0
0.0
-3.0
-6.0
0 1 2 3 4 5 6 7 8 9 A B
CHANNEL
CAL
I/P

(c)

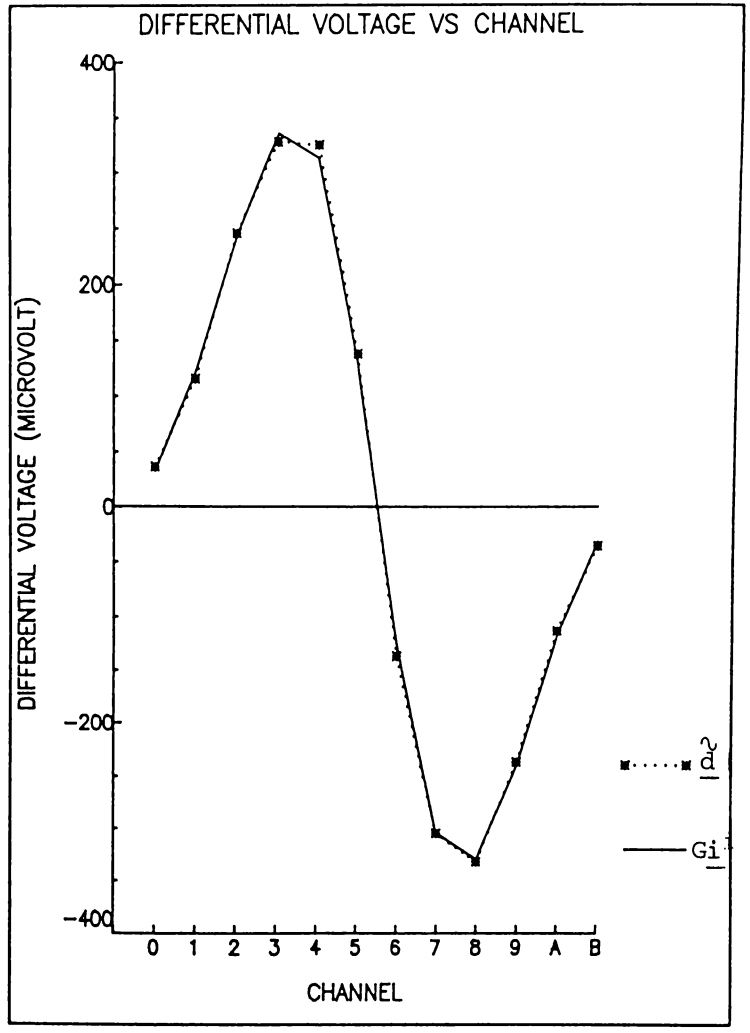
DIFFERENTIAL VOLTAGE VS CHANNEL
DIFFERENTIAL VOLTAGE (MICROVOLT)
400
200
0
-200
-400
0 1 2 3 4 5 6 7 8 9 A B
CHANNEL

(d)

Fig. 3.12

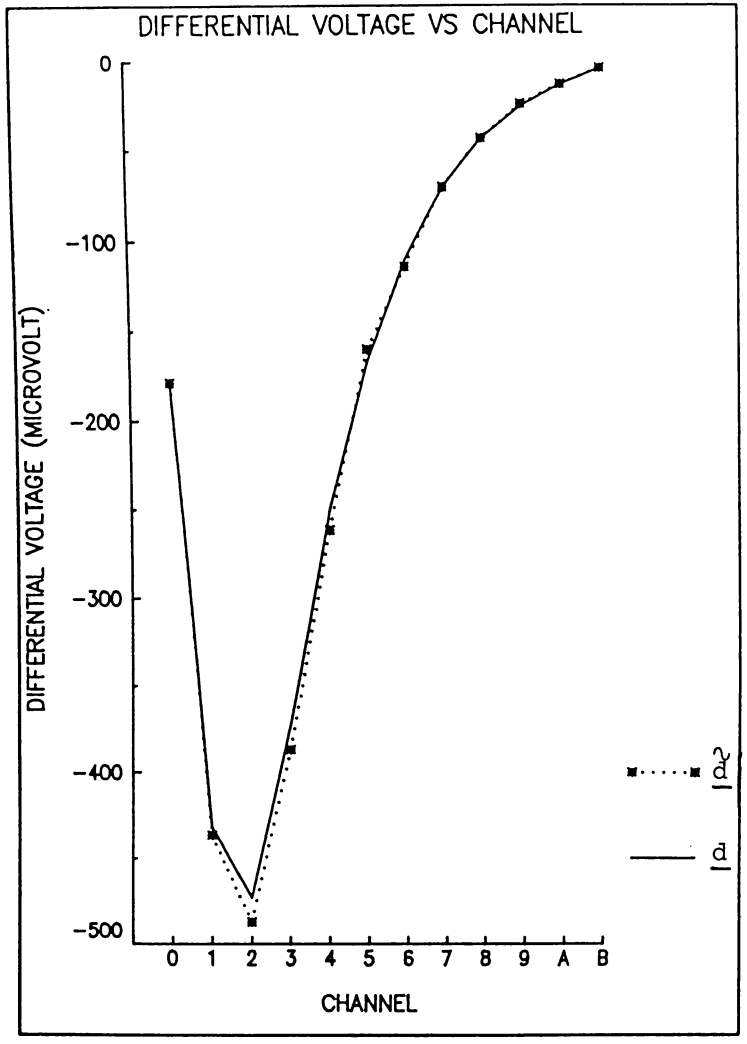
DIFFERENTIAL VOLTAGE VS CHANNEL
DIFFERENTIAL VOLTAGE (MICROVOLT)
0
-100
-200
-300
-400
-500
0 1 2 3 4 5 6 7 8 9 A B
CHANNEL
Id2
Id

(a)

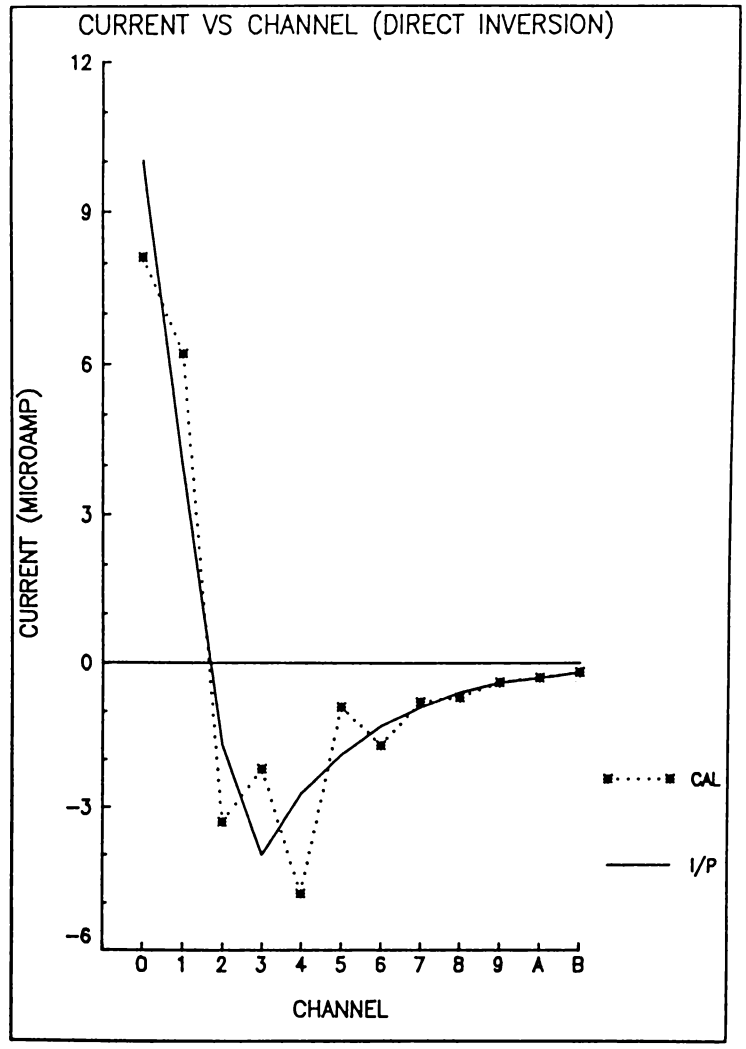
CURRENT VS CHANNEL (DIRECT INVERSION)
CURRENT (MICROAMP)
12
9
6
3
0
-3
-6
0 1 2 3 4 5 6 7 8 9 A B
CHANNEL
CAL
I/P

(b)

Fig. 3.13

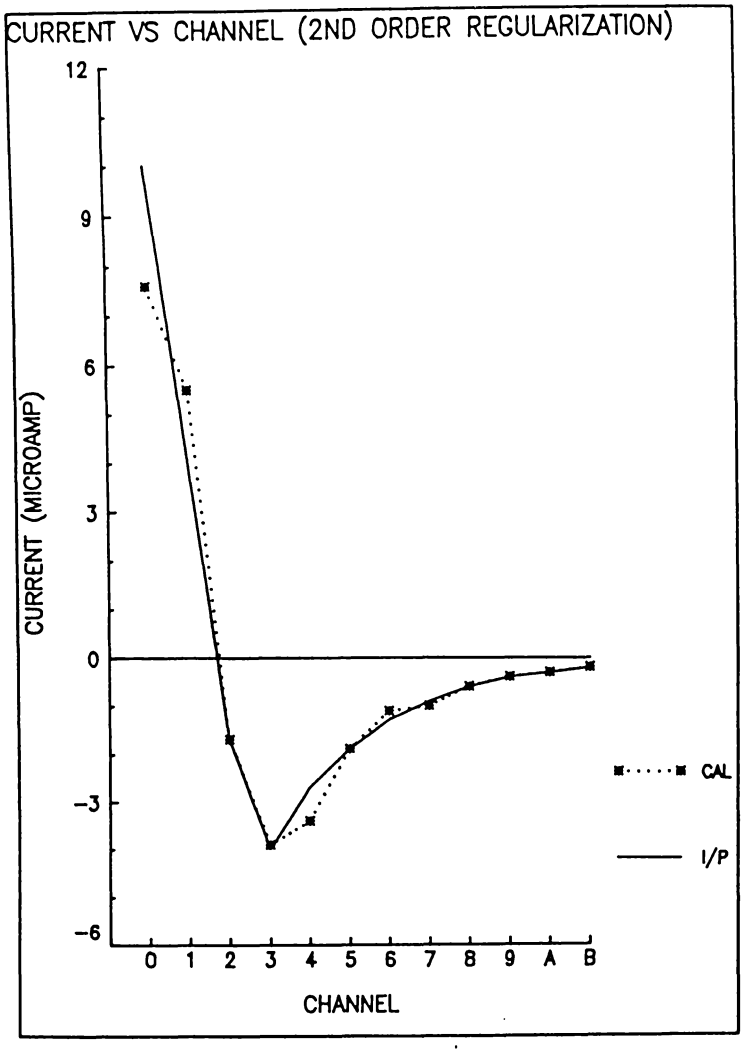
CURRENT VS CHANNEL (2ND ORDER REGULARIZATION)
CURRENT (MICROAMP)
12
9
6
3
0
-3
-6
0 1 2 3 4 5 6 7 8 9 A B
CHANNEL
CAL
I/P

(c)

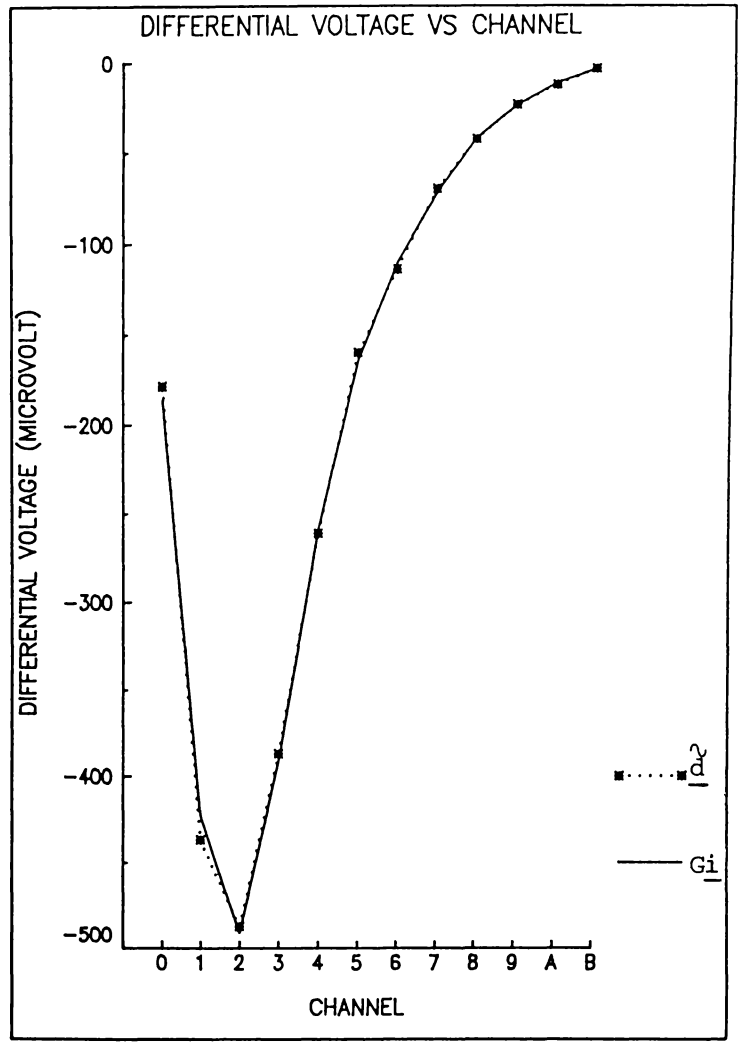
DIFFERENTIAL VOLTAGE VS CHANNEL
DIFFERENTIAL VOLTAGE (MICROVOLT)
0
-100
-200
-300
-400
-500
0 1 2 3 4 5 6 7 8 9 A B
CHANNEL
Id2
Gi

(d)

Fig. 3.13

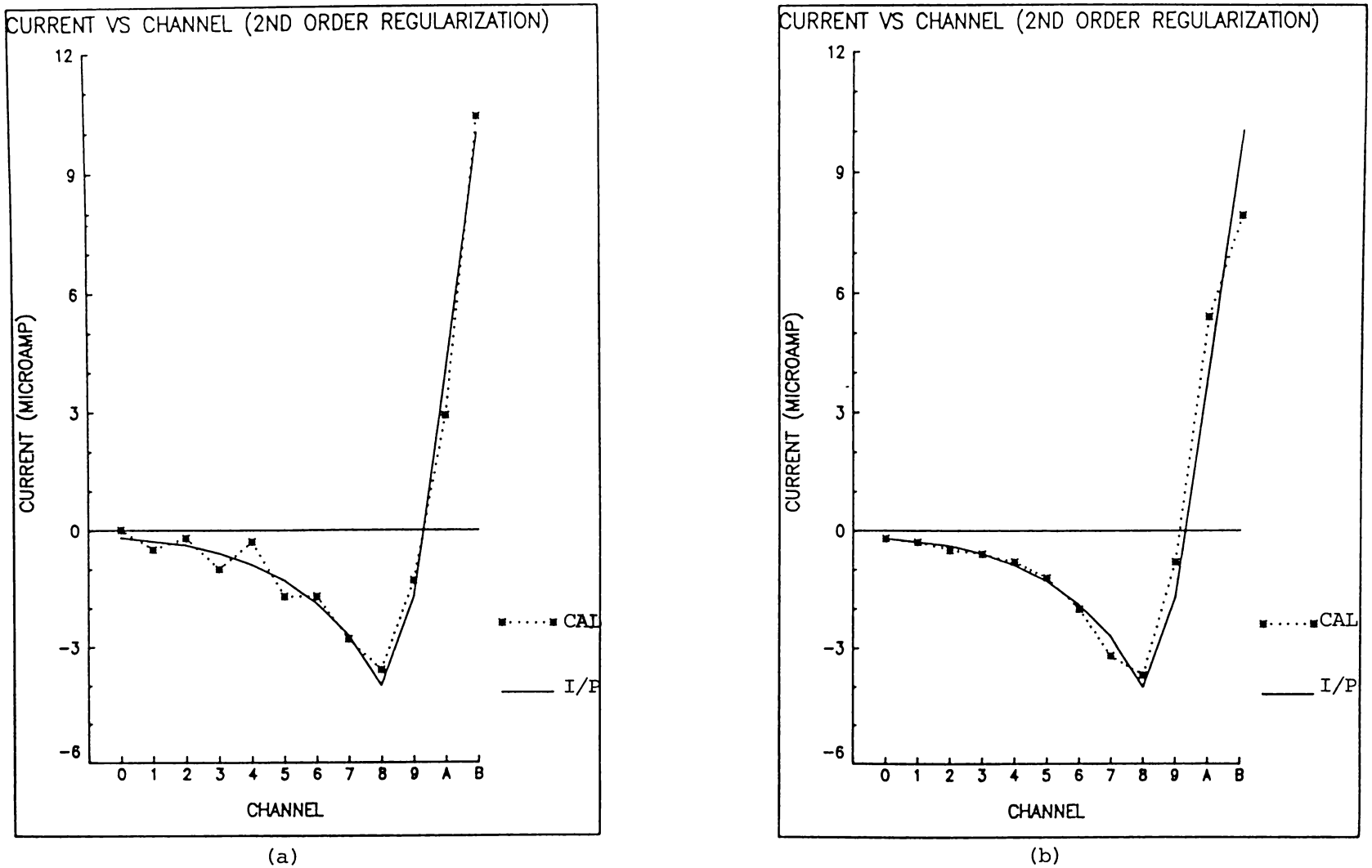

Fig. 3.14 Simulated input current distribution (I/P) as compared to calculated current distribution (CAL) obtained by second order regularization when (a) γ is too small and (b) γ is too large.

Fig. 3.15-3.17 Examples of simulated input current distributions (I/P) as compared to averages of calculated current distributions (CAL) obtained by

(a) direct inversion

(b) second order regularization

vertical bars indicate standard deviations.

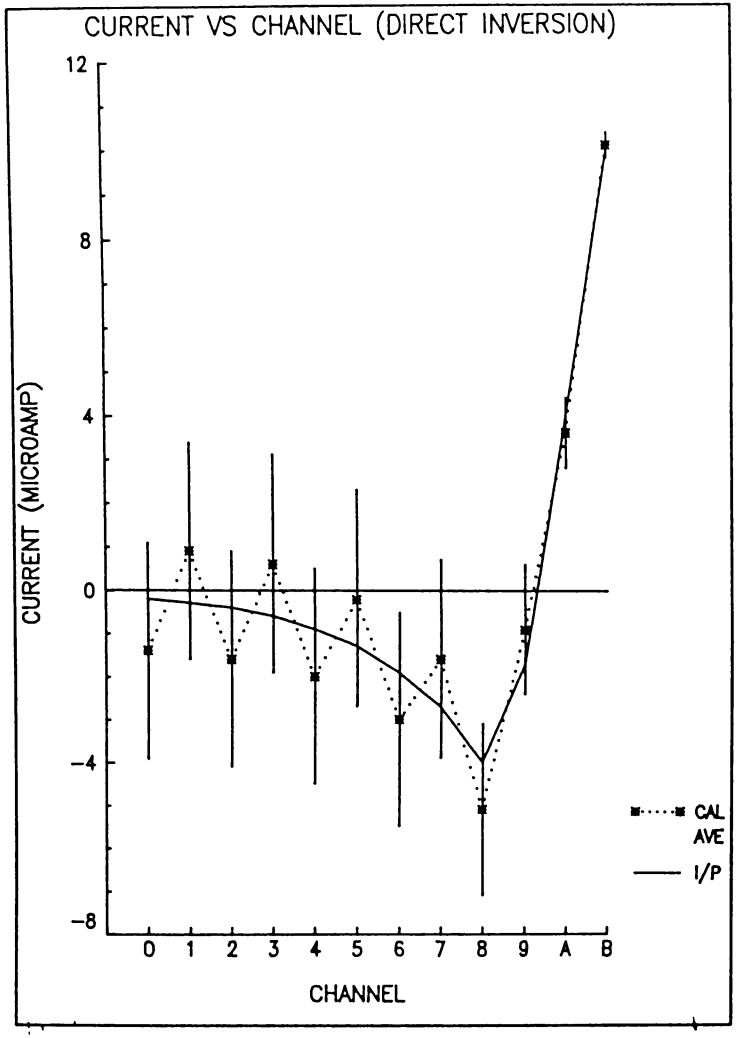
CURRENT VS CHANNEL (DIRECT INVERSION)
CURRENT (MICROAMP)
12
8
4
0
-4
-8
0 1 2 3 4 5 6 7 8 9 A B
CHANNEL
CAL AVE
I/P

(a)

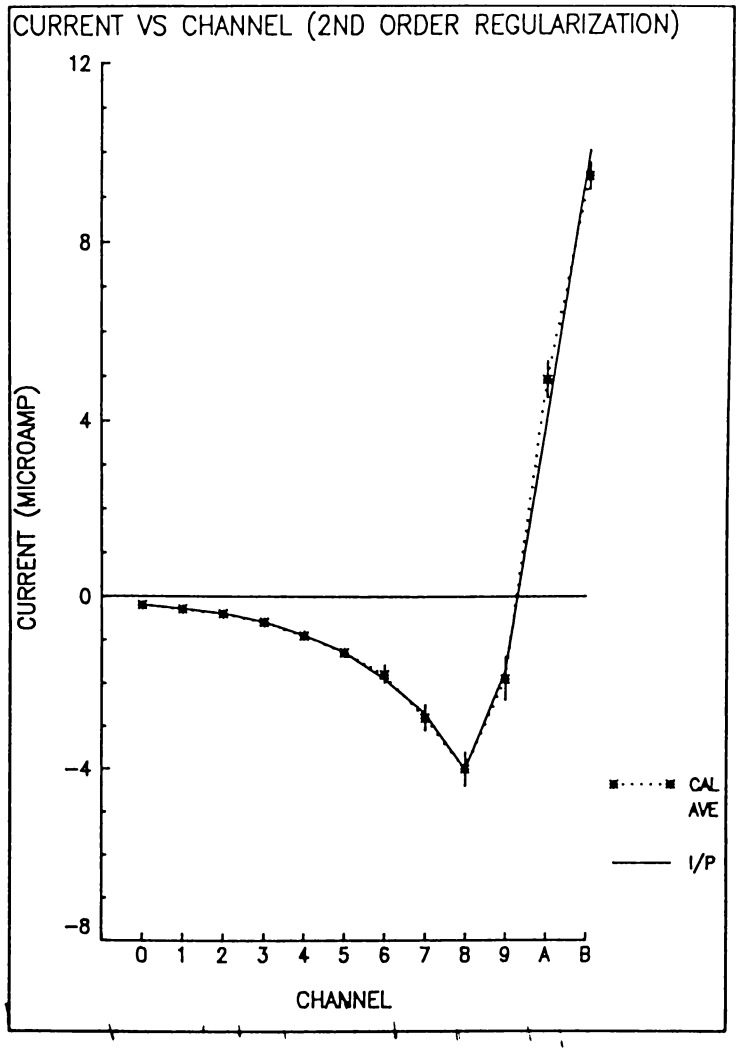
CURRENT VS CHANNEL (2ND ORDER REGULARIZATION)
CURRENT (MICROAMP)
12
8
4
0
-4
-8
0 1 2 3 4 5 6 7 8 9 A B
CHANNEL
CAL AVE
I/P

(b)

Fig. 3.15

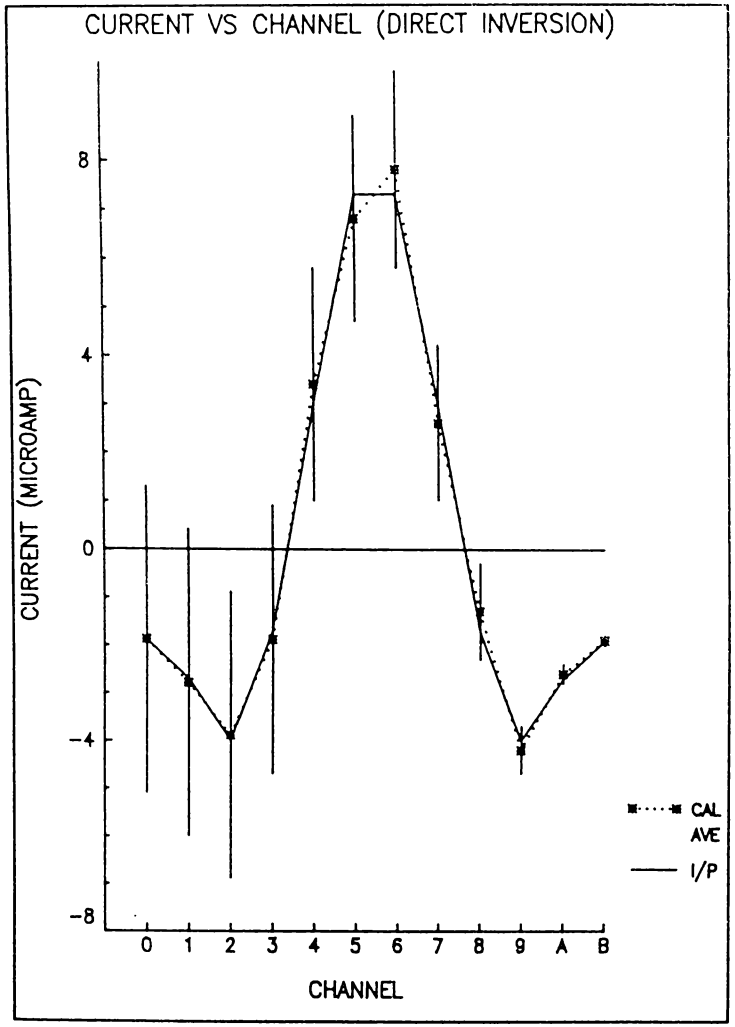
CURRENT VS CHANNEL (DIRECT INVERSION)
CURRENT (MICROAMP)
8
4
0
-4
-8
0 1 2 3 4 5 6 7 8 9 A B
CHANNEL
CAL AVE
I/P

(a)

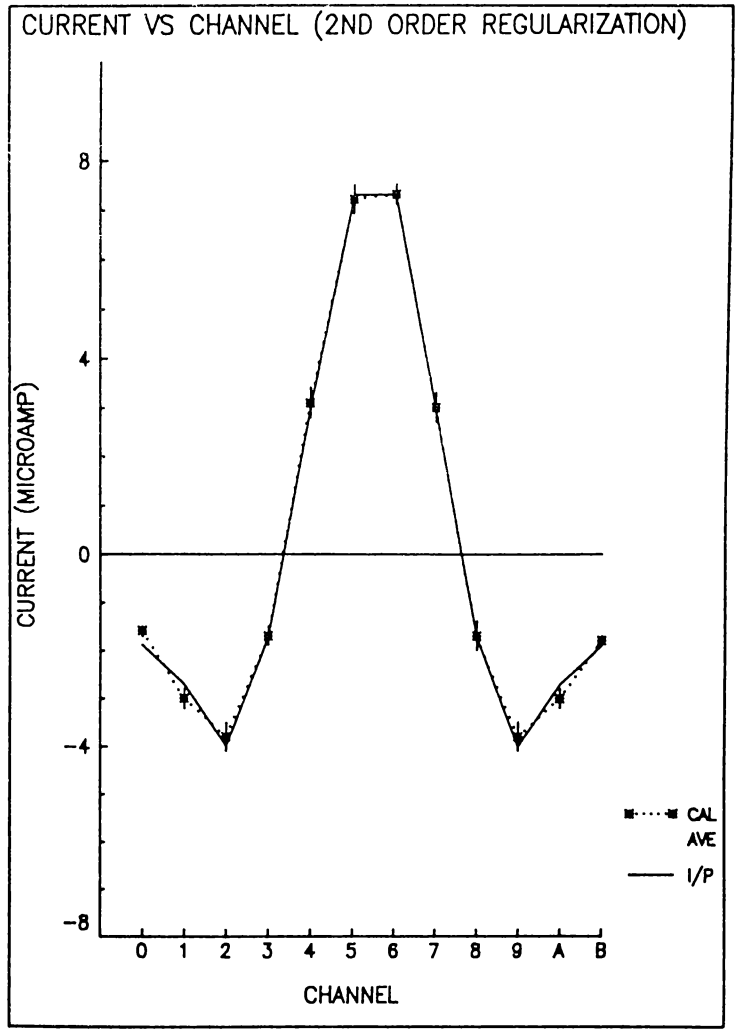
CURRENT VS CHANNEL (2ND ORDER REGULARIZATION)
CURRENT (MICROAMP)
8
4
0
-4
-8
0 1 2 3 4 5 6 7 8 9 A B
CHANNEL
CAL AVE
I/P

(b)

Fig. 3.16

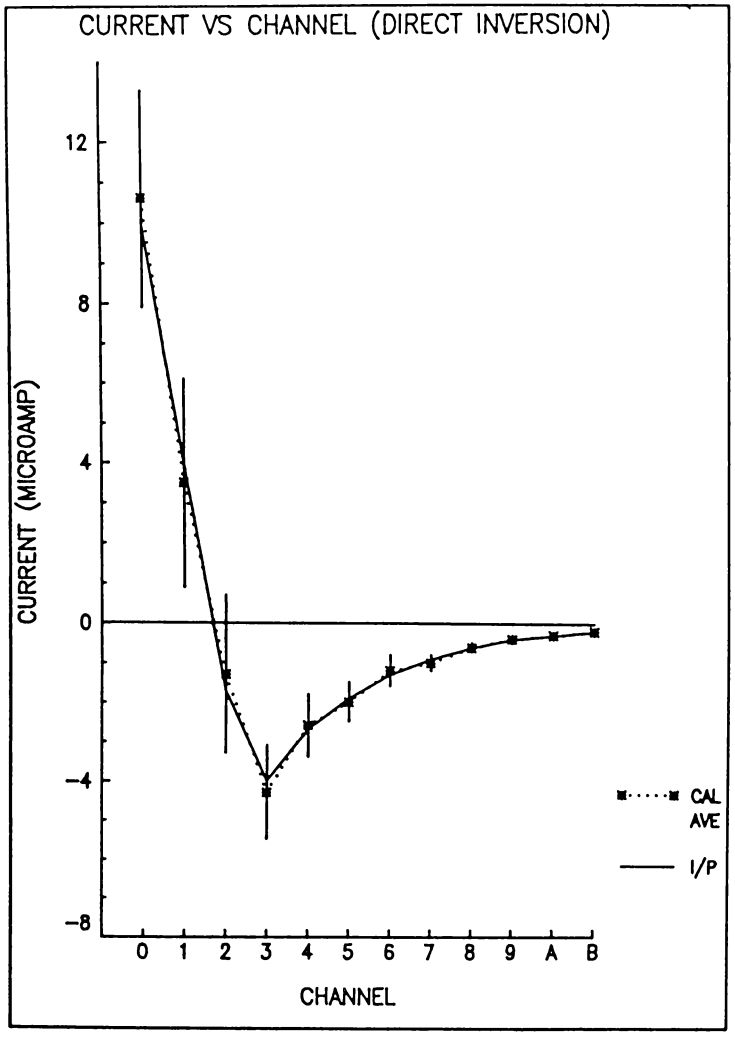
CURRENT VS CHANNEL (DIRECT INVERSION)
CURRENT (MICROAMP)
12
8
4
0
-4
-8
0 1 2 3 4 5 6 7 8 9 A B
CHANNEL
CAL AVE
I/P

(a)

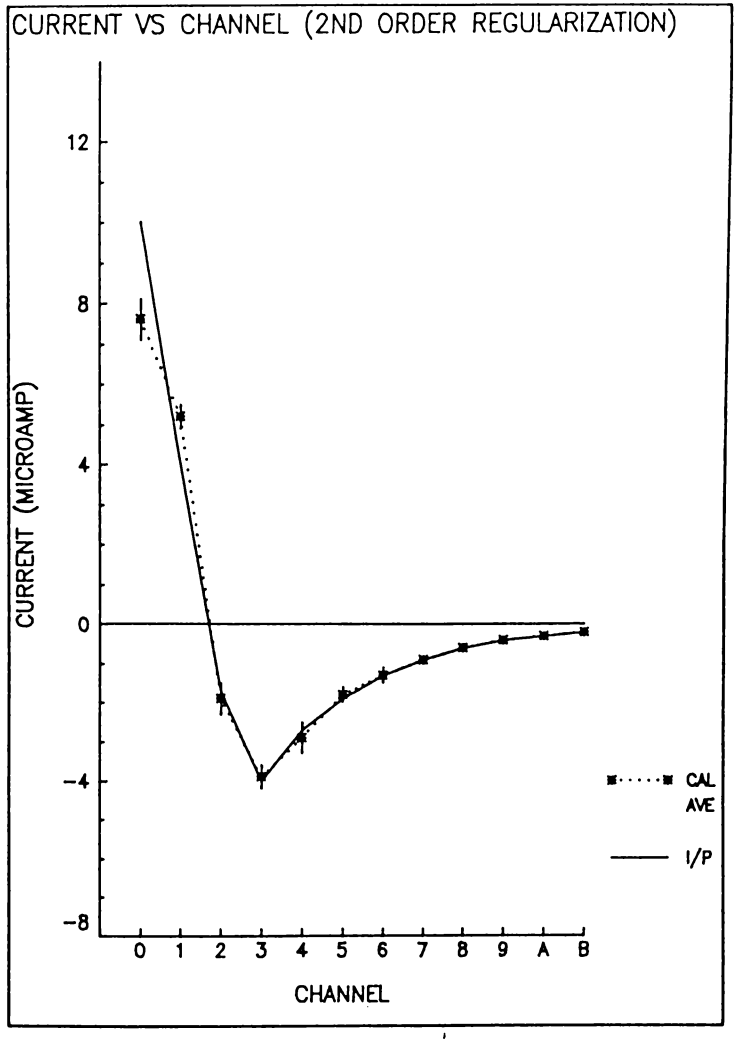
CURRENT VS CHANNEL (2ND ORDER REGULARIZATION)
CURRENT (MICROAMP)
12
8
4
0
-4
-8
0 1 2 3 4 5 6 7 8 9 A B
CHANNEL
CAL AVE
I/P

(b)

Fig. 3.17

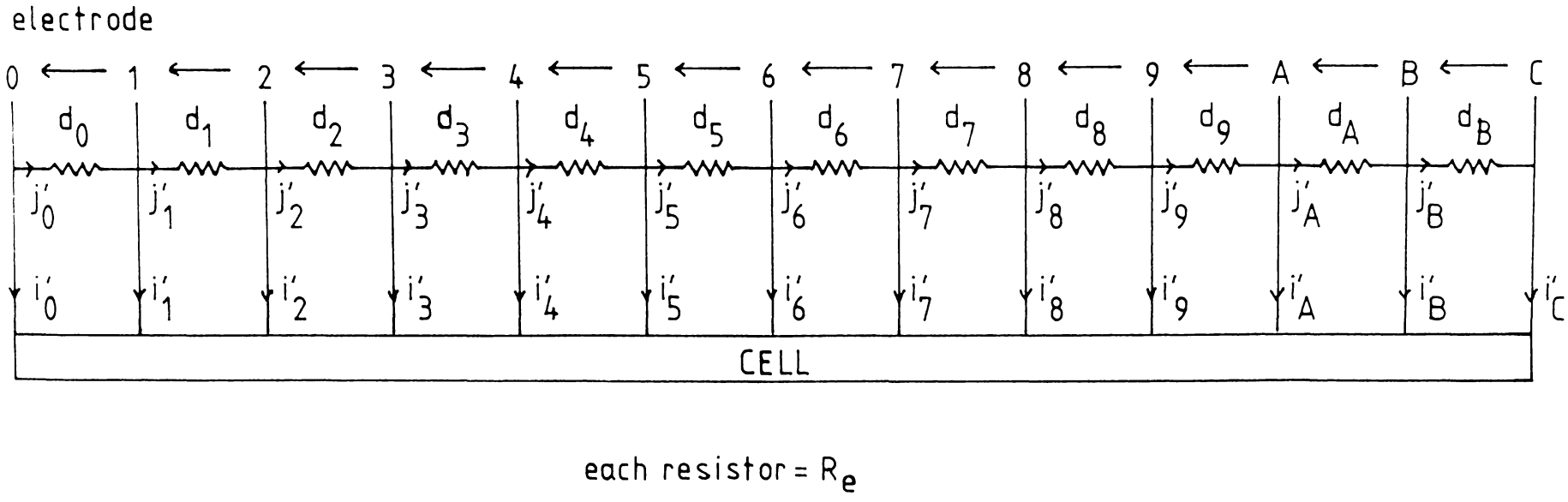

Fig. 3.18 Equivalent circuit model of a cell stem in a cylindrical holder (for simplified equations). R_e represents the resistance of the sheath of external medium between two electrodes, d_n the differential voltage between the electrode pair (n,n+1), and i'_n the transmembrane current flow at the electrode n (n = 0,1,.....,9,A,B for d_n and n = 0,1,.....,9,A,B,C for i'_n).

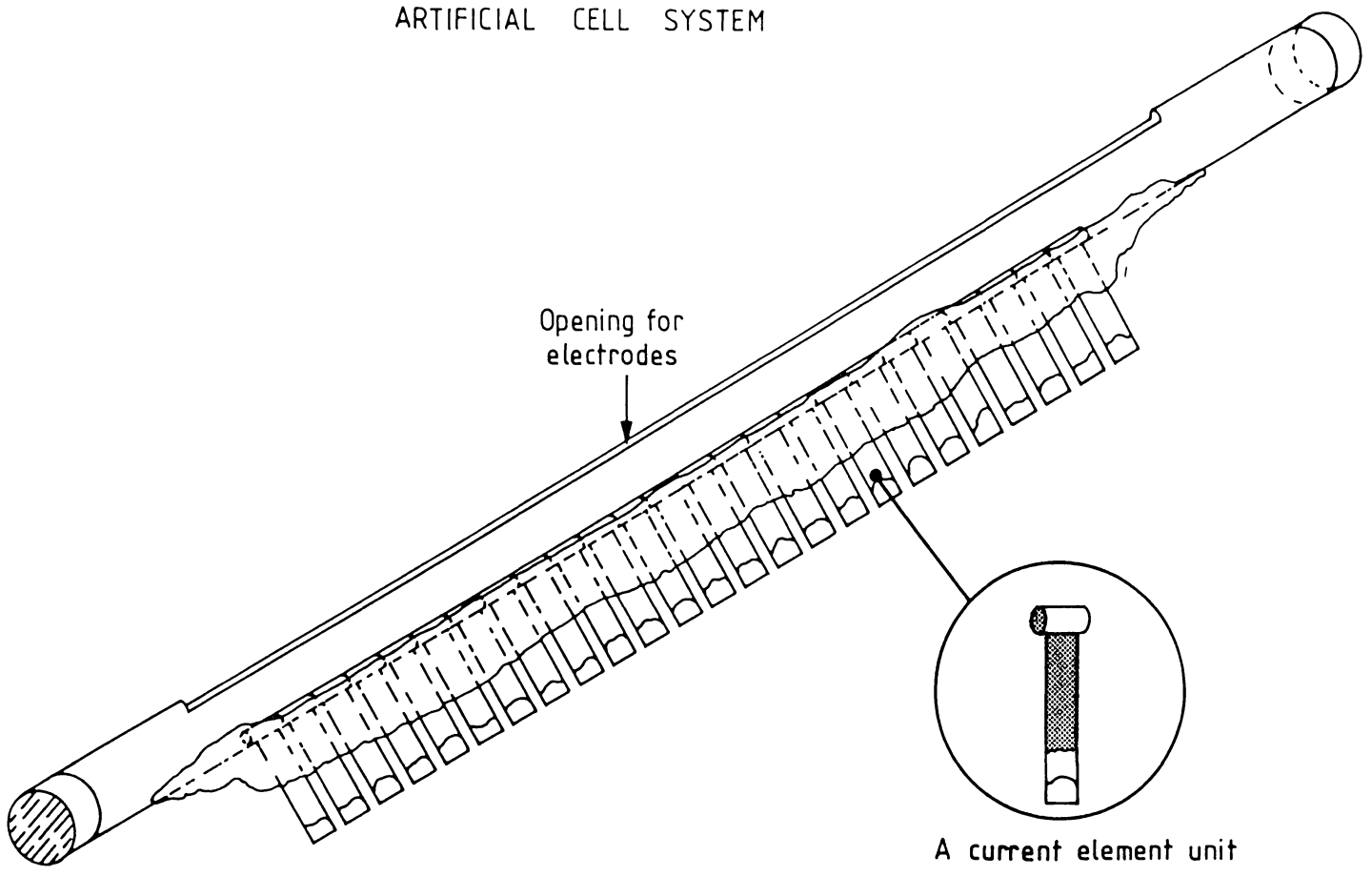

Fig. 3.19 Illustration of artificial cell system.

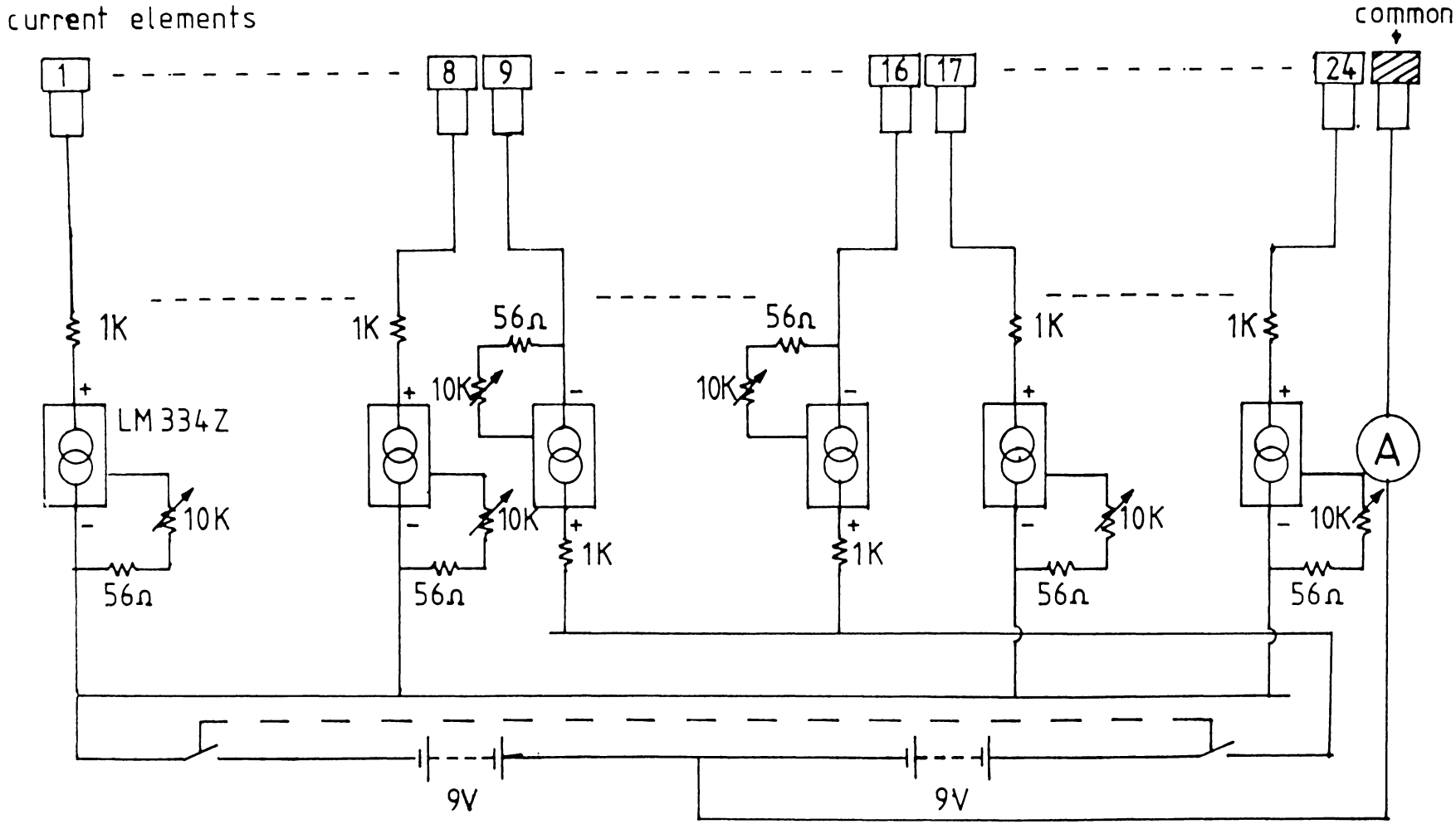

Fig. 3.20 Circuit diagram of current sources.

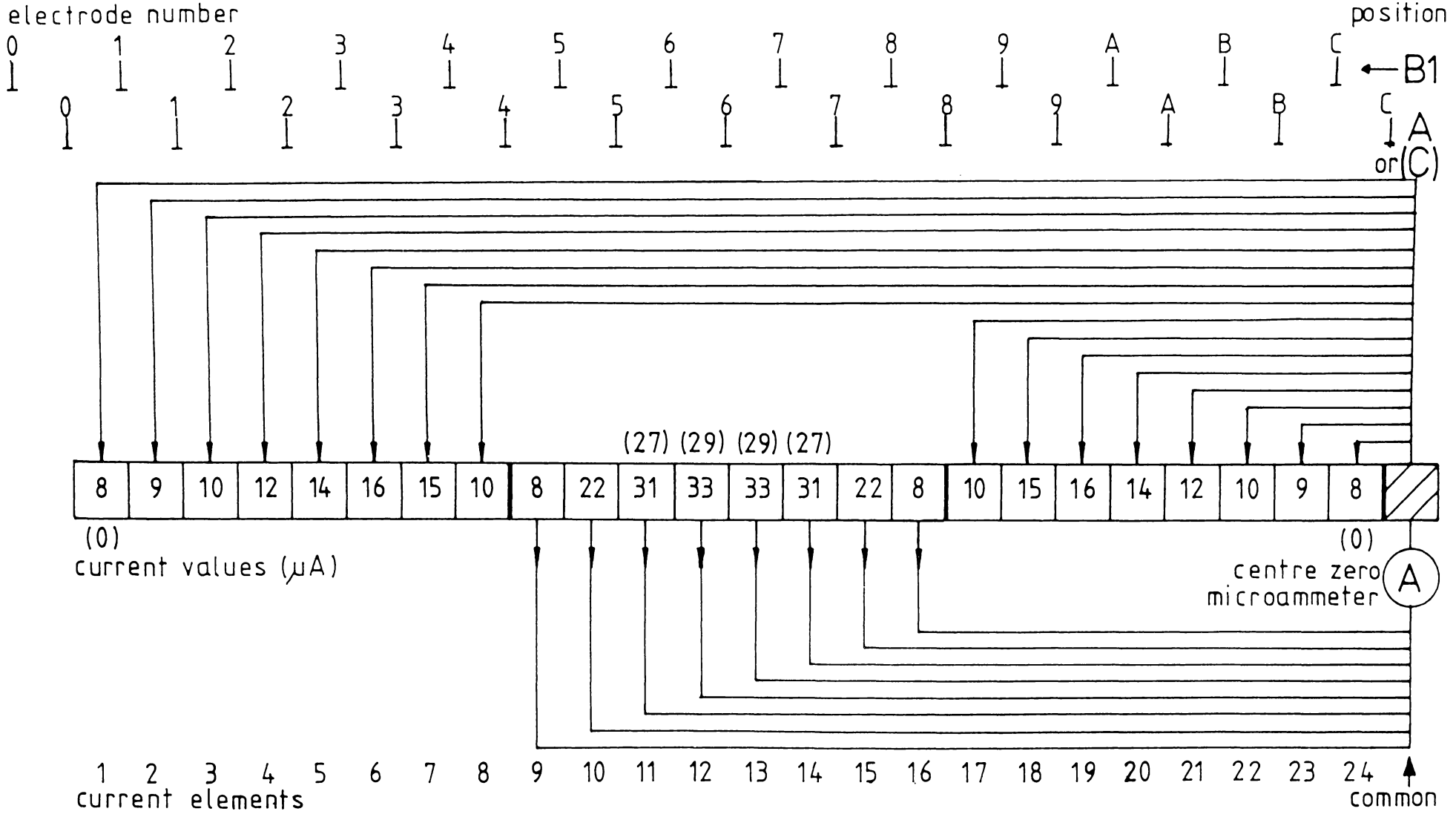

Fig. 3.21 Diagram showing current values assigned to current element units and positions of electrodes (see text).

Fig. 3.22 Examples of experimental results showing

(a) experimental measurement of differential voltage waveforms $\tilde{D}$

(b) current waveforms obtained from (a) by direct inversion

(c) current waveforms obtained from (a) by second order regularization.

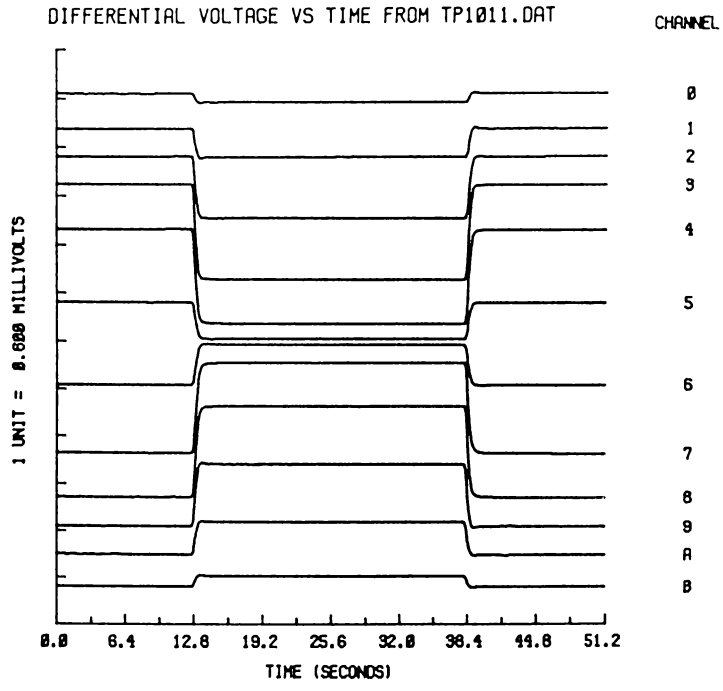

(a)

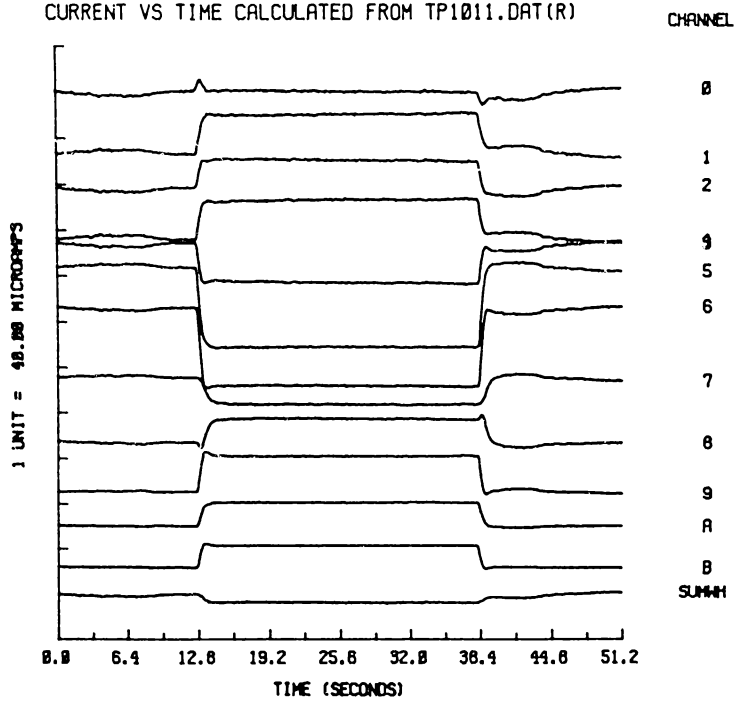
CURRENT VS TIME CALCULATED FROM TP1011.DAT(R)
CHANNEL
0
1
2
3
4
5
6
7
8
9
A
B
SUMM
1 UNIT = 40.00 MICROAMPS
0.0
6.4
12.8
19.2
25.6
32.0
38.4
44.8
51.2
TIME (SECONDS)

(b)

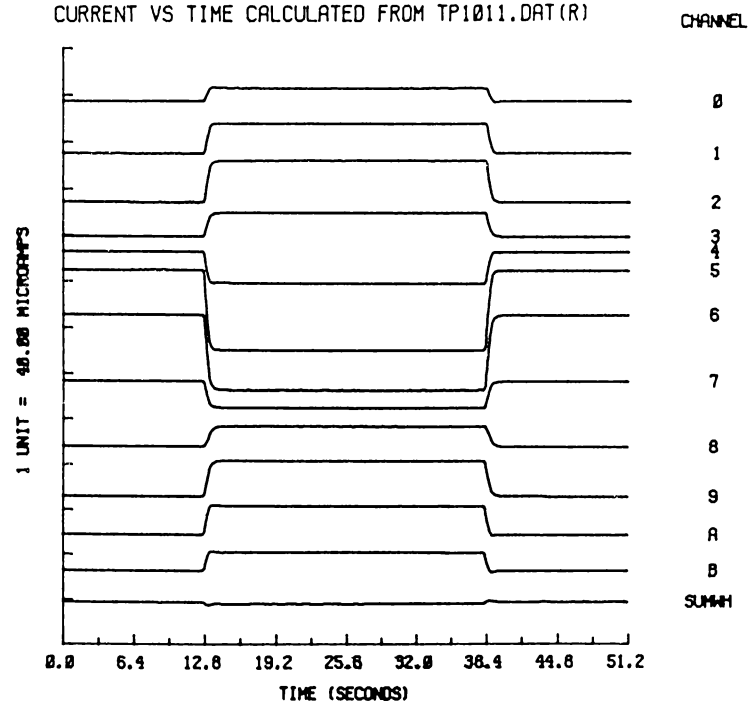
CURRENT VS TIME CALCULATED FROM TP1011.DAT(R)
CHANNEL
0
1
2
3
4
5
6
7
8
9
A
B
SUMM
1 UNIT = 40.00 MICROAMPS
0.0
6.4
12.8
19.2
25.6
32.0
38.4
44.8
51.2
TIME (SECONDS)

(c)

Fig. 3.22

Fig. 3.23-3.25 Examples of current distributions showing simulated input current (I/P) and

(a) calculated current (CAL - from experimental measurement of differential voltage distribution) by second order regularization with estimated error = 3 and 5 % for Fig. 3.23 and 3.24 and = 7.5 and 8.5 % for Fig. 3.25

(b) differences DI = CAL - I/P form calculated current in (a), also withestimated error = 0 % i.e. $\gamma = 0$ = direct inversion

(c) calculated current (CAL) using simplified equations.

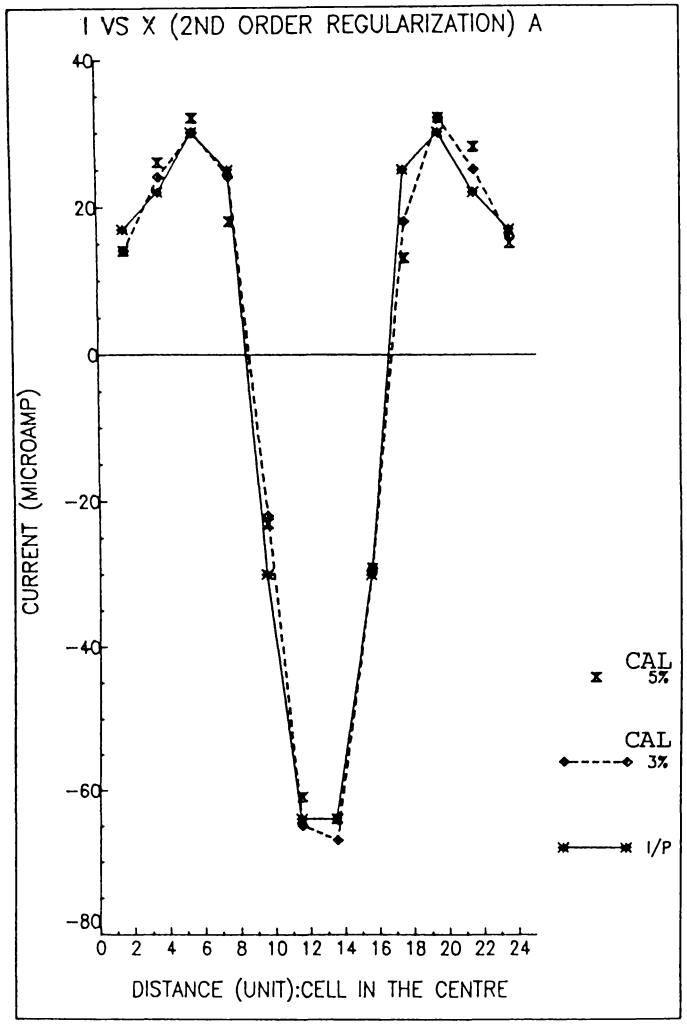
I VS X (2ND ORDER REGULARIZATION) A
CURRENT (MICROAMP)
DISTANCE (UNIT):CELL IN THE CENTRE
CAL 5%
CAL 3%
I/P

(a)

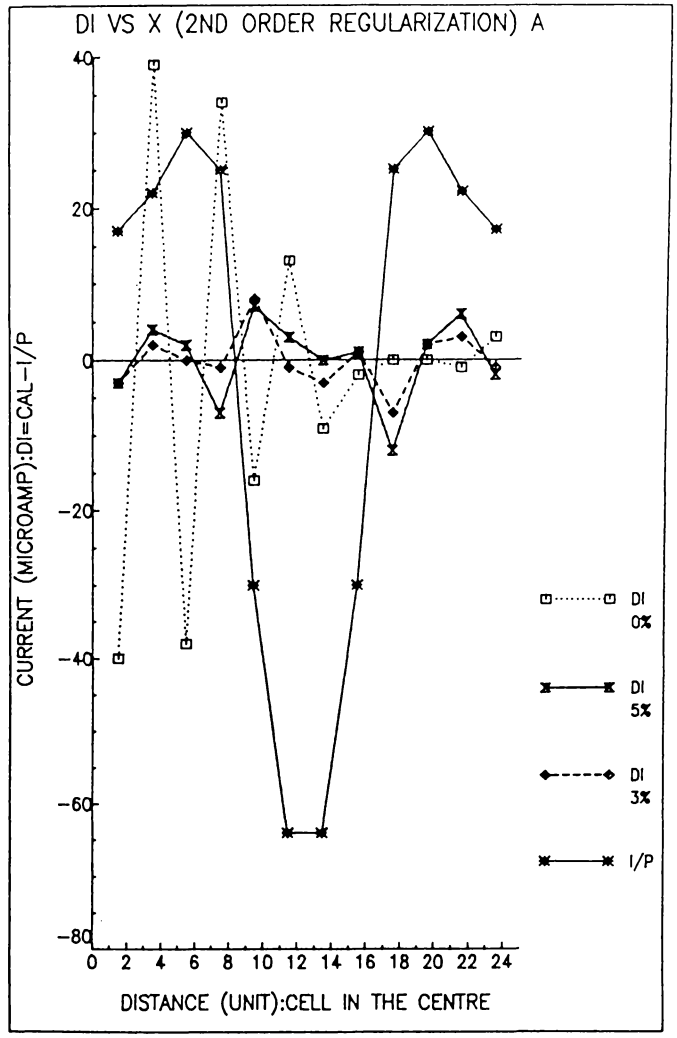
DI VS X (2ND ORDER REGULARIZATION) A
CURRENT (MICROAMP):DI=CAL-I/P
DISTANCE (UNIT):CELL IN THE CENTRE
DI 0%
DI 5%
DI 3%
I/P

(b)

Fig. 3.23

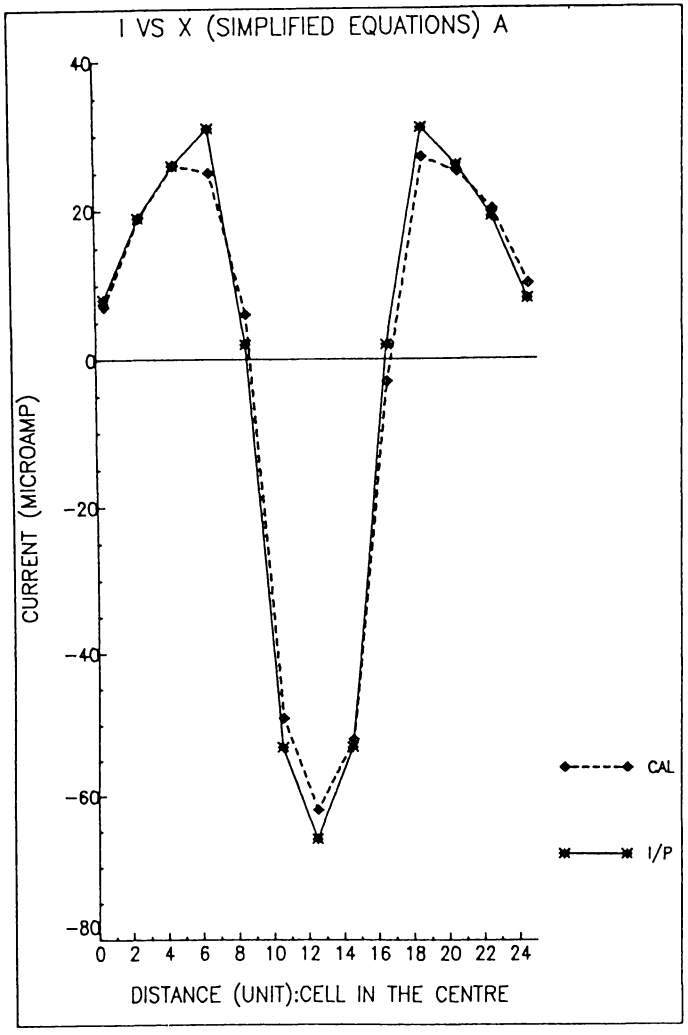
I VS X (SIMPLIFIED EQUATIONS) A
CURRENT (MICROAMP)
40
20
0
-20
-40
-60
-80
0 2 4 6 8 10 12 14 16 18 20 22 24
DISTANCE (UNIT):CELL IN THE CENTRE
CAL
I/P

Fig. 3.23 (c)

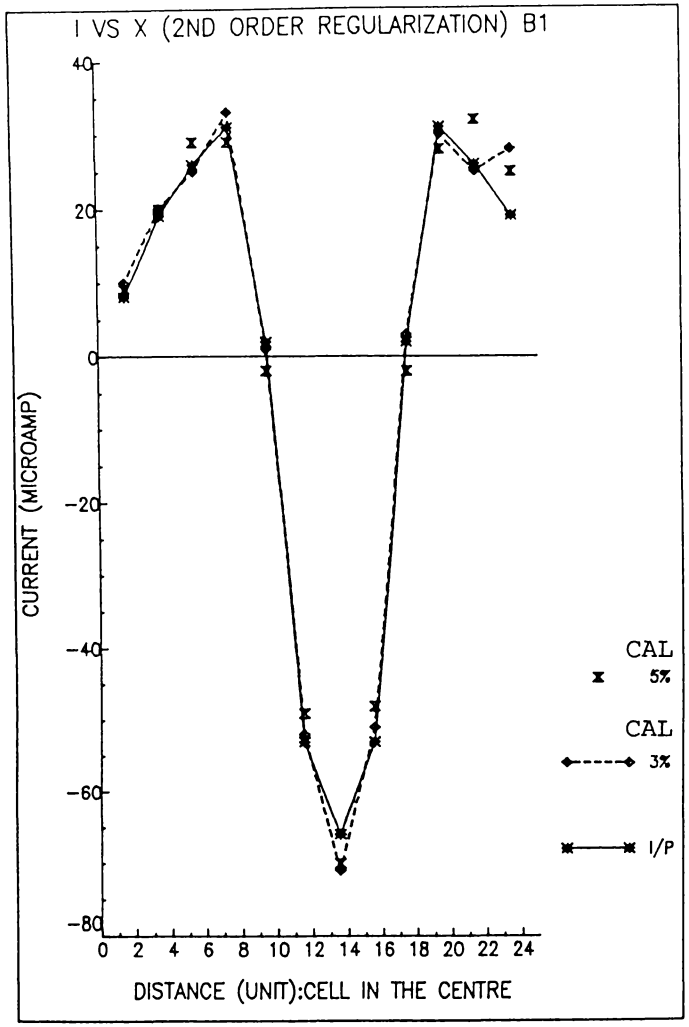
I VS X (2ND ORDER REGULARIZATION) B1
CURRENT (MICROAMP)
DISTANCE (UNIT):CELL IN THE CENTRE
CAL 5%
CAL 3%
I/P

(a)

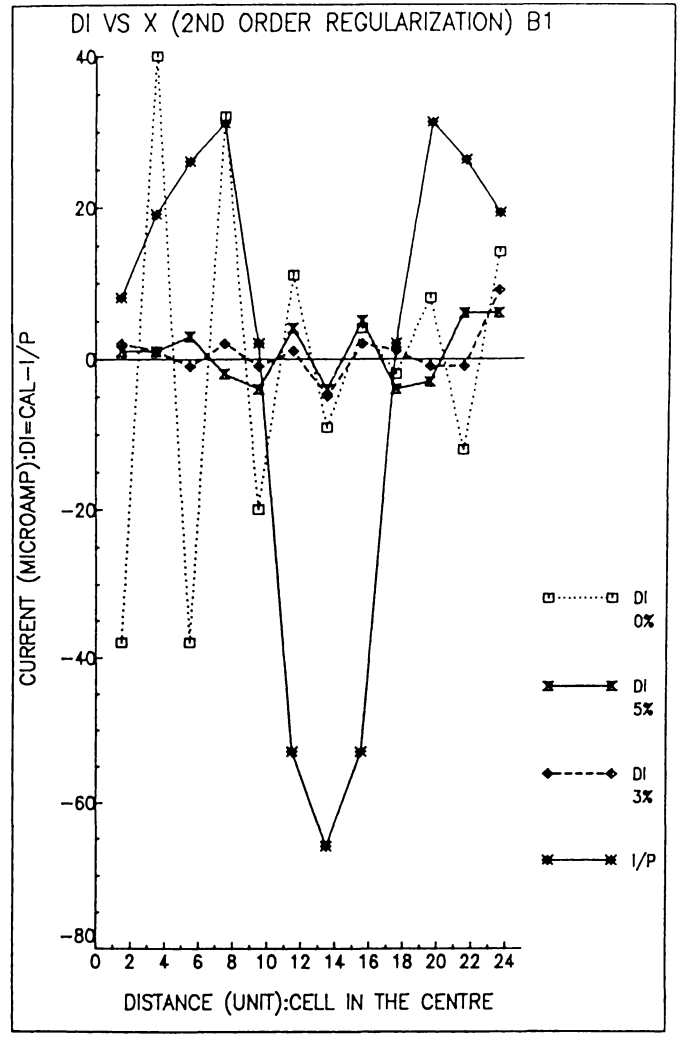
DI VS X (2ND ORDER REGULARIZATION) B1
CURRENT (MICROAMP):DI=CAL-I/P
DISTANCE (UNIT):CELL IN THE CENTRE
DI 0%
DI 5%
DI 3%
I/P

(b)

Fig. 3.24

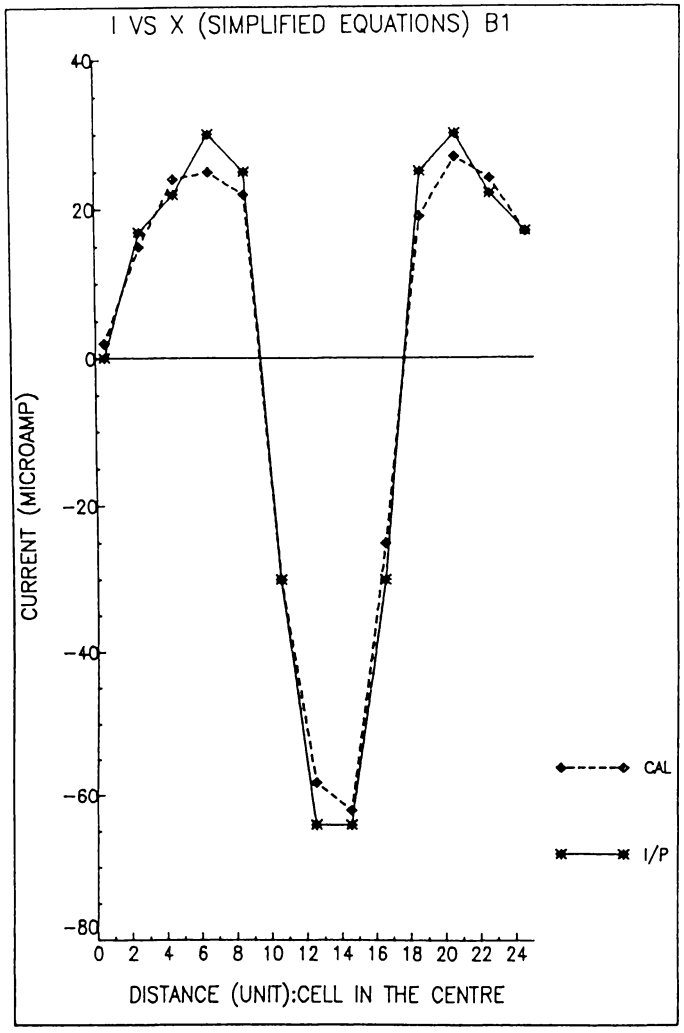
I VS X (SIMPLIFIED EQUATIONS) B1
CURRENT (MICROAMP)
40
20
0
-20
-40
-60
-80
0 2 4 6 8 10 12 14 16 18 20 22 24
DISTANCE (UNIT):CELL IN THE CENTRE
CAL
I/P

Fig. 3.24 (c)

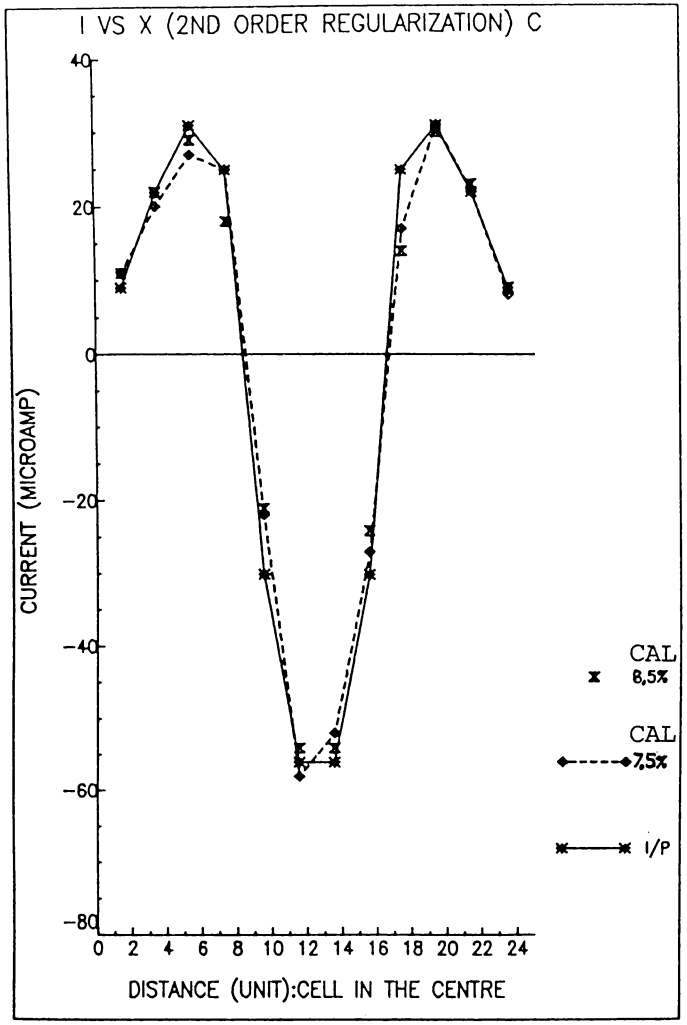
I VS X (2ND ORDER REGULARIZATION) C
CURRENT (MICROAMP)
DISTANCE (UNIT):CELL IN THE CENTRE
CAL 8.5%
CAL 7.5%
I/P

(a)

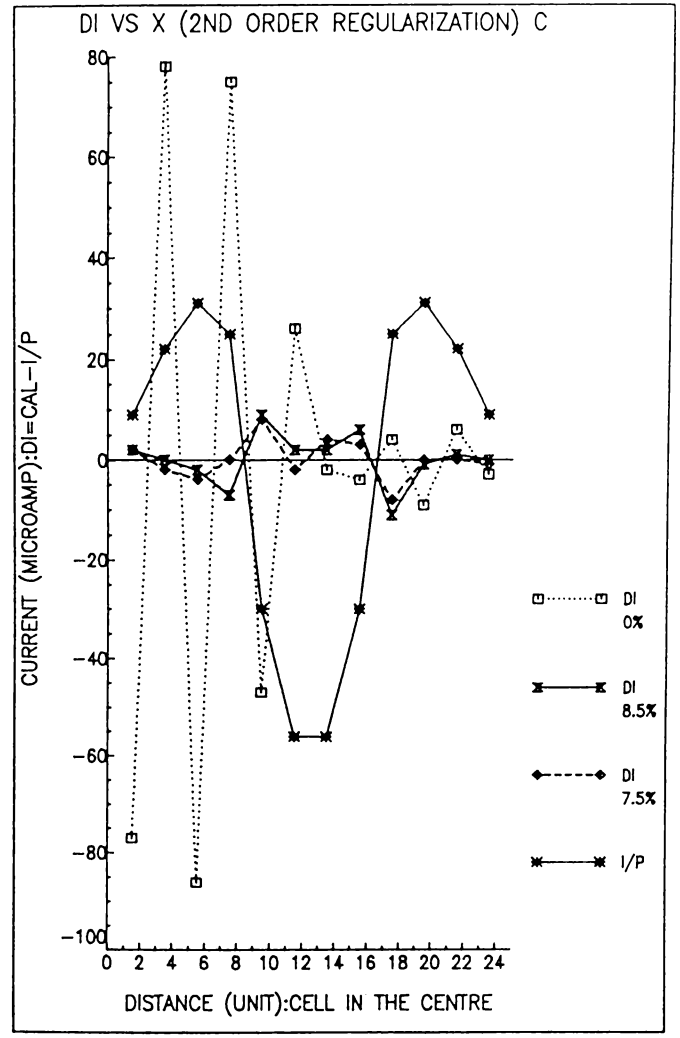
DI VS X (2ND ORDER REGULARIZATION) C
CURRENT (MICROAMP):DI=CAL-I/P
DISTANCE (UNIT):CELL IN THE CENTRE
DI 0%
DI 8.5%
DI 7.5%
I/P

(b)

Fig. 3.25

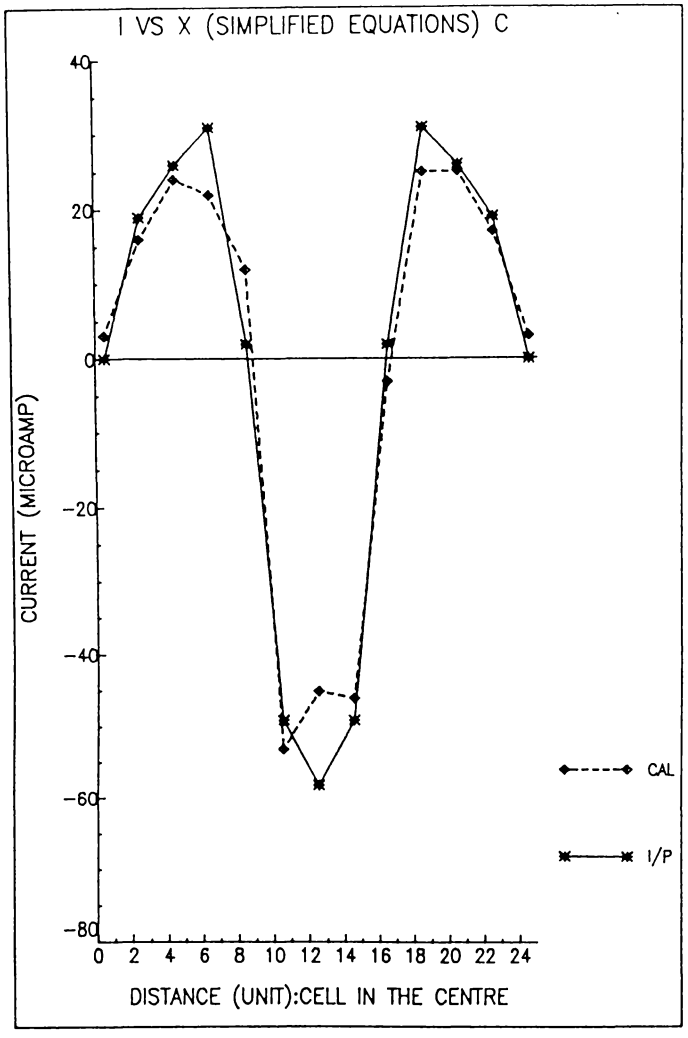
I VS X (SIMPLIFIED EQUATIONS) C
CURRENT (MICROAMP)
40
20
0
-20
-40
-60
-80
0 2 4 6 8 10 12 14 16 18 20 22 24
DISTANCE (UNIT):CELL IN THE CENTRE
CAL
I/P

Fig. 3.25 (c)

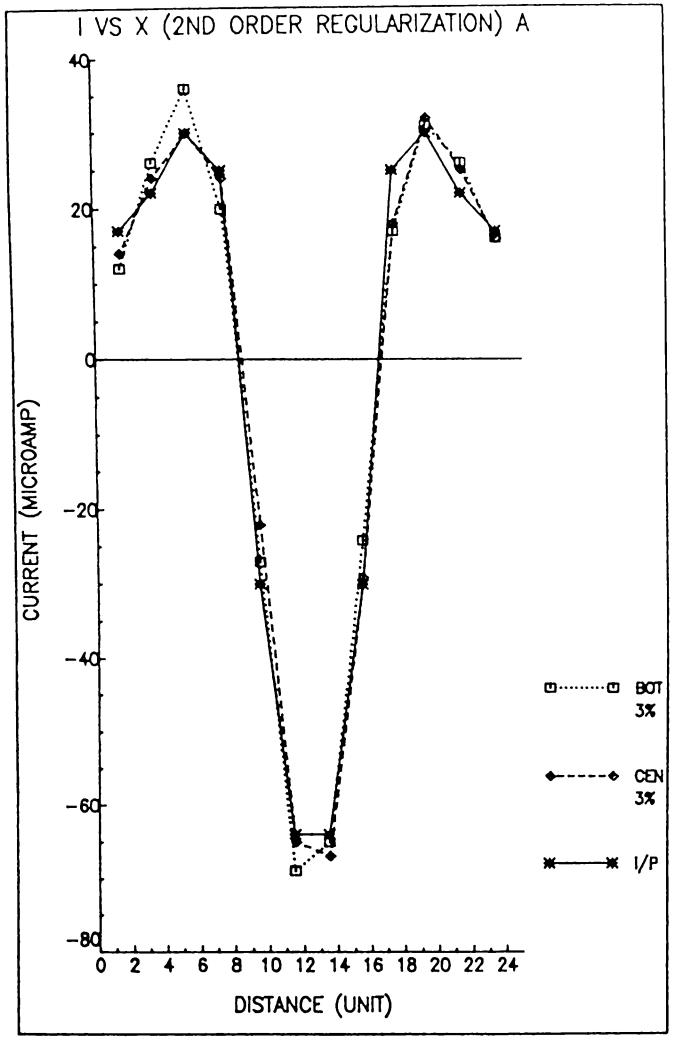

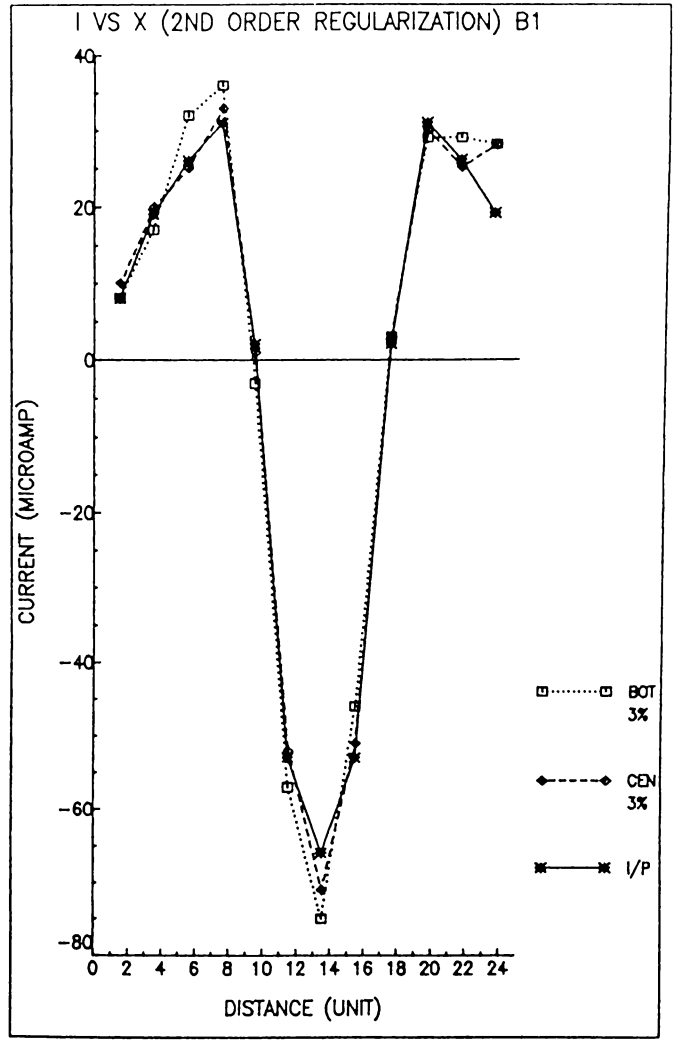

Fig. 3.26 Examples of simulated input current (I/P) and calculated current distributions by second order regularization when current cell units are at the bottom (BOT) and in the centre (CEN) of the tube.

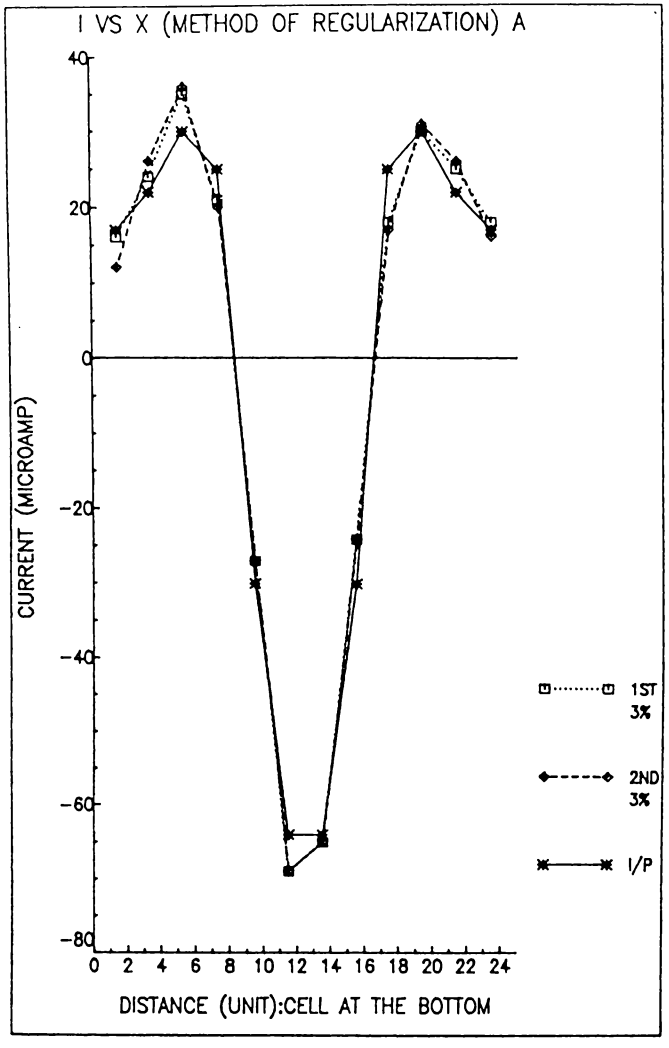

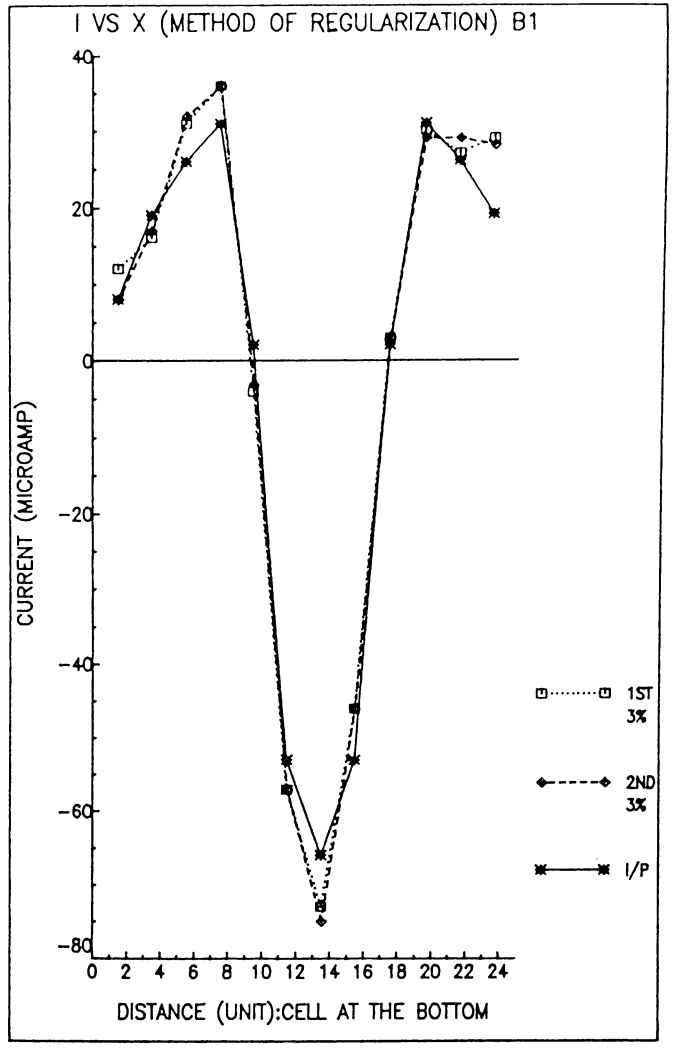

Fig. 3.27 Examples of simulated input current (I/P) and calculated current distributions by first (1ST) and second (2ND) order regularization (with estimated error = 3 %).

CHAPTER 4

MEASUREMENT OF SPONTANEOUS ACTION POTENTIALS IN DEVELOPING ANUCLEATE ISOLATED STALK SEGMENTS

4.1 Culture Conditions and Preparation of Anucleate Isolated Stalk Segments

Laboratory culture of *Acetabularia* has been described in detail by Puiseux-Dao (1970) and Shephard (1970) and the same basic procedure is used in most laboratories. The general aim of this section is to give a brief description of the culturing conditions in our laboratory for the plants of the species *Acetabularia mediterranea* used in our present work. A more detailed description can be found in the work of Lertsithichai (1980).

Young cells of *A. mediterranea* of approximately 5 mm in length were obtained from Professor B.C. Goodwin's laboratory at the University of Sussex and from the C.C.A.P. (Culture Centre of Algae and Protozoa) Cambridge, England. The cells are cultured in one litre bottles. Each of these contains approximately 400 ml of sterile AE50 growth medium, the recipe for which was also supplied by the C.C.A.P. (Appendix 3). In the early stages of growth (~5 mm in length) one bottle would contain approximately 50 cells. Once they reach the size of ~10 mm in length the medium is renewed and the cells are thinned out to ~25 cells/bottle (400 ml of AE50). This amount of medium is sufficient to support the cells until they reach the stage of full maturity (Shephard, 1970).

The culture bottles are kept in a cabinet and are partly immersed in a circulating water bath where the temperature is kept at a constant level of 21 ± 1°C. A dark-light cycle of 12 hours each with ~1400-1600 lux provided by two 65 watt, no. 55 daylight, Thorn fluorescent lamps was maintained.

The cells used in the experiments were without cap (with or without whorl) with a length of 18-25 mm. The diameter of the cells was in the range of .25-.35 mm. For each experiment 8-10 cells were selected and placed in sterile petri dishes which contained ≥ 5 ml of sterile AE50 per cell. From each cell the apical segment of 3-5 mm was cut off using a sterile surgical blade. The remaining nucleate segment was kept for six days in the dark and the rhizoid containing the nucleus was then also removed. The remaining *anucleate isolated stalk segment (ISS)* of ~10-18 mm in length was kept in the dark for another day in the first series of experiments and for 4 days in the second series. To prevent excessive loss of cytoplasmic material when the cell was cut, a strand of hair (which had been cleaned and autoclaved) was used to tie the cell at the point where it was to be cut. Approximately 12 hours after each cut, when the newly cut end was sealed, the hair was then removed. Out of these 8-10 cells, 3-5 cell fragments would survive the above preparation. One of these ISS's was then selected for the experiments.

4.2 Electrodes

The electrodes used in our experiments were of the Ag-AgCl type. This electrode consists of a metallic silver base covered with a thin coat of silver chloride. When it is immersed in an electrolytic solution containing a soluble chloride, it operates under an

approximate reversible condition i.e. the reaction which occurs when the electrode operates as a cathode is the inverse of the reaction when the electrode operates as an anode (see e.g. Benedek and Villars, 1979; Ferris, 1974; Janz and Ives, 1968). Silver chloride is relatively insoluble and therefore does not significantly contaminate the solution in which it is immersed.

Each electrode was made from Teflon coated high purity silver wire (99.99%). One of the factors which will affect the signal obtained from the electrode is the surface area. Electrodes with larger surface areas provided a more stable and less noisy signal than ones with a smaller area. In order to increase the surface area of the electrode within a certain overall length, we wound the wire into a loose helix. To prepare the electrode ~30 cm of 0.35 mm diameter wire was used. The Teflon coating over ~20 cm of this wire was removed and the wire was wound to form a loose helix of ~1 mm external diameter. This was the part which would become the Ag-AgCl electrode. The remaining 10 cm (still insulated) acted as the connection between the electrode and the signal processing system (see later). The outer ~0.05 mm of the wire which might contain excess impurity was removed by using HNO_3, and the wire was then washed thoroughly with distilled water.

When the electrodes were chlorided, an electrolytic cell was used as shown in Fig. 4.1; the electrodes were the anode. A group of wires (16) was chlorided at the same time in order to obtain the same amount of coating of AgCl so that the electrodes would vary from each other as little as possible. The electrolyte was 0.1 N HCl. The cathode material was also silver wire but of a larger diameter. The current in the cell was limited to about 1-3 mA cm^{-2} of anode surface by adjusting the variable resistance R (Fig. 4.1). The length of the

time that chloriding took place determined the depth of the AgCl layer. Generally 10-25% of the silver core should be converted to AgCl for stable electrodes (Janz and Ives, 1968). In practice we normally chlorided the electrodes twice, each time for 2-3 hours. After the first coating (of AgCl) the electrodes were left short circuited to each other for a few hours (to reduce the bias potentials between electrodes) before the electrodes were chlorided the second time. After terminating the process the electrodes were again short circuited by connecting all the non-chlorided ends together and leaving the chlorided parts in the electrolyte for at least 24 hours in order to stabilize the potential differences between them. All processes were conducted in the dark. Out of 16 electrodes, 13 with the least potential differences between them (typically 0.2-0.4 mV) were selected. These electrodes were then inserted into a set of glass tubes, which contained AE50 medium, and the tops of these tubes were sealed (see Fig. 4.5). The set of electrodes was then left short circuited together for further stabilization for another 2 days before it was used in the experiment.

4.3 Cell Holder Assembly and Medium Feed System

The cell holder assembly used in the experiments (Fig. 4.2) was designed to suit the long term measurement of the action potentials generated by the ISS of *A. mediterranea* during redevelopment. The action potentials were measured from the *action current* in the extracellular medium and hence we would like the volume of medium surrounding the cell to be limited in order to obtain a large signal but still sufficient for normal cell growth. This was achieved by

placing the cell in a glass tube with a small inner diameter and arranging a constant transport of medium through it. The use of a glass tube also provided the regular geometry of the conducting medium which was assumed in our circuit model and enabled us to observe the development of the cell through a zoom stereomicroscope.

On one side of the tube a radial slot opening was made along ~2/3 of the length to allow insertion of a set of electrodes (Fig. 4.3a). This opening was made just large enough to allow a tight fit by the tips of the electrode assembly. During the experiment the glass tube was held firmly in the cell holder by two pieces of perspex and nylon screws as shown in Figs. 4.3a, b. The part of the glass tube with no opening extended beyond the end of the perspex block. The top cover piece had a slot which allowed the electrode assembly to be inserted into the opening of the glass tube which had been aligned to be in the middle of this slot. The electrode assembly was partly supported in its position by the opening in the glass tube and partly by the bottom supporting block (Fig. 4.3b). When the cell holder was placed inside the container (made of perspex) (Fig. 4.2), the extended part of the tube, which had been fitted on with an "O" ring, was slid through the hole in the partitioning wall of the container. The presence of the "O" ring ensured a complete separation of the solution between the two compartments except through the glass tube (Fig. 4.5).

As previously mentioned the volume of medium surrounding the cell was limited due to the small size of the tube. The holder was designed to include a feeding system which would allow continuous supply of growth medium to the developing ISS. The feeding system consisted of a bottle with a controllable outlet as shown in

Fig. 4.4. In use the end of this outlet was connected to one end of an L shape glass tube. The other end of this tube was fitted with a hypodermic needle to allow fine adjustment of the amount of the feeding medium flowing into the container below. The top of the bottle was tightly fitted with a rubber bung which had two openings, one to allow inlet of air and the other to allow refill of the medium (this one was closed during the experiments). The air inlet was a long glass tube which extended deep into the bottle, its end being only a few centimetres above the medium outlet. The other end of the tube was connected to a larger glass tube filled with glasswool. Once the medium outlet was opened the medium would flow into the cell holder assembly. The air which would replace the space left by the outflow of the medium had to travel down the air inlet tube before it could float up to the medium surface to replace the lost volume. This in effect kept the flow rate of the medium constant by maintaining the same hydrostatic head (i.e. the depth of liquid between the end of the air inlet and the level of the outlet).

The medium flowed (dripped) into the left compartment of the cell holder assembly (Fig. 4.5) which created a higher level of medium in this compartment compared to its neighbour. Then the medium would flow into the next compartment through the glass tube containing the cell. The level of the medium in the right compartment was kept at a constant level by an opening in the right hand wall (Figs. 4.2, 4.5). As long as there was a constant flow of medium (from the bottle) into the left compartment, the result would be a continuous supply of medium to the cell.

4.4 Signal Processing Electronics

A block diagram of the system is shown in Fig. 4.6. Prior to each experiment the amplifiers were adjusted for correct gain. The pre-amplifiers used in the present experiments were developed in this laboratory by C. Williams (1984) using commutating auto-zero IC amplifiers to minimize DC offset drifts. This enabled us to make higher precision measurements than those obtained previously (Lertsithichai, 1980). The circuit diagram of this pre-amplifier is shown in Fig. 4.7. The advantages of this new system are the reduction of input offset voltages and the input offset voltage drifts. A gain of 500 times was selected to accommodate the offset voltages associated with the Ag-AgCl electrodes (i.e. potential difference between any pair of electrodes; for a bad pair this voltage drift can be up to ~±5 mV during the period of the experiment).

During the experiments the electrodes were connected to the inputs of the pre-amplifiers as shown in the diagram (Fig. 4.6). The output of each pre-amplifier was the input of the corresponding main amplifier which had a gain of 4.882. Altogether the signal was amplified 2441 times. This specific amplification was chosen so that the least significant bit of the ADC (analog-to-digital convertor) output and the associated computer word was equivalent to 1 μV. This avoided the need for any floating-point scaling operations in the subsequent computer processing and enabled simple integer arithmetic and print-out routines to be used.

Each of the main amplifiers also had a variable offset control in which the steady state voltage input (i.e. the bias electrode potential) could be set to zero. From the main amplifiers up to four

outputs could be connected to the inputs of a 4 channel trigger unit. This unit had a variable level at which the trigger *rate of change* of the voltage could be set for both sign and magnitude (from 0 $\mu V\ s^{-1}$ to ~$\pm 20\ \mu V\ s^{-1}$) (Fig. 4.8). Other controls on this unit included supression of triggering (which could be caused by some electrical interference or changes in the voltage values during zero offset adjustments) and manual triggering. The output of this unit was also monitored by the computer.

4.5 Computer Programs

In order to store the data during the experiment and recall it subsequently for analysis, we relied on two computer programs. One was named TR363E, the *transient recorder program* and the other was TDDP2E, the *transient data display program*. In this section we shall mention briefly the features provided in these programs which were developed by Mr S. Lertsithichai and Dr R.A. Sherlock (see Lertsithichai, 1980).

4.5.1 The Transient Recorder Program - TR363E

This program deals with the recording and storing of data. The main features of the program are as follows. After loading the program the visual display unit (VDU) which is connected to the computer will display the description of the program. A copy of the text which appears on the screen can be obtained by enabling the auxiliary port which connects the printer to the VDU. We need to enter the following parameters:

(i) time interval between samples

(ii) first channel (i.e. electrode) to be recorded

(iii) number of channels to be included

(iv) record length (i.e. number of points in time)

(v) number of samples to be included after the triggering (by trigger unit)

(vi) name of the experiment.

We should note here that the voltages at the different electrodes are sampled continuously at the prescribed intervals. If there is a transient change of the voltage (in a channel that is connected to the trigger unit) above the set rate the program will store a data record as specified by the parameters above.

The initialisation process is handled by *main-1*, which is the first of three main parts of the program. After termination of this part the program proceeds into the second part *main-2*, which controls the continuous monitoring of the electrode potentials. This is the heart of the program. It also provides a logging printout of the voltage values from all channels (as specified by (ii) and (iii) above) every 30 minutes provided there is no recording of any transient (action potential) underway. *Main-2* also keeps count of time from the starting point and if there is any transient change underway it will record the data specified by the parameters given in *main-1*. It will display the differential voltage $\tilde{D} = \underline{d}(t)$ on the CRT and printout the headings giving the transient number and the time at which the transient occurred. The program then proceeds into *main-3* where the data recorded undergoes a brief analysis for peak values (maximum and minimum), their positions and baseline values. These are displayed on the screen (and echo on a printer if it is connected to the VDU). While the data are being displayed we can decide

whether we want to keep them. If we do not want the data to be stored (due to a false trigger, for example) we press the *SENSE* console switch of the computer. Otherwise the storage of the transient data on floppy disc will take place once the display and printing is finished. Continuous monitoring is also maintained throughout this phase.

For a short period after the storage of the data (i.e. before the regular 30 minute log and provided that there is no new transient recording underway) the approximate current waveforms (using simplified equation) can be computed and displayed on the CRT by pressing the *SENSE* console switch. The peak values of these current waveforms are also analysed and displayed. This enables a useful amount of *on-line* processing to take place to monitor the progress of the experiment. The broad structure and interrelationship of these programs is summarized in Fig. 4.9.

4.5.2 The Transient Data Display Program - TDDP2E

This is the main analysis and display program which is run *off-line* on the transient data sets recorded on floppy disc during the experiment by program TR363E. It enables data to be read from the floppy disc, and various display and analysis procedures (including the solution of the current by the simplified equation) to be performed. The program is controlled by commands given through the VDU terminal. The program prompts with a question mark when it requires a command. In addition, when the laboratory and the University VAX 11/780 computers are linked, the 0 command in this program (together with a data-transfer program in the VAX) enables data files to be transferred to the VAX. This allows the solution

for the current to be obtained from the differential voltage data by second order regularization (see section 3.2.3). The set of commands in the program TDDP2E are given in Appendix 4.

4.6 Experimental Procedure and Data Analysis

Prior to each experiment the electrodes and ISS were prepared as described in sections 4.2 and 4.1 respectively. In addition the feeding bottle which contained AE50 medium and the glass tubes (L shape used in the feeding procedure and the one which held the ISS) were autoclaved. The remaining parts of the cell holder assembly which could not be autoclaved were soaked in 70% ethanol and washed thoroughly with sterile distilled water to reduce the amount of contamination which would be introduced during the experiment.

At the start of the experiment the various parts of the cell holder assembly were put together as shown in Fig. 4.2 with the electrodes connected to the signal processing system. The feeding system was adjusted to give a medium flow rate of 8-9 ml per hour. The ISS was then transferred from the dark into the glass tube under subdued light and its position adjusted so that it lay under the electrodes as shown in Fig. 4.5 (i.e. as assumed in the equivalent circuit model Fig. 3.9). The cell holder, the feeding system and the pre-amplifiers were situated inside a metal cabinet. This cabinet had a hole in the back to illuminate the ISS. The light source was a 12V, 50W tungsten halogen lamp, with a blue filter to give an approximate daylight spectrum at an intensity of ~1600 lux on the ISS. A water filter was also provided to eliminate the heat generated by the lamp and the temperature inside the cabinet was kept at 21 ± 2°C. The lamp was turned off when the ISS was being

transferred. When the ISS had been positioned properly the cabinet door was closed so the ISS remained in the dark. The *transient recorder program* was then started and the experiment was underway. Approximately 1-2 hours after the program was initiated the light was turned on and the ISS was then exposed to continuous white light until the end of the experiment which was ~3-5 days after the onset of illumination. Throughout the experiment the cabinet door was opened only occasionally when microscope observations of the ISS were made and the medium flow rate was checked.

During the experiment the amplifier offsets were adjusted occasionally to give approximately zero electrode potential. The outputs from two amplifiers (i.e. two channels) were connected to the four inputs of the trigger unit which had been set so that it would trigger the recording of the data by the transient recorder program when the signal from either channel passed the set rate of change in either direction (i.e. either positive or negative signal). The trigger rate was normally adjusted to be between $\pm$ (3-6) $\mu V\ s^{-1}$. Each of the outputs of the two channels which had been connected to the trigger unit was also connected to a Heathkit chart recorder unit to give an overall view of the occurrences of the action potentials during the experiment. The experiment was usually terminated when definite redevelopment (e.g. an extended tip) had been observed (~2-4 days) or after 4-5 days if zero or only slight growth was observed. The ISS was then removed and kept in a petri dish for further observation. After the removal of the ISS, current of known values (~10 μA) was injected into the AE50 medium in the glass tube. The voltage generated by this current was then recorded. In this way the resistance of the sheath of the medium between pairs of electrodes

(R_e's) could be analysed. The general value of R_e in an experiment was 36 ± 2 ohm (5% variation between the resistance R_e's in the same electrode assembly).

When no experiment was running the data from the previously performed experiments could be displayed and analysed using the TDDP2E program. This program allowed us to obtain the current waveform I' (in units of $1/R_e$) as calculated by the simplified equation (equation (3.18)) using the ZC or ZG command (see Appendix 4). As has been shown previously (section 3.3) the solution of the current I' obtained through the simplified equation was in general less accurate than that (I) using second order regularization (equation (3.16)). Also in the experiments the ISS's were positioned to suit the equivalent circuit model of Fig. 3.9 rather than that of the simplified equation (Fig. 3.18). Therefore the solution obtained in this way (simplified equation using ZC or ZG command) was only used as an indication of how the more accurate solutions (using equation (3.16)) would look since the general features of the two solutions (of current) are approximately the same. Fig. 4.10c shows an example of the solution of calculated current I using second order regularization, and Fig. 4.10d shows the solution I' from the simplified equation.

Generally a group of consecutive action potentials had very similar features (i.e. same initiation point, propagation behaviour - see chapter 5 for examples and more detail). from these groups one or two action potentials per group were selected and the data were transferred to the university computer for further analysis using second order regularization.

In using the method of regularization the error associated with each measurement was estimated to be ~8%. This error was probably

caused by error in R_e (~±5% see above), amplifier gain (~±1-2%), the different length of the cell between pairs of electrodes e.g. a straight cell section would have less length between a pair of electrodes than a non-straight section (~±4-5%) (i.e. less current was generated within the medium between the two electrodes which it spanned compared to the non-straight section), and amplifier and electrode noise (~±3%).

When using second order regularization the γ chosen was that which gives

$$\text{average } \|R\| \leqslant \text{average } \|E(8\%)\|$$

(see section 3.3). This normally corresponded to the value of $(3\text{-}5)\times10^{-6}$ Fig. 4.10a shows an example of the experimental measurement of an action potential. The direct inversion solution is given in Fig. 4.10b. It shows oscillatory behaviour which is not reasonable and useless for any kind of analysis while the method of regularization produced a well-behaved smooth solution (Fig. 4.10c). From this solution (Fig. 4.10c) the initiation point of a depolarized region could be found by taking into consideration the fact that current enters the cell at the depolarized region (positive current) and leaves the cell outside this region (negative current). Therefore, the region where the current became positive first was the initiation point of a depolarized region or an action potential. In this case (Fig. 4.10c) since i_8, i_9 and i_A were positive the depolarized region was initiated between electrodes 8 and B (c.f. Fig. 3.9). Fig. 4.10c could also be used to investigate the propagation of the depolarized region. Here the depolarized region was initially between electrodes 8 and B and extended towards electrode 0 (see Fig. 4.11). As the depolarization spread the

originally polarized region outside the region between electrodes 8 and B became depolarized i.e. current at that region changed from negative to positive value and this is shown in Fig. 4.11. In this particular action potential the depolarized region extended until it reached electrode 4 before part of it became repolarized (at 75.2 s). The region between electrodes 8 and A which was part of the original depolarized region (8-B) was the last region to return to normal polarized condition. That is, after 88 seconds the signs of $\underline{i}$ remained the same as shown at the 88th second and slowly returned to approximate zero current. Similar behaviour of the movements of the depolarized region(s) (associated with an action potential) were also found in other experiments. Other types of movements of the depolarized region will be given in chapter 5.

Another property of the propagating action potential, the propagation velocity, could also be determined from the time which the depolarized region took to travel a certain distance. Since in the depolarized region the transmembrane current is positive, the velocity of the propagating positive current waveform would give us the approximate propagation velocity of the depolarized region i.e. the action potential. The easiest procedure was to note the peak positions of the positive values of current i_n's. These were provided by the printout of the peak positions and values analysis of the calculated current as shown in fig. 4.10c (note: in this example the first positive peak of i_8 had to be obtained from the graph since the first positive peak was less than the second positive peak and therefore the peak position in the printout was that of the second peak). The plot of these positions is shown in Fig. 4.12 which is a linear graph (correlation coefficient = 0.99). This indicates an approximate uniform propagation. from the slope of this graph the

propagation velocity could be obtained. In this example

$$\text{slope} = \frac{\text{channel \#4 - channel \#9}}{\text{position 91 - position 83}}$$

$$= \frac{5}{8} \frac{\text{channel}}{\text{position}}$$

Since the distance between two electrodes (i.e. from one channel to the next) is = 1.6 ± 0.1 mm and the time between each position is = 0.8 second. We have

$$\text{slope} \times \frac{1.6 \pm 0.1}{0.8} = \frac{5}{8} \times \frac{1.6 \pm 0.1}{0.8} \frac{\text{mm}}{\text{s}}$$

i.e. propagation velocity = 1.3 ± 0.1 mm s^{-1}.

Thus through these procedures a number of properties of the action potentials generated by the ISS'S during redevelopments could be found. This method of analysis (using I) helps to make this task much easier than using the differential voltage $\tilde{D}$ (section 3.2.1) in which we need to look for both the maximum positive and maximum negative values of $\underline{\tilde{d}}$ to be able to identify the position of the depolarized region. By using the current I (as shown above) we need to look only for the positive components of $\underline{i}$ to locate the depolarized region. Also in most cases, using the current I proved to be more accurate. For example Fig. 4.13a shows a differential voltage $\tilde{D}$ which seems to indicate a propagating action potential due to the delay of the peak positions from $\tilde{d}_2(t)$ to $\tilde{d}_6(t)$. However, the current solution I (Fig. 4.13b) reveals otherwise i.e. it is a non-propagating action potential. Although the method of analysis using $\tilde{D}$ is less accurate in predicting the propagating behaviour than using the current I, it has been shown to be accurate in identifying

the initiation site of an action potential (Thavarungkul, 1980, see also section 3.2.1) and has proved useful in some cases where we were unable to obtain the solution of current I. This occurred in two experiments (AH and BG, see chapter 5) where there was a data storage unit malfunction and some of the data could not be stored during the experiments. In these cases we were left with the printout of the extrema of the measured $\tilde{D}$ as shown in Fig. 4.14 for each action potential and the waveforms as recorded by the chart recorders (increased to 4 recorders instead of the normal 2). From these we were still able to identify the initiation sites of the action potentials. Thus by using the combinations of these three methods of analysis the features and the properties of the spontaneous action potentials produced by the regenerating ISS's could be studied. The results of the experiments are presented in chapter 5.

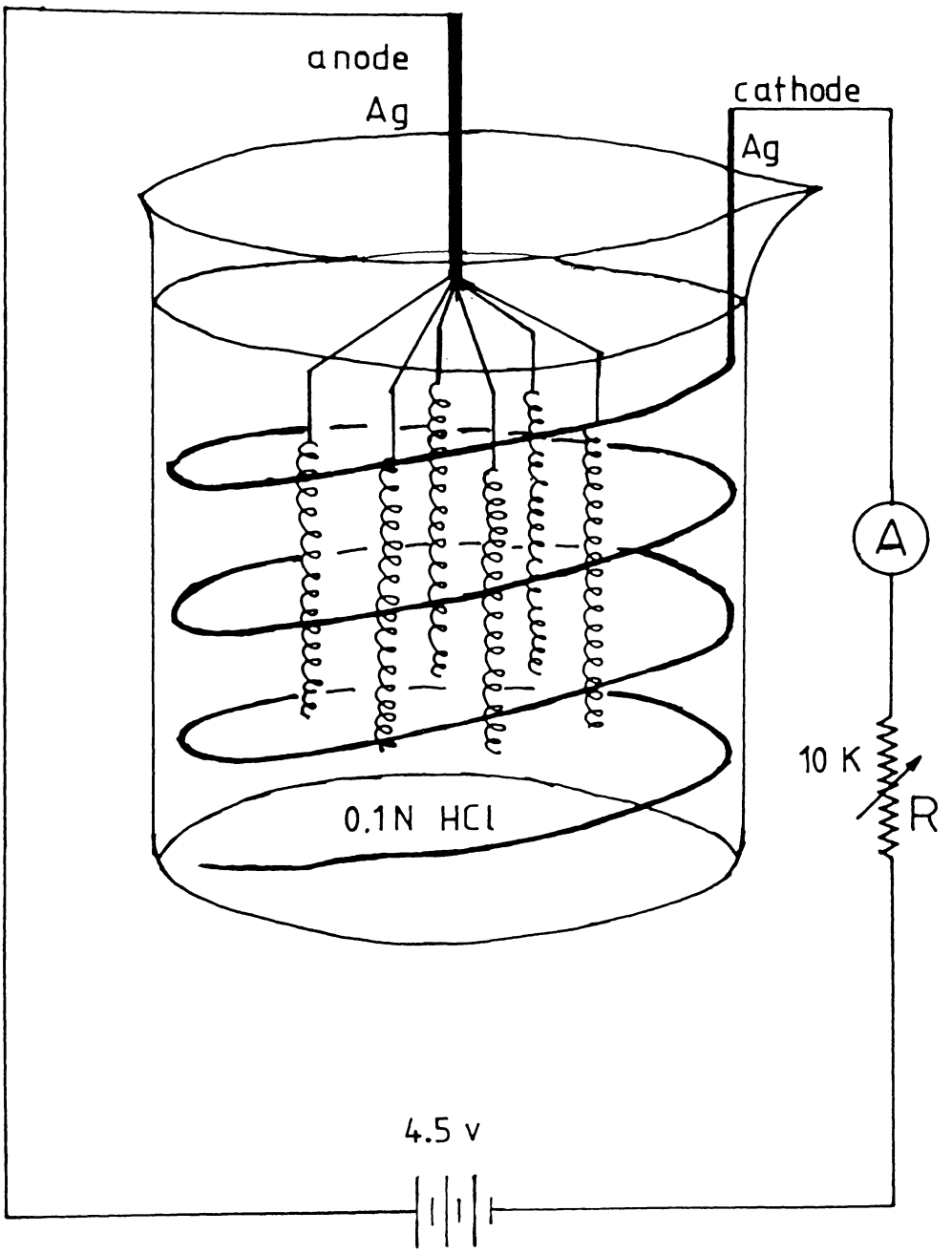

Fig. 4.1 An electrolytic cell used to chloride electrodes (six only shown).

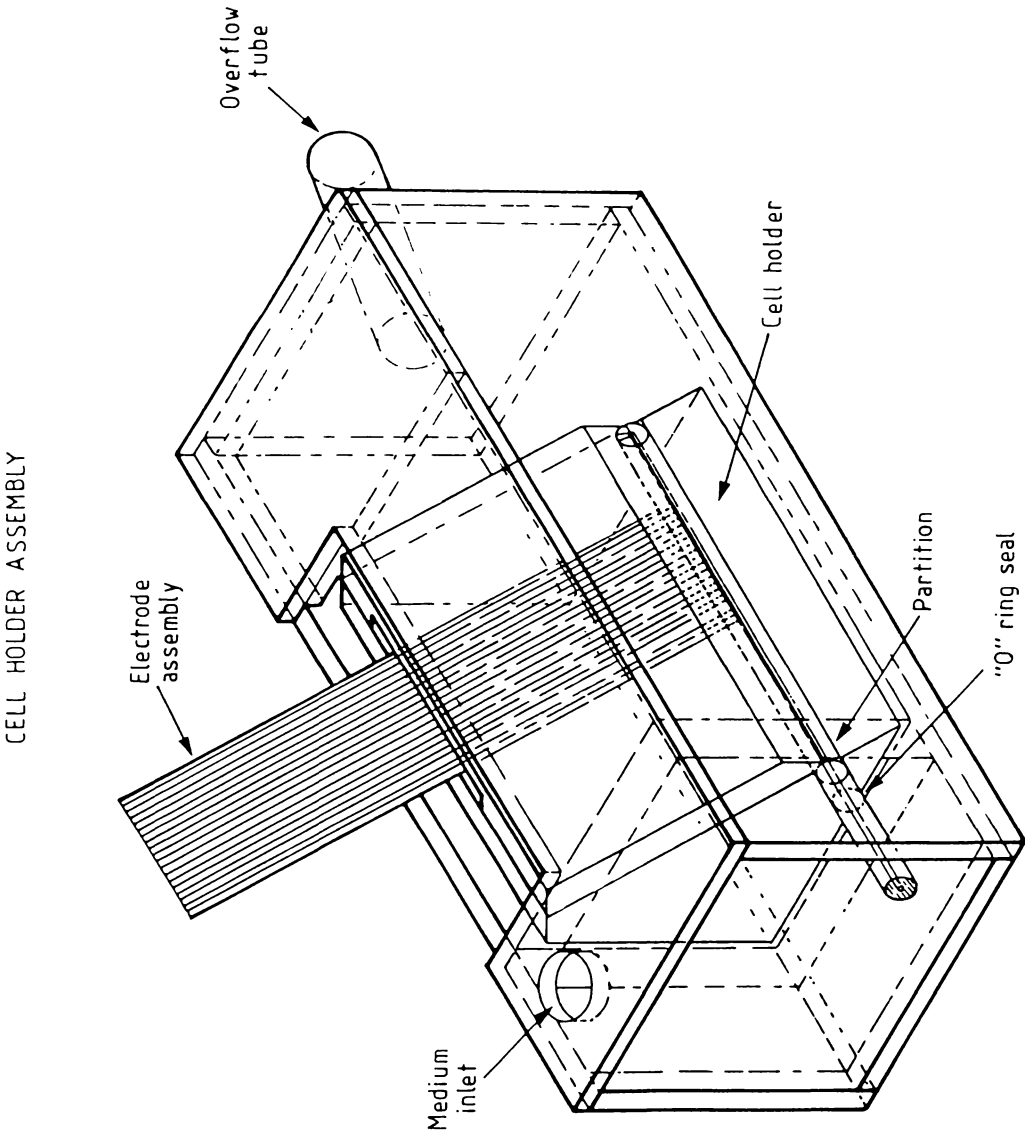

Fig. 4.2 Illustration of cell holder assembly.

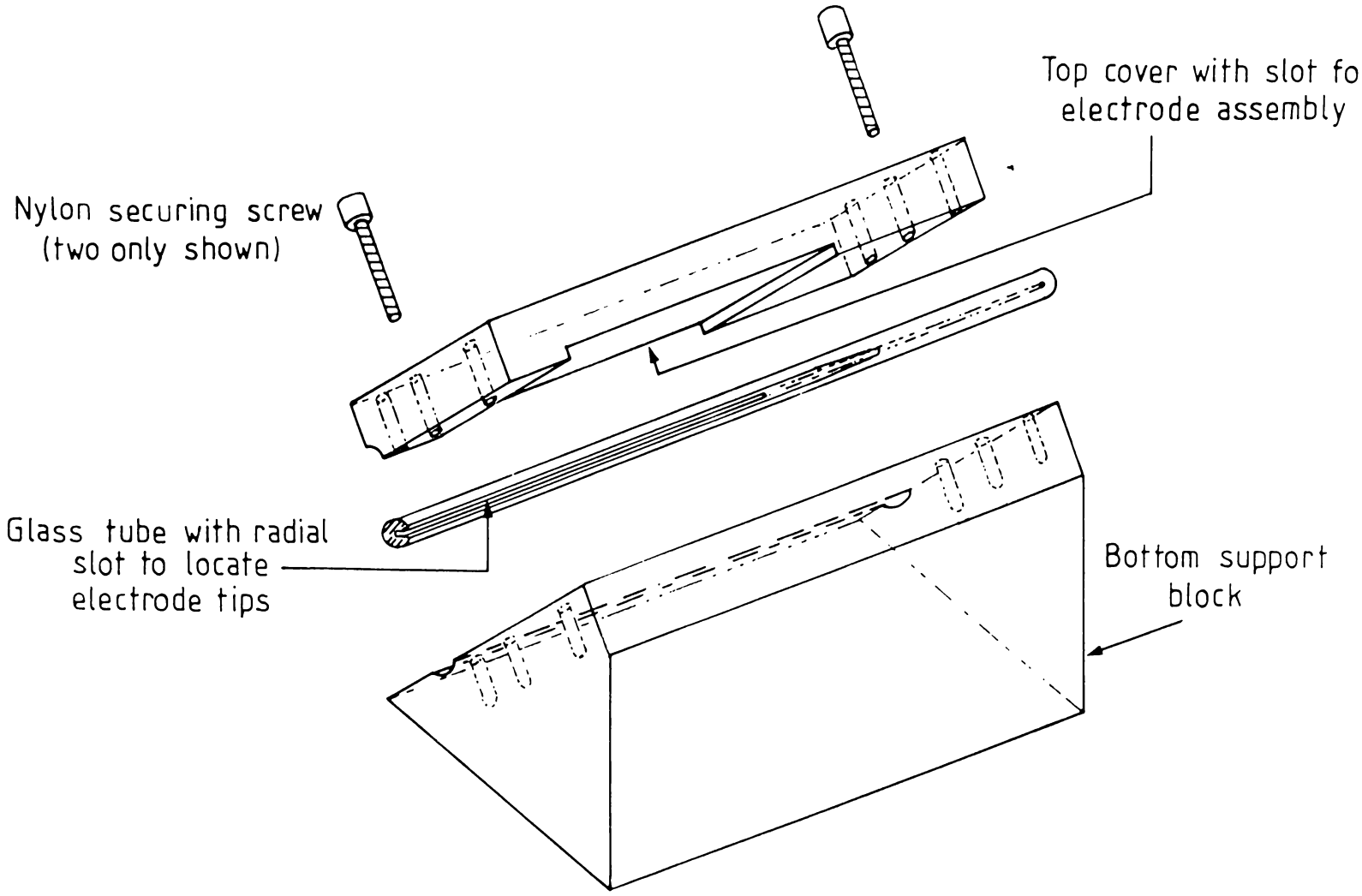

Fig. 4.3 (a) Illustration of various parts of the cell holder.

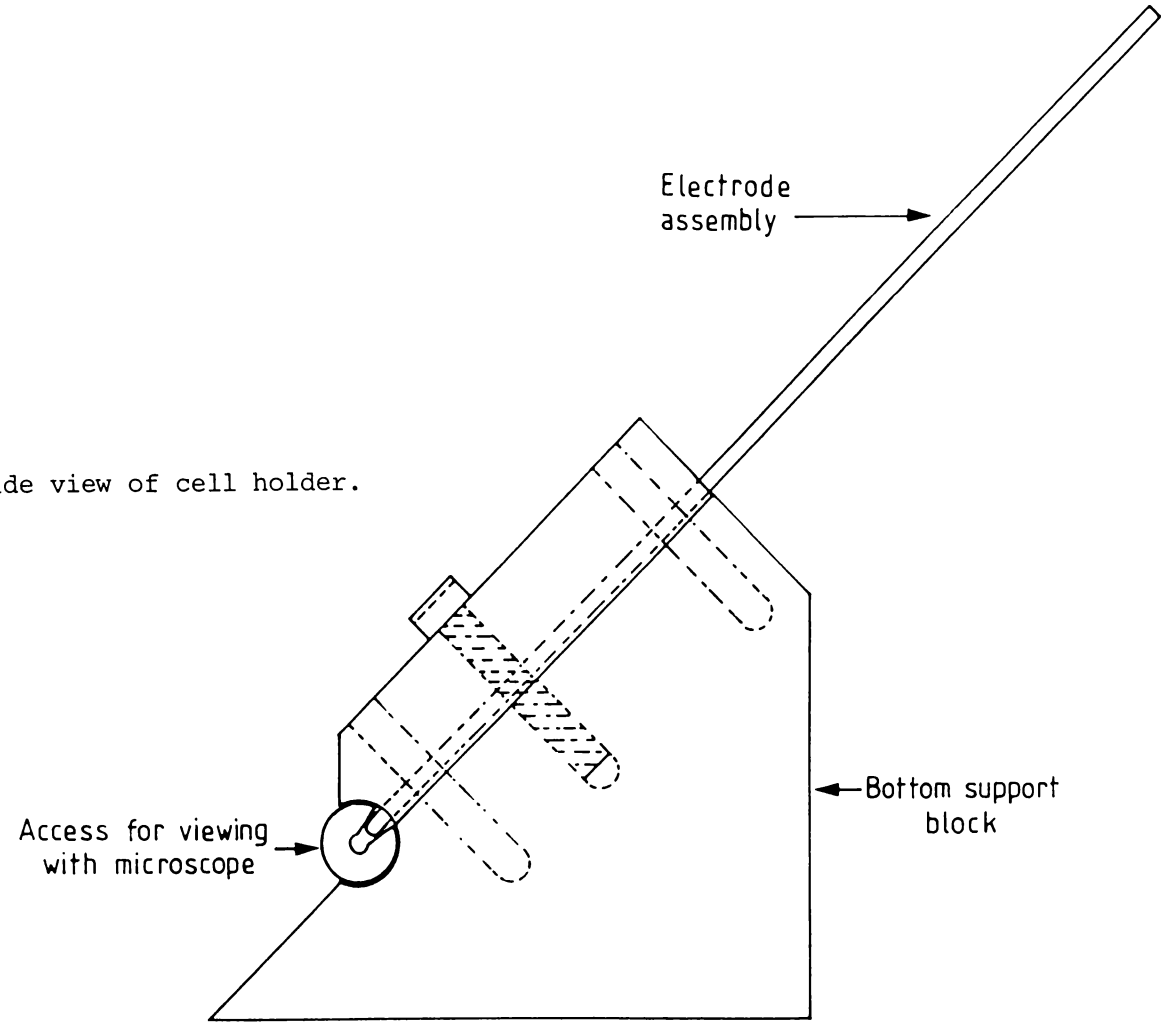

Fig. 4.3 (b) Side view of cell holder.

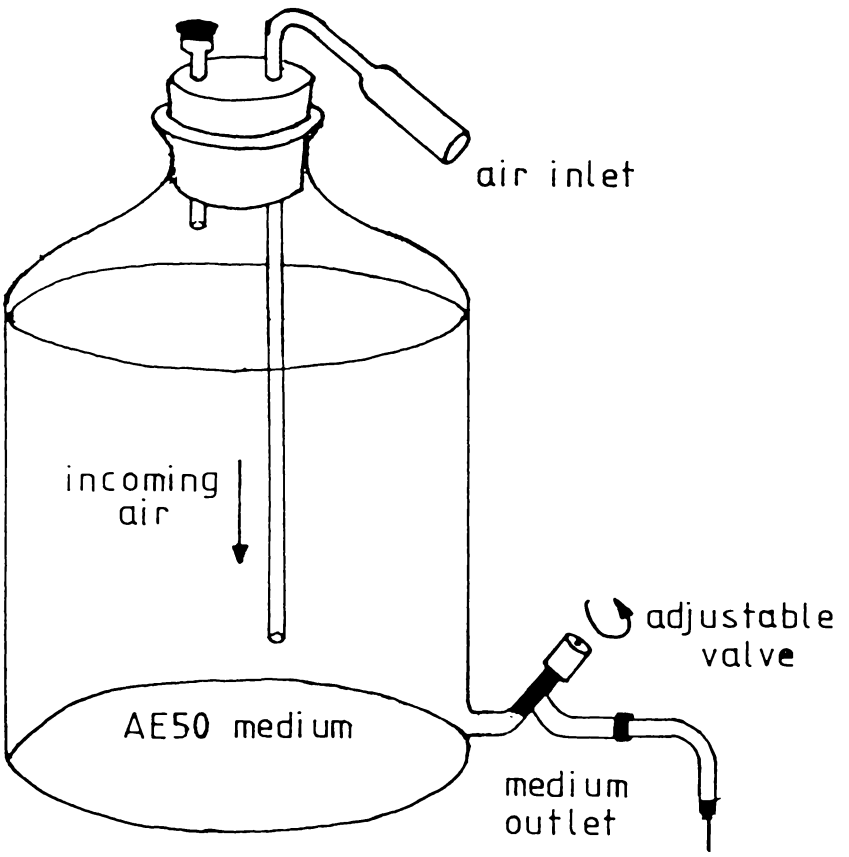

Fig. 4.4 Feeding bottle.

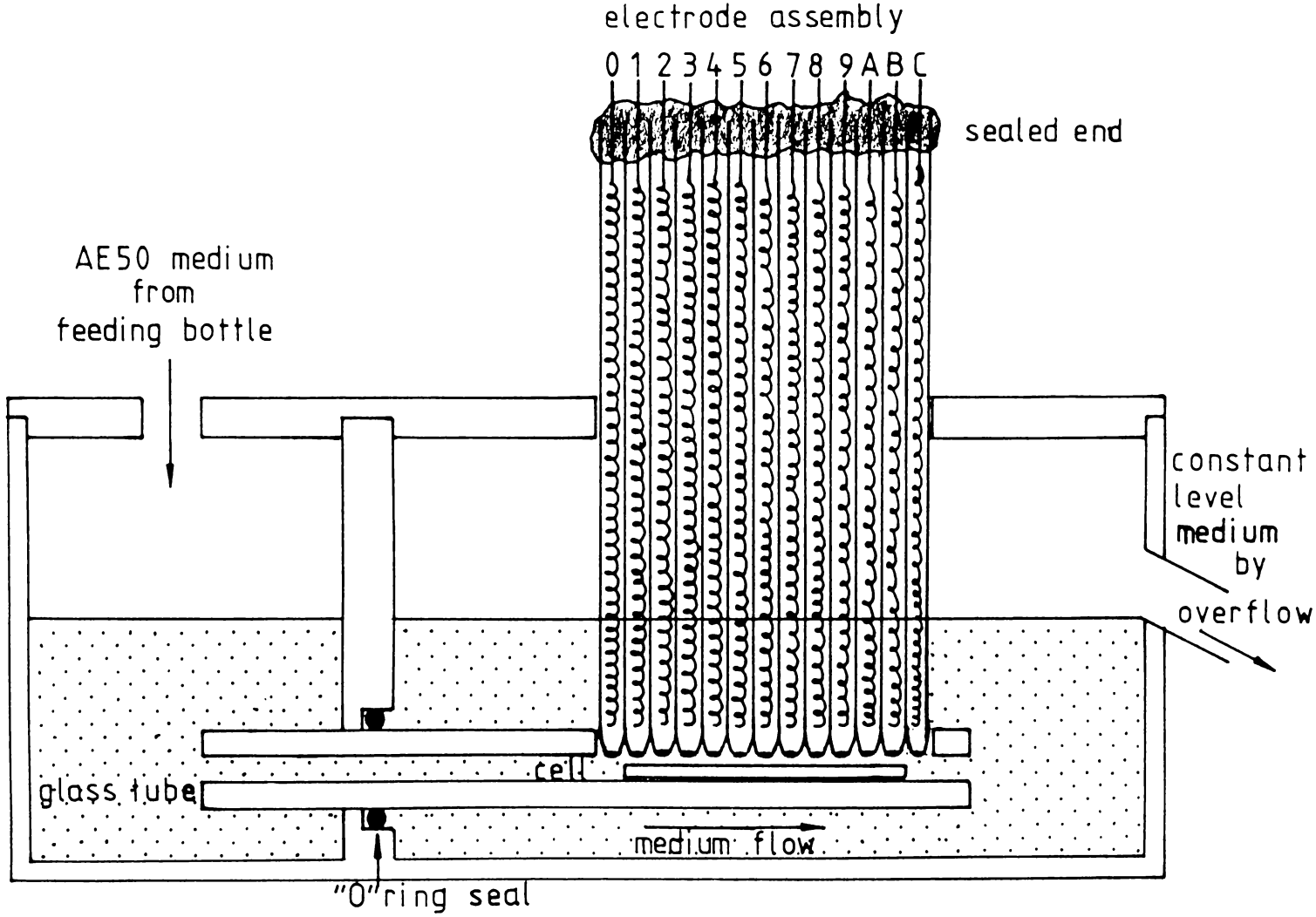

Fig. 4.5 Cross section of the cell holder assembly showing cell position and direction of medium flow.

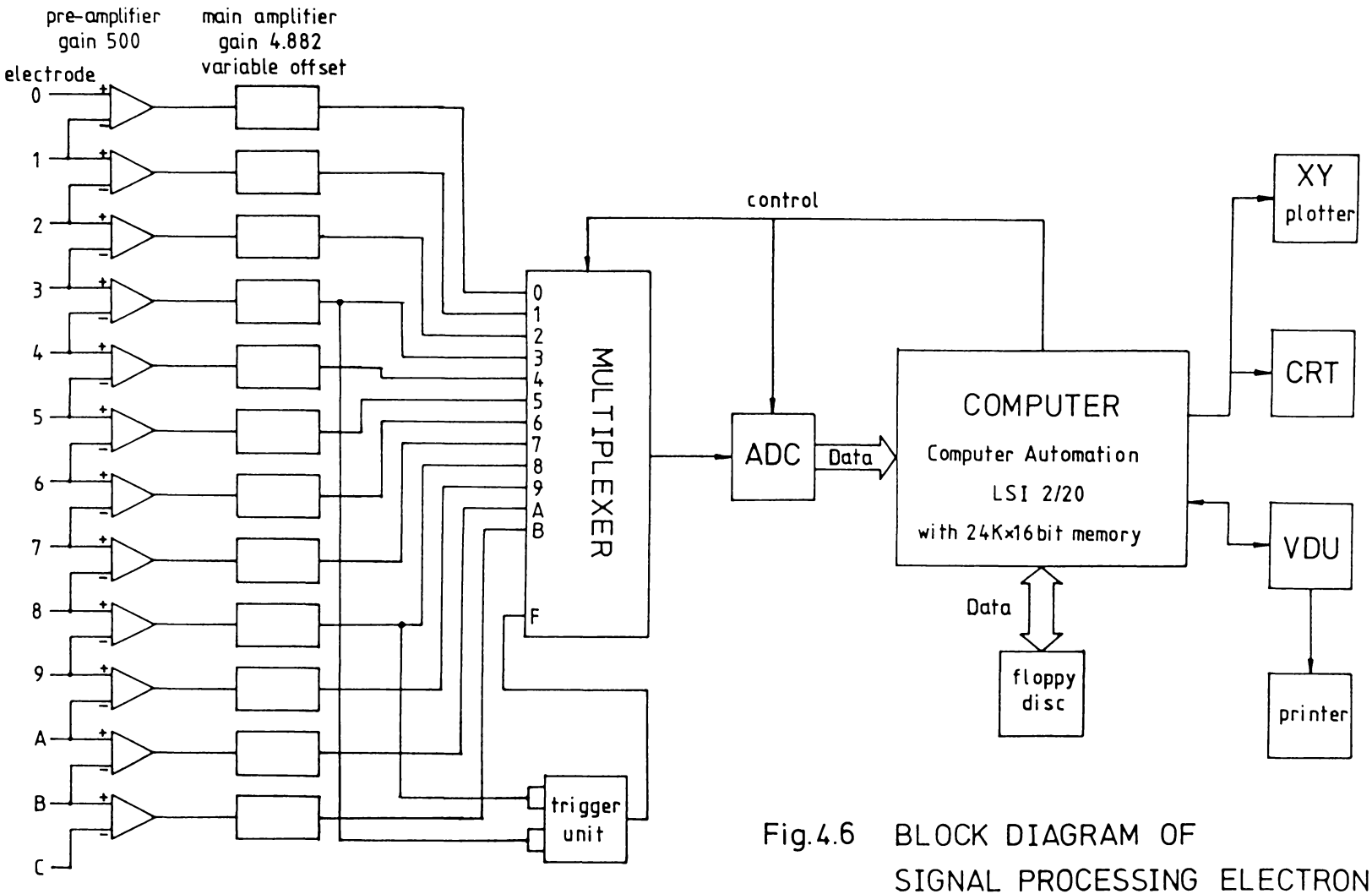

Fig.4.6 BLOCK DIAGRAM OF
SIGNAL PROCESSING ELECTRONICS

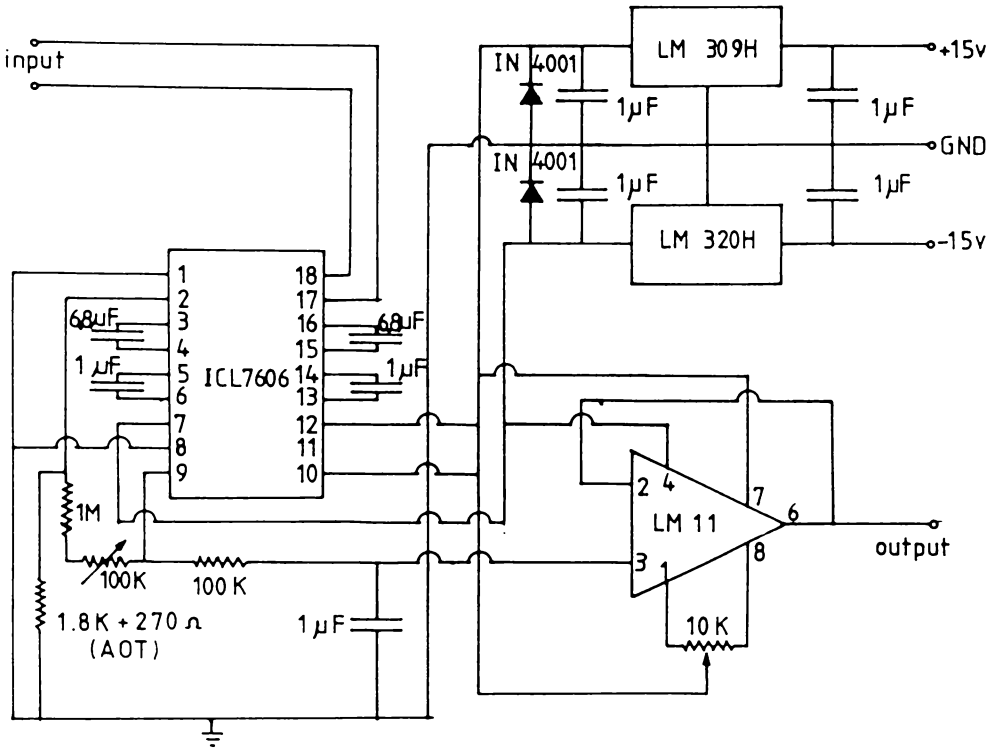

Fig. 4.7 Circuit diagram of pre-amplifier (from Williams, 1984).

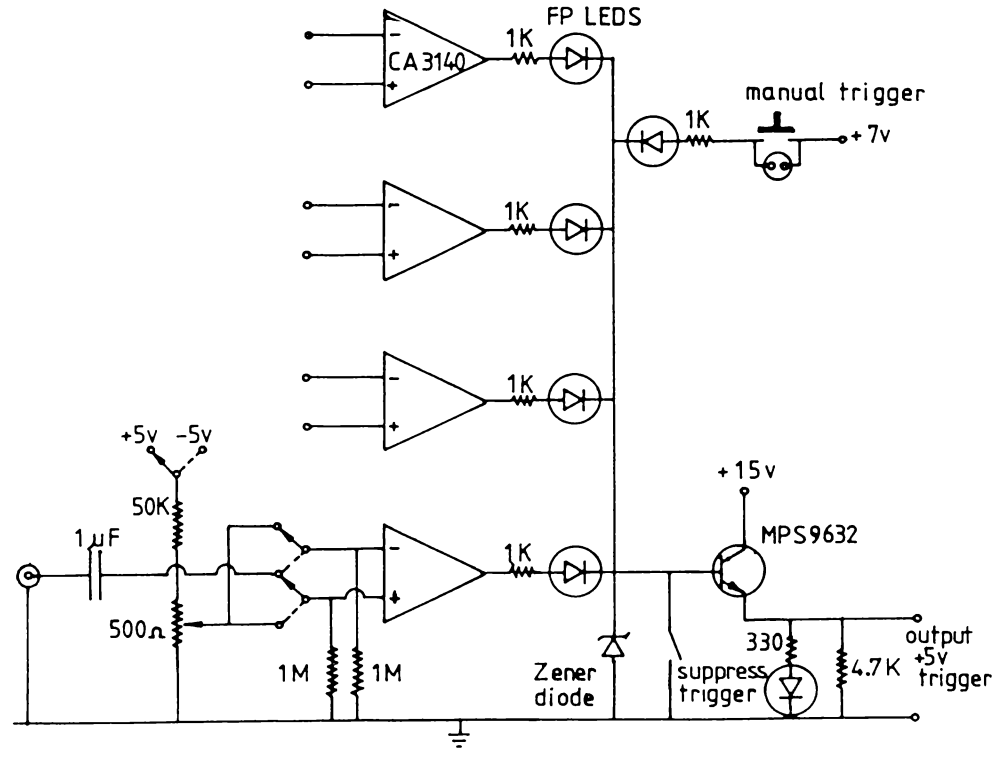

Fig. 4.8 Circuit diagram of trigger unit.

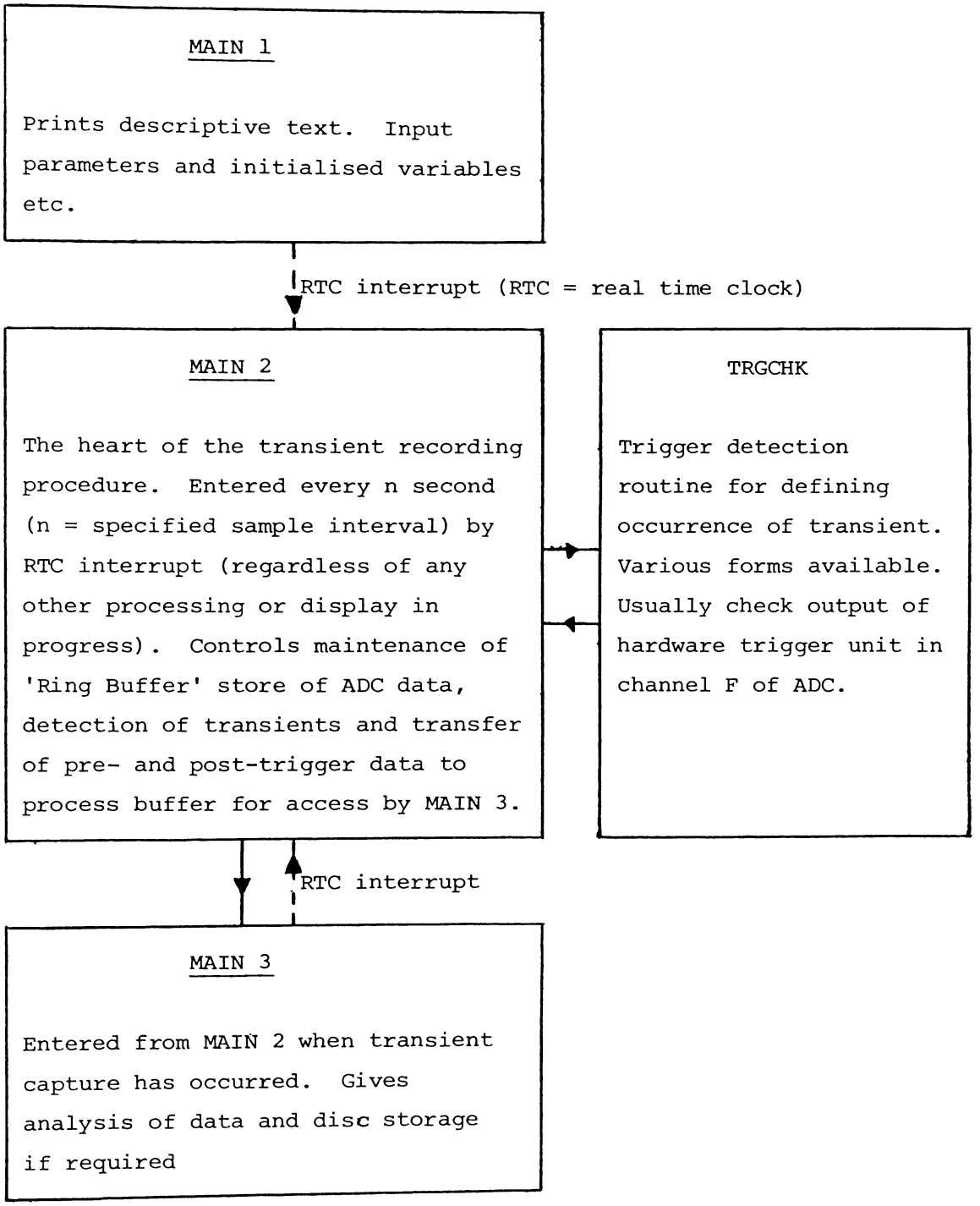

Fig. 4.9 Transient Recorder Program - TR3 series outline structure (from Lertsithichai, 1980).

Fig. 4.10 An example of a spontaneous action potential showing

(a) differential voltage waveforms, $\tilde{D}$

(b) current waveforms, I, calculated from (a) by direct inversion

(c) current waveforms, I, calculated from (a) by second order regularization with $\gamma = 5 \times 10^{-6}$ and estimated error of 8 %. The printout indicates the corresponding peak values and positions (note: time = position × sample interval which in this example = 0.8 s)

(d) current waveforms, I′, calculated from (a) by simplified equations.

(a)

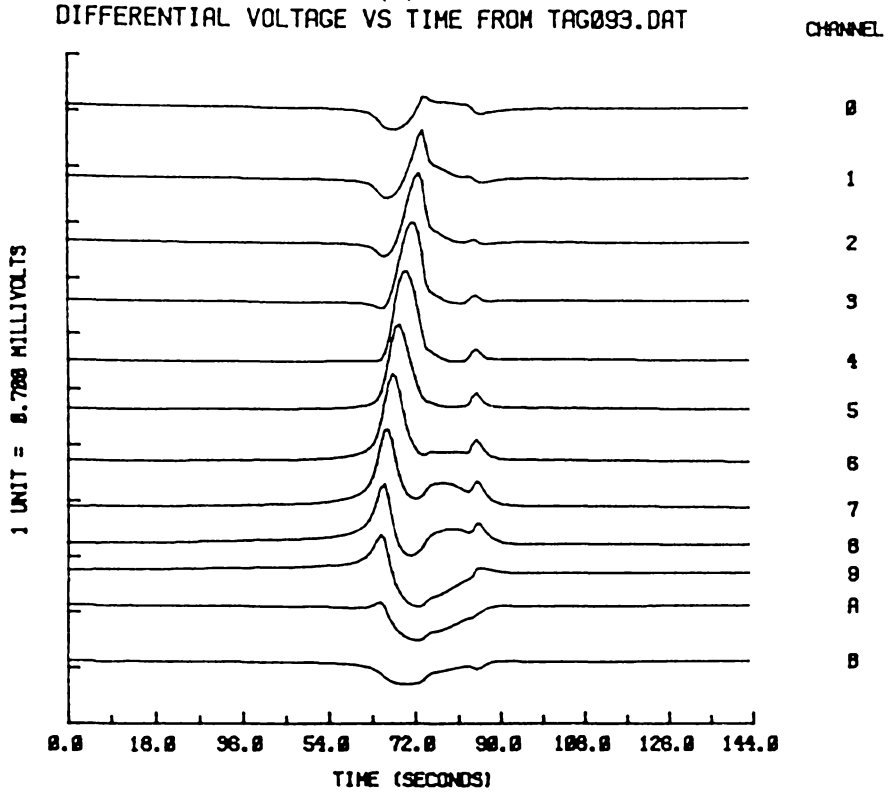

(b)

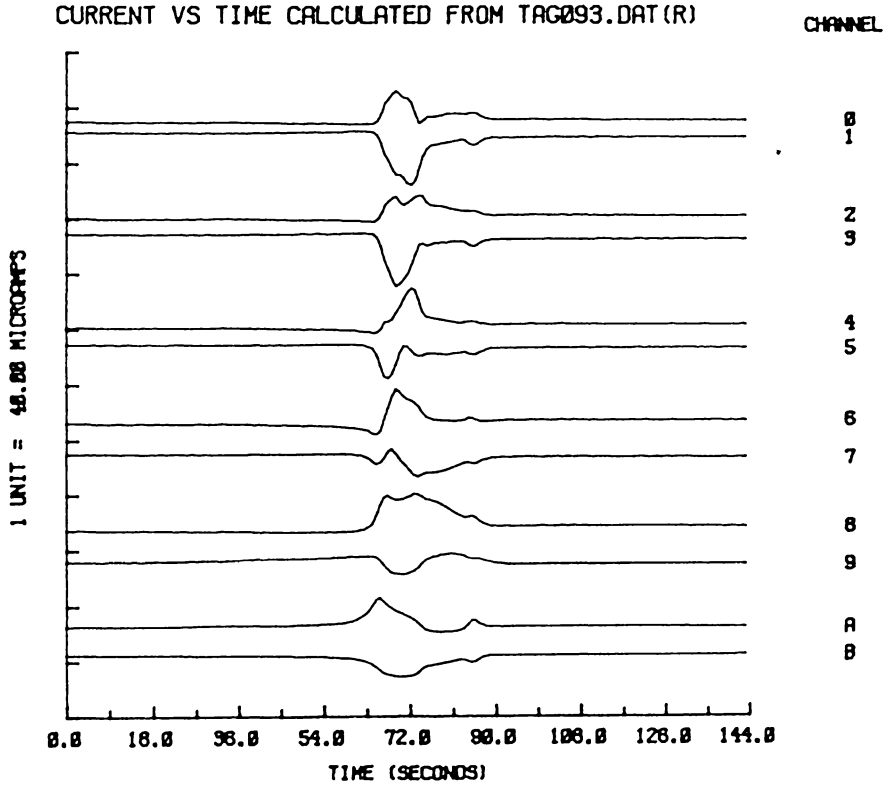

Fig. 4.10 (a) and (b)

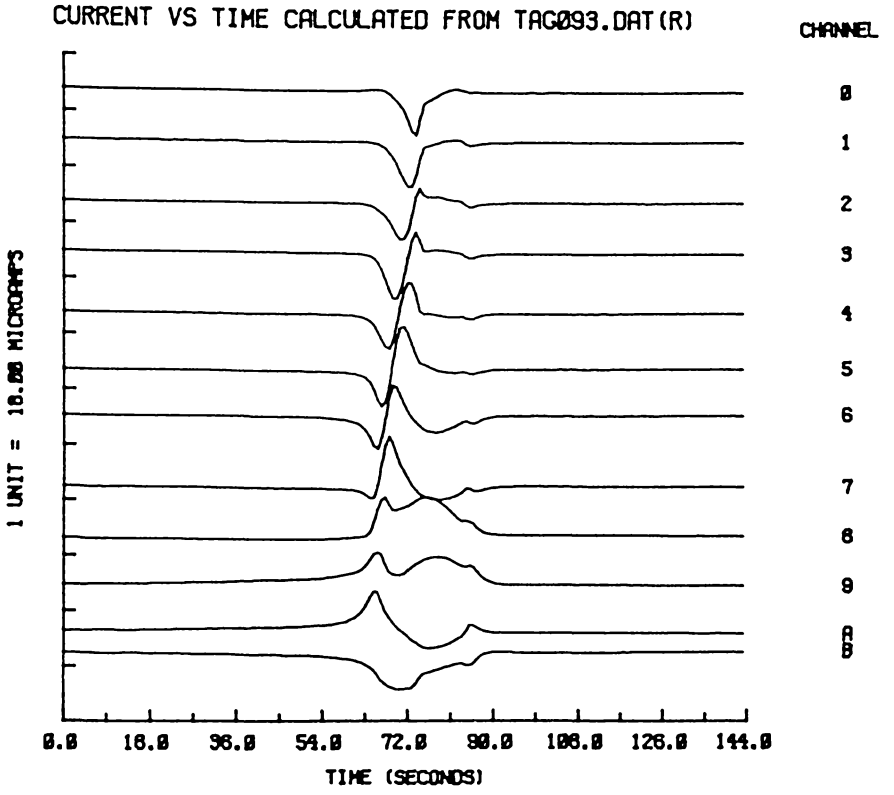

CHAN	MAXVAL	MAXPOS	MINVAL	MINPOS	SPAN
****	******	******	******	******	****
0	0.745	104	-14.196	93	14.941
1	0.540	104	-14.570	91	15.111
2	4.746	94	-12.137	89	16.882
3	6.853	93	-14.863	87	21.716
4	10.113	91	-11.566	86	21.678
5	14.160	90	-11.737	84	25.898
6	10.105	87	-10.703	83	20.807
7	16.453	86	-4.145	99	20.597
8	13.569	96	-0.449	63	14.018
9	10.589	83	-0.636	237	11.225
A	12.730	82	-5.765	96	18.495
B	0.580	237	-11.982	90	12.562

Fig. 4.10 (c)

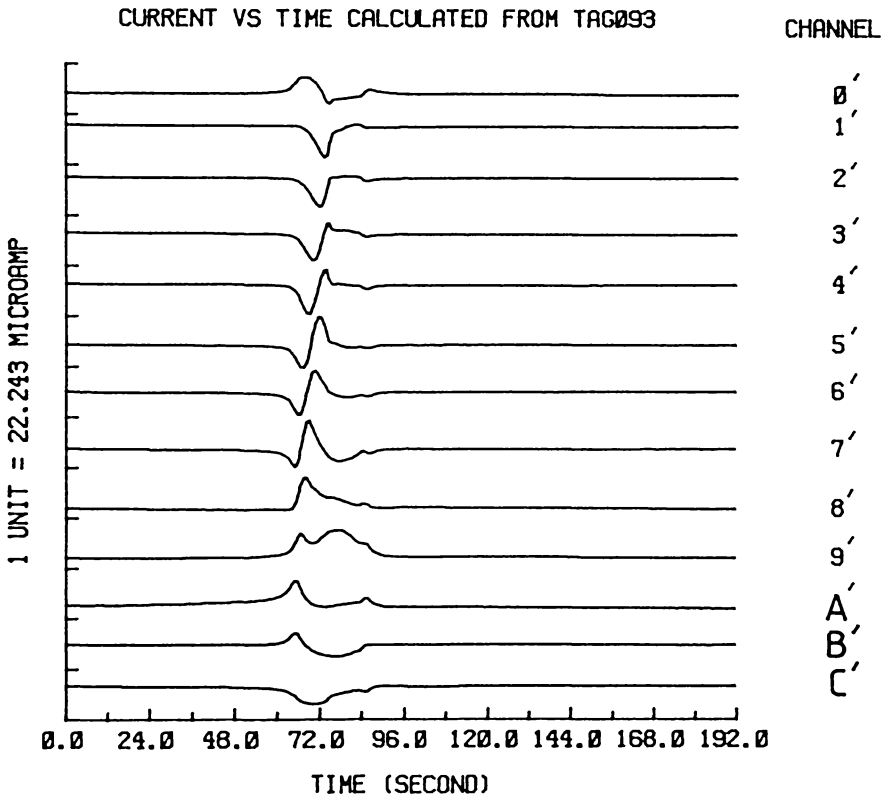
CURRENT VS TIME CALCULATED FROM TAG093
CHANNEL
0'
1'
2'
3'
4'
5'
6'
7'
8'
9'
A'
B'
C'
1 UNIT = 22.243 MICROAMP
0.0 24.0 48.0 72.0 96.0 120.0 144.0 168.0 192.0
TIME (SECOND)

Fig. 4.10 (d)

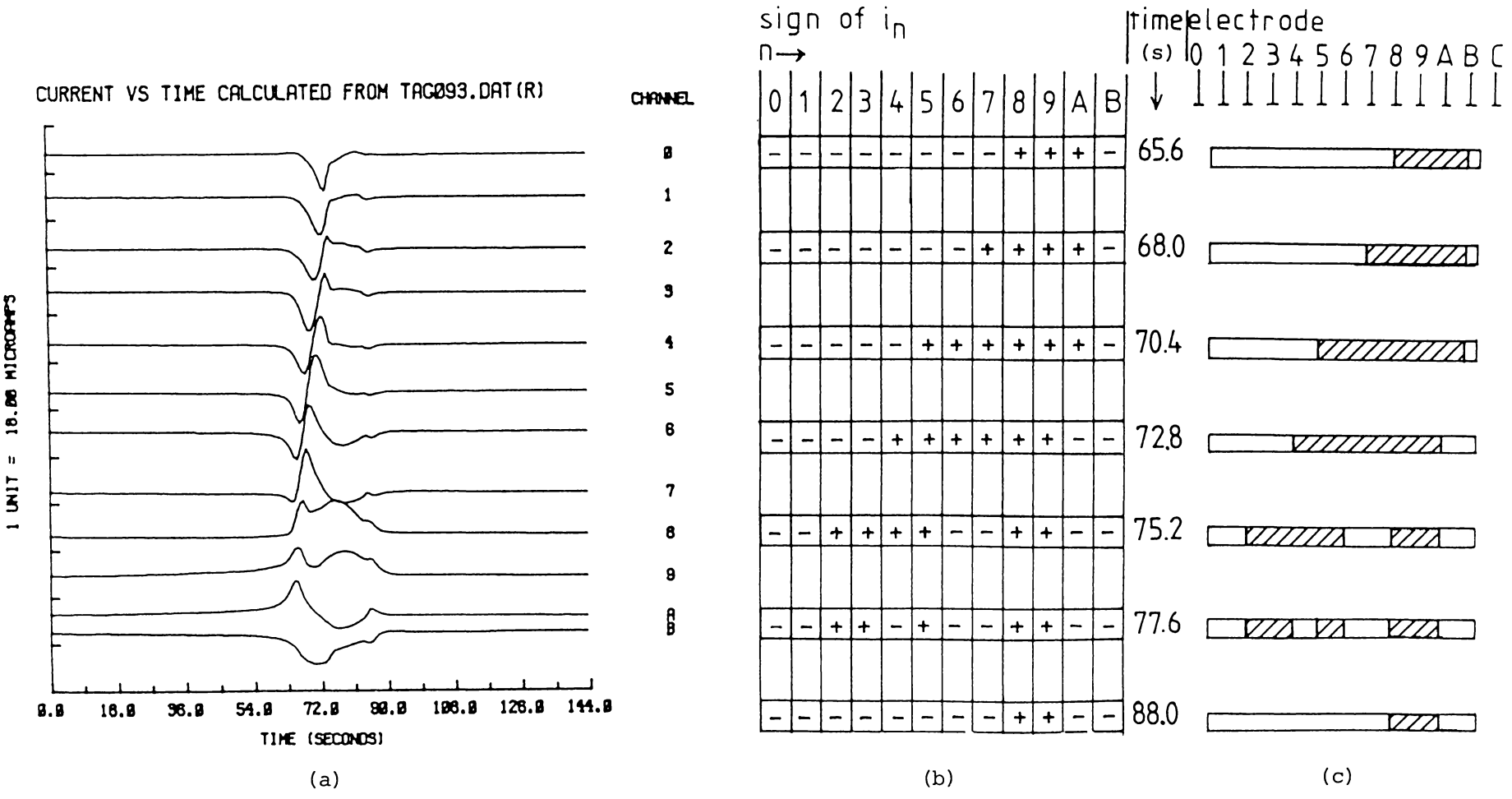

Fig. 4.11 An example of the calculated current waveforms by second order regularization (a), the corresponding table of signs of currents (b) and the resulting analysed depolarized region(s) (▨) (c).

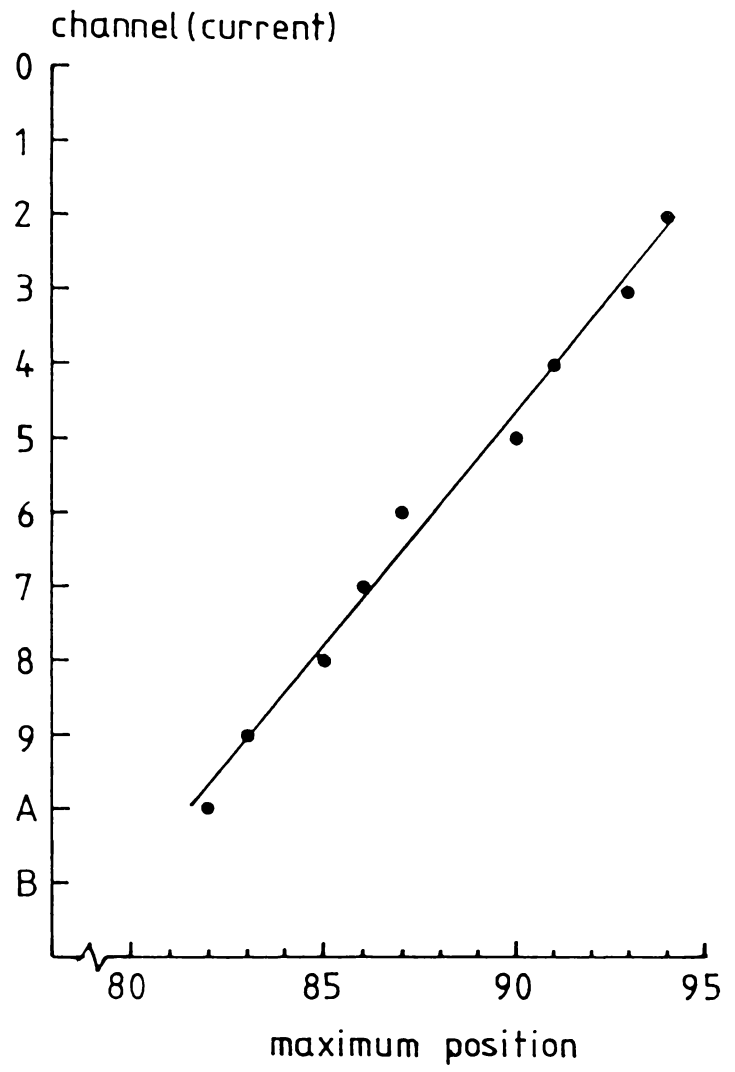

Fig. 4.12 An example of a plot used in the analysis for propagation velocity of an action potential (see text).

Fig. 4.13 An example of a spontaneous action potential showing

(a) differential voltage waveforms (from Lertsithichai, 1980)

(b) current waveforms calculted form (a) by second order regularization which indicate a non-propagating action potential (see text).

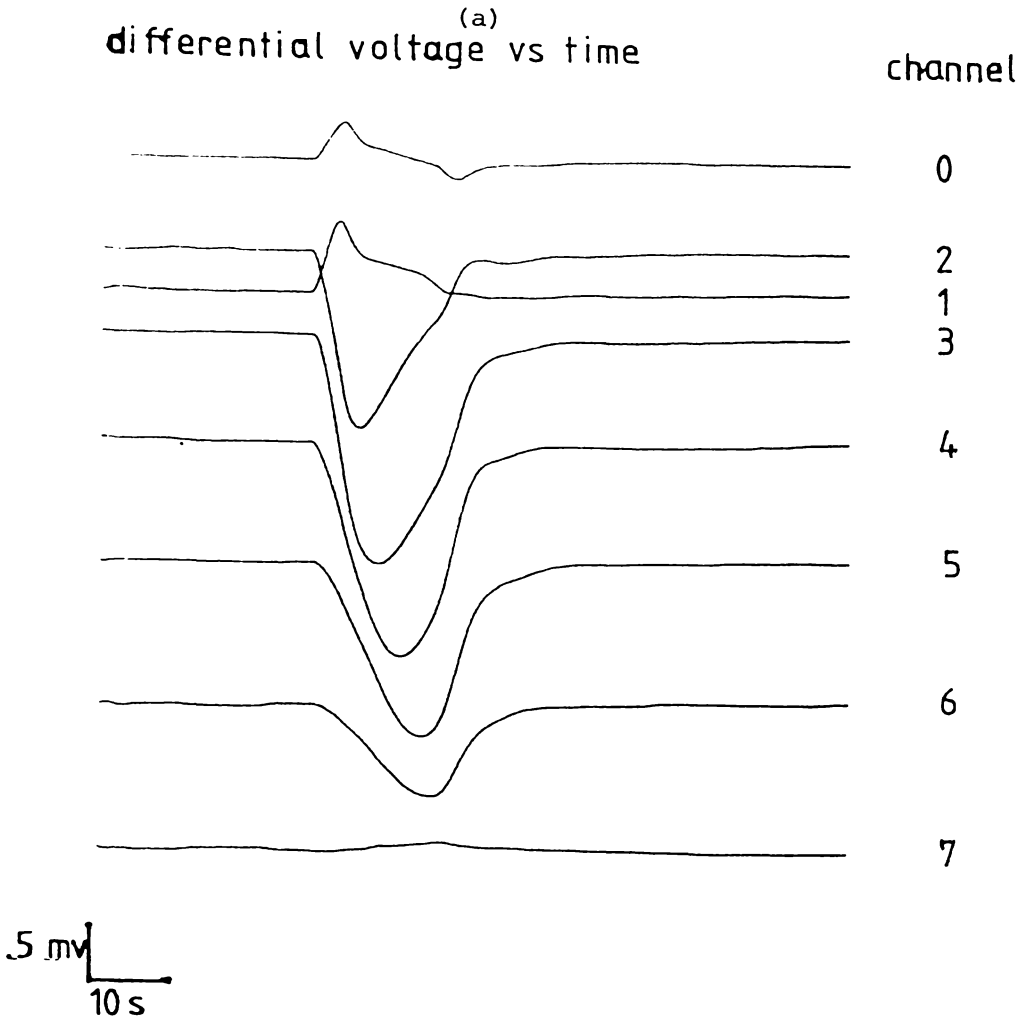

Fig. 4.13 (a) and (b).

```
*** TRANSIENT NUMBER   80 TRIG ON CH F AT 5363 MIN 53.0 S

SET SENSE IF DISK STOREAGE NOT REQUIRED

 CHAN  MINVAL MINPOS MAXVAL MAXPOS  SPAN  0-20%AV 80-100%AV

  :0   -0157    99   +0147    80   +0304   -0081   -0061
  :1   -0490    76   +0160    84   +0650   -0010   +0013
  :2   -0764    77   +0082    85   +0846   -0058   -0042
  :3   -0710    77   +0170    85   +0880   +0032   +0037
  :4   -0707    78   +0165    86   +0872   -0005   -0001
  :5   -0611    80   +0182    97   +0793   -0005   -0011
  :6   -0615    81   +0229    98   +0844   +0013   +0000
  :7   -0589    83   +0352    98   +0941   +0104   +0087
  :8   -0606    84   +0331    99   +0937   +0077   +0061
  :9   -0834    85   +0082    99   +0916   -0154   -0173
  :A   -0636    86   +0042    78   +0678   -0077   -0087
  :B   -0275    87   +0149    78   +0424   +0028   +0024

TRANSIENT NUMBER    80 SAVED ON DISK

SET SENSE TO DISPLAY DIFFERENCE DATA & PRINT SUMMARY
```

Fig. 4.14 An example of a printout of analysed peak values and positions of differential voltage waveforms which is displayed during an experiment (i.e. part of TR363E program).

CHAPTER 5

EXPERIMENTAL RESULTS

The results summarized in this chapter were obtained from the investigations of the spontaneous action potentials generated by anucleate isolated stalk segments (ISS's) of *Acetabularia mediterranea* during their redevelopment. The experimental procedures were as described in section 4.6. A total of eighteen experiments were carried out; nine of these had the former apical ends facing the incoming AE50 medium (i.e. near electrode 0, see Fig. 4.5) while the others had the former basal ends facing the incoming medium. The names given to these experiments start with *A* or *B* respectively (see Table 5.1, page 186). The reason for this division was to attempt to establish whether there was any major effect on the direction of growth by the direction of medium flow. In group *A*, 7 out of the 9 cells redeveloped at the former apical end compared with 5 out of 8 in the *B* group (excluding one cell which had no observable growth). These results suggest that there is no significant effect on the direction of new growth from the direction of the medium flow. The higher percentage of redevelopment of the ISS's at the former apical end indicates that some *memory* of the original developmental polarity was still preserved in most cases.

5.1 Redevelopments of ISS's

The eighteen experiments were also divided into two series depending on the time the ISS's had been kept in the dark. In the

first series of nine experiments the ISS's were kept in the dark for only ~1 day after the rhizoids had been amputated (following Novak and Bentrup, 1972, see section 4.1 for procedures). In this series, 8 out of 9 ISS's redeveloped with only two (i.e. ~25% of the redeveloped ISS's) regenerating at the former basal ends. In an attempt to obtain more redevelopment at the former basal end the ISS's were kept slightly longer in the dark (i.e. 4 days) in the second series. Some improvement was obtained in that ~33% of the ISS's regenerated at the former basal ends (3/9 from the experiments and 6/18 from ISS's not used in the experiments). The reason for wanting the ISS's to regenerate at their former basal ends is that these are the cases which clearly indicate the loss of the ISS's original developmental polarities. They are therefore the cases where the possible involvement of the action potentials in the process of symmetry-breaking could be best investigated.

When illumination was given to the ISS in each experiment, redevelopment was generally observed after ~30-50 hours. In our experiments *growth* was taken as the stage where a definite redevelopment was observed, normally when the new tip was ≈0.1 mm in length. The *regeneration time* for each ISS was then taken as the period from the *onset of illumination* to the time where *growth* was observed. Out of the eighteen experiments only thirteen were chosen for detailed analysis. The other five experiments were discarded because the results obtained might not truly represent the behaviour of normal redeveloping ISS's. In these experiments the ISS's either died within the experimental period (2-3 days) due to some unknown cause(s) or had some observable contamination on the surface of the cell stem. From this point onwards the results presented will be

from the thirteen experiments (Table 5.1, page 186) unless otherwise stated as pertaining to a *dying cell* or a *contaminated cell*.

In the experiments three types of redevelopment were observed and these are shown in Figs. 5.1 and 5.2. They are classified as

(i) *a-tip* or *b-tip*, the ISS only developed a new tip (Figs. 5.1a, 5.2a)

(ii) *a-whl* or *b-whl*, the ISS developed a new tip followed later by a whorl (Figs. 5.1b, 5.2b).

(iii) *a-cap* or *b-cap*, the ISS developed a new tip followed later by a whorl and then a small cap (Figs. 5.1c, 5.2c).

a and *b* indicate the redevelopments at the former apical and basal ends respectively. The most common type was a-whl or b-whl.

The regeneration time (light on → growth) varied from cell to cell. The average time was found to be 39 ± 11 hours. This average value excluded the regeneration time of experiment BH which was unusually long (for regeneration time see Table. 5.1). The first whorl of hair appeared at about 55 hours. In a few cases where small caps were formed, the time taken was about 80 hours. In all experiments the final stage of redevelopment of the individual ISS (either as a tip, a whorl or a cap) was observed during the experiments i.e. no further development (into the following stage) occurred after the experiments were completed.

5.2 The Spontaneous Action Potentials During the Redevelopment

In this section the results of the analysis of some of the properties of spontaneous action potentials associated with the regenerating ISS's are described.

5.2.1 Action Potential Activity

The transient changes in the membrane potential which occurred during the experiments could be divided into two groups as follows:

(i) A major group consisted of transient changes which gave rise to large amplitude pulses which we called action potentials.

(ii) A minor group (very few c.f. (i)) consisted of small amplitude pulses, generally <20% of the amplitude of (i) (probably subthreshold responses) which were not taken into consideration in our analysis.

The amplitude of the action potentials varied from cell to cell and to a lesser degree from pulse to pulse in the same cell. They were generally in the range of 0.4-1.0 mV (measured as extracellular $\tilde{D}$) corresponding to peak membrane current of ~10 $\mu A\ mm^{-2}$.

The general pattern of occurrence of the action potentials observed in our experiments can be described as follows. After the onset of illumination there was a period where a few, normally non-propagating, action potentials occurred. This period varied from cell to cell and had an average of 4 ± 2 hours. This was followed by a *rest period* where no action potentials were observed, lasting for 6 ± 5 hours (note great variation between the cells). After the *rest period* the action potentials occurred again and seemed to follow

a rhythm, alternating between *active* (where action potentials were observed) and *rest* periods. Figs. 5.3a and 5.4a show examples of the number of action potentials which occurred (in a 3 hour interval) during the experimental period for two experiments. Both the frequency of the action potentials and the time for each cycle (active to active or rest to rest period) varied from cell to cell. The highest action potential frequency during the active period was normally in the range of 1-3 pulse h^{-1} with the overall average frequency (i.e. number of action potentials/experimental period) being ~0.3-1.3 pulse h^{-1}. In addition the number of the action potentials also changed from cycle to cycle e.g. in experiment AF (Fig. 5.4a) where the number in the third cycle was lower than the previous two cycles.

In order to estimate the period of the rhythm we calculated the auto-correlation coefficients of the number of action potentials starting from the point after the first rest period i.e. at the 13th hour in our examples. The equation used to calculate the auto-correlation coefficient of lag k = 1, ..., K (where K = maximum lag = number of interval -1) is

$$r_k = \frac{\sum_{i=1}^{n-k} (x_i - \bar{x})(x_{i+k} - \bar{x})}{\sum_{i=1}^{n} (x_i - \bar{x})^2}$$

where x_i is the number of action potentials at interval i, and n is the number of intervals. Figs. 5.3b,c and 5.4b,c show the plots of the number of action potentials during the considered period and the corresponding coefficients at lag 1 to k, the latter being called the correlogram (e.g. Chatfield, 1980). These figures (5.3c and 5.4c)

clearly indicated the existence of a rhythm in the occurrences of the action potentials since the correlogram will generally exhibit an oscillation at the same frequency as the time series which contains a periodic fluctuation (Chatfield, 1980). This feature could be distinguished more or less clearly in all the experiments. From the correlogram the period of each cycle could be found from the interval between the consecutive peaks and this was found to lie in the range of 24-30 hours.

5.2.2 Initiation Sites of the Action Potentials

In section 4.6 we have demonstrated the process by which the initiation site of an action potential could be found from the calculated current waveform I i.e. the region where i_n's were first positive. An example showing the initiation site at the end near electrode C (i.e. the right hand end) was also given (Fig. 4.11). In this section we shall give more examples of the action potentials initiated at various sites along the ISS.

In our experiments the action potentials generated by the ISS's were found to initiate predominantly at the ends (see section 5.2.3 for more detail) and occasionally in the middle region of the ISS's. The initial depolarized region of an action potential was normally found to span the length covered by two pairs of electrodes i.e. $(1.6 \pm 0.1) \times 2 = 3.2 \pm 0.2$ mm. Figs. 5.5-5.10 show examples of spontaneous action potentials initiated at various sites along the ISS. The initiation site is located at the region where i_n's are first positive and the positive i_n's are indicated by + signs in Figs. 5.5c-5.10c. We should also note here that, for example in Fig. 5.5b, in addition to the positive i_0 and i_1, i_B is also

initially positive. However, this positive current is due to a systematic error rather than a depolarized region. This error is caused by a small amount of current-flow (due to the depolarized region) being leaked from the glass tube (containing the ISS) through the gaps between the electrode tips and the slot walls. (Thus, the measured differential voltage waveforms will contain this error which then passes onto the calculated current waveforms). This error (when observable) appears in the current i_n furthest away from the initiation site, that is, the region with a small amount of current in the conducting medium and hence the error due to the leaked current becomes significant (e.g. i_B in Fig. 5.5b). This error was reduced in the experiments where the tips of the electrode assembly had a tighter fit in the slot (i.e. less leak). Also in the experiments by Lertsithichai (1980) where the gaps were sealed by epoxy resin this feature was not observed (e.g. Fig. 4.13) thus supporting the above argument.

For all experiments the analysed initiation sites of the action potentials were also plotted as a function of time and these are shown in Figs. 5.11-5.23. In order to describe the association of the occurrences of the action potentials with the various regions of the ISS we divided the ISS into 3 regions i.e.

(i) *the regenerating end, R-end*

the region of ~3-4 mm from the end of the original ISS which possesses the new apex.

(ii) *the other end, 0-end*

the region of ~3-4 mm from the end of the ISS which has no observable development.

(iii) *the middle region, mid*

the region between (i) and (ii).

The action potentials were then broadly classified as initiating in one of these three regions. in the case where the initiation site lay in more than one region the action potential was classified as being in the region where the maximum of the positive i_n's was located. The reason for choosing the length of 3-4 mm for the end regions was the fact that the initial depolarized region (initiation site of an action potential) was generally found to be ~3 mm in length (see above).

As can be seen from Figs. 5.11-5.23, the action potentials initiated predominantly at the ends. Frequently a few action potentials with similar features would initiate at one end before the initiation site moved to the opposite end and remained there for the next few action potentials.

For example, in experiment BF (Fig. 5.15) the action potentials initiated mainly at the R-end (near electrode C) and propagated to the other end as indicated by the arrow before moving to the O-end at ~55 hours after the onset of illumination. The initiation site remained at the O-end for ~6 hours (these action potentials propagated to the R-end) followed by a rest period after which the initiation site moved back to the R-end at ~68 hours. Then at ~86 hours the initiation site again moved to the O-end and the same pattern continued for the remaining period of the experiment. The action potentials initiating at the R-end all had similar features, e.g. Fig. 5.24a. Similarly those action potentials initiating at the O-end also had similar features as shown in Figs. 5.24b (the propagating behaviours of the action potentials shown in Figs. 5.24a and b are shown in Fig. 5.29 and Fig. 5.30 respectively).

The movements of the initiation sites of the action potentials seem to be characteristic of individual cells. In some cases, during

the time in which the initiation site moved from one end to the other the ISS could also generate one or more action potentials along this path (Figs. 5.19, 5.20). From our experiments the movements of the initiation sites can be summarized as follows:

(i) initiation sites were found at *the R-end* right from the start and *occasionally moved to the O-end* - experiments AC, AI, BF, AH, BD, BE, Figs. 5.12, 5.13, 5.15, 5.19, 5.20, 5.21.

(ii) initiation sites were found more at *the O-end* before growth was observed but the situation *reversed after growth* had been established - experiment BG, Fig. 5.14.

(iii) initiation sites were found more at *the O-end* and then *remained* in this region *long after growth* had been established. However, the initiation sites of the *later action potentials did move to the R-end* - experiments AG, AB, Figs. 5.16, 5.17.

note in experiment AG (Fig. 5.16) the *initiation sites moved* to the R-end a few hours *before a cap was observed.*

(iv) initiation sites were found *scattered* along the ISS's *before growth* but the action potentials increasingly *initiated at the R-end after growth* - experiments AE, BH, Figs. 5.11, 5.23.

(v) initiation sites were found *scattered* along the ISS (predominantly at the ends) *through out the experimental period* - experiment B1 Fig. 5.22.

(vi) initiation sites were found *only at the O-end* - experiment AF, Fig. 5.18.

The number of the action potentials initiated in the three different regions together with other results are shown in Tables 5.1

and 5.2. Since the number of action potentials varied from one experiment to another, we calculated the percentage of the action potentials in the different regions with respect to the total number in each experiment and these are shown in Fig. 5.25. The histograms were plotted according to the regeneration time of the ISS's, starting from the experiment with the lowest regeneration time i.e. experiment AE (Fig. 5.11).

From Fig. 5.25, the average values of all experiments (last 3 columns) indicate that the action potentials initiated mostly at the R-end, followed by the O-end, and least in the middle region. However, any conclusion from these averages should be taken with caution since the high standard deviations indicate great variations between the ISS's. In fact there are a few experiments in which the action potentials were initiated predominantly at the O-end i.e. experiments AG, AB, AF, and B1 (Figs. 5.16, 5.17, 5.18 and 5.22) with AF having *all* action potentials initiated at the O-end. It is interesting to see that three of these four experiments i.e. AG, AB, and AF (see Fig. 5.25 also 5.16-5.18) regenerated at approximately the same time (~40 hours) and that growth in each case was observed after a rest period rather than after an active period like others.

Experiment AG (Fig. 5.16) in this group provided another interesting result. In this experiment the action potentials initiated predominantly at the O-end at first (even when tip and whorl developments were observed). Fig. 5.26 shows a typical action potential initiated at the O-end. However, a few hours before a small cap had been observed the initiation site of the action potentials moved to the R-end. After the change of initiation site, the action potentials remained a propagating type though they propagated for a shorter distance than when they had initiated at the O-end

(Fig. 5.27, see also Fig. 5.16). However, they later changed to a non-propagating type (Fig. 5.28) with a longer duration. In this particular case the current waveform I (Fig. 5.28b) showed no positive i_n in the first peak and hence we were unable to find the initiation site using I (note: i_B is positive but this is due to a systematic error as described in section 5.2.2). By observing the differential voltage $\tilde{D}$ (Fig. 5.28a) we see that $\tilde{d}_0(t)$ has a negative peak and hence indicates that the depolarized region is on the left of the electrode pair (0,1) i.e. beyond electrode 0. This is possible in this case since in this experiment at the time where this particular action potential was recorded the ISS had grown a new tip, a whorl, and a cap beyond electrode 0. Also at the time when a cap was observed the end which was regenerating had acquired a darker green colour than the O-end. This is most likely due to the translocation of part of the cytoplasmic substances into the cap region as described by Lüttke (1983, see also chapter 1).

Other features observed from Fig. 5.25 are

(i) the percentage of action potentials initiated in the middle region seems to increase with regeneration time, especially in experiment BH.

(ii) in many cases the percentage of the action potentials initiated at the R-end, as compared to the O-end, increases after growth e.g. experiments AE, BG, BF, AB, AH, BD, BE, BH.

(iii) for the few experiments where the ISS's regenerated at the former basal ends (i.e. experiments BG, AB, B1 and BH) the percentages of the action potentials initiated at the R-ends befor growth are in all cases lower than those initiated at the O-ends.

5.2.3 Propagating and Non-Propagating Action Potentials

The use of the multi-extracellular recording technique enabled us to demonstrate clearly the propagation of the action potential, or, to be more precise, the propagation of the depolarization region. An example of this type of action potential has already been shown in chapter 4. In this section various propagating behaviours are demonstrated. However, not all action potentials propagate and some examples of the non-propagating action potentials will also be given.

As described in section 4.6, the propagating behaviour of a depolarized region (i.e. an action potential) could be found by locating the positive current i_n's at different points in time e.g. Figs. 5.29-5.33. The last depolarized region pattern shown in these figures is the last of the individual action potentials before they return to the normal polarized condition. From these results we found the following.

(i) The depolarized region normally initiates at one region and extends in length.

(ii) In most cases the depolarized region initiates at one end and extends towards the other until it covers more than half of the cell before it starts to repolarize.

(iii) The repolarization can either start at the region which is first depolarized (Fig. 5.30), or in some other region (Fig. 5.29), even at the region where it has just been depolarized (Fig. 5.31 from 99 s to 103 s) i.e. depolarized last but repolarized first.

(iv) If the depolarization initiates at any region other than the ends it normally extends to the side which has a longer length (Fig. 5.33) and very rarely extends both

ways (Fig. 5.31). Normally, when a depolarized region initiates further from the ends its extension is very limited (Fig. 5.33) or non-existent i.e. a non-propagating action potential (see later). Fig. 5.31 shows a rare case of propagation of an action potential initiating in the middle region of the cell.

(v) In a few cases more than one depolarized region may initiate at approximately the same time (Figs. 5.29, 5.31, 5.32). In Fig. 5.29 one depolarized region initiates between electrodes 8 and B and propagates to electrode 3. Another depolarized region initiates at the end near electrode 0 and extends slightly towards electrode 1 when the first depolarized region returns to the normal polarized state (at ~100 s). The reason for considering that the second depolarized region is a new one is that the current i_0 becomes positive without having i_1 or i_2 become positive (as it would have been if the first depolarized region was extended to this region - see Fig. 5.29b, where signs of i_1 and i_2 from 83-91 seconds are negative). Similar arguments apply to Figs. 5.31 and 5.32.

(vi) In most cases the depolarized region does not propagate to the very end of the ISS.

(vii) Figs. 5.29 and 5.30 show action potentials obtained from the same ISS (experiment BF). It can be seen that the action potential initiating at the end near electrode C (Fig. 5.29), the R-end, propagates a shorter distance than the action potential initiating at the end near

electrode 0 (Fig. 5.30), the 0-end. This is in fact true for most experiments where propagating action potentials were found to initiate from both ends e.g. experiments AI, BF, BH (Figs. 5.13, 5.15, 5.23). The distance travelled by action potentials initiating at the R-end is on average ~2-3 mm less than those initiating at the 0-end.

(viii) The average velocity of the action potentials which had propagated $\geq$ 4 channels (> 6.5 mm), over all experiments, was found to be 1.4 $\pm$ 0.3 mm s^{-1}.

For the non-propagating action potentials the waveform of the current I appears much simpler i.e. only the current at the depolarized region becomes positive and slowly returns to zero value. Figs. 5.34-5.36 show examples of some non-propagating action potentials initiating in different regions. (Note the very long duration of the action potential in Fig. 5.36, ~5 min as compared to 1-2 min in other action potentials. This was found in one cell only.) These non-propagating action potentials are not subthreshold responses (see chapter 2) since their amplitudes are approximately the same as the propagating ones i.e. ~0.4-0.8 mV (differential voltage $\tilde{D}$).

The ratio of occurrences of these two types of action potential (i.e. propagating and non-propagating) varied from cell to cell, from zero to near 100% propagating (see Table 5.1). The fact that the depolarized region which initiates further from the ends rarely propagates or only propagates to the side of the cell with a longer length ((iv) above) seems to indicate that the length of the ISS may affect the propagation behaviour of the action potential. Fig. 5.37

shows the relationship between the percentage of propagating action potentials in each experiment (values in Table 5.1) as a function of ISS's length. Although the number of results are limited it does indicate that the number of propagating action potentials increases as the length increases. The correlation coefficient of the percentage of propagating action potentials and ISS's length was calculated to be = 0.88.

5.2.4 Sharp and Slow Take-Off Action Potentials

Another interesting feature of the observed action potentials is the way the waveforms start. In all the examples presented so far the differential voltage $\tilde{D}$ (and hence I) changed gradually as the action potentials initiated. We shall call this type of action potential a *slow take-off*. Another type of take-off will be called a *sharp take-off* when waveforms change abruptly from the steady state baselines. An example of a sharp take-off action potential is shown in Fig. 5.38. This type of action potential was generally observed at the beginning of the experiments just after the onset of illumination and was mostly non-propagating (these were shown in Figs. 5.11-5.23 by an orange colouring). Only occasionally was this type of action potential found in other periods (e.g. experiment BH, Fig. 5.23). Although most of these sharp take-off action potentials were non-propagating a few did occur as the propagating type (e.g. in experiment AG, Fig. 5.16).

These sharp take-off action potentials were also found in *dying* and *contaminated* cells. The following observations suggested that this characteristic may also be associated with the injury of the cell.

(i) In one of the dying cells a clear region was observed. Before the action potential shown in Fig. 5.39 occurred the clear region was between electrodes 5 and 7 (Fig. 5.39c). The action potential then initiated between electrodes 4 and 6 (Fig. 5.39d) i.e. just next to the clear region. Immediately after the action potential the clear region was observed to increase in size i.e. it spanned between electrodes 4 and 7 (Fig. 5.39e). It seems that shrinking of the green region (cytoplasm) gives rise to an action potential. A few similar action potentials also initiated at the sites of the shrinking cytoplasm. The cell eventually died.

(ii) In another cell which suffered similar injury (by injury we mean that the cell showed a clear patch which was normally associated with a damaged region but the cause of the injury was unknown since no obvious physical interference was observed) but later recovered, the following were observed.

Fig. 5.40, *slow take-off* action potential, observed before the injury occurred.

Fig. 5.41, *sharp take-off* action potential, observed when the cell was injured and had a clear region.

Fig. 5.42, *slow take-off* action potential, observed when the cell had recovered from injury i.e. clear region became green again.

(iii) In Figs. 5.43 and 5.44 the cell was contaminated by some filament type organism (maybe bacterial) at one end. The action potentials which initiated at the contaminated end

had the *sharp take-off* features as shown in Fig. 5.43. During the same period action potentials initiating at the opposite end (i.e. with no observable contamination) had the *slow take-off* characteristic (Fig. 5.44).

5.3 Other Observations

5.3.1 Mottled and Even Colour Appearances

During the period of the experiments we normally observed periodic changes in the colour of the ISS's. Two distinct types of appearance were

(i) *mottled appearance*, when there were some dark green patches in parts of the ISS.

(ii) *even appearance*, when the dark green patches disappeared and the colour of the ISS was evenly green.

The mottled appearance is probably caused by the migration of the chloroplasts as described by Schmid and Koop (1983) as *banding* or *clodding* and by Kof *et al.* (1982) as chloroplast *clusters*. In two of the experiments the occurrences of (i) and (ii) were noted and these were indicated in Fig. 5.15 (experiment BF) and Fig. 5.16 (experiment AG). The mottled appearance seems to be associated with the active period while the even appearance seems to be associated with the rest period. This behaviour tends to suggest that these two types of appearance also appear in a rhythm which may be similar to the action potential rhythm. We should also note here that the dark green patches in (i) also moved along the ISS. However, directions of the movement were not recorded since only occasional observations were made.

5.3.2 The Action Potential Rhythm

As already described in section 5.2.1, the occurrences of the action potentials follow a definite rhythm. This rhythm was also observed by Borghi *et al.* (1983) and Dazy *et al.* (1980) and was found to be closely related to the cytoplasmic streaming and the longitudinal potential gradient rhythms.

In a few experiments where the ISS's were *dying* or *contaminated* this rhythm was not observed. The action potentials seemed to occur regularly without a rest period and the action potential frequency increased with time. The amplitudes of the action potentials also decreased as the experiments progressed. Fig. 5.45 shows the number of action potentials occurring (in 3 hour interval) in such an ISS (c.f. Figs. 5.3 and 5.4 note different scales).

Tables 5.1 and 5.2 Summary of experimental results.

Before = period after the onset of illumination until growth was observed.

After = period after growth was observed until the end of the experiment.

$\sum$ = number of action potentials for the whole experimental period.

R-end = the regenerating end.

O-end = the other end.

Mid = the region between R and O-ends.

= first series.

† = experiments in which the initiation sites of action potentials were analysed by using differential voltage distributions. Propagation behaviour of the action potentials in these experiments was not established due to limited information (see end of section 4.6).

Experiment		Cell type	ISS length (mm)	Regeneration		Action potential					
Name	Period (hour)			Type	Time (hour)	Number			Frequency (pulse h^{-1})	Propagating	
						Before	After	Σ		Number	%
AE	47	whorl	11	a-whl	21	18	35	53	1.13	4	8
AC	72	no whorl	9	a-whl	27	27	46	73	1.01	10	14
AI	120	whorl	15	a-cap	27	8	47	55	0.46	54	98
BG†	120	whorl	12	b-cap	28	9	29	38	0.32	-	-
BF	120	whorl	18	a-cap	34	14	44	58	0.48	53	91
AG	120	whorl	18	a-cap	40	27	43	70	0.58	54	77
AB	104	no whorl	11	b-whl	40	23	55	78	0.75	21	27
AF	101	whorl	8	a-whl	45	20	31	51	0.50	0	0
AH†	120	whorl	15	a-cap	45	19	36	55	0.46	-	-
BD	92	no whorl	12	a-whl	47	70	46	116	1.26	30	26
BE	96	whorl	15	a-tip	55	17	16	33	0.34	19	58
B1	71	no whorl	11	b-whl	55	21	7	28	0.39	9	32
BH	144	whorl	17	b-whl	112	51	20	71	0.49	37	52

Table 5.1 SUMMARY OF EXPERIMENTAL RESULTS I.

Experiment		Regeneration		Number of action potentials										Percentage of action potentials w.r.t Σ								
Name	Period	Time	Type	Before growth			After growth			Total				Before growth			After growth			Total		
	(hour)	(hour)		R-end	0-end	Mid	R-end	0-end	Mid	R-end	0-end	Mid	Σ	R-end	0-end	Mid	R-end	0-end	Mid	R-end	0-end	Mid
AE	47	21	a-whl	6	10	2	35	0	0	41	10	2	53	11	19	4	66	0	0	77	19	4
AC	72	27	a-whl	23	2	2	35	11	0	58	13	2	73	31	3	3	48	15	0	79	18	3
AI	120	27	a-cap	8	0	0	42	4	1	50	4	1	55	15	0	0	76	7	2	91	7	2
BG†	120	28	b-cap	3	6	0	27	0	2	30	6	2	38	8	16	0	71	0	5	79	16	5
BF	120	34	a-cap	7	1	6	28	14	2	35	15	8	58	12	2	10	48	24	3	60	26	14
AG	120	40	a-cap	2	23	2	19	22	2	21	45	4	70	3	33	3	27	31	3	30	64	6
AB	104	40	b-whl	7	15	1	23	30	2	30	45	3	78	9	19	1	29	38	3	38	58	4
AF	101	45	a-whl	0	20	0	0	31	0	0	51	0	51	0	39	0	0	61	0	0	100	0
AH†	120	45	a-cap	7	8	4	30	3	3	37	11	7	55	13	15	7	54	5	5	67	20	13
BD	92	47	a-whl	48	9	13	38	3	5	86	12	18	116	41	8	11	33	3	4	74	10	16
BE	96	55	a-tip	9	6	2	7	0	9	16	6	11	33	27	18	6	21	0	27	48	18	33
B1	71	55	b-whl	8	10	3	2	5	0	10	15	3	28	29	36	11	7	18	0	36	54	11
BH	144	112	b-whl	14	17	20	0	7	3	24	24	23	71	20	24	28	14	10	4	34	34	32
																			Average	55±26	34±27	11±11

Table 5.2 SUMMARY OF EXPERIMENTAL RESULTS II.

Fig. 5.1 Different types of redevelopment of ISS's at former apical end (a) a-tip; (b) a-whl(whorl); (c) a-cap (see text).

Fig. 5.2 Different types of redevelopment of ISS's at former basal end (a) b-tip; (b) b-whl (whorl); (c) b-cap (see text).

Fig. 5.3 and 5.4 Plots of results from experiments BG and AF respectively showing:-

(a) number of spontaneous action potentials at three hour intervals for the whole period of the experiment

(b) same as (a) but starting after the first *rest period* (see text)

(c) auto-correlation coefficients of (b) at lag k = 1,2,.....,K (K = maximum interval in (b) - 1).

NUMBER OF ACTION POTENTIALS FROM EXPERIMENT BG

AT 3 HOUR INTERVALS STARTING FROM THE 1st HOUR

INTVL	VALUE	0 2 4 6
		-*---------*---------*---------*
1	4.	I##########################
2	1.	I#######
3	0.	I#
4	0.	I#
5	1.	I#######
6	1	I#######
7	1.	I#######
8	0.	I#
9	1.	I#######
10	0	I#
11	0.	I#
12	0	I#
13	0.	I#
14	1.	I#######
15	2.	I############
16	2.	I############
17	2.	I############
18	0.	I#
19	0.	I#
20	0.	I#
21	0.	I#
22	1.	I#######
23	2.	I############
24	2.	I############
25	2.	I############
26	3.	I##################
27	1.	I#######
28	0.	I#
29	0.	I#
30	0.	I#
31	0.	I#
32	2.	I############
33	2.	I############
34	3.	I##################
35	1.	I#######
36	2.	I############
37	1.	I#######
38	0.	I#
39	0.	I#
40	0.	I#

Fig. 5.3 (a)

NUMBER OF ACTION POTENTIALS FROM EXPERIMENT BG

AT 3 HOUR INTERVALS STARTING FROM THE 13th HOUR

INTVL	VALUE	0 2 4 6
		-*---------*---------*---------*
1	1.	I######
2	1.	I######
3	1.	I######
4	0.	I#
5	1.	I######
6	0	I#
7	0.	I#
8	0.	I#
9	0.	I#
10	1.	I######
11	2.	I##########
12	2.	I##########
13	2.	I##########
14	0.	I#
15	0.	I#
16	0.	I#
17	0.	I#
18	1.	I######
19	2.	I##########
20	2.	I##########
21	2.	I##########
22	3.	I##################
23	1.	I######
24	0.	I#
25	0.	I#
26	0.	I#
27	0.	I#
28	2.	I##########
29	2.	I##########
30	3.	I##################
31	1.	I######
32	2.	I##########
33	1.	I######
34	0.	I#
35	0.	I#
36	0.	I#

Fig. 5.3 (b)

AUTO-CORRELATION COEFFICIENTS OF NUMBER OF ACTION POTENTIALS

FROM EXPERIMENT BG AT 3 HOUR INTERVALS STARTING FROM THE 13th HOUR

LAG	VALUE	-1.0	0.0	1.0
		--*----------+----------*----------+----------*		
1	0.5443	I	##########	
2	0.2108	I	#####	
3	-0.2449	I	######	
4	-0.5479	I	##########	
5	-0.6117	I	##########	
6	-0.3651	I	########	
7	-0.0015	I	#	
8	0.3342	I	########	
9	0.4866	I	##########	
10	0.5195	I	##########	
11	0.2445	I	######	
12	-0.1221	I	###	
13	-0.3666	I	########	
14	-0.4559	I	##########	
15	-0.3365	I	########	
16	-0.1535	I	####	
17	0.1516	I	####	
18	0.1794	I	#####	
19	0.2377	I	######	
20	0.1459	I	####	
21	-0.0070	I	#	
22	-0.1319	I	####	
23	-0.1906	I	#####	
24	-0.1908	I	#####	
25	-0.0689	I	##	
26	-0.0386	I	##	
27	0.0859	I	###	
28	0.0551	I	##	
29	0.0549	I	##	
30	0.0522	I	##	
31	0.0240	I	#	
32	0.0212	I	#	
33	-0.0070	I	#	
34	-0.0047	I	#	
35	-0.0023	I	#	

Fig. 5.3 (c)

NUMBER OF ACTION POTENTIALS FROM EXPERIMENT AF

AT 3 HOUR INTERVALS STARTING FROM THE 1st HOUR

INTVL	VALUE	0 2 4 6
		-*---------*---------*---------*
1	2.	I###########
2	0.	I#
3	0.	I#
4	0.	I#
5	2.	I###########
6	1.	I#######
7	1.	I#######
8	2.	I###########
9	3.	I##################
10	5.	I##############################
11	2.	I###########
12	1.	I#######
13	0.	I#
14	1.	I#######
15	1.	I#######
16	3.	I##################
17	2.	I###########
18	3.	I##################
19	5.	I##############################
20	3.	I##################
21	2.	I###########
22	1.	I#######
23	0.	I#
24	1.	I#######
25	1.	I#######
26	2.	I###########
27	1.	I#######
28	2.	I###########
29	2.	I###########
30	2.	I###########
31	0.	I#
32	0.	I#
33	0.	I#

Fig. 5.4 (a)

NUMBER OF ACTION POTENTIALS FROM EXPERIMENT AF

AT 3 HOUR INTERVALS STARTING FROM THE 13th HOUR

INTVL	VALUE	0 2 4 6
		-*---------*---------*---------*
1	2.	I###########
2	1.	I######
3	1.	I######
4	2.	I###########
5	3.	I##################
6	5.	I##############################
7	2.	I###########
8	1.	I######
9	0.	I#
10	1	I######
11	1.	I######
12	3.	I##################
13	2	I###########
14	3.	I##################
15	5.	I##############################
16	3.	I##################
17	2.	I###########
18	1.	I######
19	0.	I#
20	1	I######
21	1.	I######
22	2.	I###########
23	1.	I######
24	2.	I###########
25	2.	I###########
26	2.	I###########
27	0.	I#
28	0.	I#
29	0.	I#

Fig. 5.4 (b)

AUTO-CORRELATION COEFFICIENTS OF NUMBER OF ACTION POTENTIALS

FROM EXPERIMENT AF AT 3 HOUR INTERVALS STARTING FROM THE 13th HOUR

LAG	VALUE	-1.0	0.0	1.0
		--*--------------------*--------------------*		
1	0.5130	I	##########	
2	0.1155	I	###	
3	-0.2821	I	#######	
4	-0.3463	I	########	
5	-0.2718	I	######	
6	-0.1272	I	####	
7	-0.0397	I	##	
8	0.1929	I	#####	
9	0.4176	I	##########	
10	0.3663	I	########	
11	0.0932	I	###	
12	-0.2200	I	#####	
13	-0.3879	I	##########	
14	-0.2576	I	######	
15	-0.1737	I	####	
16	-0.0227	I	#	
17	-0.0247	I	#	
18	0.1185	I	###	
19	0.1359	I	####	
20	0.1052	I	###	
21	-0.0849	I	###	
22	-0.1842	I	#####	
23	-0.1797	I	#####	
24	-0.0351	I	##	
25	0.0395	I	##	
26	0.0375	I	##	
27	0.0133	I	#	
28	-0.0109	I	#	

Fig. 5.4 (c)

Fig. 5.5-5.10 Examples of spontaneous action potentials initiating at various points along a redeveloping ISS showing:-

(a) differential voltage waveforms

(b) calculated current waveforms (by second order regularization)

(c) initial depolarized region (▨) analysed from (b). The + sign indicates position of the positive current at the specified time.

(a)

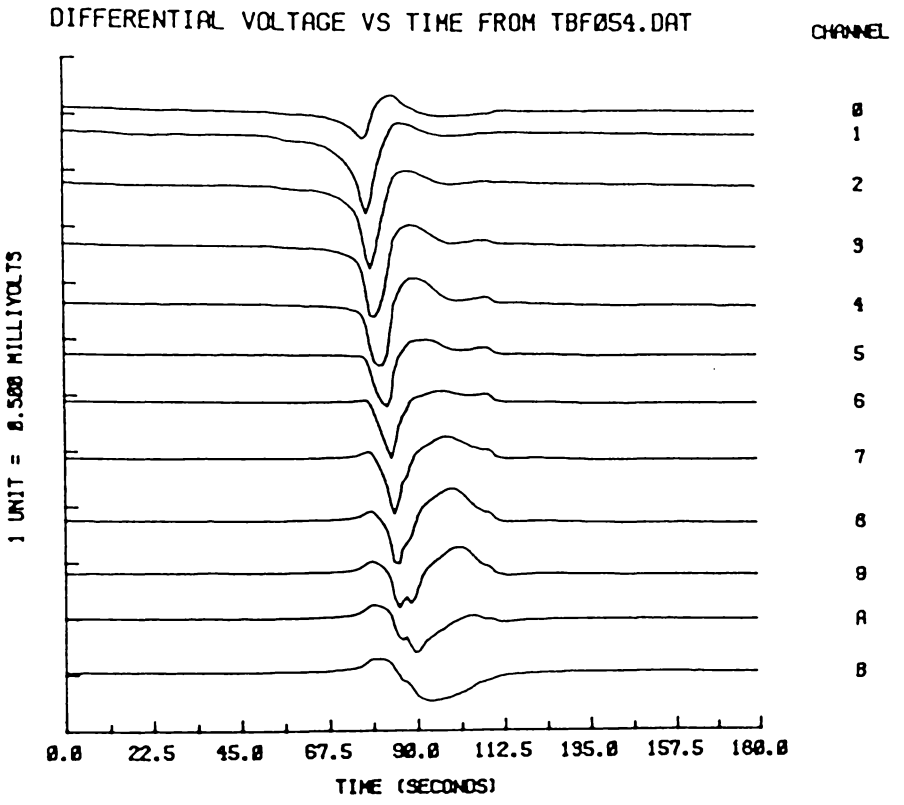
DIFFERENTIAL VOLTAGE VS TIME FROM TBF054.DAT
CHANNEL
0
1
2
3
4
5
6
7
8
9
A
B
1 UNIT = 0.500 MILLIVOLTS
0.0 22.5 45.0 67.5 90.0 112.5 135.0 157.5 180.0
TIME (SECONDS)

(b)

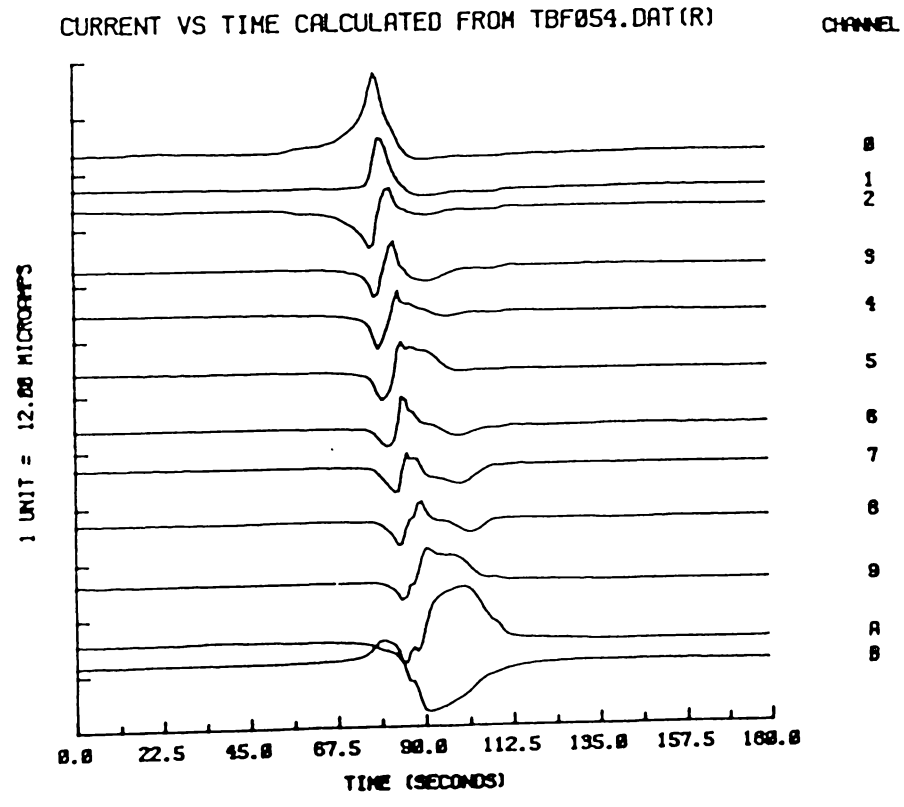
CURRENT VS TIME CALCULATED FROM TBF054.DAT(R)
CHANNEL
0
1
2
3
4
5
6
7
8
9
A
B
1 UNIT = 12.00 MICROAMPS
0.0 22.5 45.0 67.5 90.0 112.5 135.0 157.5 180.0
TIME (SECONDS)

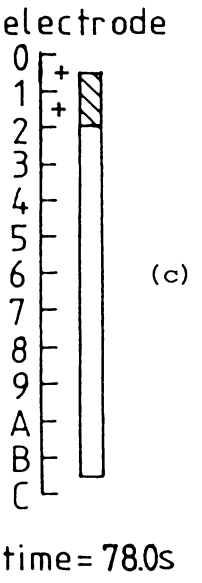
electrode
0
1
2
3
4
5
6
7
8
9
A
B
C
+
+
(c)
time = 78.0s

Fig. 5.5

(a)

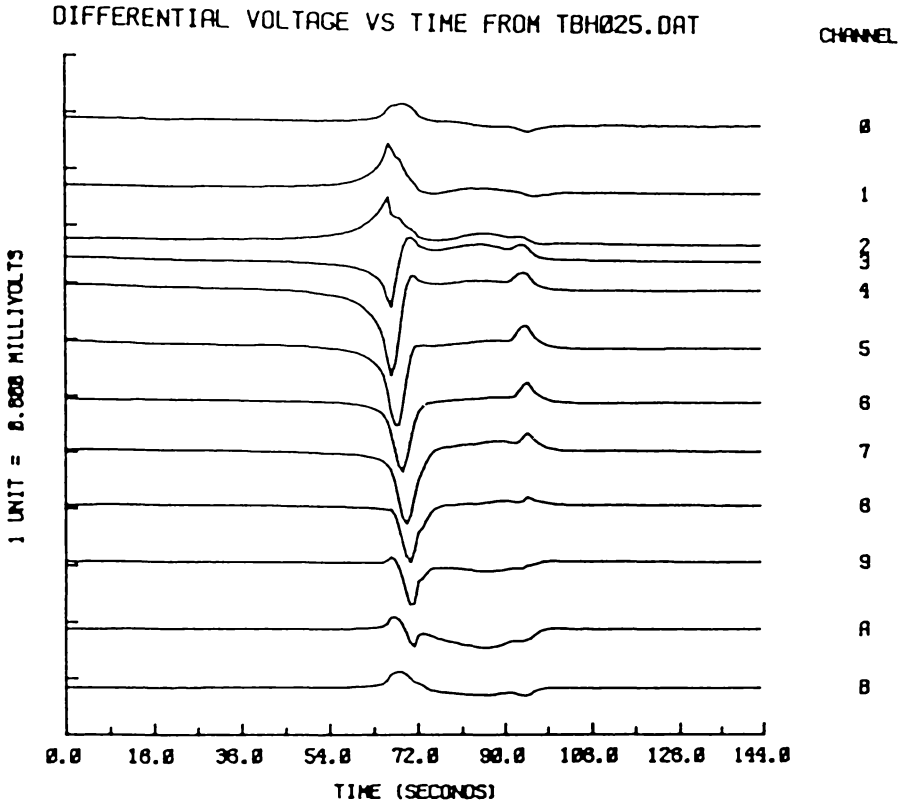
DIFFERENTIAL VOLTAGE VS TIME FROM TBH025.DAT
CHANNEL
0
1
2
3
4
5
6
7
8
9
A
B
1 UNIT = 0.800 MILLIVOLTS
0.0
18.0
36.0
54.0
72.0
90.0
108.0
126.0
144.0
TIME (SECONDS)

(b)

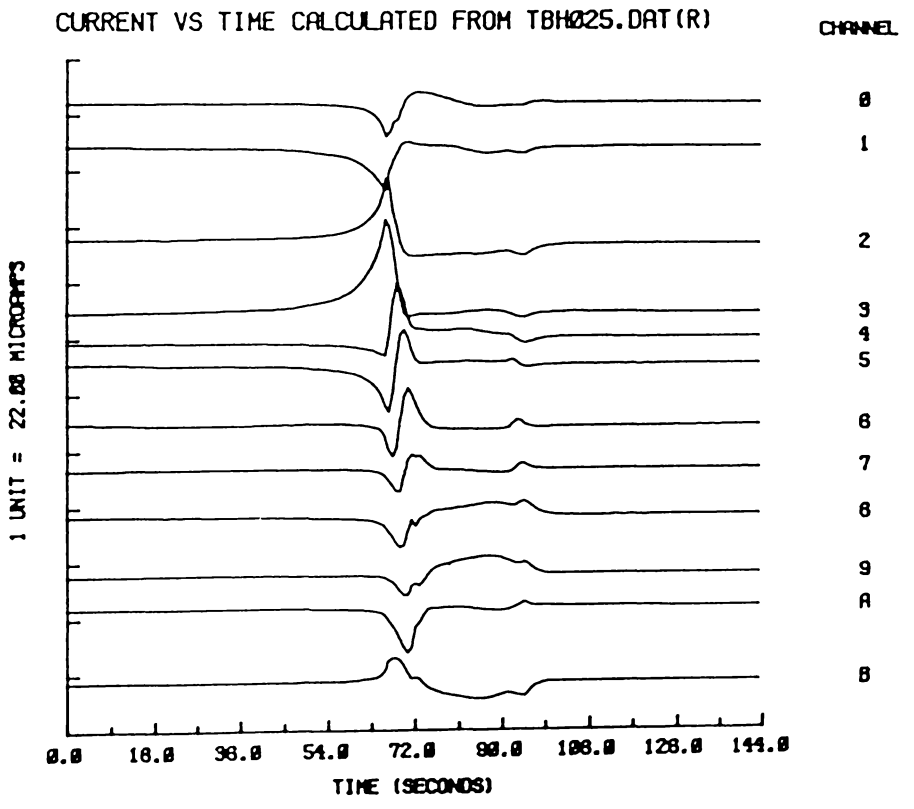
CURRENT VS TIME CALCULATED FROM TBH025.DAT(R)
CHANNEL
0
1
2
3
4
5
6
7
8
9
A
B
1 UNIT = 22.00 MICROAMPS
0.0
18.0
36.0
54.0
72.0
90.0
108.0
126.0
144.0
TIME (SECONDS)

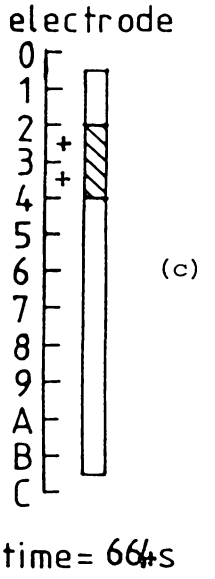
electrode
0
1
2
3
4
5
6
7
8
9
A
B
C
+
+
time= 664s

(c)

Fig. 5.6

(a)

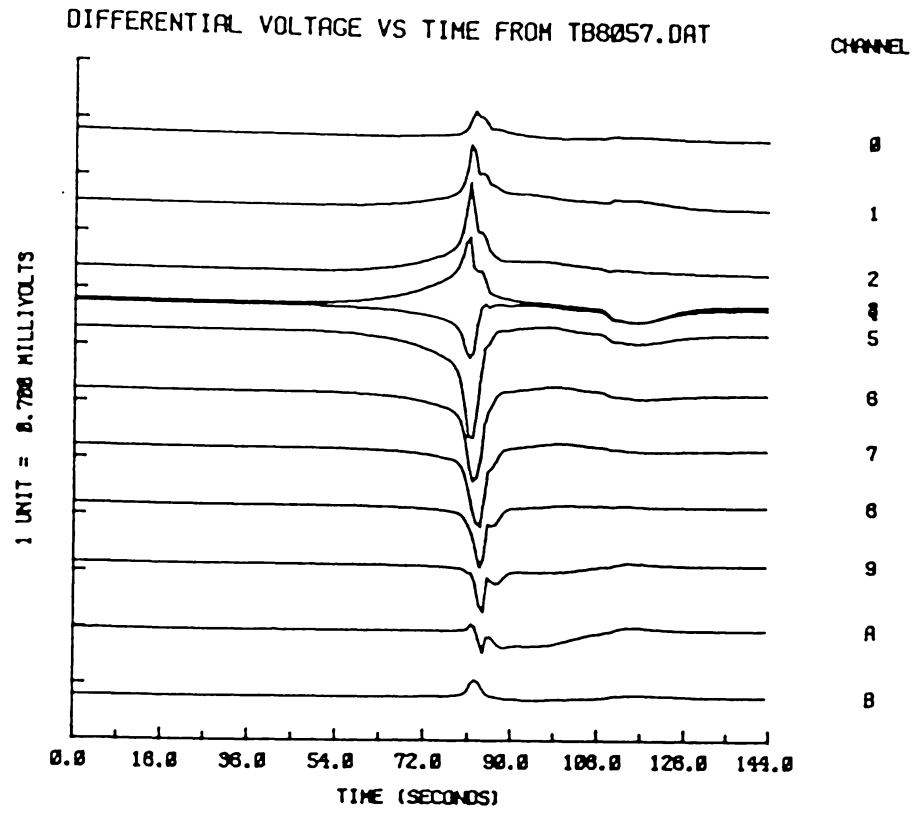
DIFFERENTIAL VOLTAGE VS TIME FROM TB0057.DAT
CHANNEL
0
1
2
3
4
5
6
7
8
9
A
B
1 UNIT = 0.700 MILLIVOLTS
0.0
18.0
36.0
54.0
72.0
90.0
108.0
126.0
144.0
TIME (SECONDS)

(b)

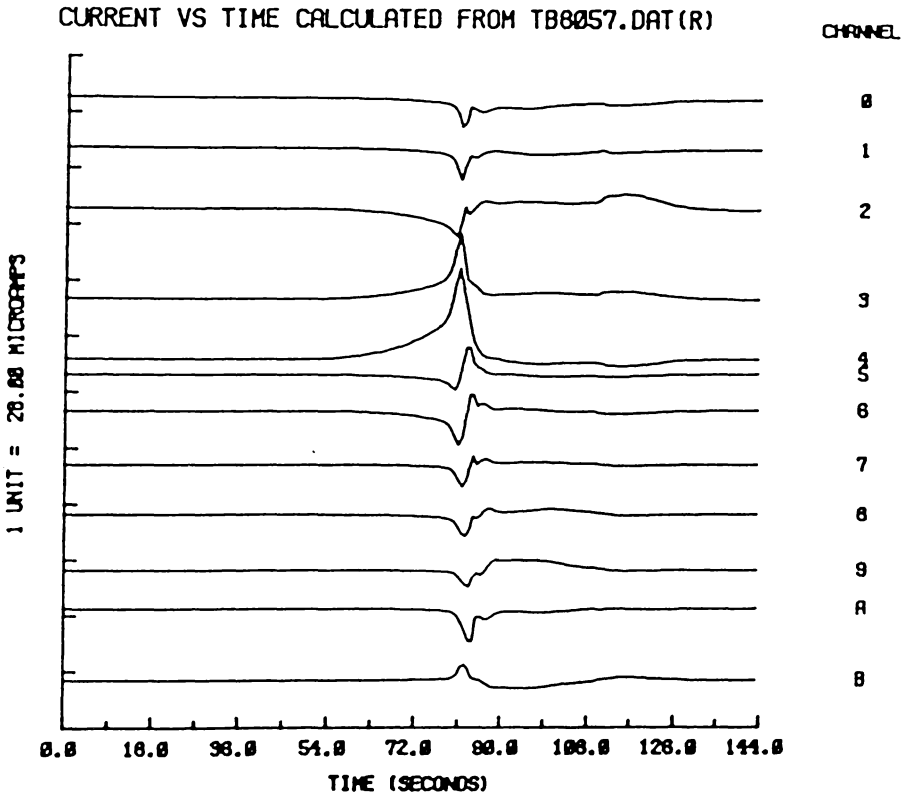
CURRENT VS TIME CALCULATED FROM TB0057.DAT(R)
CHANNEL
0
1
2
3
4
5
6
7
8
9
A
B
1 UNIT = 20.00 MICROAMPS
0.0
18.0
36.0
54.0
72.0
90.0
108.0
126.0
144.0
TIME (SECONDS)

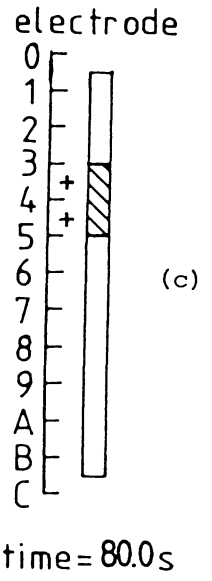
electrode
0
1
2
3
4
5
6
7
8
9
A
B
C
time = 80.0s

(c)

Fig. 5.7

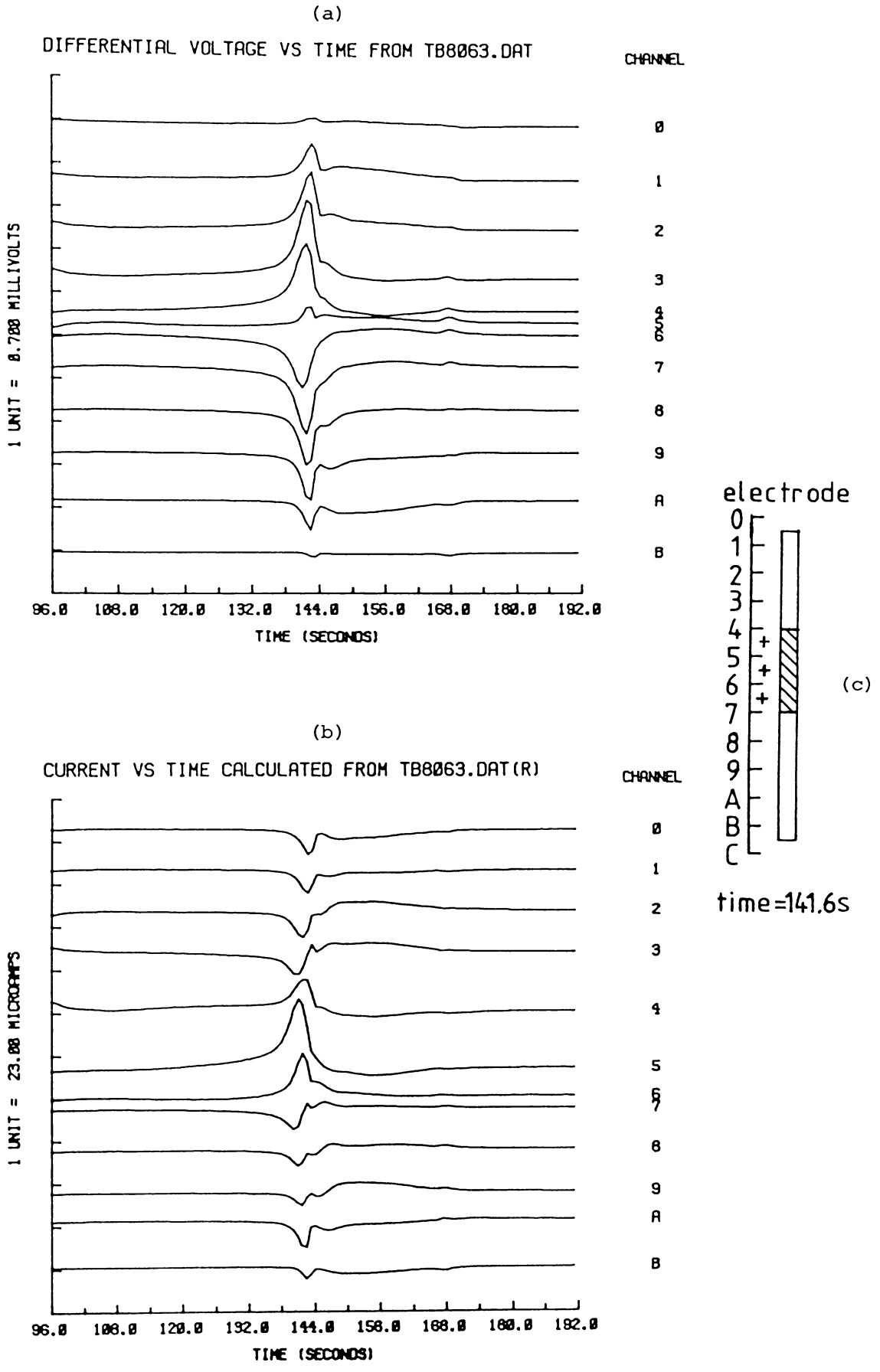
(a)
DIFFERENTIAL VOLTAGE VS TIME FROM TB8063.DAT
CHANNEL
0
1
2
3
4
5
6
7
8
9
A
B
1 UNIT = 0.700 MILLIVOLTS
96.0 108.0 120.0 132.0 144.0 156.0 168.0 180.0 192.0
TIME (SECONDS)
(b)
CURRENT VS TIME CALCULATED FROM TB8063.DAT(R)
CHANNEL
0
1
2
3
4
5
6
7
8
9
A
B
1 UNIT = 23.00 MICROAMPS
96.0 108.0 120.0 132.0 144.0 156.0 168.0 180.0 192.0
TIME (SECONDS)
electrode
0
1
2
3
4
5
6
7
8
9
A
B
C
(c)
time=141.6s

Fig. 5.8

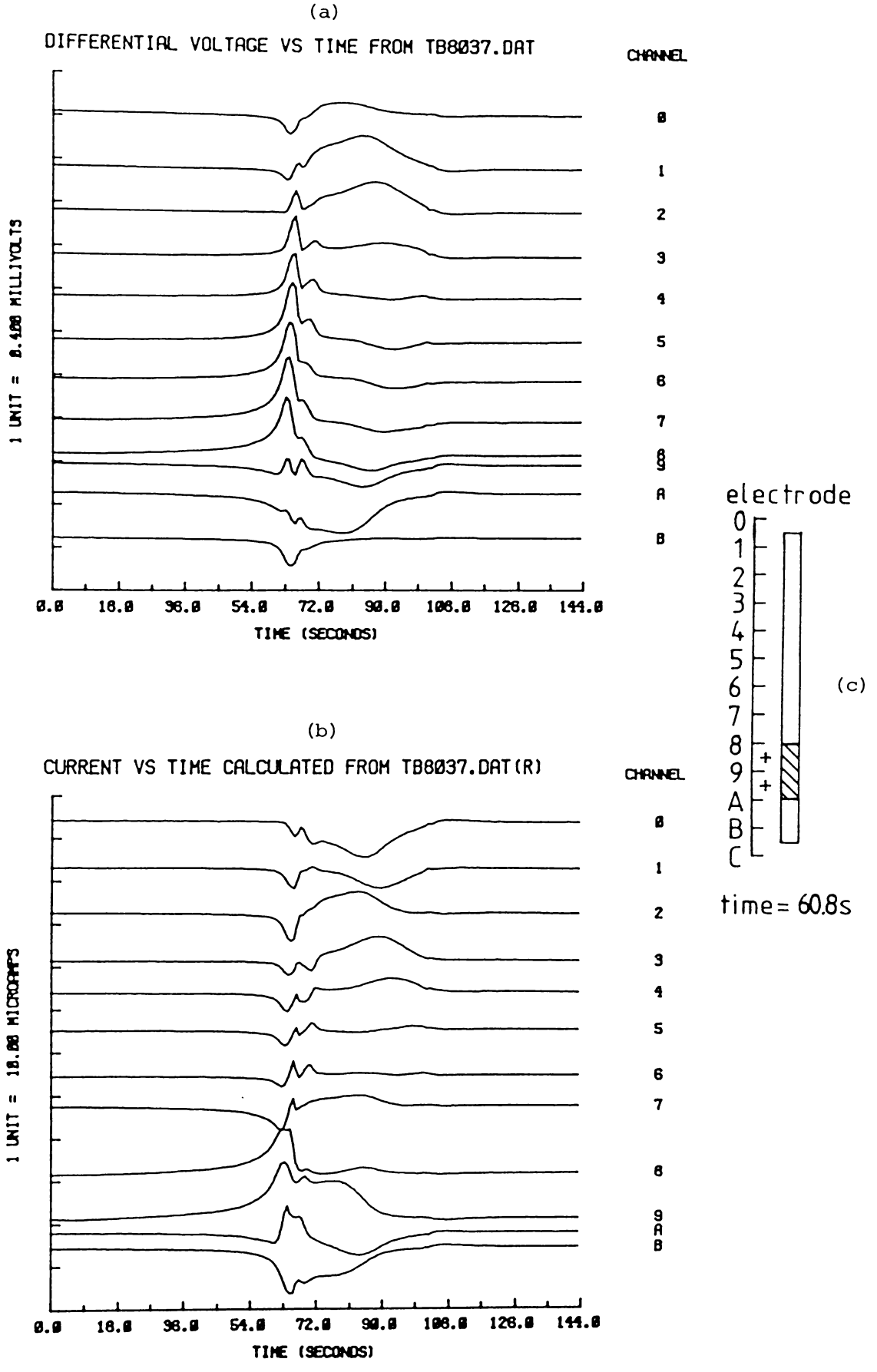
(a)
DIFFERENTIAL VOLTAGE VS TIME FROM TB0037.DAT
CHANNEL
0
1
2
3
4
5
6
7
8
9
A
B
1 UNIT = 0.400 MILLIVOLTS
0.0 18.0 36.0 54.0 72.0 90.0 108.0 126.0 144.0
TIME (SECONDS)
(b)
CURRENT VS TIME CALCULATED FROM TB0037.DAT(R)
CHANNEL
0
1
2
3
4
5
6
7
8
9
A
B
1 UNIT = 10.00 MICROAMPS
0.0 18.0 36.0 54.0 72.0 90.0 108.0 126.0 144.0
TIME (SECONDS)
electrode
0
1
2
3
4
5
6
7
8
9
A
B
C
+
+
(c)
time = 60.8s

Fig. 5.9

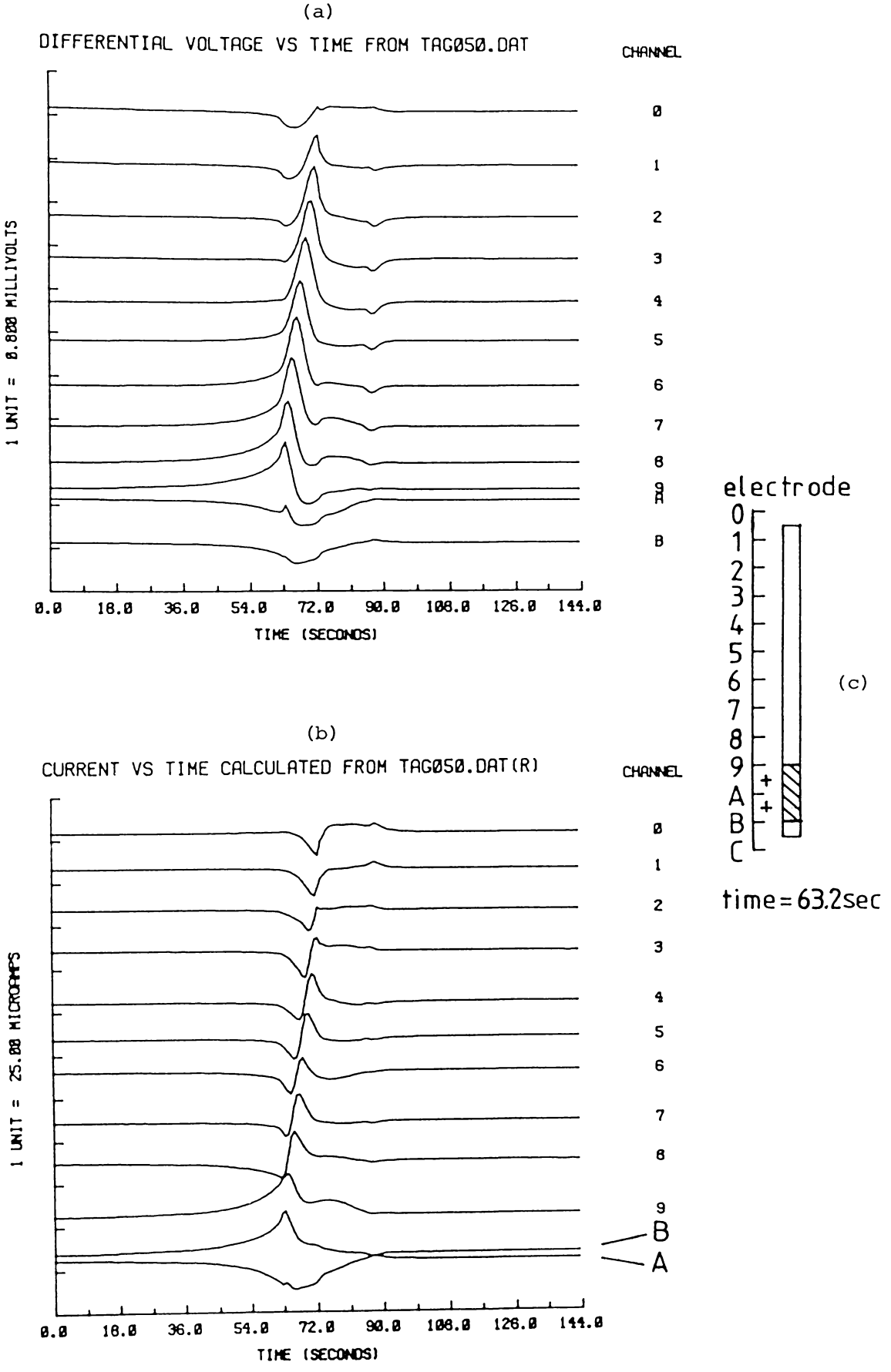
(a)
DIFFERENTIAL VOLTAGE VS TIME FROM TAG050.DAT
CHANNEL
1 UNIT = 0.000 MILLIVOLTS
0
1
2
3
4
5
6
7
8
9
A
B
0.0 18.0 36.0 54.0 72.0 90.0 108.0 126.0 144.0
TIME (SECONDS)
(b)
CURRENT VS TIME CALCULATED FROM TAG050.DAT(R)
CHANNEL
1 UNIT = 25.00 MICROAMPS
B
A
0.0 18.0 36.0 54.0 72.0 90.0 108.0 126.0 144.0
TIME (SECONDS)
electrode
0
1
2
3
4
5
6
7
8
9
A
B
C
(c)
time=63.2sec

Fig. 5.10

Fig. 5.11-5.23 Plots of initiation sites of spontaneous action potentials produced by ISS's after illumination showing:-

 - initiation site of a non-propagating action potential (except for Fig. 5.14 and 5.19 see † below)

 or  - initiation site of a propagating action potential with its propagation direction towards electrode 'O' or 'C' respectively. The length of the arrow indicates the distance travelled by the depolarized region (i.e. action potential)

 - action potential with sharp take-off

† - denotes experiments in which the initiation sites of action potentials were analysed by using differential voltage distributions (otherwise the current waveforms were used). Propagation behaviour of the action potentials was not established due to limited information (see end of section 4.6)

a and b - former apical and basal ends.

For Fig. 5.15 and 5.16 only

M - mottled appearance (see section 5.3.1)

E - even appearance.

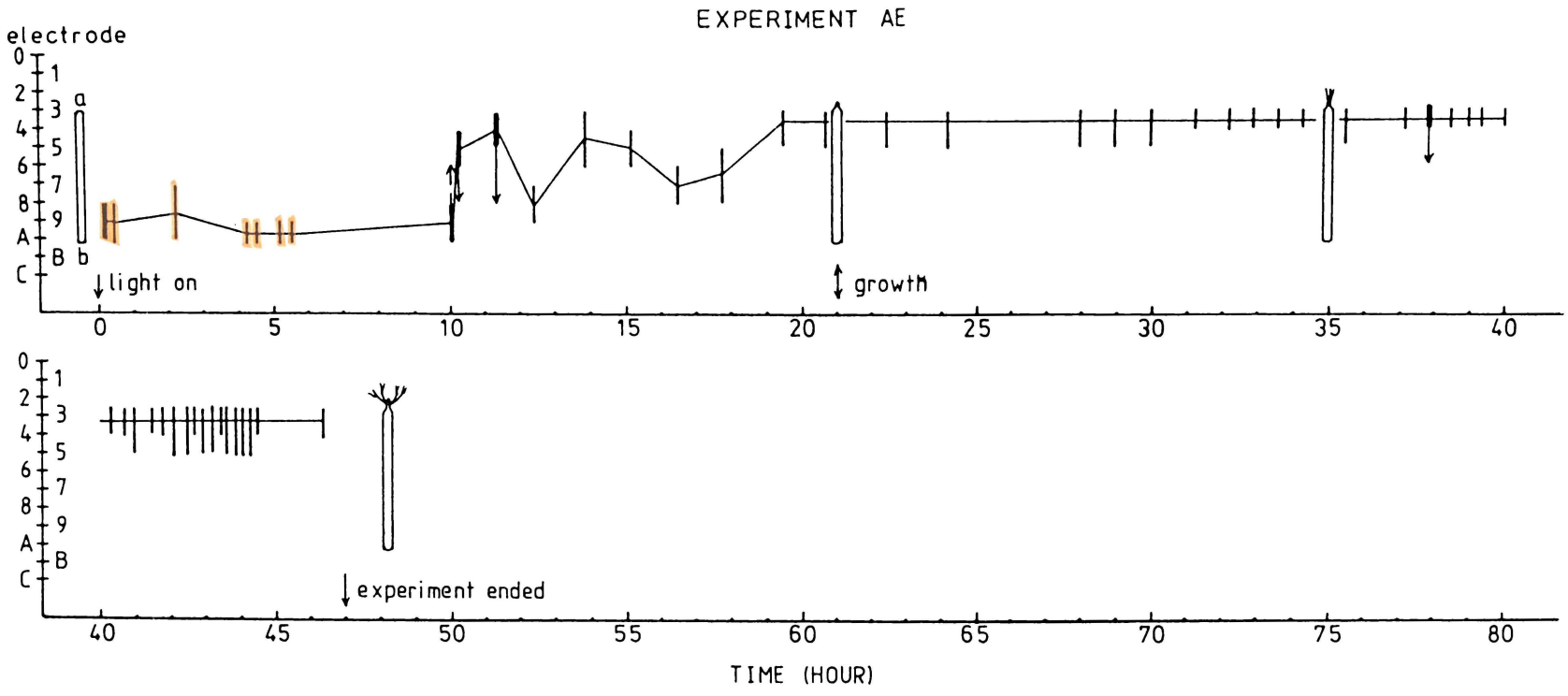
EXPERIMENT AE
electrode
0
1
2
3
4
5
6
7
8
9
A
B
C
a
b
light on
growth
0
5
10
15
20
25
30
35
40
experiment ended
40
45
50
55
60
65
70
75
80
TIME (HOUR)

Fig. 5.11

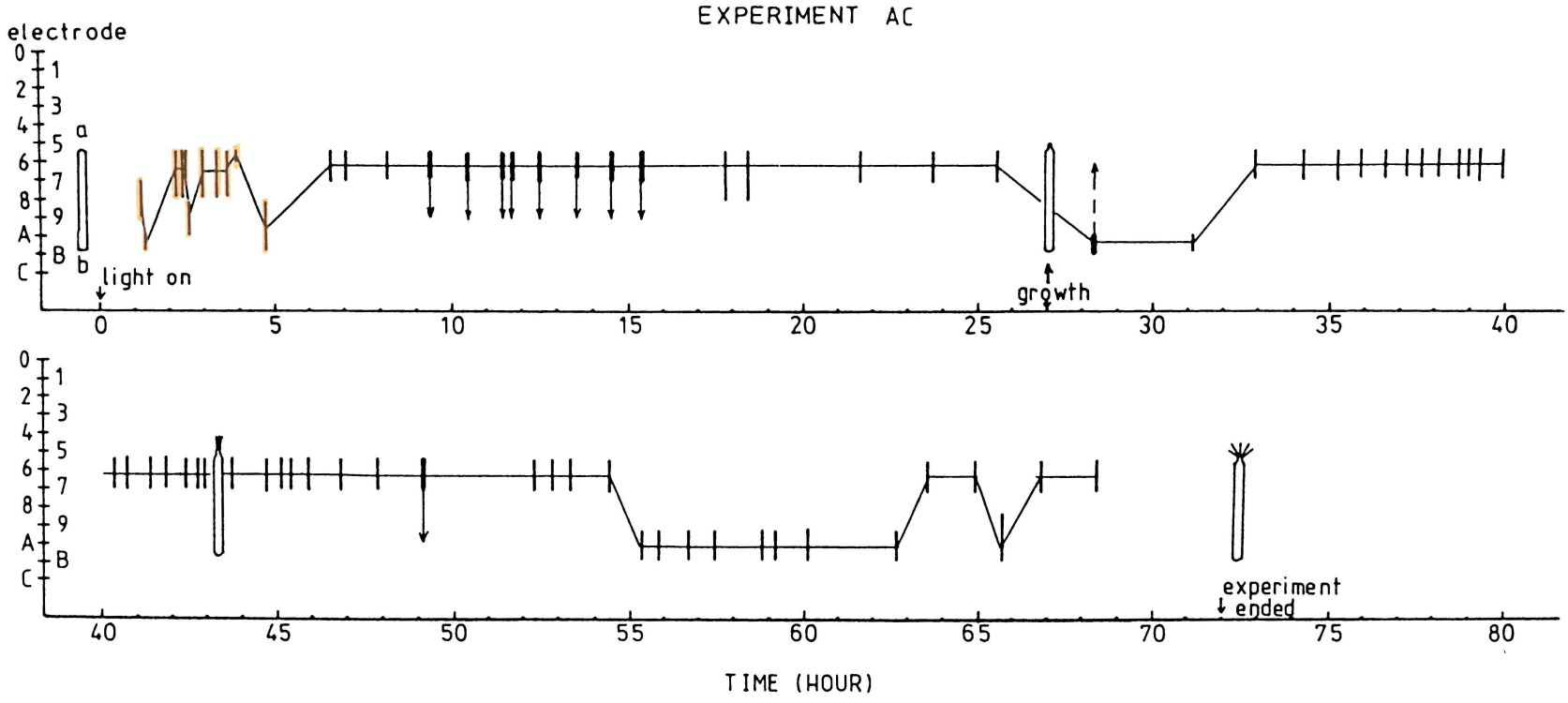
EXPERIMENT AC
electrode
0
1
2
3
4
5
a
6
7
8
9
A
B
b
C
light on
growth
0
5
10
15
20
25
30
35
40
experiment
ended
45
50
55
60
65
70
75
80
TIME (HOUR)

Fig. 5.12

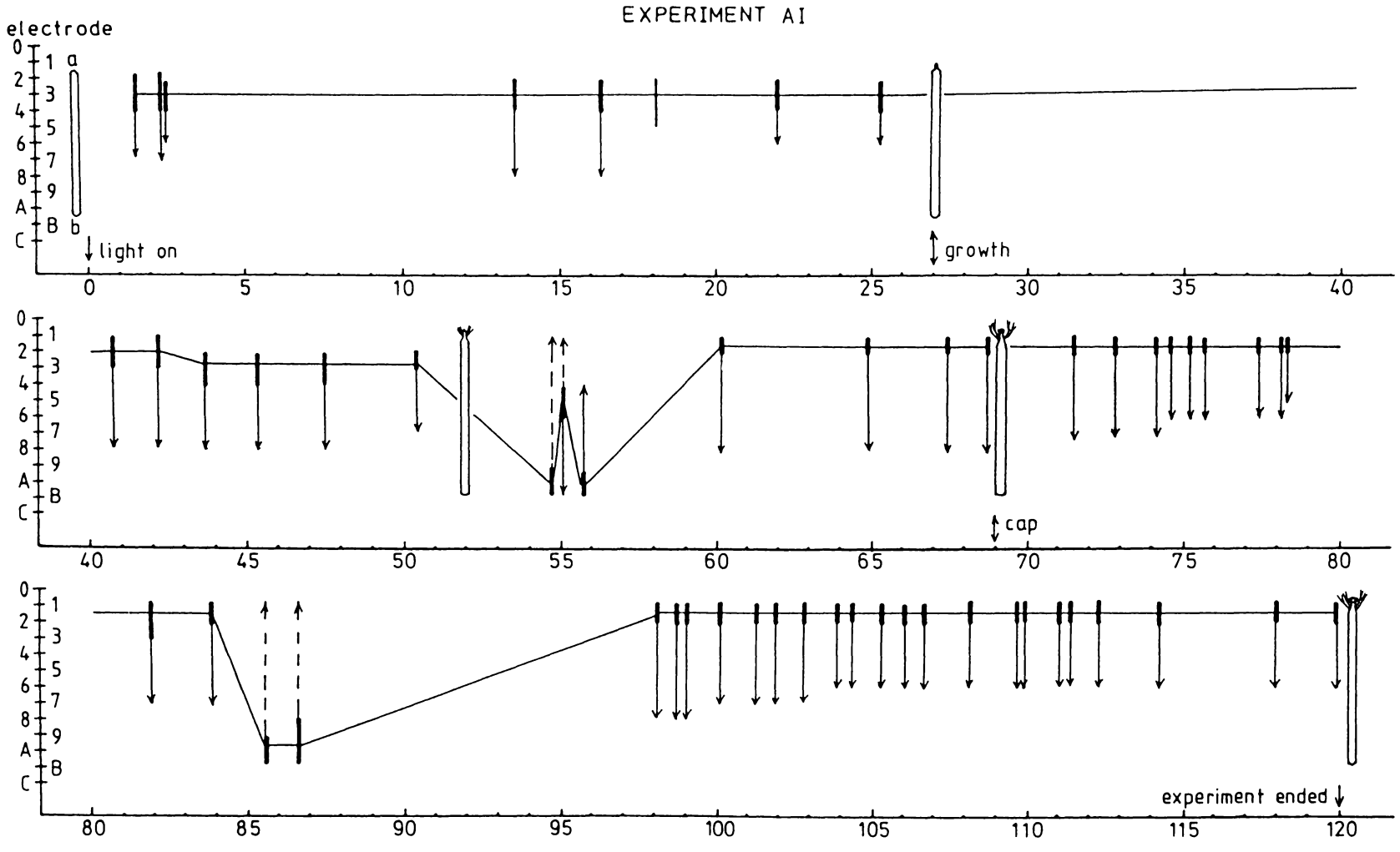
EXPERIMENT AI
electrode
0
2
4
6
8
A
C
1 a
3
5
7
9
B b
light on
growth
0
5
10
15
20
25
30
35
40
1
3
5
7
9
B
cap
40
45
50
55
60
65
70
75
80
85
90
95
100
105
110
115
120
experiment ended
TIME (HOUR)

Fig. 5.13

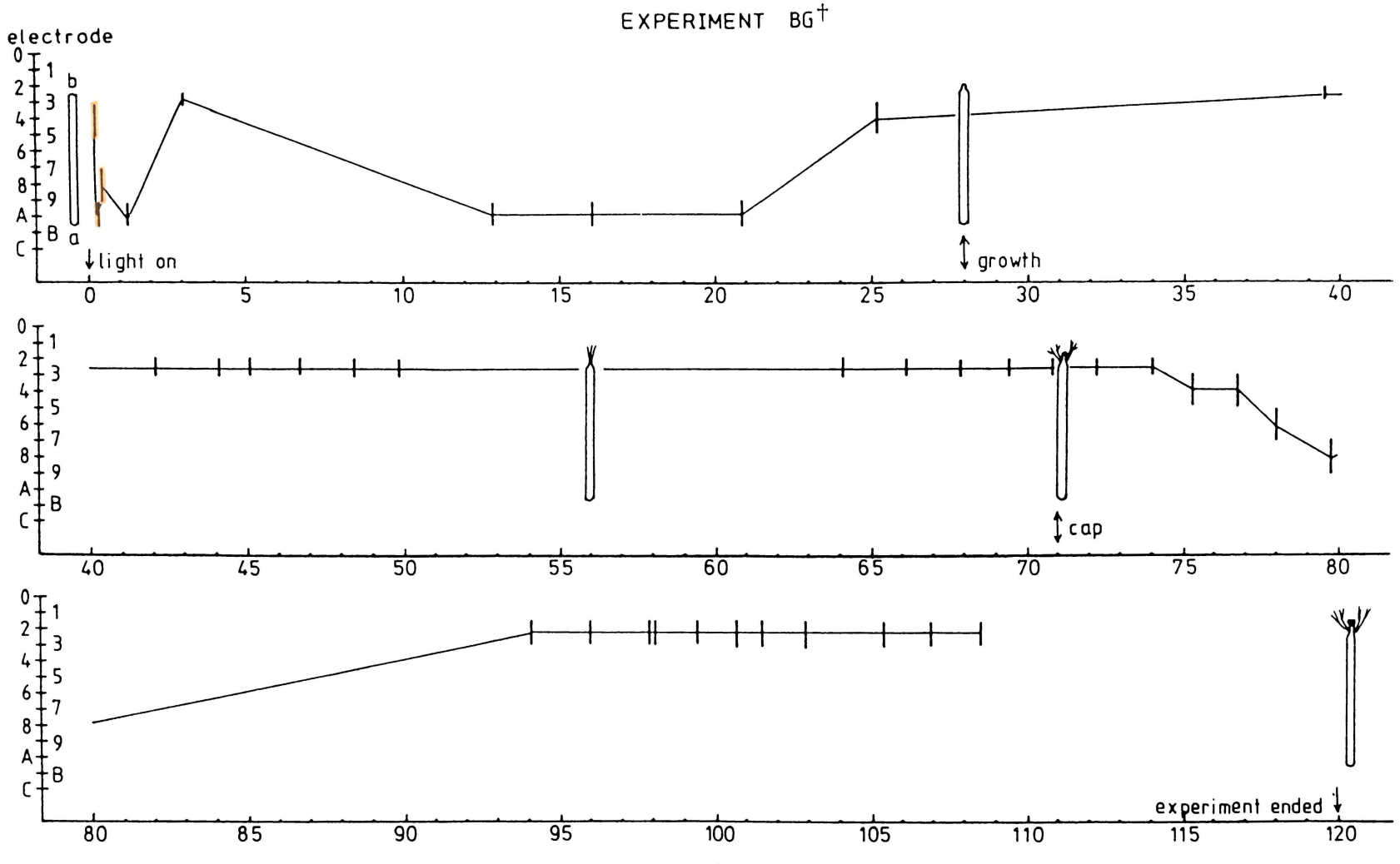
EXPERIMENT BG†
electrode
0 1 2 3 4 5 6 7 8 9 A B C
b
a
light on
growth
cap
experiment ended
0 5 10 15 20 25 30 35 40
40 45 50 55 60 65 70 75 80
80 85 90 95 100 105 110 115 120
TIME (HOUR)

Fig. 5.14

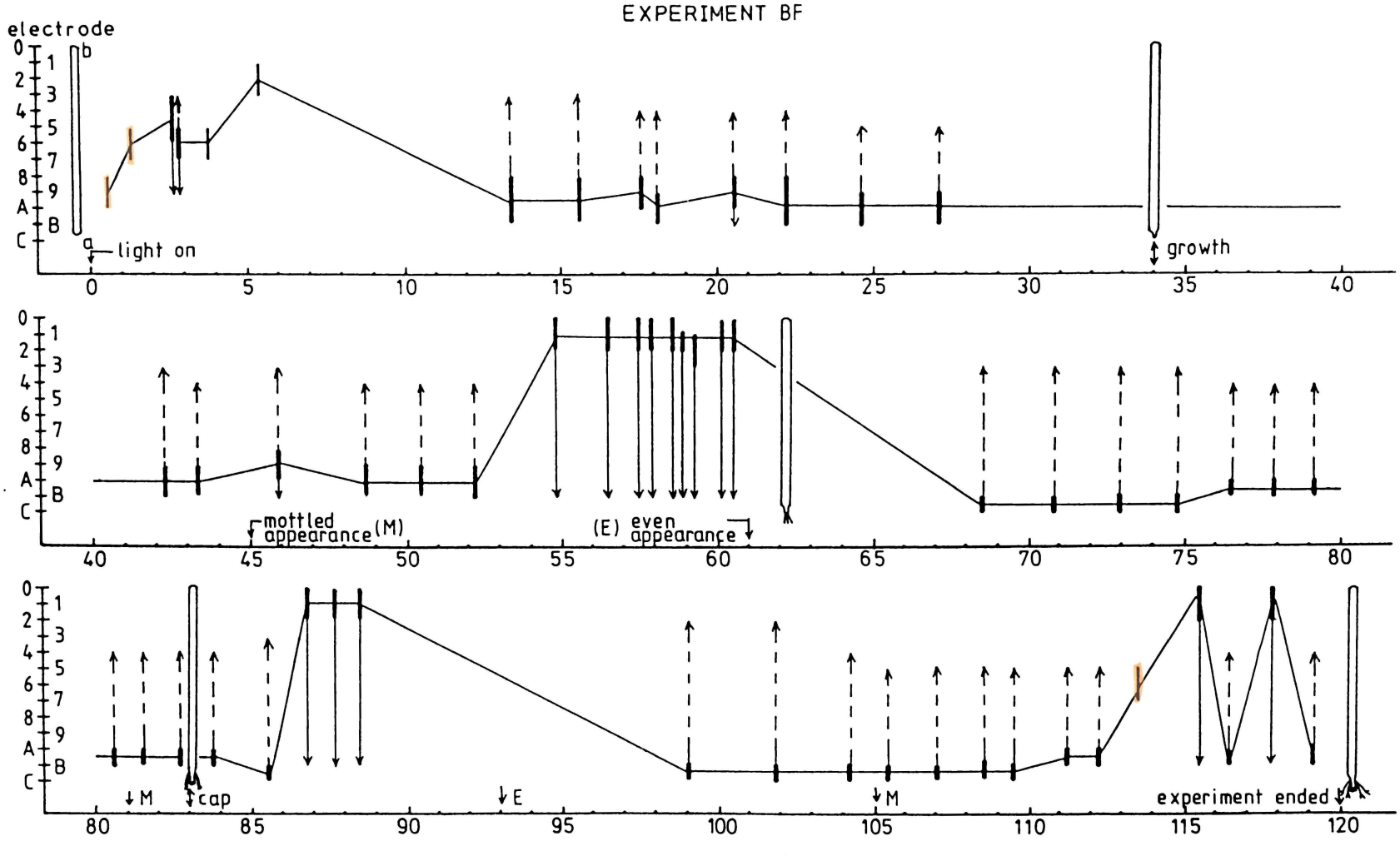
EXPERIMENT BF
electrode
b
a
light on
growth
mottled appearance (M)
(E) even appearance
M
cap
E
M
experiment ended
TIME (HOUR)

Fig. 5.15

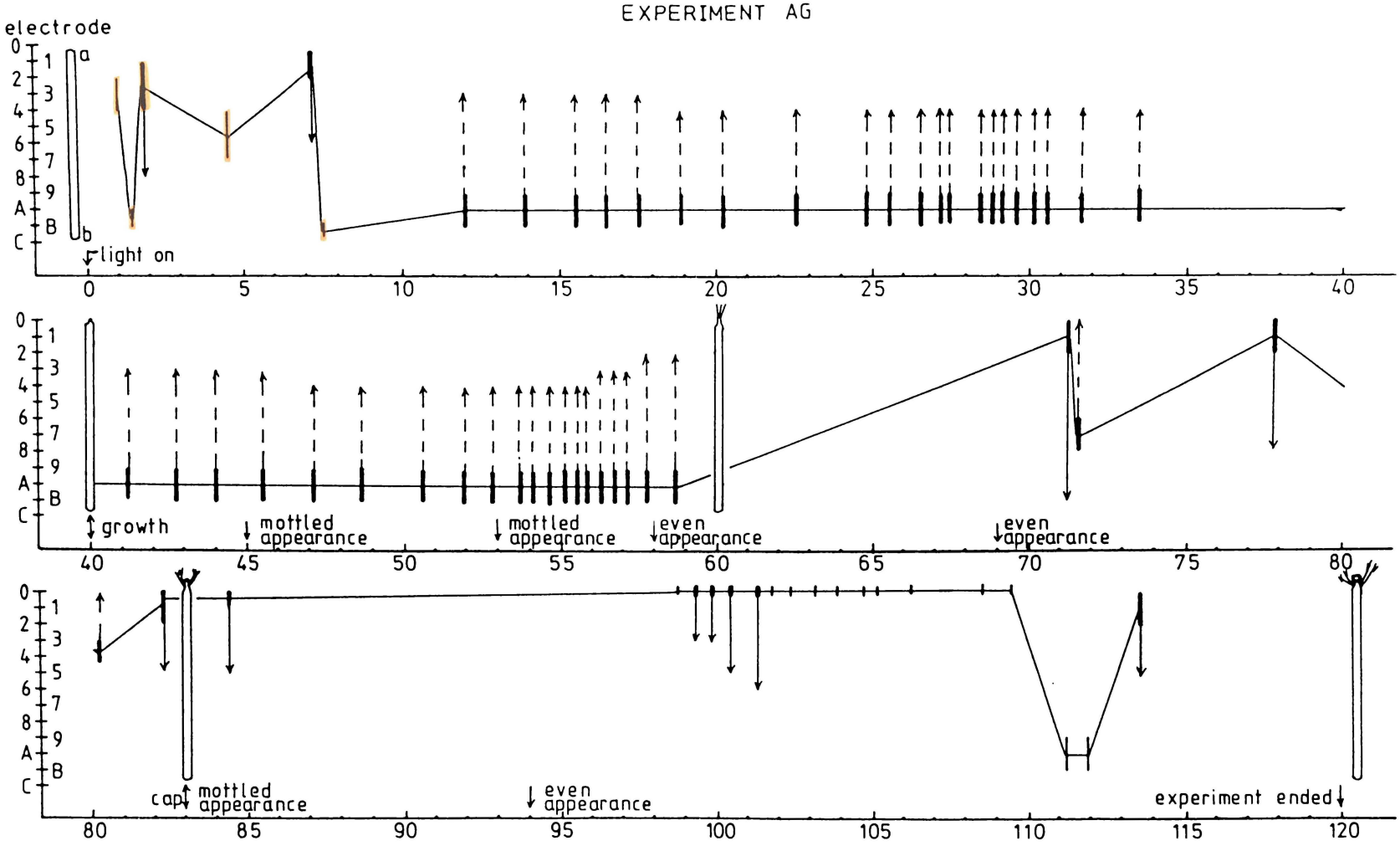
EXPERIMENT AG
electrode
a
b
light on
growth
mottled appearance
mottled appearance
even appearance
even appearance
cap
mottled appearance
even appearance
experiment ended
TIME (HOUR)

Fig. 5.16

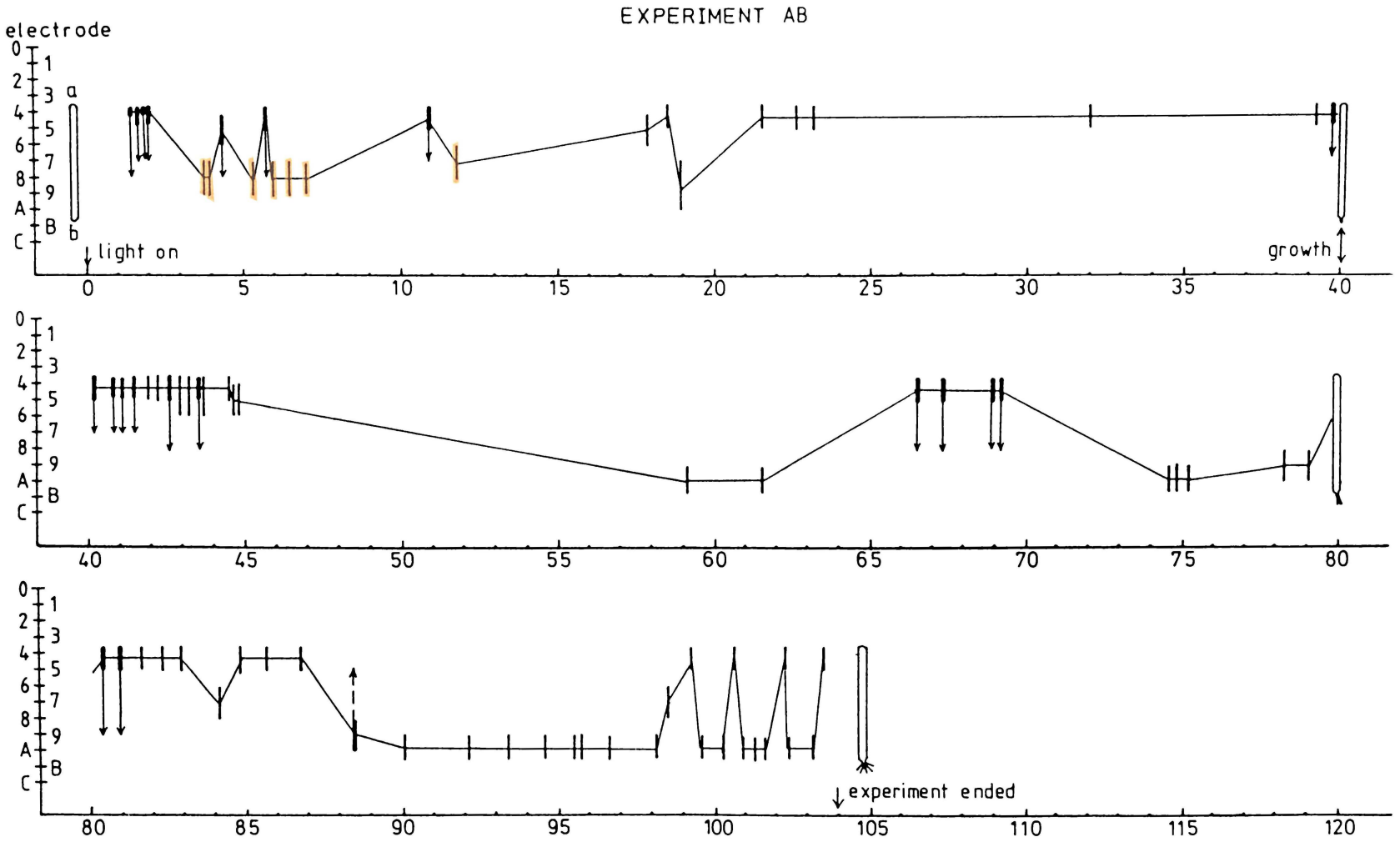
EXPERIMENT AB
electrode
0
2
4
6
8
A
C
1
3
5
7
9
B
a
b
light on
growth
0
5
10
15
20
25
30
35
40
45
50
55
60
65
70
75
80
85
90
95
100
105
110
115
120
experiment ended
TIME (HOUR)

Fig. 5.17

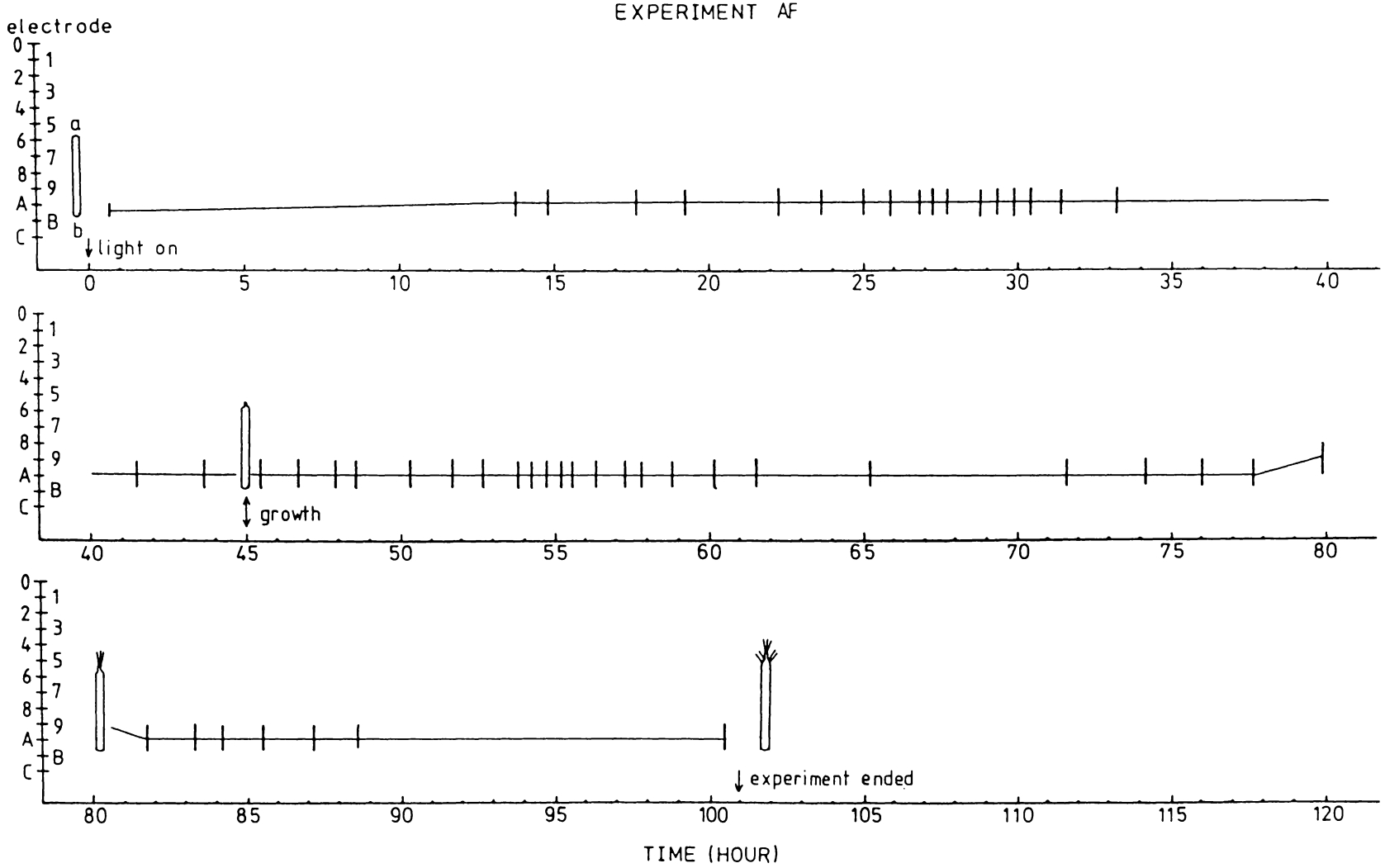
EXPERIMENT AF
electrode
0
1
2
3
4
5
a
6
7
8
9
A
B
b
C
light on
0
5
10
15
20
25
30
35
40
growth
45
50
55
60
65
70
75
80
experiment ended
85
90
95
100
105
110
115
120
TIME (HOUR)

Fig. 5.18

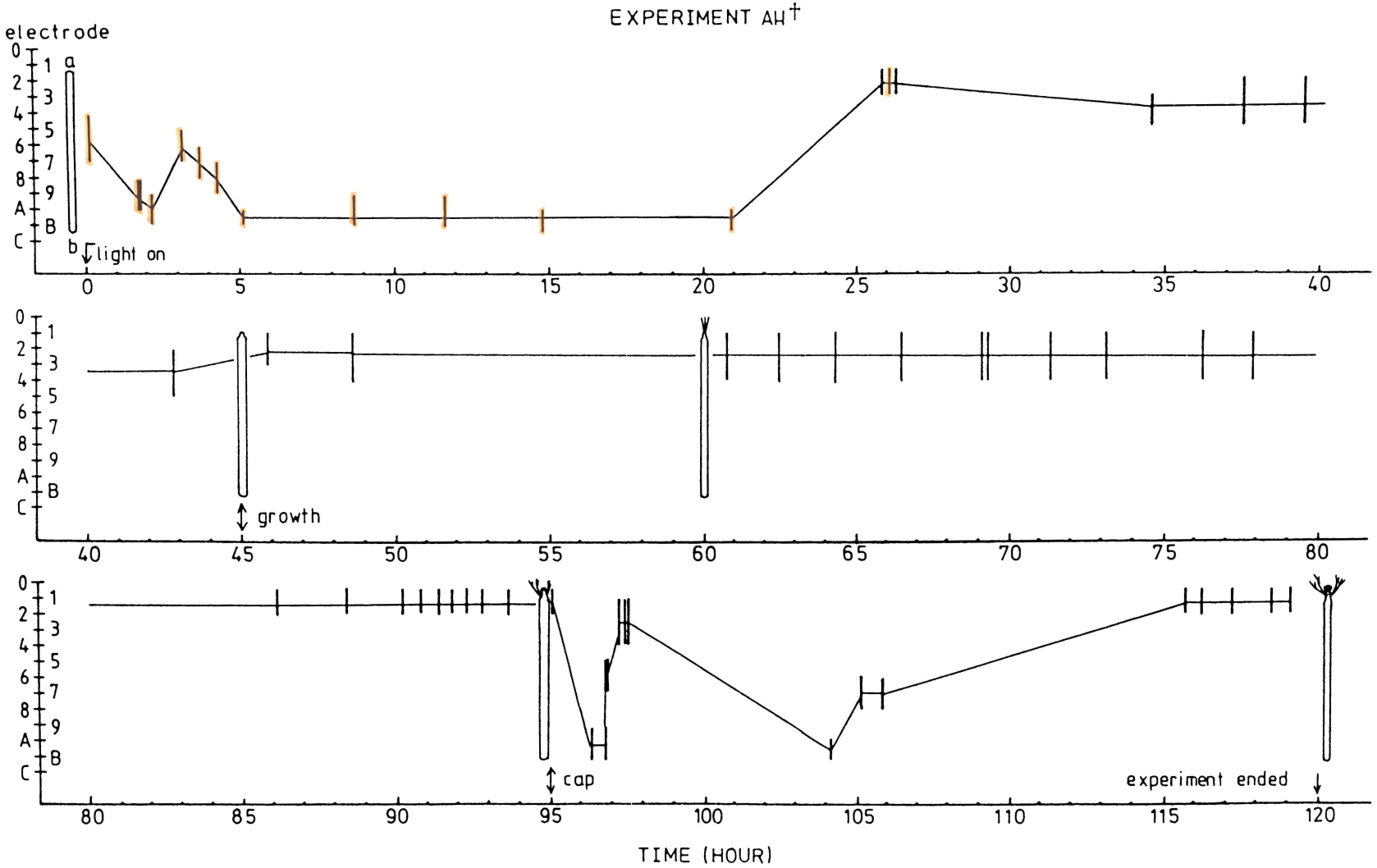
EXPERIMENT AH†
electrode
0
1 a
2
3
4
5
6
7
8
9
A
B
C
b
light on
0
5
10
15
20
25
30
35
40
growth
45
50
55
60
65
70
75
80
cap
experiment ended
85
90
95
100
105
110
115
120
TIME (HOUR)

Fig. 5.19

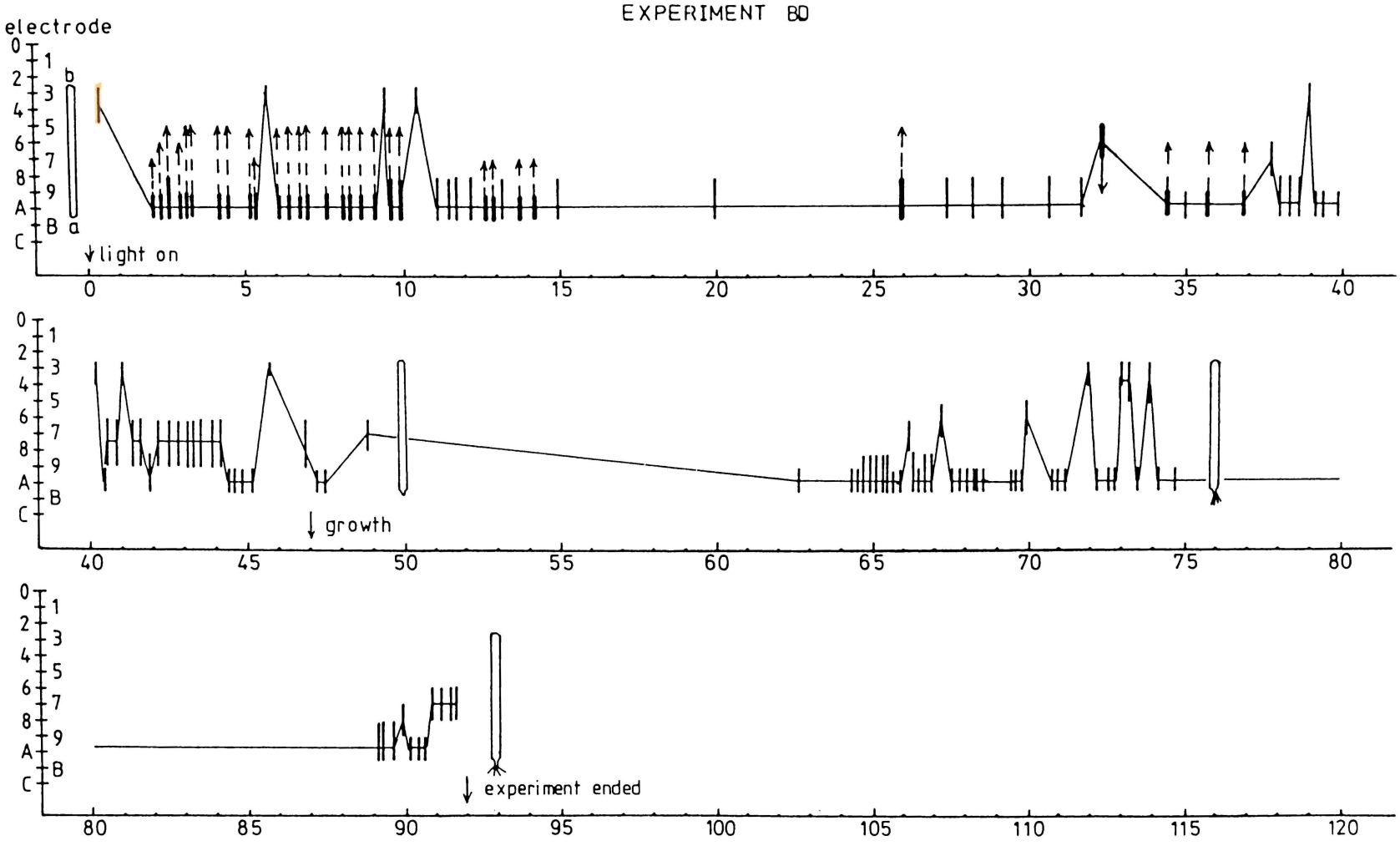
EXPERIMENT BD
electrode
0 1 2 3 4 5 6 7 8 9 A B C
b
a
light on
0 5 10 15 20 25 30 35 40
growth
40 45 50 55 60 65 70 75 80
experiment ended
80 85 90 95 100 105 110 115 120
TIME (HOUR)

Fig. 5.20

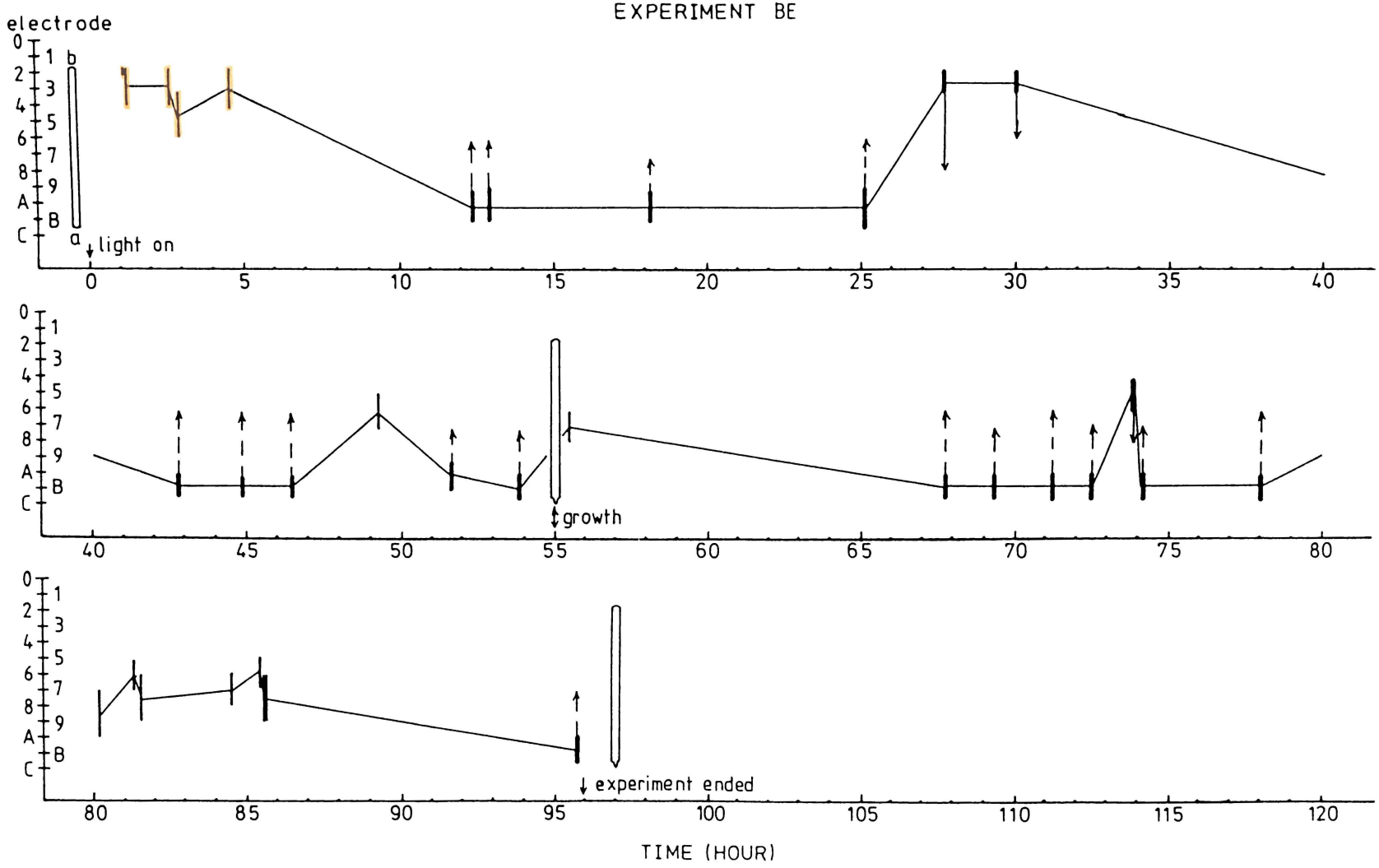
EXPERIMENT BE
electrode
0
1
2
3
4
5
6
7
8
9
A
B
C
b
a
light on
0
5
10
15
20
25
30
35
40
growth
40
45
50
55
60
65
70
75
80
experiment ended
80
85
90
95
100
105
110
115
120
TIME (HOUR)

Fig. 5.21

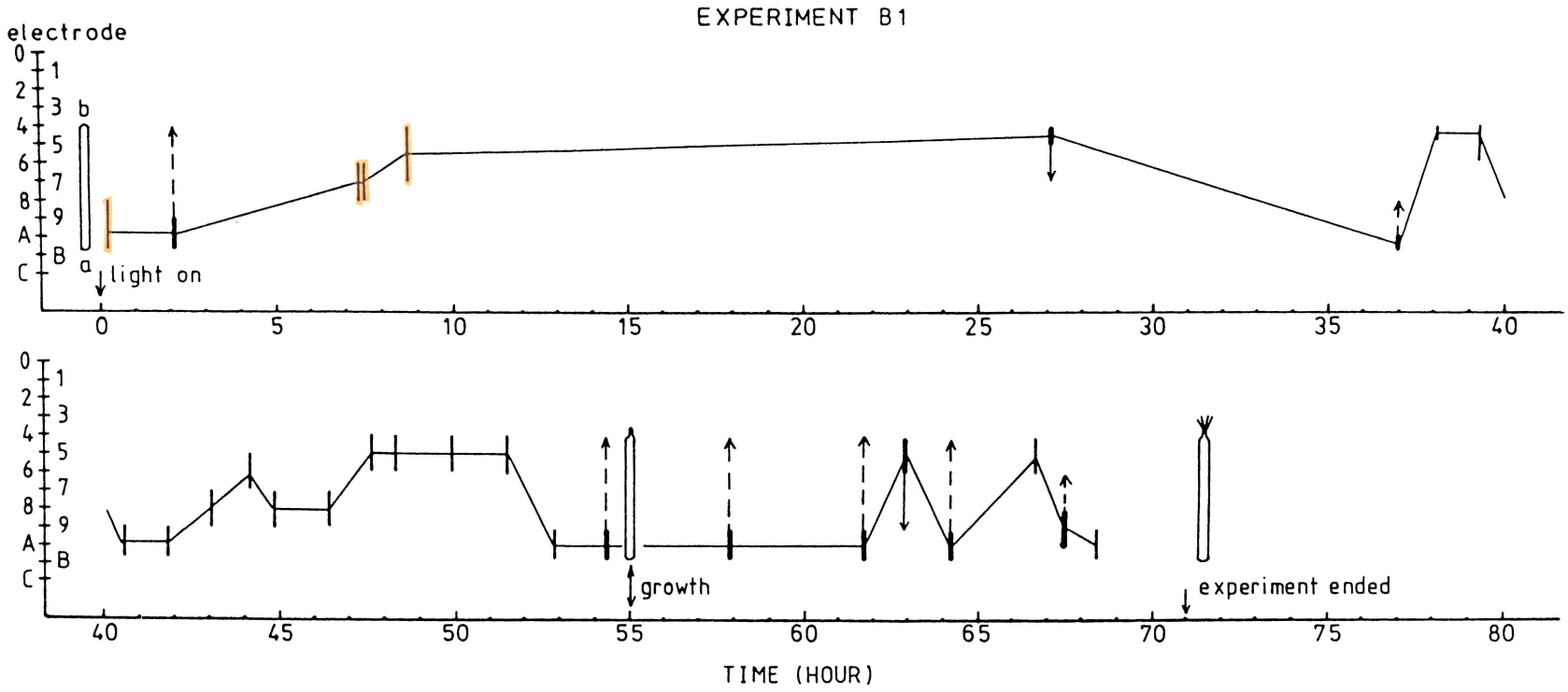
EXPERIMENT B1
electrode
0
1
2
3
4
5
6
7
8
9
A
B
C
b
a
light on
0
5
10
15
20
25
30
35
40
growth
experiment ended
45
50
55
60
65
70
75
80
TIME (HOUR)

Fig. 5.22

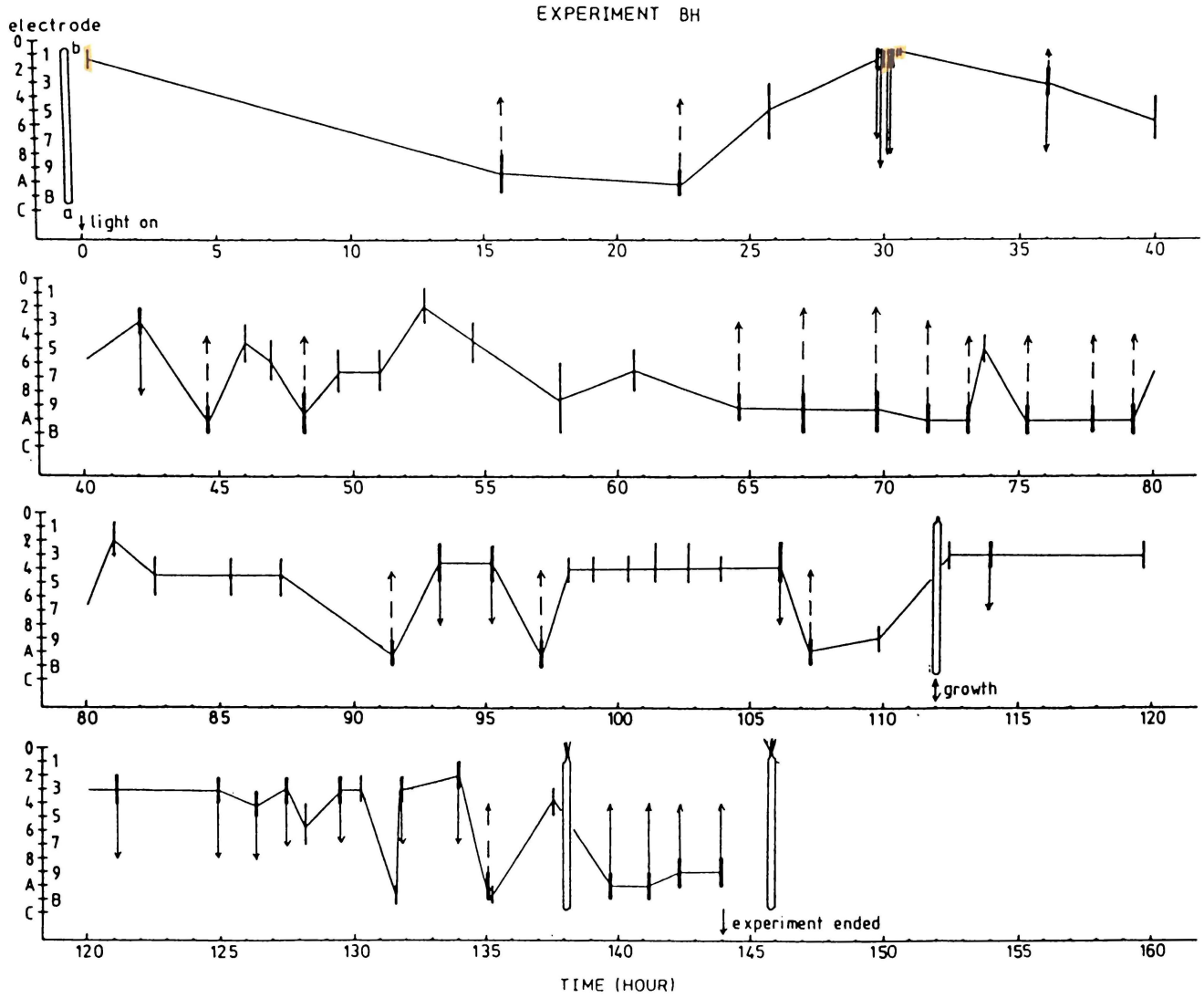
EXPERIMENT BH
electrode
0
2
4
6
8
A
C
1
3
5
7
9
B
b
a
light on
0
5
10
15
20
25
30
35
40
45
50
55
60
65
70
75
80
85
90
95
100
105
110
115
120
growth
125
130
135
140
145
150
155
160
experiment ended
TIME (HOUR)

Fig. 5.23

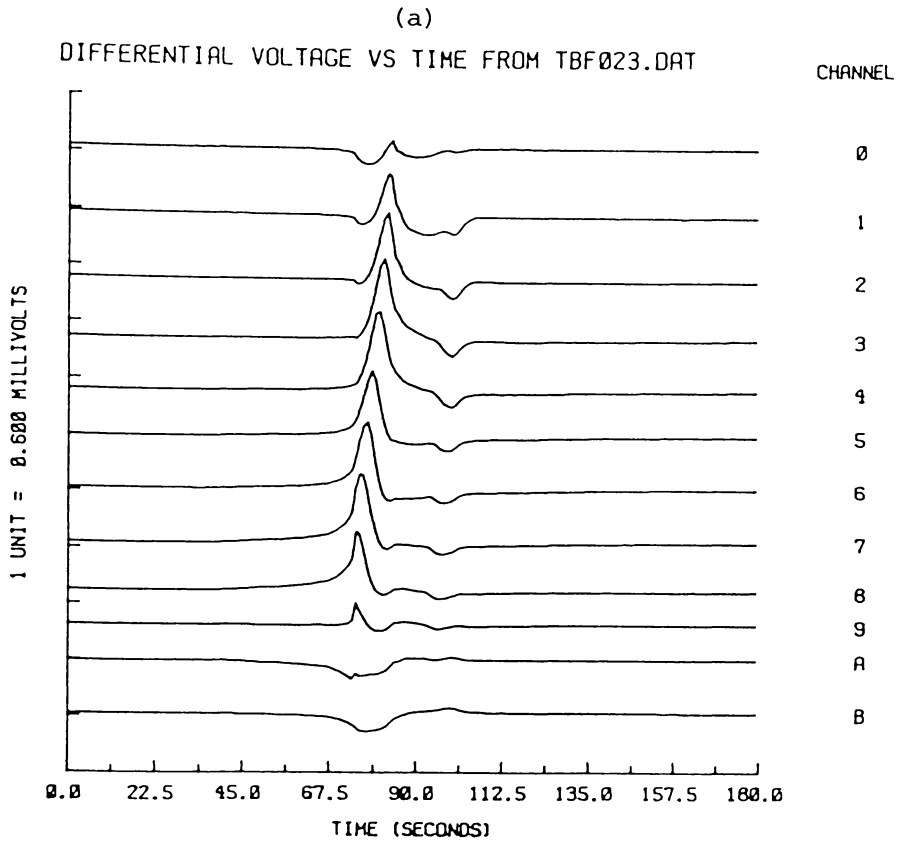

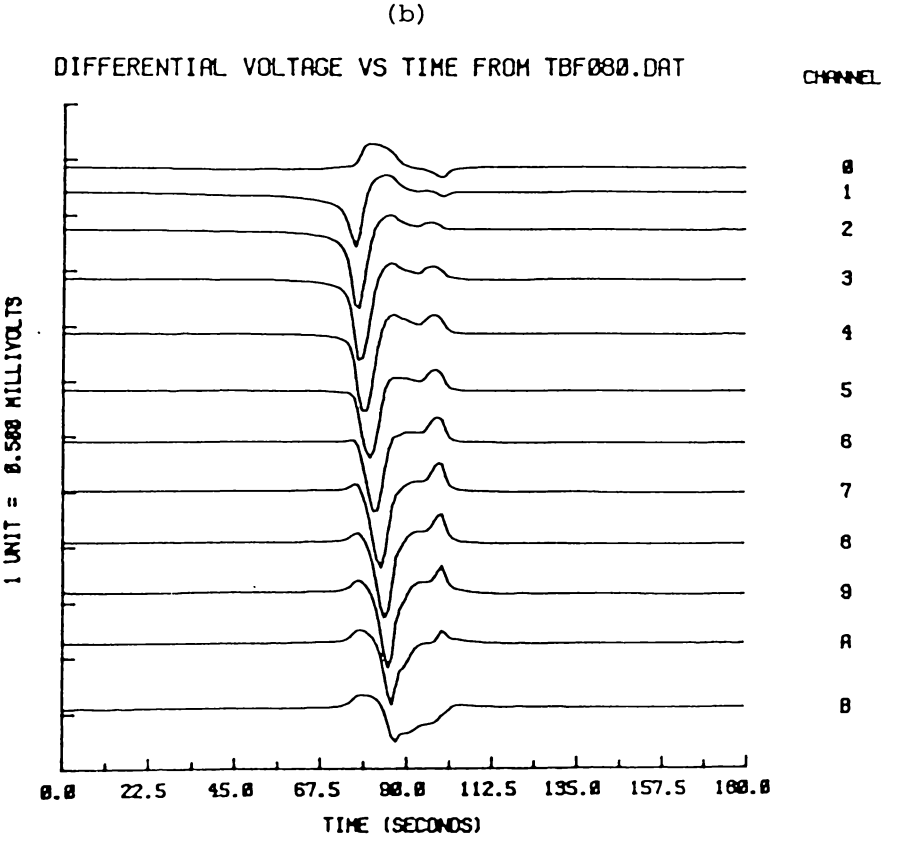

Fig. 5.24 Examples of spontaneous action potentials produced by the same ISS, initiating at (a) the regenerating end and (b) the other end (see text).

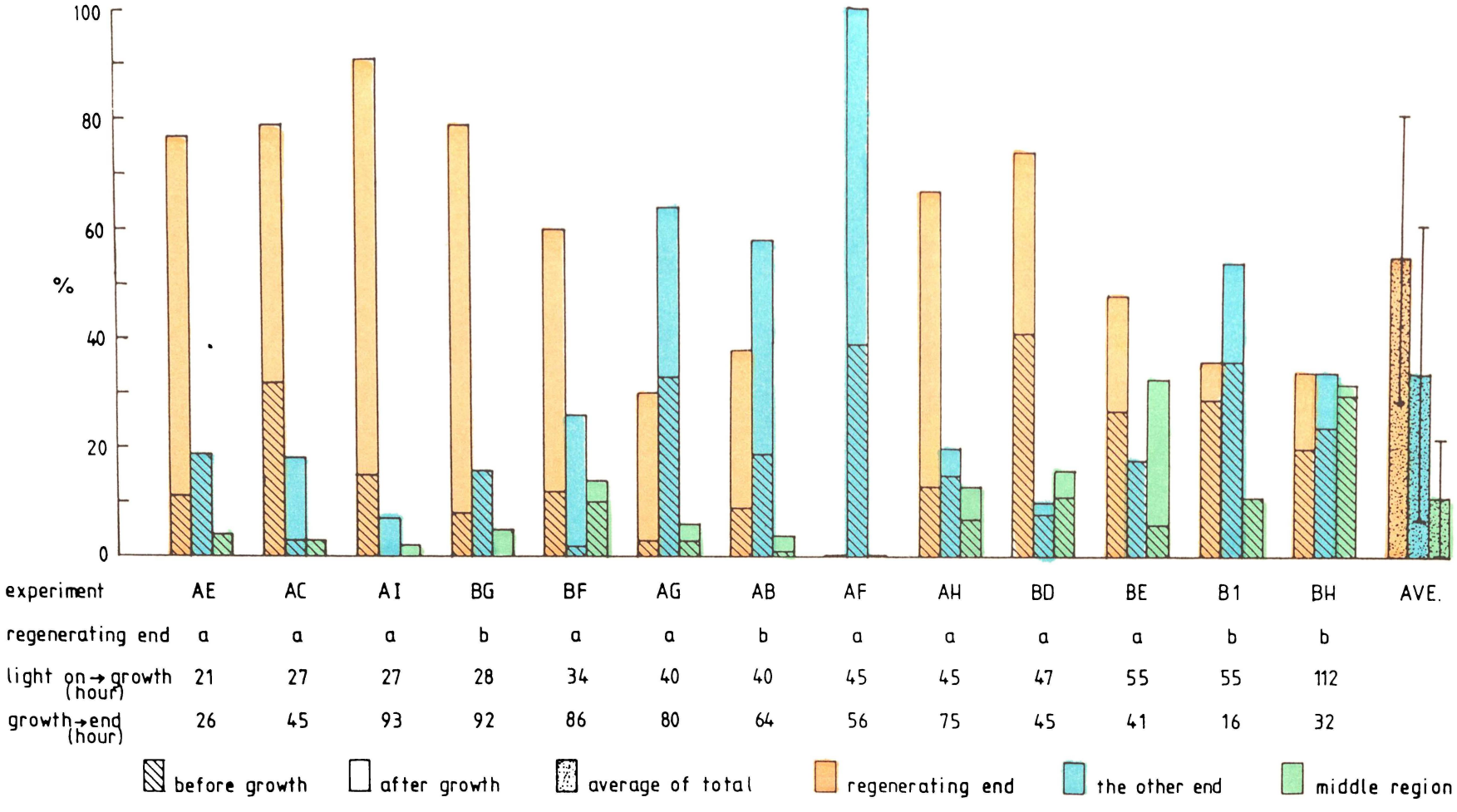

Fig. 5.25 Percentage of action potential initiations in the three different regions.

Fig. 5.26-5.28 Examples of spontaneous action potentials from experiment AG where the ISS redeveloped at the end near electrode '0'.

Fig. 5.26 Propagating action potential initiating at the *0-end* (other end).

Fig. 5.27 Propagating action potential initiating at the *R-end* (regenerating end).

Fig. 5.28 Non-propagating action potential initiating at the *R-end*.

Each Fig. shows

(a) differential voltage waveforms

(b) calculated current waveforms

(c) initial depolarized region (▨) analysed from (b). The + sign indicates position of the positive current at the specified time.

Note: * indicates the use of (a) instead of (b) to locate the depolarized region

(see ∿ end of section 5.2.2 for details).

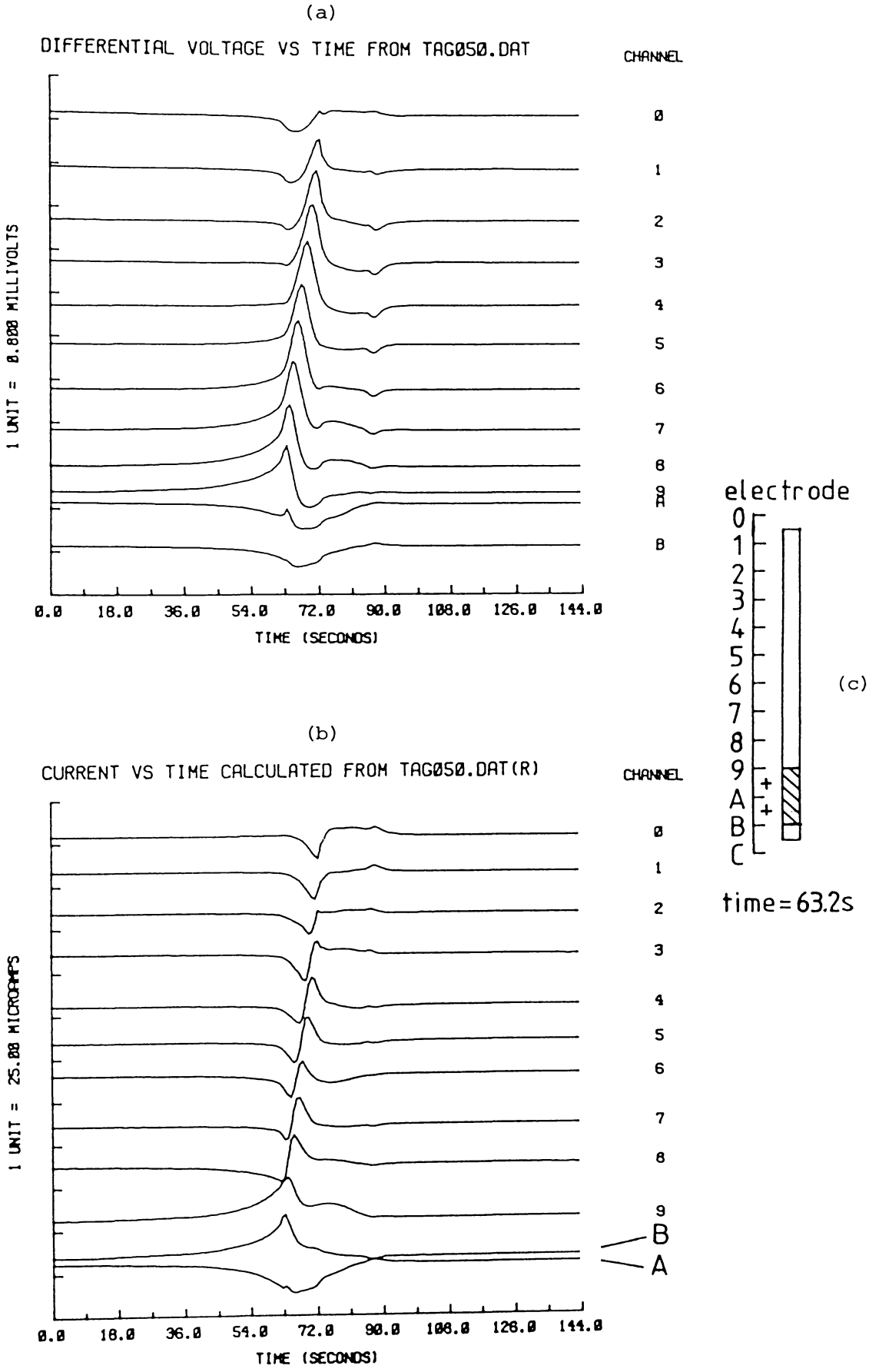
(a)
DIFFERENTIAL VOLTAGE VS TIME FROM TAG050.DAT
CHANNEL
1 UNIT = 0.000 MILLIVOLTS
0
1
2
3
4
5
6
7
8
9
A
B
0.0
18.0
36.0
54.0
72.0
90.0
108.0
126.0
144.0
TIME (SECONDS)
(b)
CURRENT VS TIME CALCULATED FROM TAG050.DAT(R)
CHANNEL
1 UNIT = 25.00 MICROAMPS
B
A
TIME (SECONDS)
electrode
0
1
2
3
4
5
6
7
8
9
A
B
C
(c)
time=63.2s

Fig. 5.26

(a)

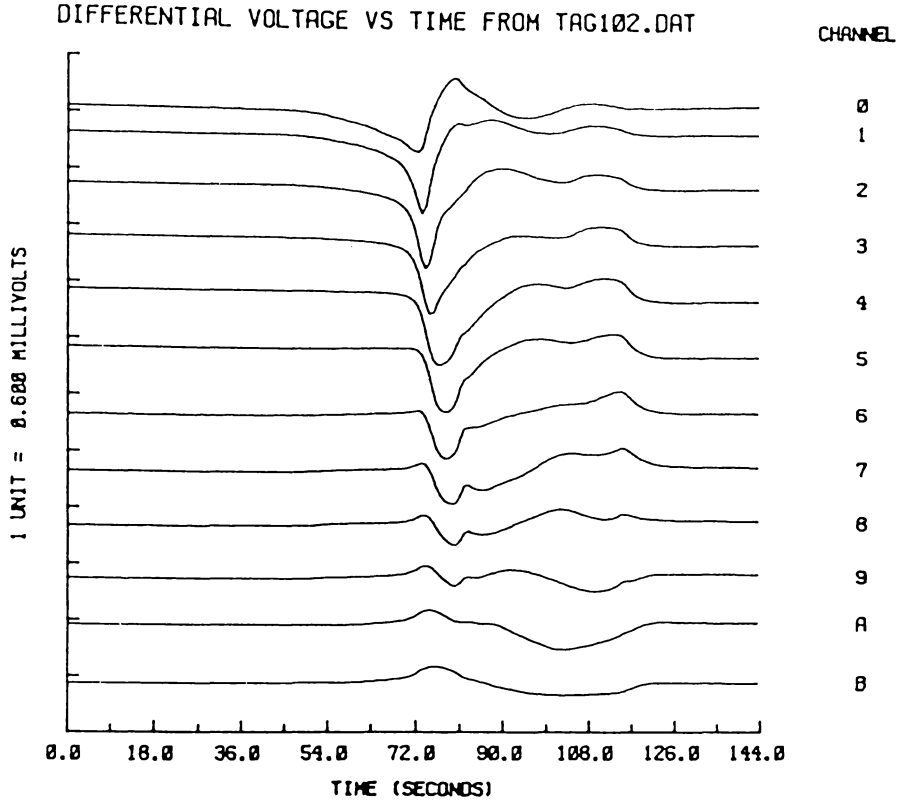
DIFFERENTIAL VOLTAGE VS TIME FROM TAG102.DAT
CHANNEL
0
1
2
3
4
5
6
7
8
9
A
B
1 UNIT = 0.600 MILLIVOLTS
0.0
18.0
36.0
54.0
72.0
90.0
108.0
126.0
144.0
TIME (SECONDS)

(b)

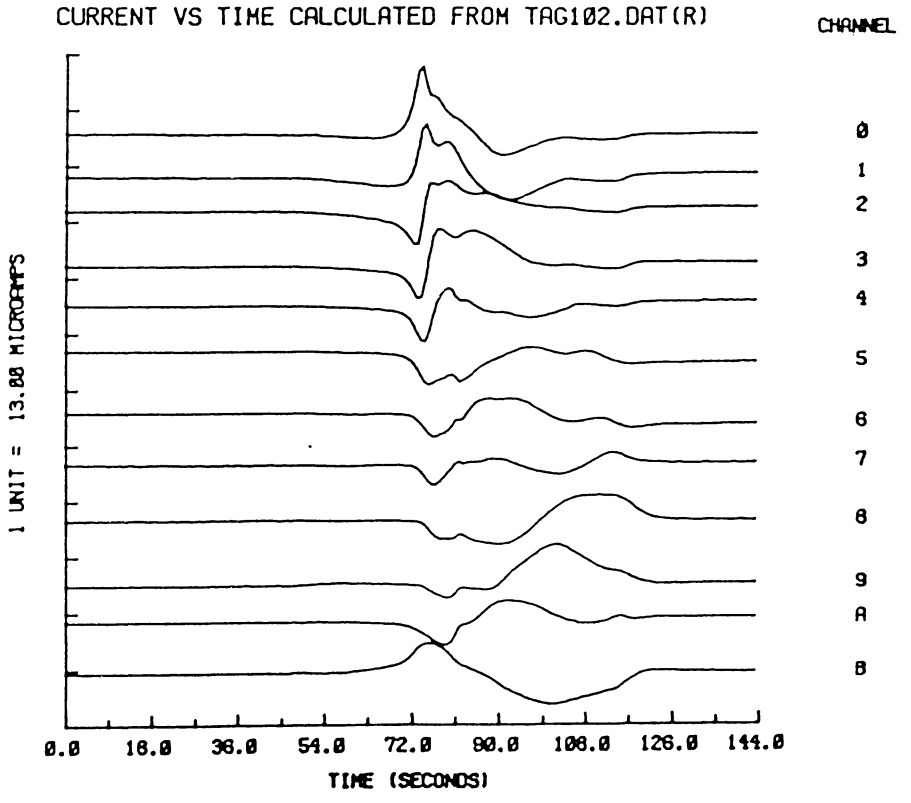
CURRENT VS TIME CALCULATED FROM TAG102.DAT(R)
CHANNEL
0
1
2
3
4
5
6
7
8
9
A
B
1 UNIT = 13.80 MICROAMPS
0.0
18.0
36.0
54.0
72.0
90.0
108.0
126.0
144.0
TIME (SECONDS)

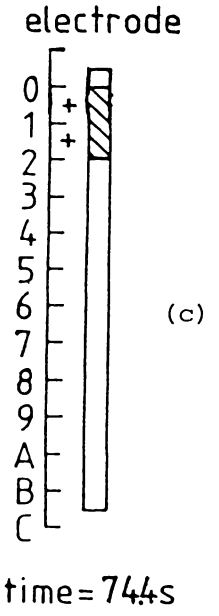
electrode
0
1
2
3
4
5
6
7
8
9
A
B
C
time=744s

(c)

Fig. 5.27

(a)

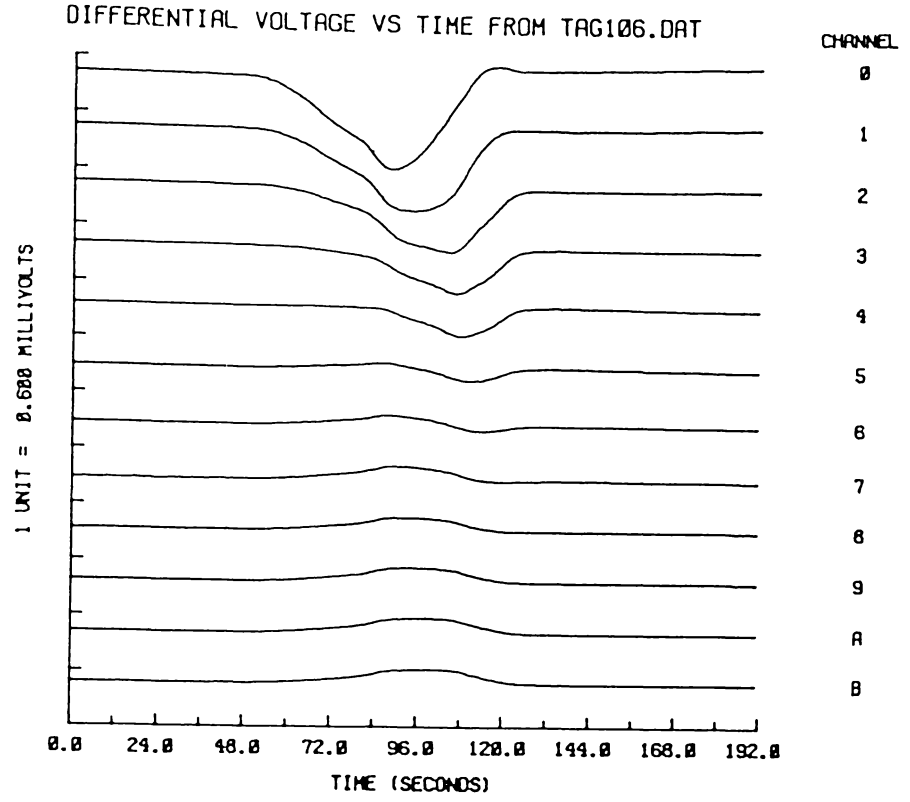
DIFFERENTIAL VOLTAGE VS TIME FROM TAG106.DAT
CHANNEL
0
1
2
3
4
5
6
7
8
9
A
B
1 UNIT = 0.600 MILLIVOLTS
0.0 24.0 48.0 72.0 96.0 120.0 144.0 168.0 192.0
TIME (SECONDS)

(b)

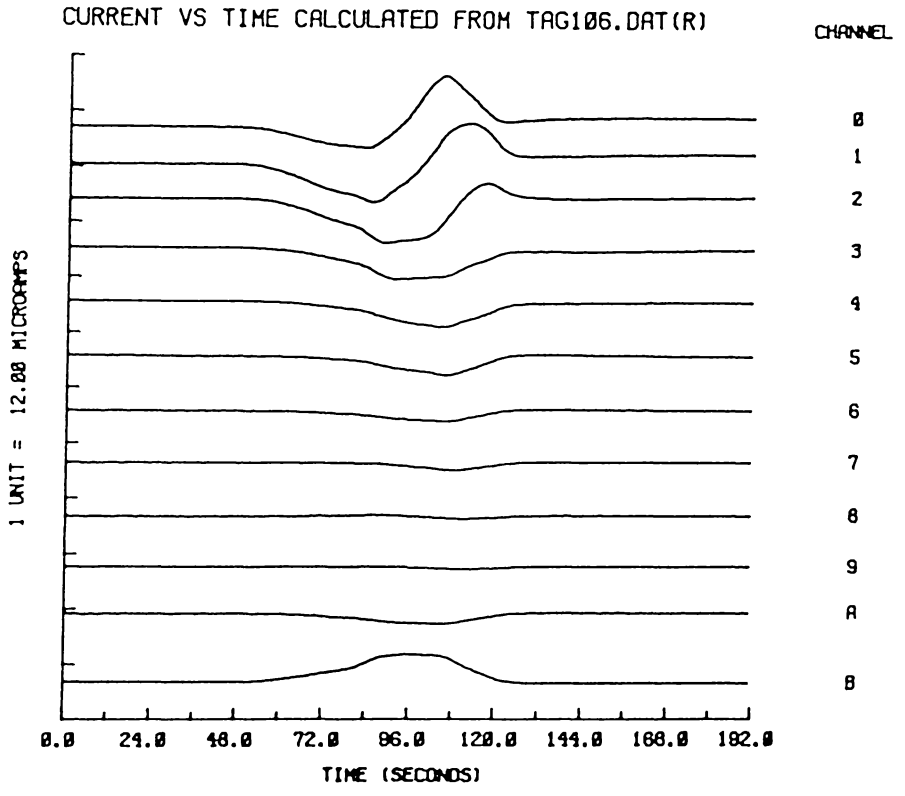
CURRENT VS TIME CALCULATED FROM TAG106.DAT(R)
CHANNEL
0
1
2
3
4
5
6
7
8
9
A
B
1 UNIT = 12.00 MICROAMPS
0.0 24.0 48.0 72.0 96.0 120.0 144.0 168.0 192.0
TIME (SECONDS)

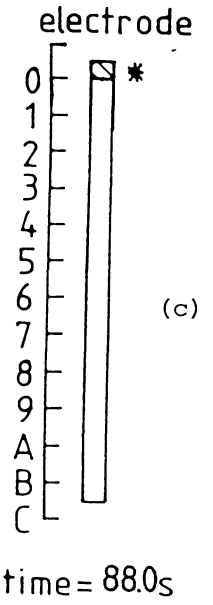
electrode
0
1
2
3
4
5
6
7
8
9
A
B
C
(c)
time = 88.0s

Fig. 5.28

Fig. 5.29-5.33 Examples of the propagating behaviour of various spontaneous action potentials showing:-

(a) calculated current waveforms

(b) the corresponding table of signs of currents at various points in time

Note: the + sign in brackets (Fig. 5.30) indicates that it was probably caused by systematic error (see ∿ beginning of section 5.2.2)

(c) the resulting analysed depolarized region(s) (or).

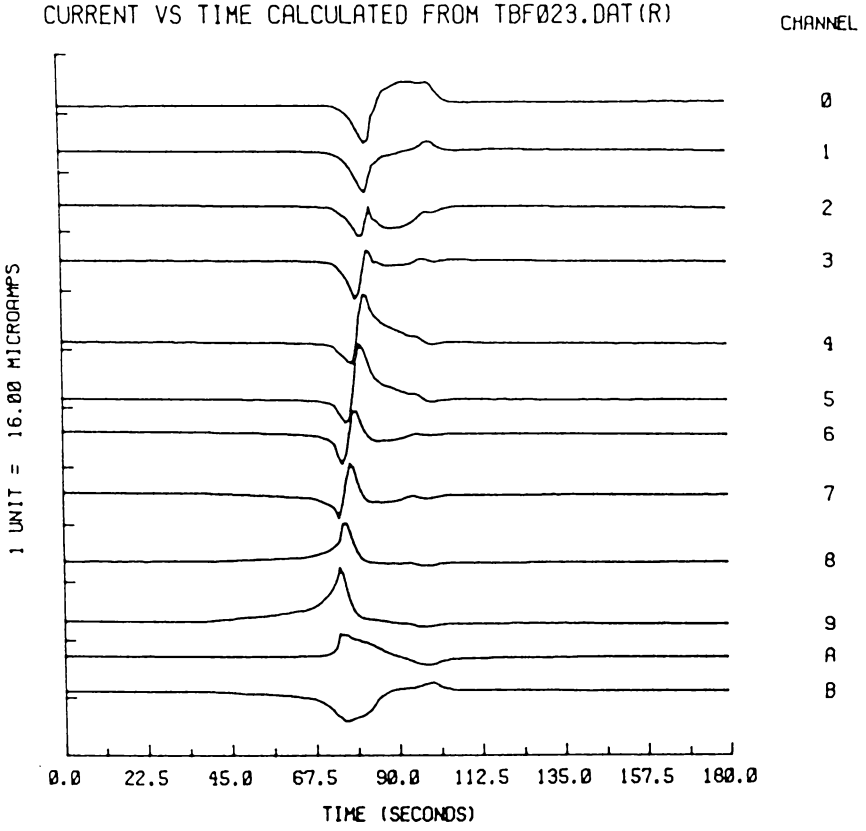
CURRENT VS TIME CALCULATED FROM TBF023.DAT(R)
CHANNEL
0
1
2
3
4
5
6
7
8
9
A
B
1 UNIT = 16.00 MICROAMPS
0.0
22.5
45.0
67.5
90.0
112.5
135.0
157.5
180.0
TIME (SECONDS)

(a)

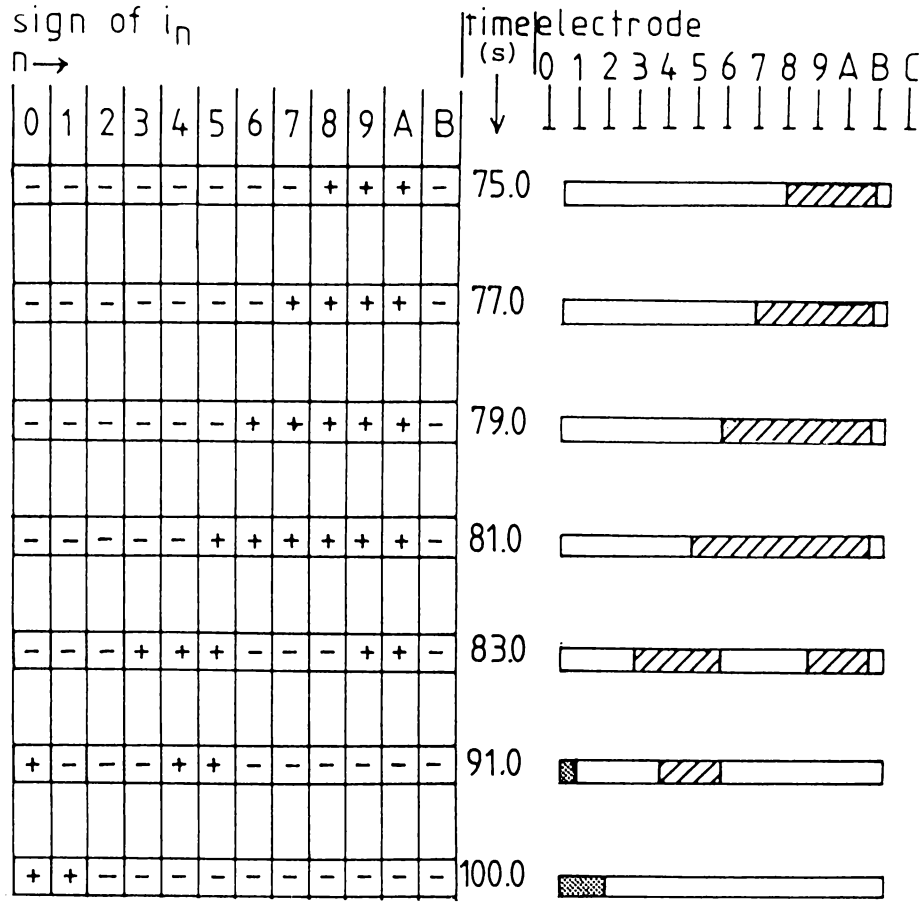
sign of i_n
n→
time (s)
electrode
0 1 2 3 4 5 6 7 8 9 A B C
0 1 2 3 4 5 6 7 8 9 A B
75.0
77.0
79.0
81.0
83.0
91.0
100.0

(b) (c)

Fig. 5.29

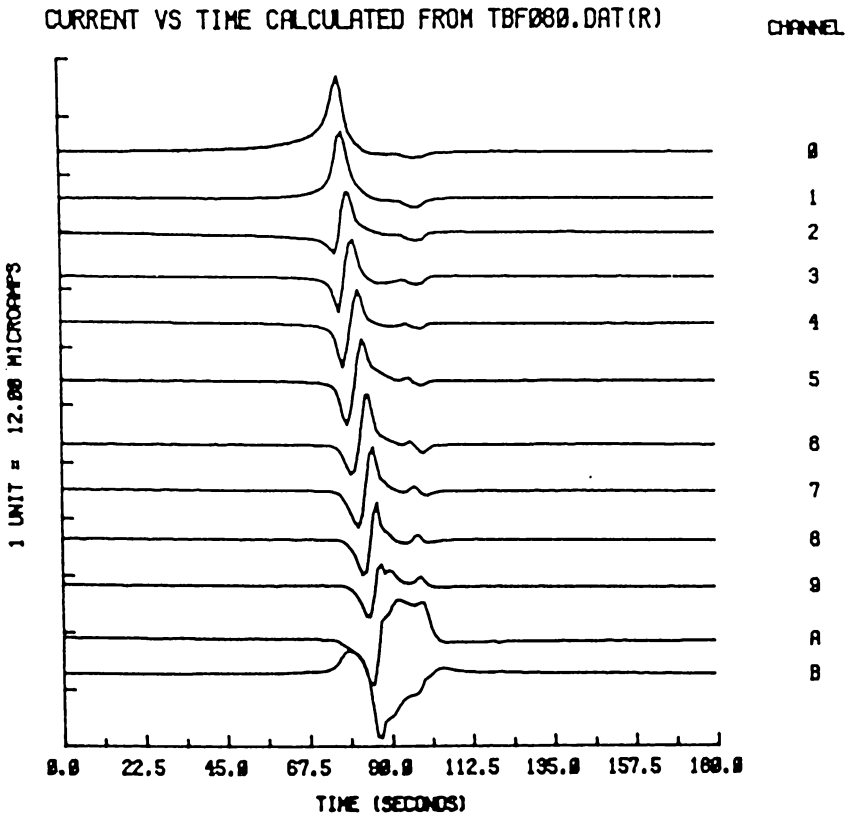
CURRENT VS TIME CALCULATED FROM TBF080.DAT(R)
CHANNEL
1 UNIT = 12.00 MICROAMPS
0
1
2
3
4
5
6
7
8
9
A
B
0.0
22.5
45.0
67.5
90.0
112.5
135.0
157.5
180.0
TIME (SECONDS)

(a)

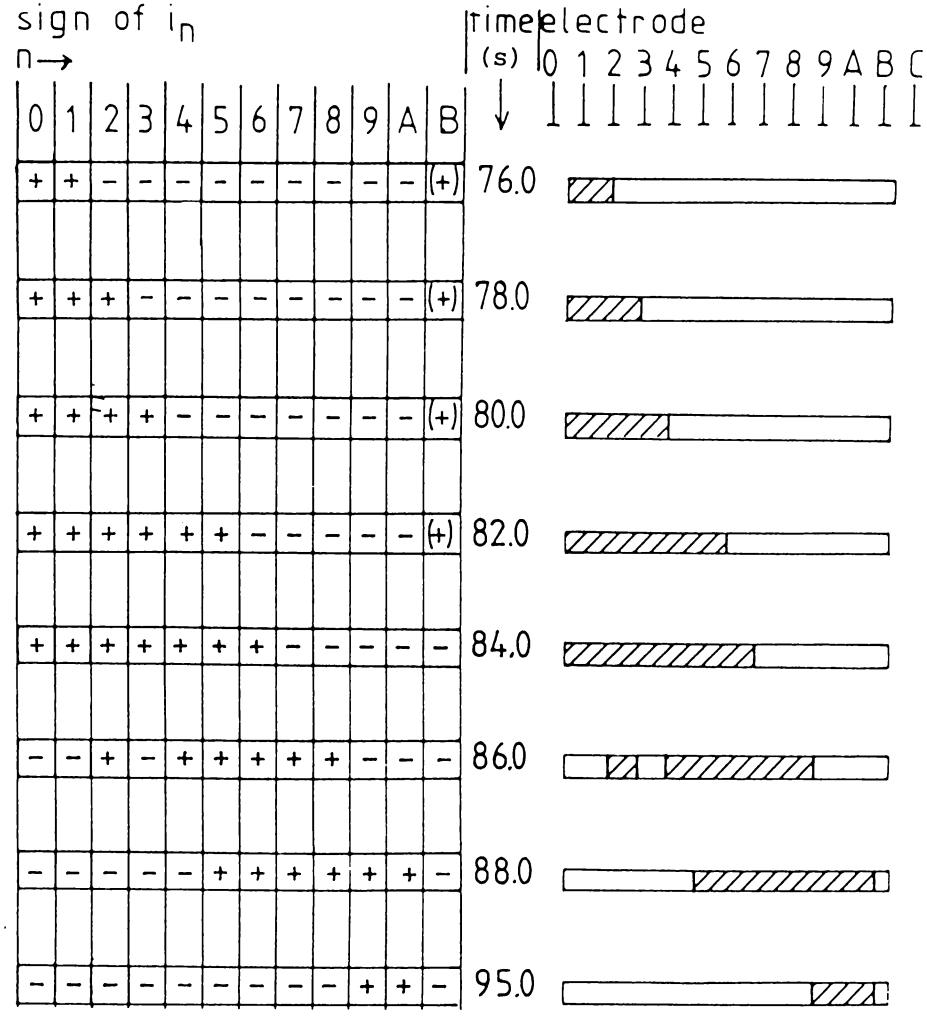
sign of i_n
n→
time (s)
electrode
0 1 2 3 4 5 6 7 8 9 A B C
0 1 2 3 4 5 6 7 8 9 A B
76.0
78.0
80.0
82.0
84.0
86.0
88.0
95.0

(b) (c)

Fig. 5.30

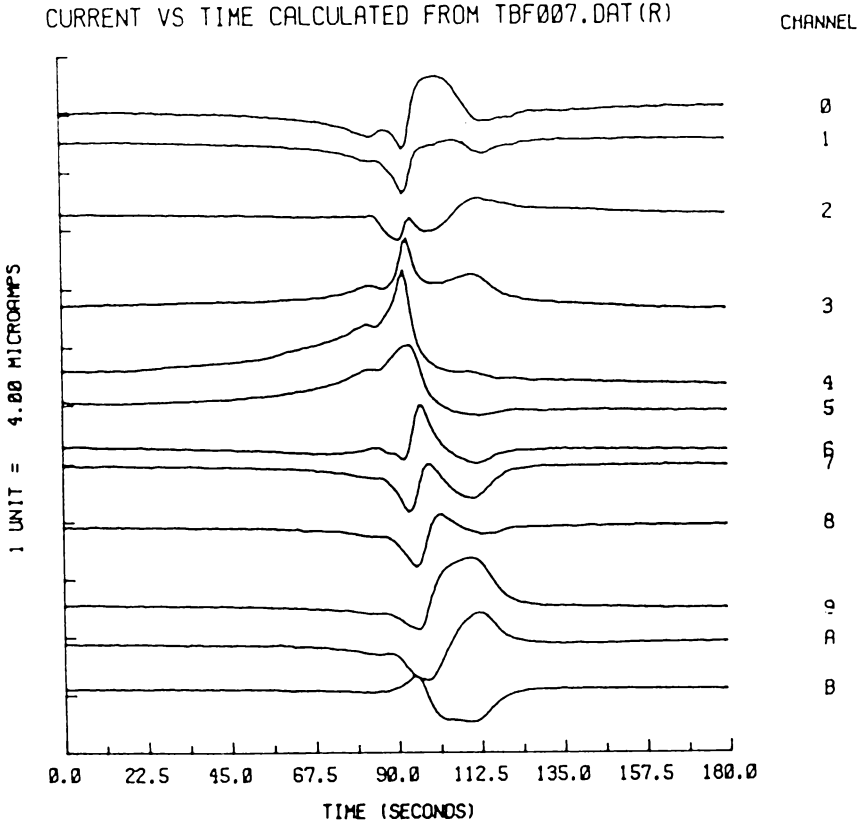
CURRENT VS TIME CALCULATED FROM TBF007.DAT(R)
CHANNEL
1 UNIT = 4.88 MICROAMPS
0
1
2
3
4
5
6
7
8
9
A
B
0.0
22.5
45.0
67.5
90.0
112.5
135.0
157.5
180.0
TIME (SECONDS)

(a)

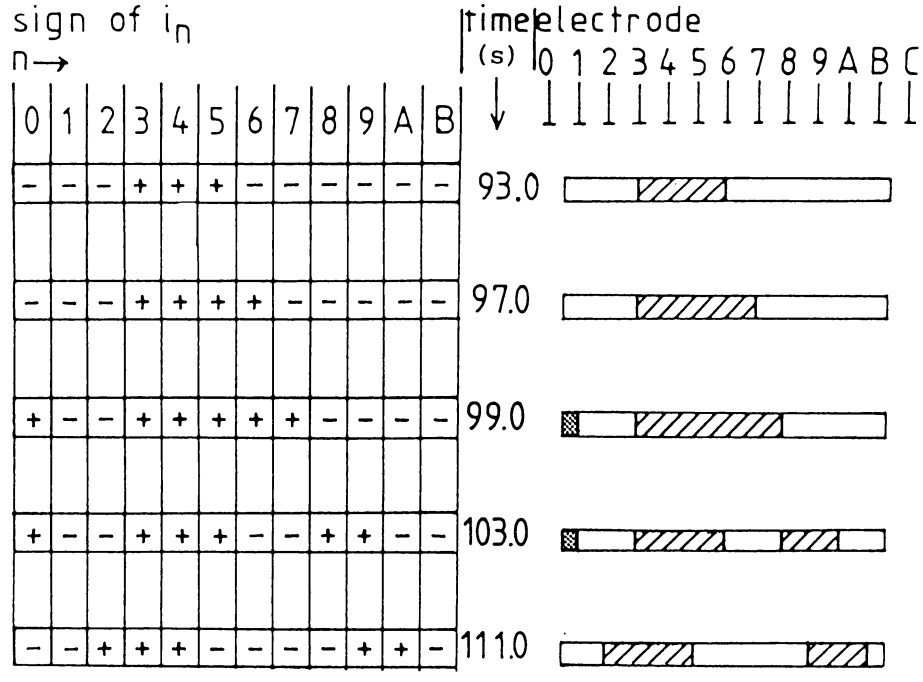
sign of i_n
n→
0 1 2 3 4 5 6 7 8 9 A B
time (s)
electrode
0 1 2 3 4 5 6 7 8 9 A B C
93.0
97.0
99.0
103.0
111.0

(b) (c)

Fig. 5.31

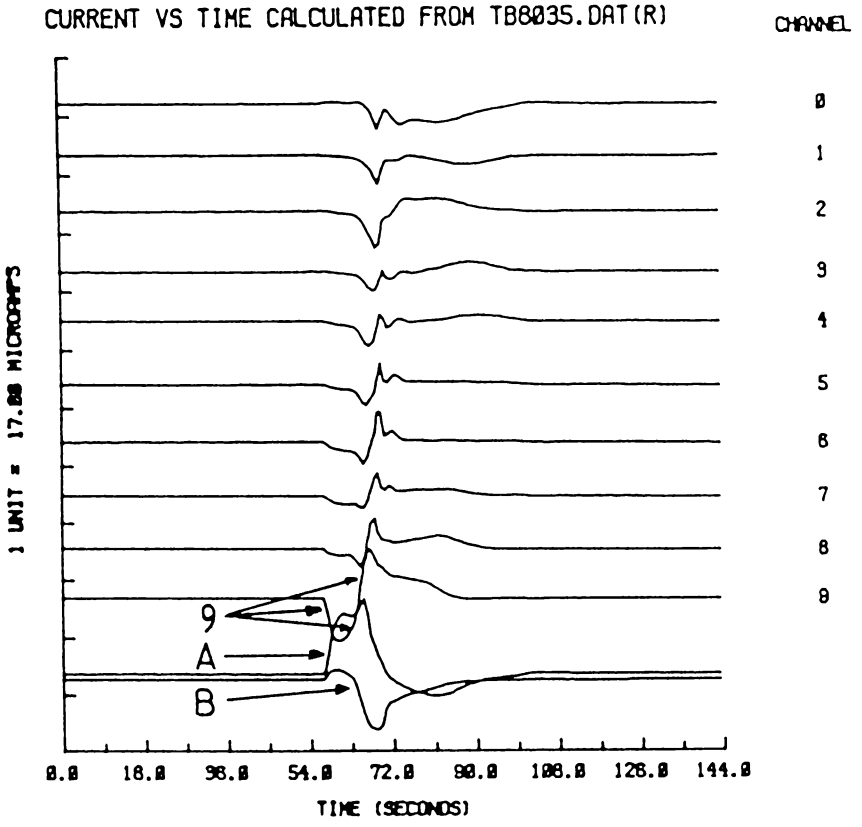
CURRENT VS TIME CALCULATED FROM TB8035.DAT(R)
CHANNEL
0
1
2
3
4
5
6
7
8
9
1 UNIT = 17.88 MICROAMPS
9
A
B
0.0
18.0
36.0
54.0
72.0
90.0
108.0
126.0
144.0
TIME (SECONDS)

(a)

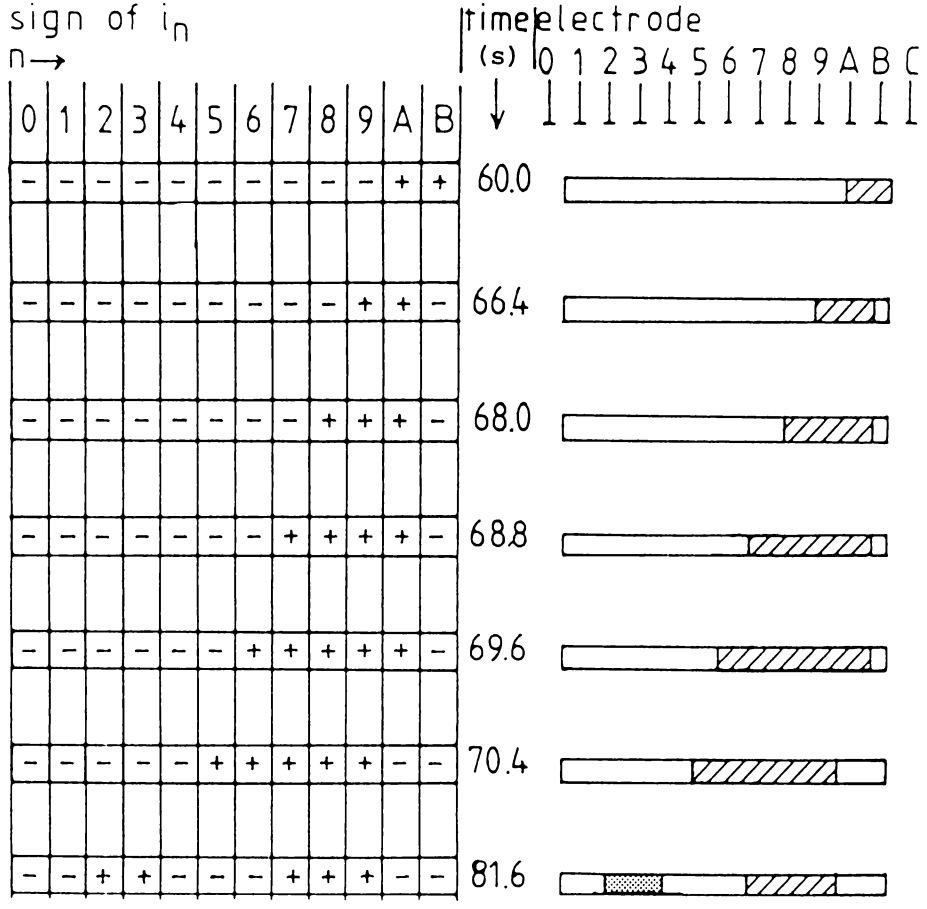
sign of i_n
n→
time (s)
electrode
0 1 2 3 4 5 6 7 8 9 A B C
0 1 2 3 4 5 6 7 8 9 A B
60.0
66.4
68.0
68.8
69.6
70.4
81.6

(b) (c)

Fig. 5.32

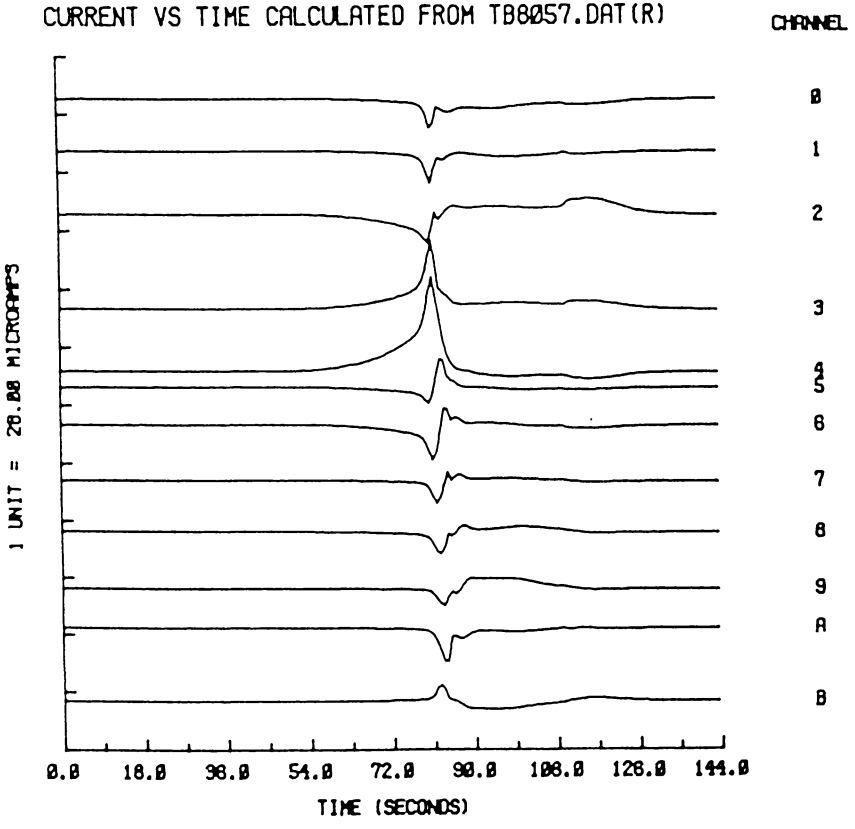
CURRENT VS TIME CALCULATED FROM TB8057.DAT(R)
CHANNEL
0
1
2
3
4
5
6
7
8
9
A
B
1 UNIT = 20.00 MICROAMPS
0.0
18.0
36.0
54.0
72.0
90.0
108.0
126.0
144.0
TIME (SECONDS)

(a)

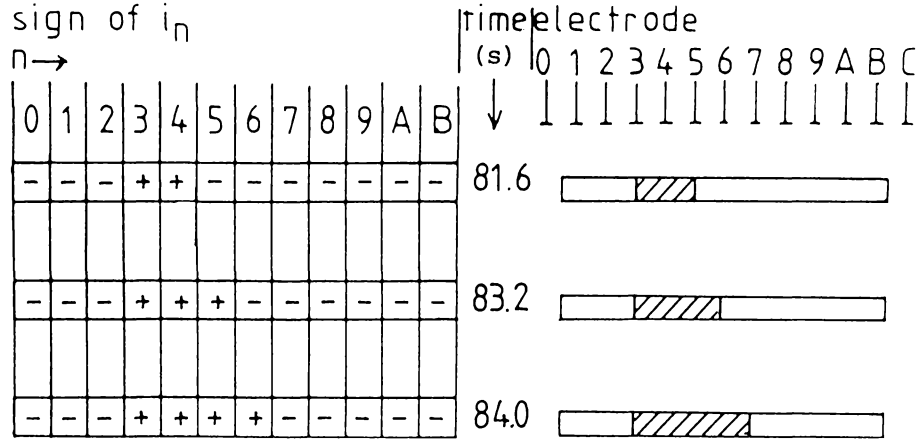
sign of i_n
n→
time (s)
electrode
0 1 2 3 4 5 6 7 8 9 A B C
0 1 2 3 4 5 6 7 8 9 A B
81.6
83.2
84.0

(b) (c)

Fig. 5.33

Fig. 5.34-5.36 Examples of non-propagating action potentials initiating at various points along a redeveloping ISS showing:-

(a) differential voltage waveforms

(b) calculated current waveforms

(c) depolarized region (▨) analysed from (b). The + sign indicates position of the positive current at the specified time.

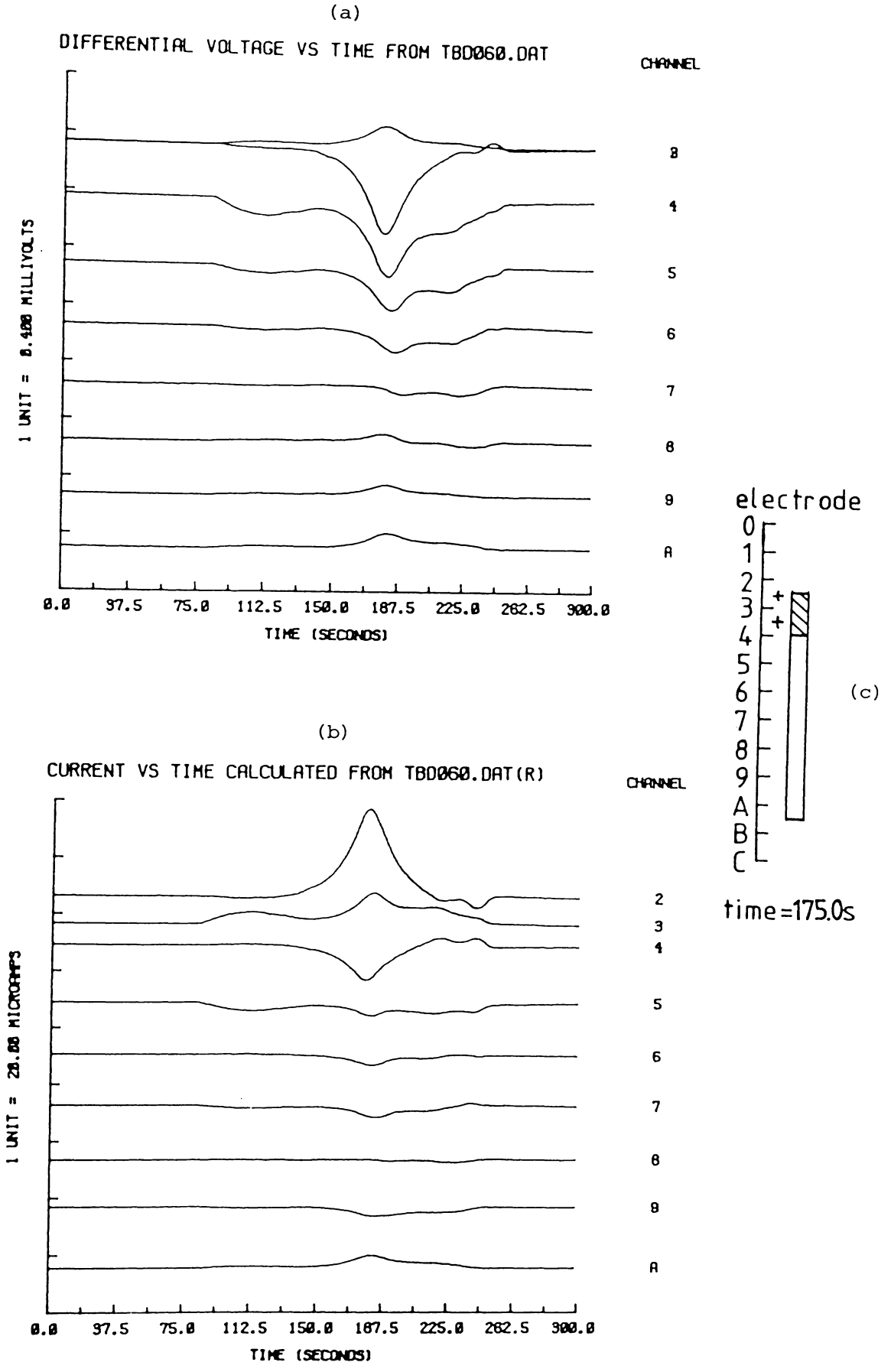
(a)
DIFFERENTIAL VOLTAGE VS TIME FROM TBD060.DAT
CHANNEL
8
4
5
6
7
8
9
A
1 UNIT = 0.400 MILLIVOLTS
0.0 37.5 75.0 112.5 150.0 187.5 225.0 262.5 300.0
TIME (SECONDS)
(b)
CURRENT VS TIME CALCULATED FROM TBD060.DAT(R)
CHANNEL
2
3
4
5
6
7
8
9
A
1 UNIT = 20.00 MICROAMPS
0.0 37.5 75.0 112.5 150.0 187.5 225.0 262.5 300.0
TIME (SECONDS)
electrode
0
1
2
3
4
5
6
7
8
9
A
B
C
(c)
time=175.0s

Fig. 5.34

(a)

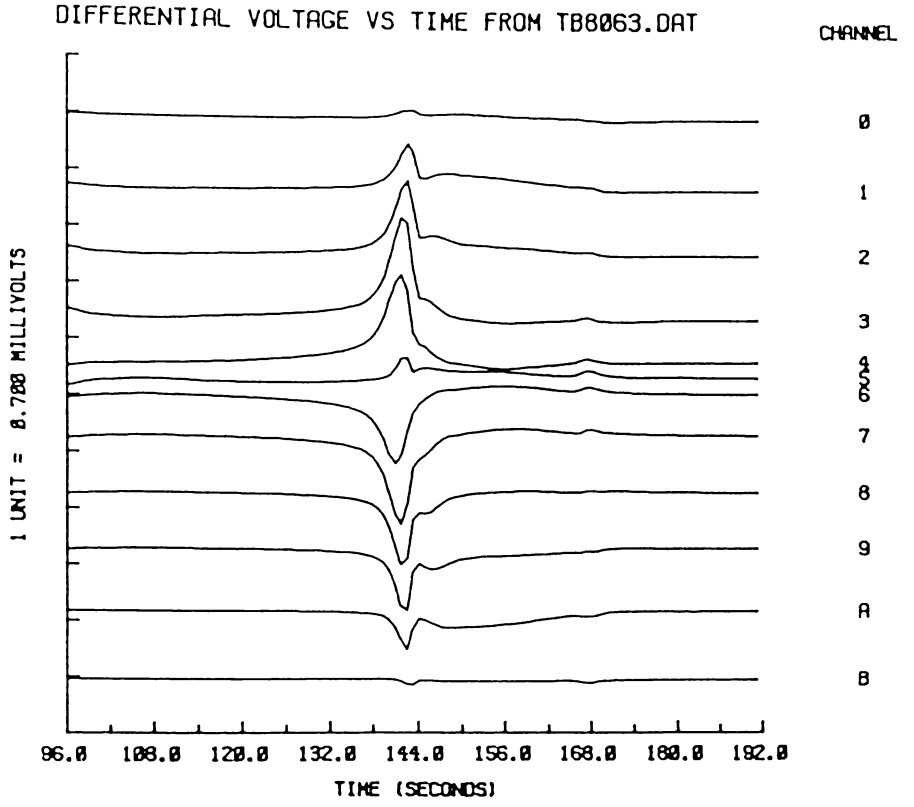
DIFFERENTIAL VOLTAGE VS TIME FROM TB8063.DAT
CHANNEL
0
1
2
3
4
5
6
7
8
9
A
B
1 UNIT = 8.788 MILLIVOLTS
96.0 108.0 120.0 132.0 144.0 156.0 168.0 180.0 192.0
TIME (SECONDS)

(b)

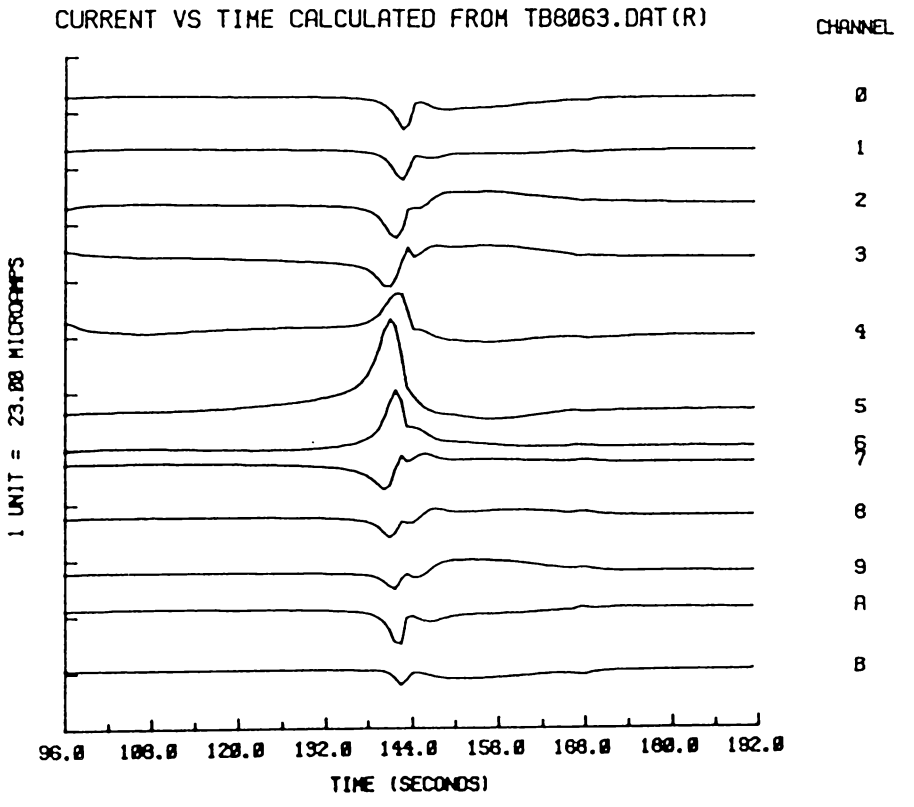
CURRENT VS TIME CALCULATED FROM TB8063.DAT(R)
CHANNEL
0
1
2
3
4
5
6
7
8
9
A
B
1 UNIT = 23.88 MICROMHOS
96.0 108.0 120.0 132.0 144.0 156.0 168.0 180.0 192.0
TIME (SECONDS)

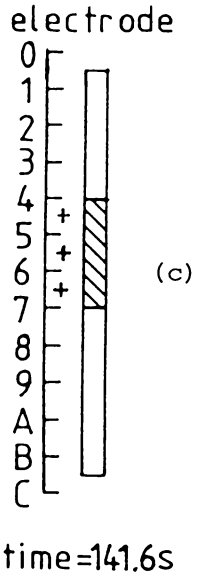
electrode
0
1
2
3
4
5
6
7
8
9
A
B
C
(c)
time=141.6s

Fig. 5.35

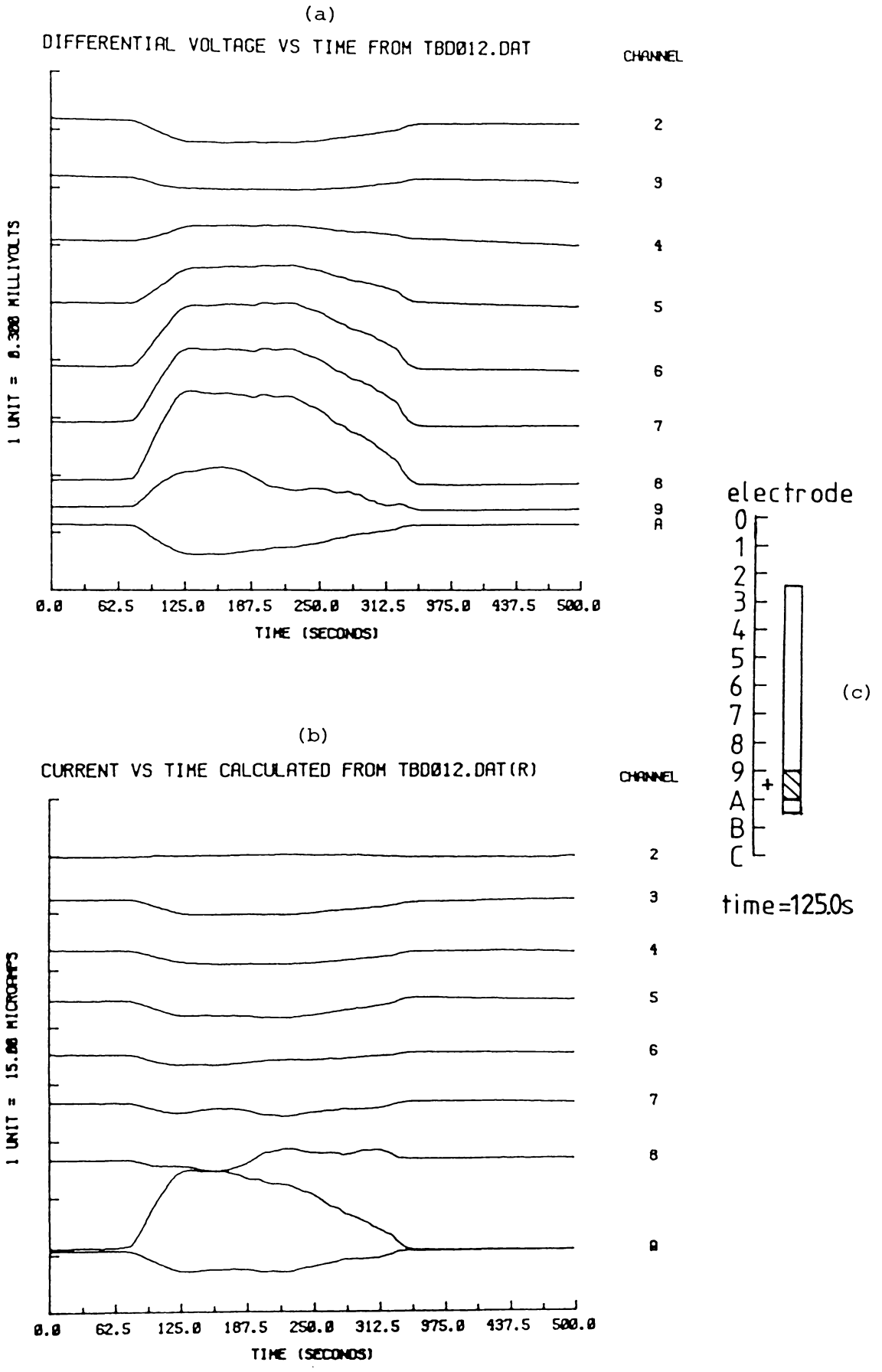
(a)
DIFFERENTIAL VOLTAGE VS TIME FROM TBD012.DAT
CHANNEL
2
3
4
5
6
7
8
9
A
1 UNIT = 0.300 MILLIVOLTS
0.0 62.5 125.0 187.5 250.0 312.5 375.0 437.5 500.0
TIME (SECONDS)
electrode
0
1
2
3
4
5
6
7
8
9
A
B
C
+
(c)
time=125.0s
(b)
CURRENT VS TIME CALCULATED FROM TBD012.DAT(R)
CHANNEL
2
3
4
5
6
7
8
A
1 UNIT = 15.00 MICROAMPS
0.0 62.5 125.0 187.5 250.0 312.5 375.0 437.5 500.0
TIME (SECONDS)

Fig. 5.36

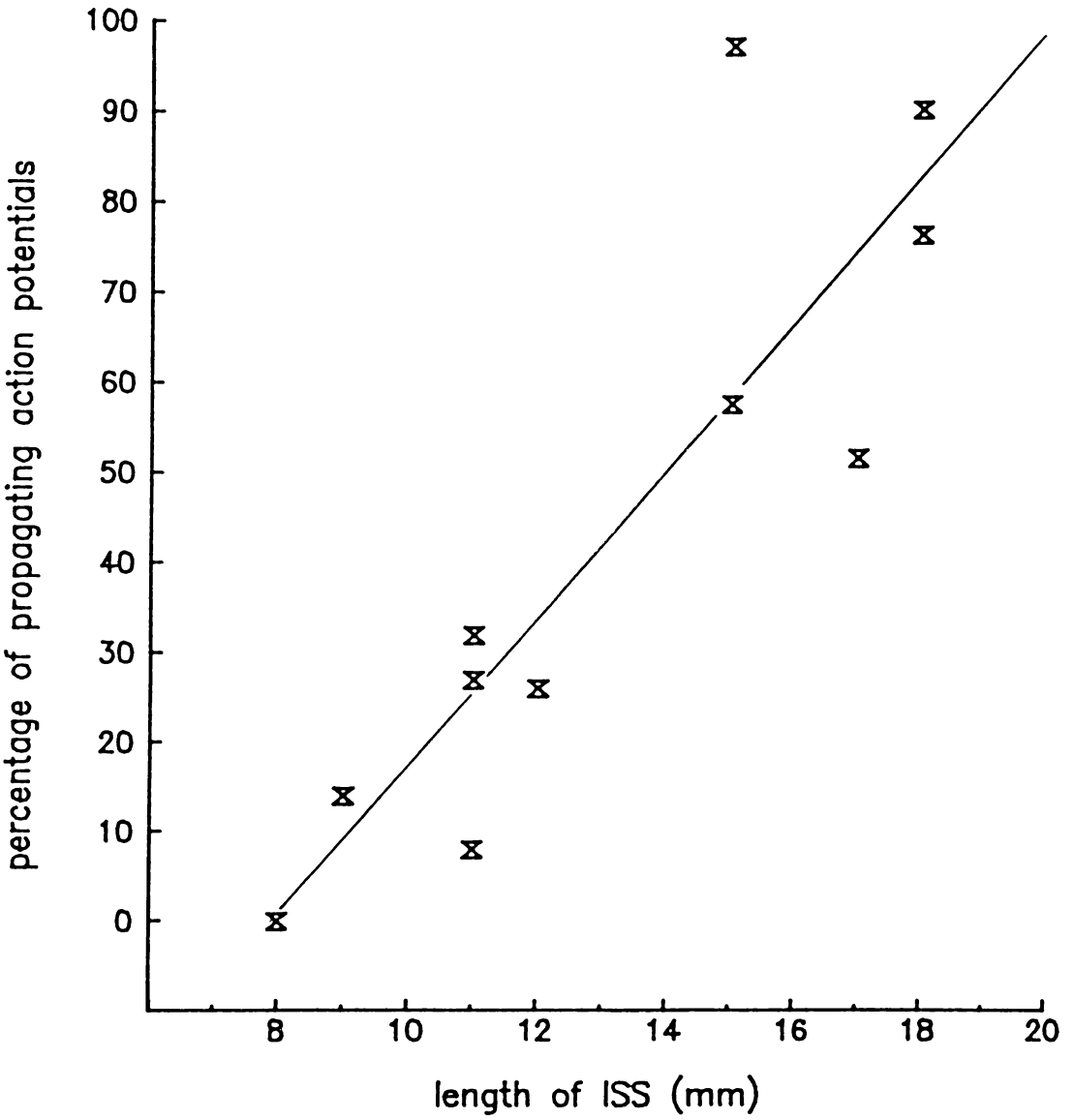

Fig. 5.37 Percentage of propagating action potentials in relation to the length of ISS.

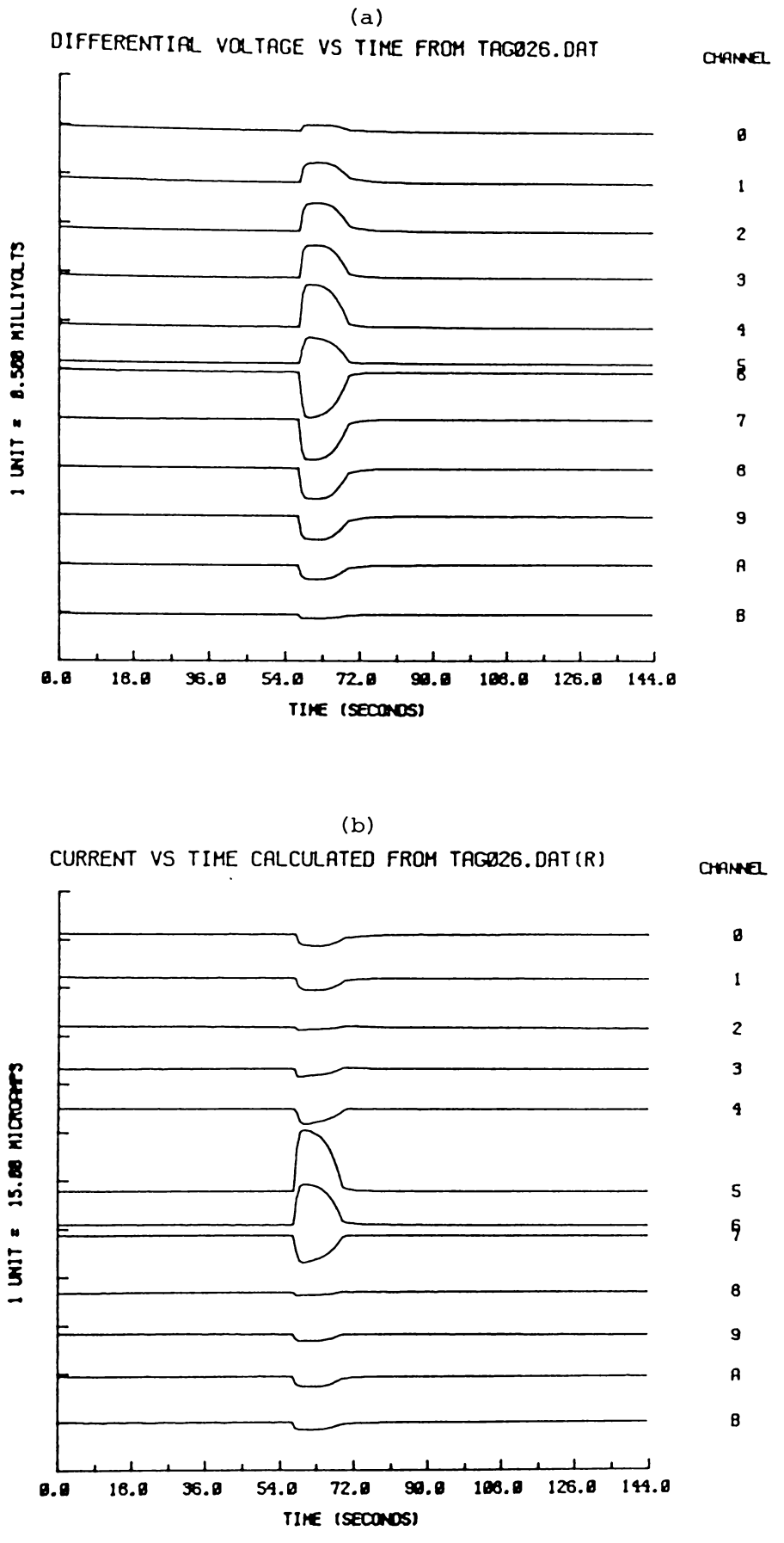

Fig. 5.38 An example of a *sharp take-off* spontaneous action potential showing (a) the differential voltage waveforms and (b) the calculated current waveforms.

Fig. 5.39 A *sharp take-off* action potential associated with a clear region in the *dying* ISS (see section 5.2.4) showing:-

(a) the differential voltage waveforms

(b) the calculated current waveforms

(c) the clear region (▭) observed before the initiation of the action potential

(d) the depolarized region of the action potential (▨) analysed from (b)

(e) the extended clear region (▭) observed after the action potential.

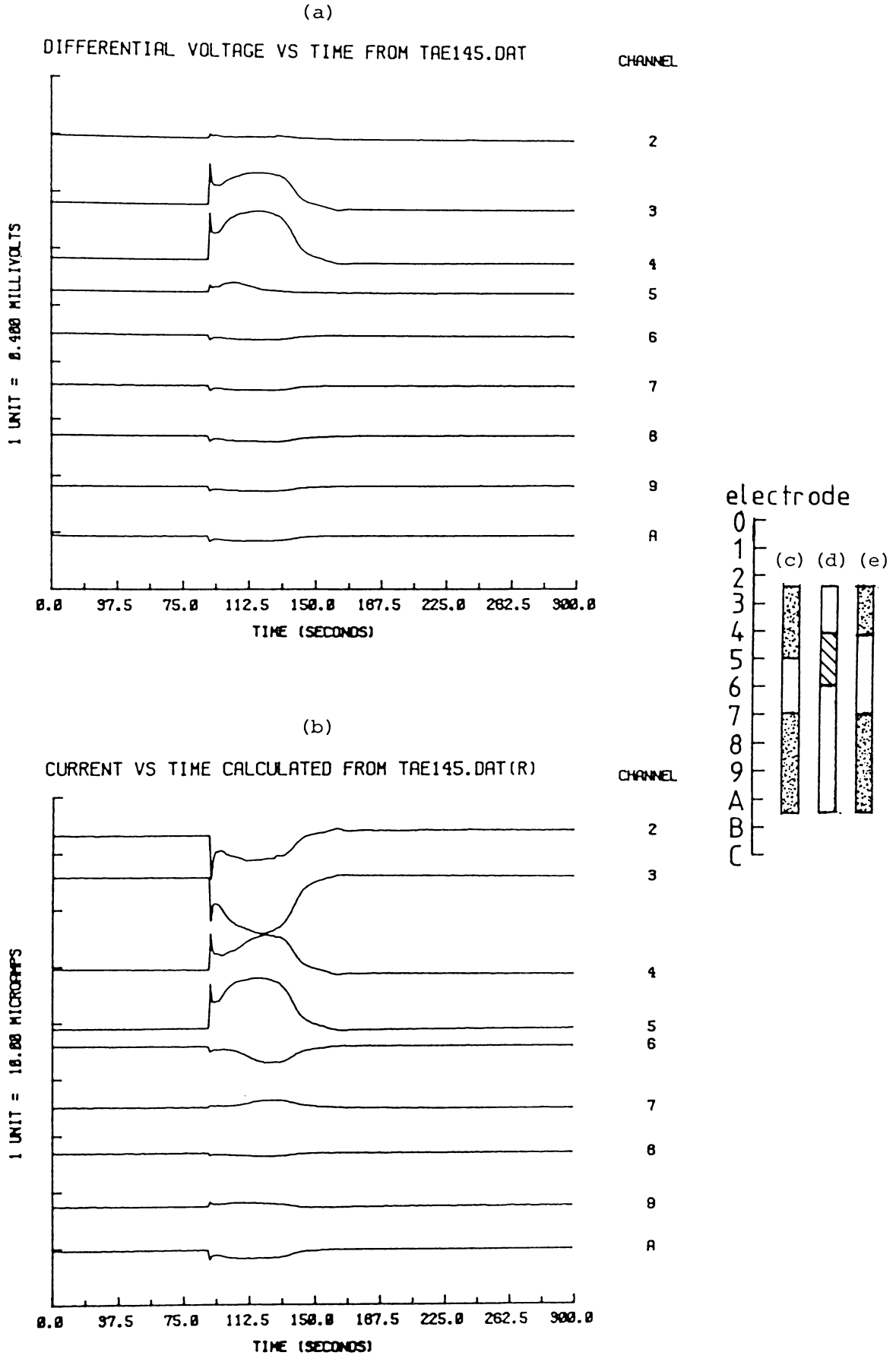
(a)
DIFFERENTIAL VOLTAGE VS TIME FROM TAE145.DAT
CHANNEL
2
3
4
5
6
7
8
9
A
1 UNIT = 0.400 MILLIVOLTS
0.0 97.5 75.0 112.5 150.0 187.5 225.0 262.5 300.0
TIME (SECONDS)
(b)
CURRENT VS TIME CALCULATED FROM TAE145.DAT(R)
CHANNEL
2
3
4
5
6
7
8
9
A
1 UNIT = 10.00 MICROAMPS
0.0 97.5 75.0 112.5 150.0 187.5 225.0 262.5 300.0
TIME (SECONDS)
electrode
0
1
2
3
4
5
6
7
8
9
A
B
C
(c) (d) (e)

Fig. 5.39

Fig. 5.40-5.42 Spontaneous action potentials observed in an injured ISS i.e. ISS showing a clear region (see section 5.2.4 for details).

Fig. 5.40 A *slow take-off* action potential observed before injury occurred.

Fig. 5.41 A *sharp take-off* action potential observed when the ISS had developed a clear region.

Fig. 5.42 A *slow take-off* action potential observed when the ISS had recovered from injury i.e. the clear region had disappeared.

Each Fig. shows

(a) differential voltage waveforms

(b) calculated current waveforms.

(a)

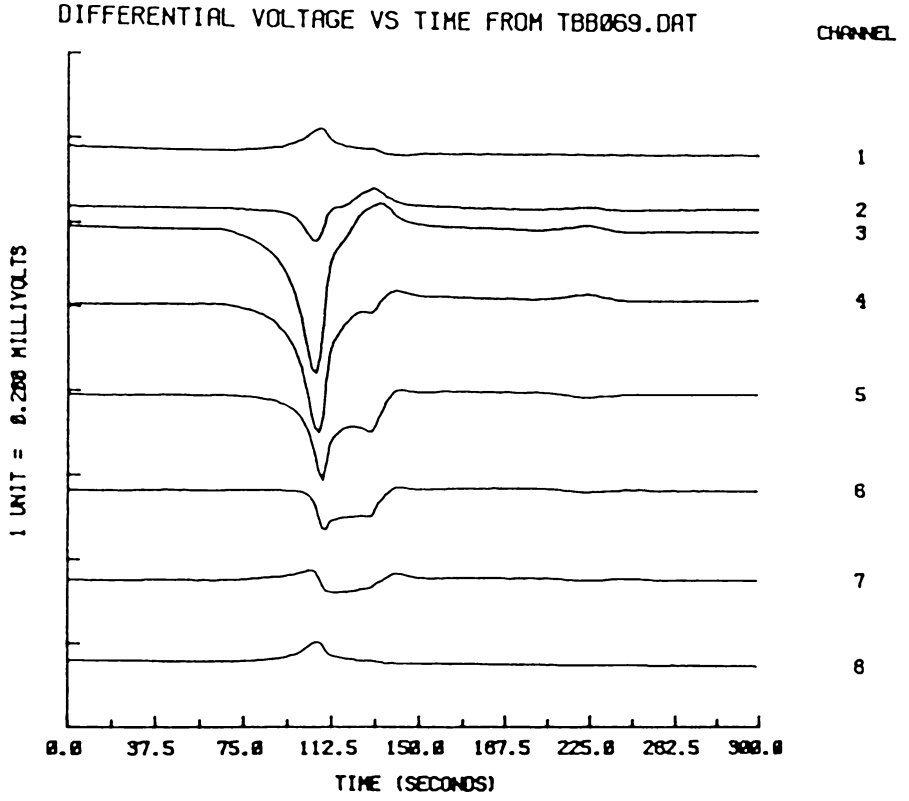
DIFFERENTIAL VOLTAGE VS TIME FROM TBB069.DAT
CHANNEL
1
2
3
4
5
6
7
8
1 UNIT = 0.200 MILLIVOLTS
0.0
37.5
75.0
112.5
150.0
187.5
225.0
262.5
300.0
TIME (SECONDS)

(b)

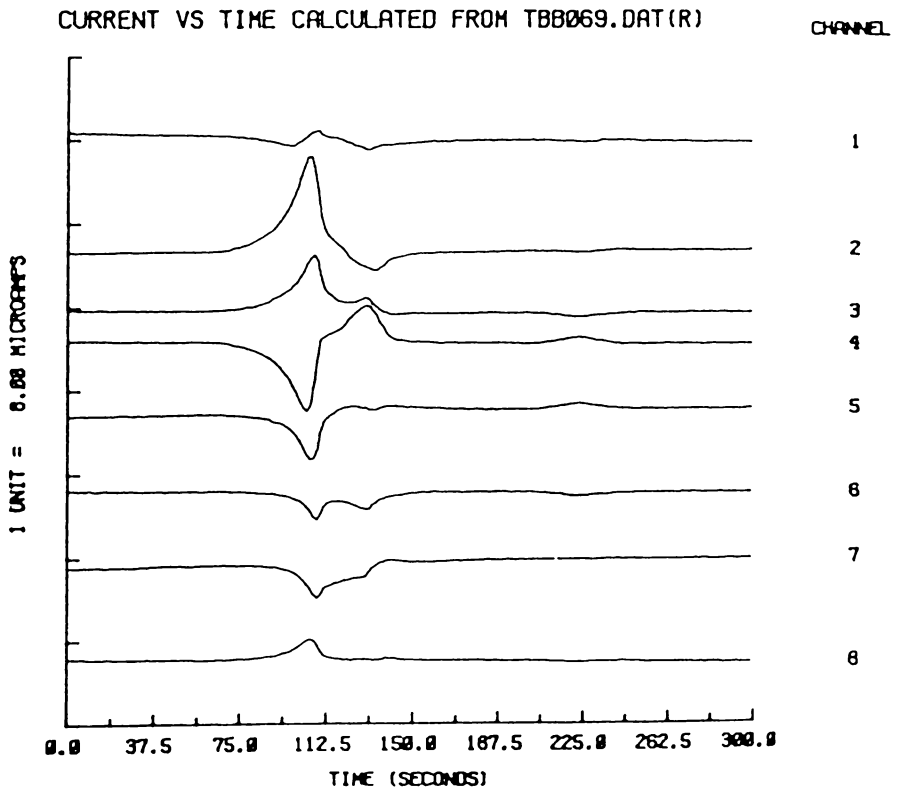
CURRENT VS TIME CALCULATED FROM TBB069.DAT(R)
CHANNEL
1
2
3
4
5
6
7
8
1 UNIT = 0.00 MICROAMPS
0.0
37.5
75.0
112.5
150.0
187.5
225.0
262.5
300.0
TIME (SECONDS)

Fig. 5.40

(a)

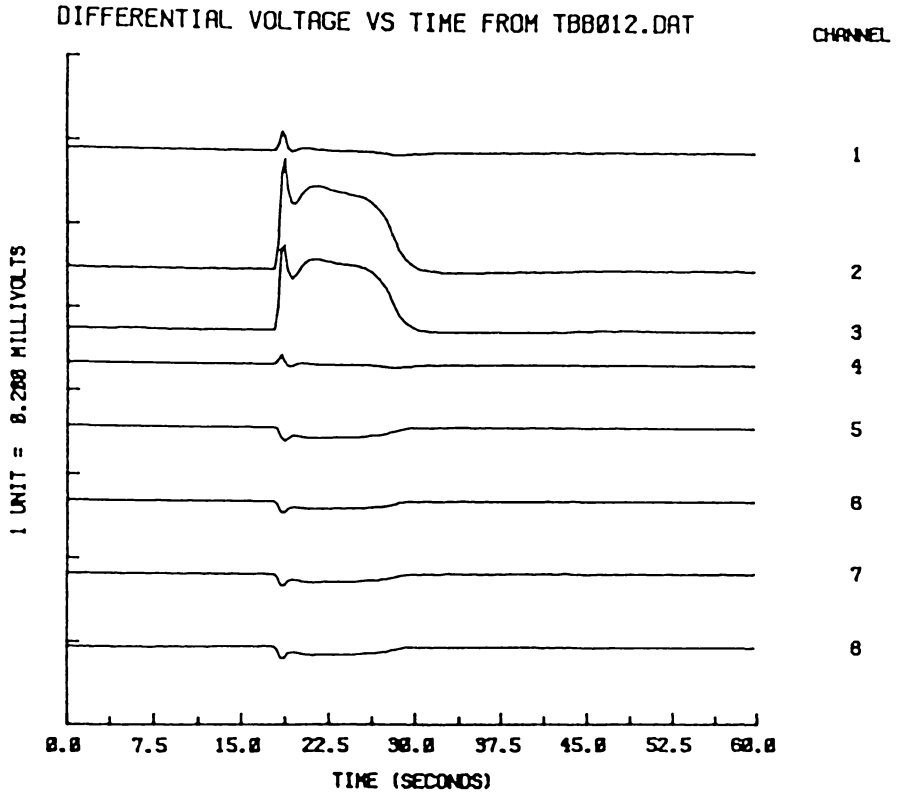
DIFFERENTIAL VOLTAGE VS TIME FROM TBB012.DAT
CHANNEL
1
2
3
4
5
6
7
8
1 UNIT = 0.200 MILLIVOLTS
0.0
7.5
15.0
22.5
30.0
37.5
45.0
52.5
60.0
TIME (SECONDS)

(b)

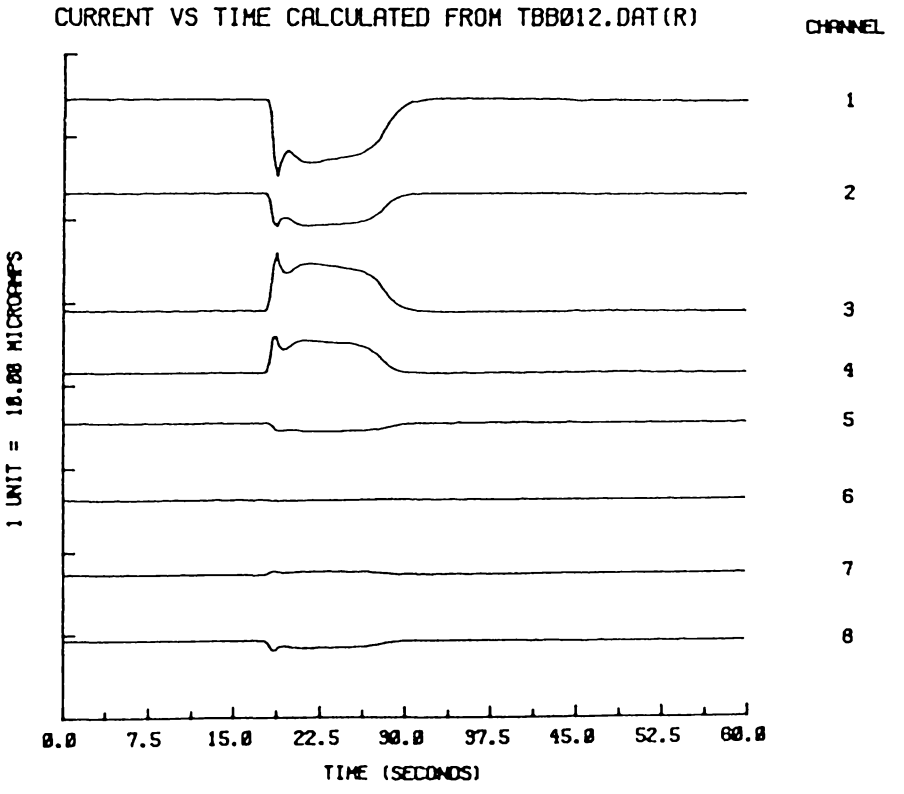
CURRENT VS TIME CALCULATED FROM TBB012.DAT(R)
CHANNEL
1
2
3
4
5
6
7
8
1 UNIT = 10.00 MICROAMPS
0.0
7.5
15.0
22.5
30.0
37.5
45.0
52.5
60.0
TIME (SECONDS)

Fig. 5.41

(a)

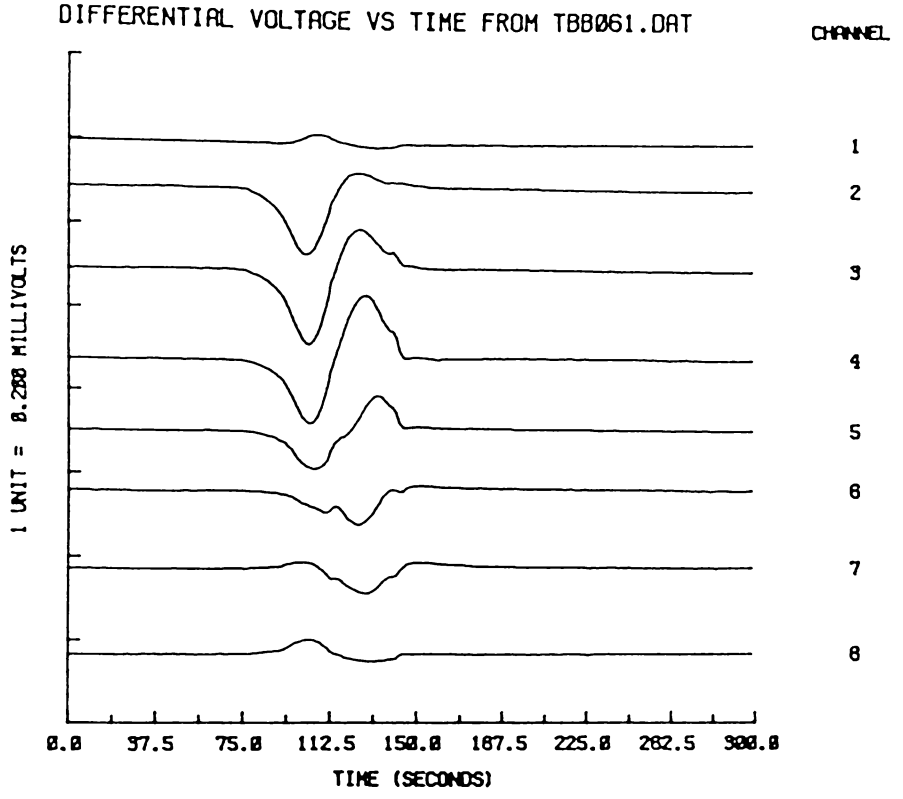
DIFFERENTIAL VOLTAGE VS TIME FROM TBB061.DAT
CHANNEL
1
2
3
4
5
6
7
8
1 UNIT = 0.200 MILLIVOLTS
0.0
37.5
75.0
112.5
150.0
187.5
225.0
262.5
300.0
TIME (SECONDS)

(b)

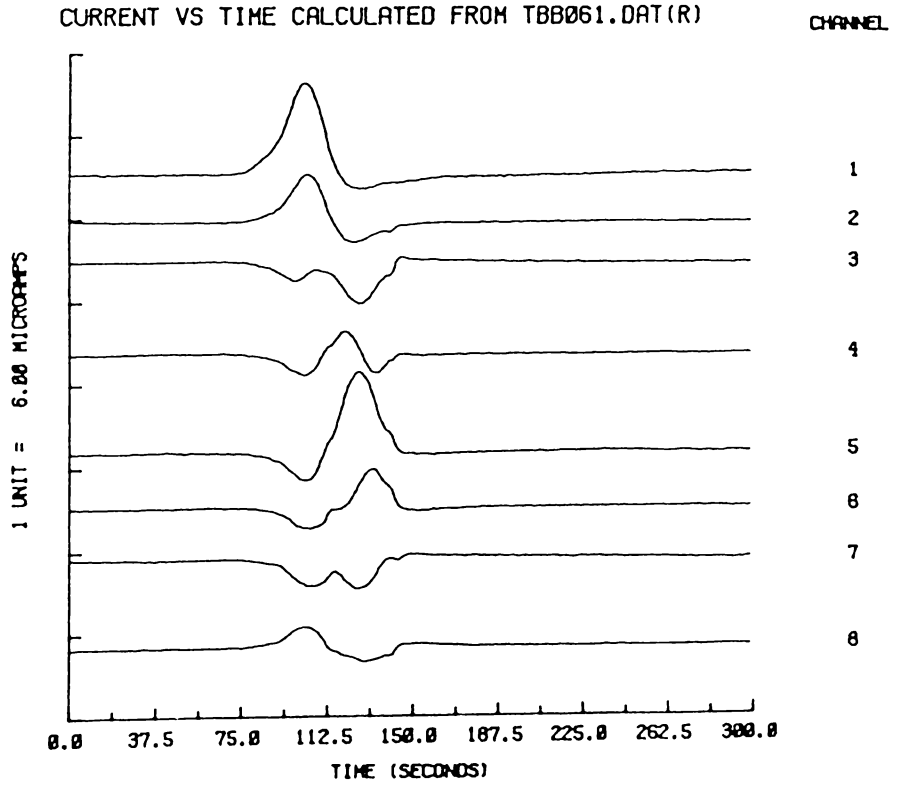
CURRENT VS TIME CALCULATED FROM TBB061.DAT(R)
CHANNEL
1
2
3
4
5
6
7
8
1 UNIT = 6.00 MICROAMPS
0.0
37.5
75.0
112.5
150.0
187.5
225.0
262.5
300.0
TIME (SECONDS)

Fig. 5.42

Fig. 5.43-5.44 Spontaneous action potentials observed in a *contaminated* ISS (see section 5.2.4).

Fig. 5.43 A *sharp take-off* action potential initiated at the contaminated end.

Fig. 5.44 A *slow take-off* action potential initiated at the opposite end with no (observable) contamination.

Each Fig. shows

(a) differential voltage waveforms

(b) calculated current waveforms.

(a)

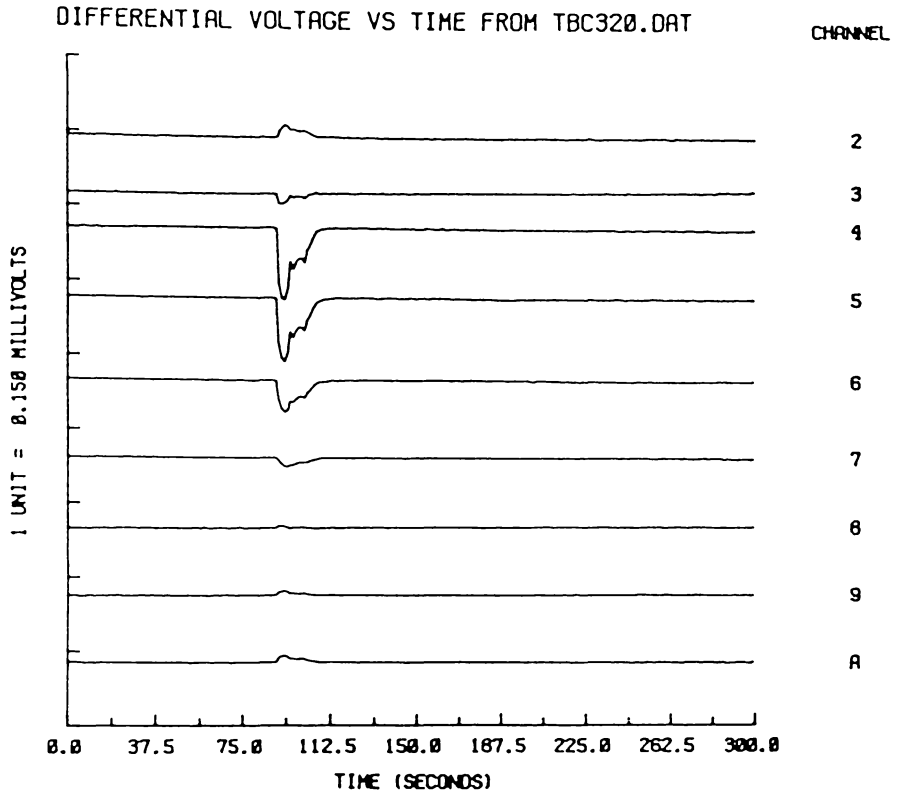
DIFFERENTIAL VOLTAGE VS TIME FROM TBC320.DAT
CHANNEL
2
3
4
5
6
7
8
9
A
1 UNIT = 0.150 MILLIVOLTS
0.0
37.5
75.0
112.5
150.0
187.5
225.0
262.5
300.0
TIME (SECONDS)

(b)

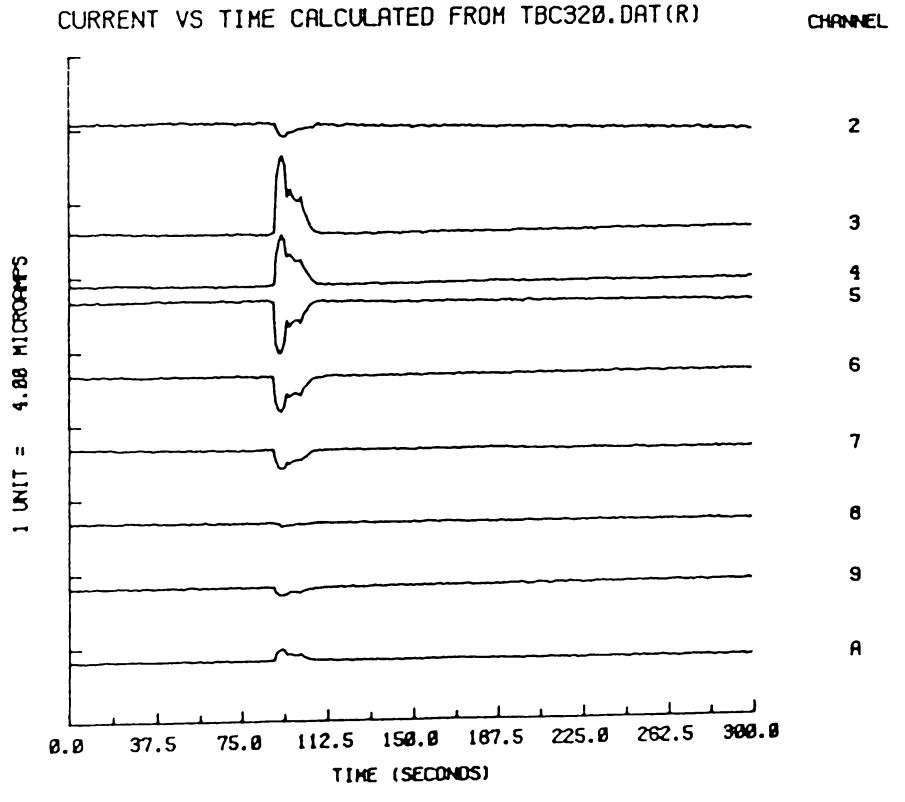
CURRENT VS TIME CALCULATED FROM TBC320.DAT(R)
CHANNEL
2
3
4
5
6
7
8
9
A
1 UNIT = 4.00 MICROAMPS
0.0
37.5
75.0
112.5
150.0
187.5
225.0
262.5
300.0
TIME (SECONDS)

Fig. 5.43

(a)

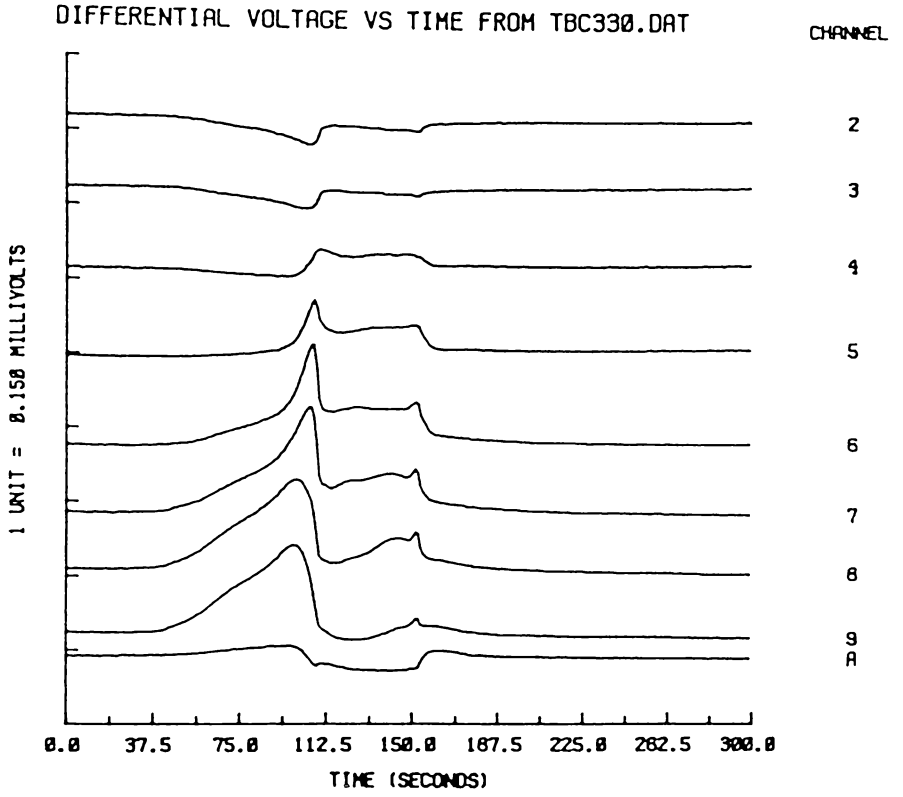
DIFFERENTIAL VOLTAGE VS TIME FROM TBC330.DAT
CHANNEL
1 UNIT = 0.150 MILLIVOLTS
2
3
4
5
6
7
8
9
A
0.0
37.5
75.0
112.5
150.0
187.5
225.0
262.5
300.0
TIME (SECONDS)

(b)

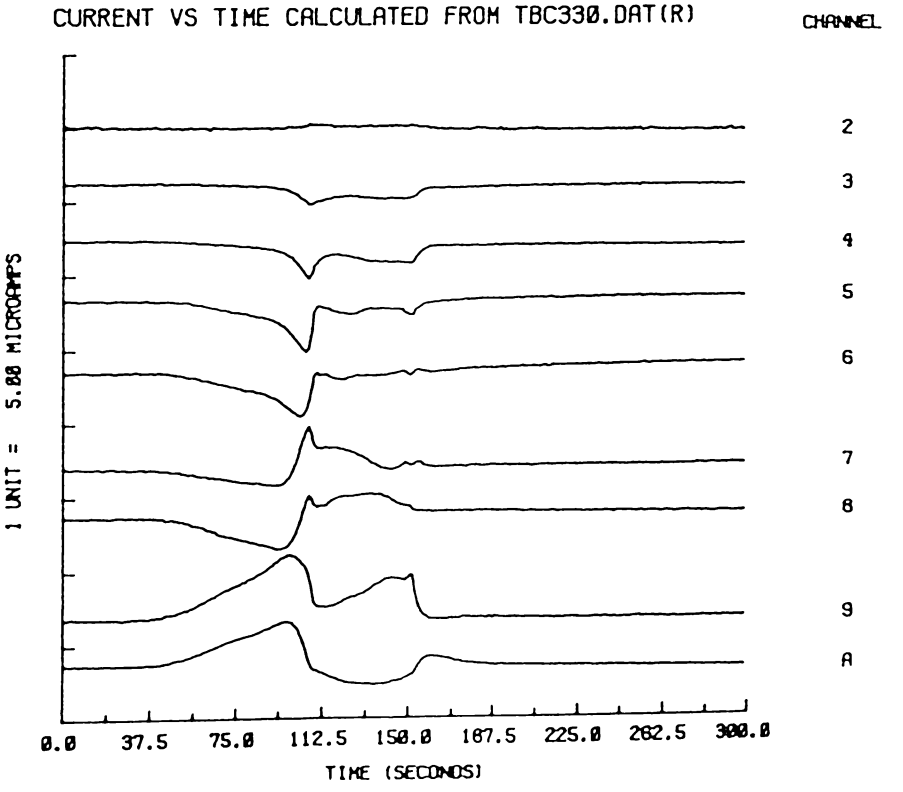
CURRENT VS TIME CALCULATED FROM TBC330.DAT(R)
CHANNEL
1 UNIT = 5.00 MICROAMPS
2
3
4
5
6
7
8
9
A
0.0
37.5
75.0
112.5
150.0
187.5
225.0
262.5
300.0
TIME (SECONDS)

Fig. 5.44

NUMBER OF SPONTANEOUS ACTION POTENTIALS

AT 3 HOUR INTERVALS STARTING FROM THE 1st HOUR

INTVL	VALUE	0 5 10 15
		-*---------*---------*---------*
1	10.	I##########################
2	1.	I###
3	1.	I###
4	5.	I############
5	3.	I########
6	5.	I############
7	3.	I########
8	2.	I######
9	1.	I###
10	2.	I######
11	2.	I######
12	1.	I###
13	1.	I###
14	2.	I######
15	3.	I########
16	4.	I##########
17	5.	I############
18	5.	I############
19	4.	I##########
20	5.	I############
21	4.	I##########
22	7.	I##################
23	9.	I#######################
24	6.	I###############
25	6.	I###############
26	4.	I##########
27	6.	I###############
28	10.	I##########################
29	9.	I#######################
30	10.	I##########################
31	9.	I#######################
32	9.	I#######################
33	8.	I###################
34	8.	I###################
35	9.	I#######################
36	9.	I#######################
37	13.	I##################################

Fig. 5.45 Number of spontaneous action potentials (at three hour intervals generated by a *dying* ISS during the period of the experiment (111 hours).

CHAPTER 6

DISCUSSION

6.1 Validity of the Technique

The first aim of this work was to develop a technique to identify the initiation sites of the action potentials and their subsequent propagation behaviour (if any) in cells or cell segments of *Acetabularia* in conditions as close to natural as possible. The second was the application of the technique to the measurements of the spontaneous action potentials generated by developing ISS's (anucleate isolated stalk segments) to see if any identifiable patterns or correlations with growth and development could be discerned.

The first objective was achieved by measuring the potential distribution generated by the current-flow in the surrounding medium of the cell (or cell segment) during an action potential using an array of exracellular electrodes. The initiation site and the propagation behaviour were then identified by using the calculated current waveform I, obtained from the measured differential voltage $\tilde{D}$ by the method of regularization. The application of the method was necessary because of the ill-conditioned nature of the inversion problem. The experiments described in section 3.3 as well as the tests in section 3.2.3 strongly support the validity of this technique.

When the technique was applied to the measured differential voltage $\tilde{D}$ in the main experiments (i.e. the developing ISS's) the errors in $\tilde{D}$ arose from

(i) uneven spacing of the electrodes which gave rise to differences in the external resistances between pairs of electrodes

(ii) electrode noise + amplifier noise and gain variations

(iii) the unequal length of the ISS sections between pairs of electrodes (due to a curved ISS - even if the ISS was straight at the beginning of the experiment its ends would generally bend towards the light as the experiment progressed)

(iv) the slight leakage of the current out of the tube which held the ISS.

However, these factors did not have a great effect on the calculation of the current I when the method of regularization was applied.

This technique enabled us to identify easily the patterns of movement of the depolarized region and also proved to be more accurate than the previous method of analysis using the differential voltage $\tilde{D}$ (Thavarungkul, 1980, see also section 3.2.1).

6.2 Conclusions and Comparisons with Other Work

The redevelopments of the ISS's in our experiments still showed significant retention of the original developmental polarity, indicated by the higher number of regenerations at the former apical end. Our results showed a lower percentage of ISS's regeneration at the former basal end than that reported by Novak and Bentrup (1972). In their experiments in which anucleate stalk segments were kept only

one day in the dark they obtained a 39% regeneration at the former basal end. This same condition in our experiments (first series) only provided a 25% redevelopment at this end. A further series of experiments in which the ISS's were kept longer in the dark (4 days) showed a slightly higher percentage of regeneration at the former basal end i.e. 33%. However, this was still lower than that obtained by Novak and Bentrup.

Although regenerating (at an average time of 39 ± 11 hours) most of the ISS's did not reach the stage of cap formation. That is, they only formed new extended tips with one or two whorls. For those which did form caps, the sizes of these caps were smaller than would be expected from a normal nucleate cell i.e. only ~2-3 mm in diameter compared to ⩾ 5 mm. Our main interest in this work is, however, the behaviour of the spontaneous action potentials during the course of development.

In most of the previous electrophysiological studies of the cell of *Acetabularia*, either as a complete cell or a cell segment, the technique used by Novak and Bentrup (1972, see chapter 1) was usually employed (e.g. Borghi *et al.*, 1983; Broda and Schweiger, 1981; Christ-Adler and Bentrup, 1976; Dazy *et al.*, 1980; Goodwin and Pateromichelakis, 1979). Since this technique could give rise to serious pertubations in the environment of the cell it is of special interest to compare some of our observations with those made by others using the Novak and Bentrup technique.

6.2.1 General Features

Action potentials observed in our experiments during the redevelopments of the ISS's in constant external conditions showed frequencies in the range of 0.3-1.3 pulse h^{-1} over the period of the experiment. The action potential frequency seems to be characteristic of the individual cell (Dazy *et al.*, 1980). From our observations there is no indication of a correlation between the action potential frequency and the regeneration time i.e. high frequency does not always indicate a short regeneration time, and vice versa.

The occurrences of spontaneous action potentials during the course of ISS development can be divided into two stages. First, within 4 ± 2 hours of the onset of illumination, a few sharp take-off non-propagating action potentials generally occurred followed by a rest period of ~6 ± 5 hours. The second stage occurred after this rest period where the occurrences of the slow take-off propagating and/or non-propagating action potentials seem to follow a rhythm, alternating between an active period (where action potentials occurred) and a rest period (where there were no action potentials). The time between consecutive active (or rest) periods was found to be between 24-30 hours depending on the cell as well as the cycle. A system which was being developed to measure the extracellular potential gradient along the cell (Williams, 1984) was unfortunately not ready when our experiments were being carried out. Therefore, simultaneous measurements of the action potentials and the potential gradient were not possible. However, results obtained by Dazy *et al.* (1980) indicated the variations of the occurrences of the action potentials and the extracellular potential gradient followed a

very similar rhythm. Experiments by Borghi *et al.* (1983) on *nucleate* cells of *Acetabularia* also indicated the similarity of the potential gradient rhythm and the rhythm of the cytoplasmic streaming. One interesting feature in their experiments was the observation of the cytoplasmic "vibration" (or in some cases plasmolysis which seemed to indicate water movement) just after the onset of illumination (lasting for ~1-3 min) followed by a short period of cytoplasmic streaming (~30 min). This seems to correspond to the period in which we normally observed the *first few* sharp take-off, non-propagating action potentials. This may indicate a relationship between cytoplasmic and/or water movements (which influences ion concentrations) and the sharp take-off action potential. The observations of the sharp take-off action potentials initiating at the sites of the shrinking cytoplasm in an injured cell also tend to support this possibility.

A rhythm of the occurrences of the spontaneous action potentials in *nucleate Acetabularia* cells has been observed for cells in a light:dark cycle of 16:8 h which also persisted under constant illumination (Dazy *et al.*, 1980). The rhythm was also detected on illumination after the cells had been subjected to a prolonged dark period (> 1 week and up to 6-8 weeks). It also persisted in constant light (Borghi *et al.*, 1983). This feature was also observed in our experiments with ISS's i.e. in *anucleate* cells. This seems to indicate that the necessary components of the *"rhythm oscillator"* for the occurrences of spontaneous action potentials are contained in the cytoplasm and/or the plasmalemma and can still function after several days in darkness. Although the persistence of the rhythm under

constant illumination is one of the characteristics of the circadian rhythm, additional data would be needed (e.g. on the temperature dependence of the period etc., see Schweiger and Schweiger, 1977) to establish its true circadian nature.

The existence of the action potential rhythm in our experiments, although agreeing with some workers (Borghi *et al.*, 1983; Dazy *et al.*, 1980), contradicted the results obtained by Novak and Bentrup (1972) in which the rate of the occurrences of the spontaneous action potentials increased steadily with time until it reached a constant level. Most of the ISS's in our experiments generated a clear rhythm, except for the dying and contaminated cells which showed similar behaviour to that observed by Novak and Bentrup. This may be evidence of the perturbatory or unnatural environment in the Novak and Bentrup work.

Another feature which seems to exhibit a rhythm is the colour appearance of the ISS's. The dark green patches observed during the mottled appearance period were probably the chloroplast *clusters, bands*, or *clods* observed by Kof *et al.* (1982) and Schmid and Koop (1983). This banding was observed during the migration of the chloroplasts to and from the apical region at the beginning and the end of the normal circadian light period respectively (Schmid and Koop, 1983). This seems to correspond to our observations that the mottled appearance occurred during the active period (which is probably the period described as the circadian light period by Schmid and Koop (1983)).

6.2.2 Initiation Sites of the Action Potentials

The results obtained in this work supported the work by Lertsithichai (1980), that in developing ISS's action potentials initiated at *both* ends with only a few initiating in the middle region. These observations together with the fact that in some experiments most of the action potentials did not propagate do not provide any support to the symmetry-breaking role of the propagating action potentials as proposed by Novak and Bentrup (1972) and Novak (1975). Furthermore, in the four cases (experiments BG, AB, B1 and BH) where the redevelopments occurred at the basal ends (i.e. in which the original developmental polarities were lost and hence symmetry-breaking must have taken place before growth), the action potentials which occurred before growth initiated at both ends.

The number of action potentials initiating in the middle region seems to increase with regeneration time. In one case where the regeneration time was extremely long (experiment BH) the action potentials seemed to initiate randomly along the ISS with approximately equal numbers in each of the three regions. This makes an interesting comparison with the results of Goodwin and Pateromichelakis (1979) who observed that in a cell with no apical elongation there is an instability in the membrane potential gradient i.e. the sign of the extracellular potential gradient between the tip and the other part of the plant varied with time.

In general there seemed to be a weak tendency for predominant action potential initiation at the regenerating end (observed in 8/13 experiments, see Fig. 5.25). However, in some cases (4/13 experiments) the reverse were observed. From these results it seems

reasonable to conclude that there is no firm correlation between the site of the action potential initiations and the site of apex regeneration. This result is in agreement with Bentrup (1977), Christ-Adler and Bentrup (1976), and Lertsithichai (1980).

An interesting point which should be noted here is the fact that 3 out of the 4 cases where regenerations occurred at the end with fewer action potential initiations, a tip growth was first observed shortly after a rest period had finished. (Past experiments by Lertsithichai (1980) also showed 2 out of 3 similar cases). Tip growths in other experiments, however, were first observed shortly after an active period had finished. This seems to indicate that under constant illumination the direction of development of the ISS may depend on a different level (or type) of electrical activity (which may involve different mechanism(s), see below). So far this possibility in *Acetabularia* has not been suggested by any other worker. However, in *Fucus* eggs similar behaviour seems to exist. In the experiments carried out by Peng and Jaffe (1976) 16 batches of the same species of *Fucus* eggs were subjected to external electric fields. The results were such that 11 batches germinated towards the positive electrode and 2 batches germinated towards a negative electrode. Three batches had mixed reactions in that they germinated towards a positive electrode in strong fields and towards the negative electrode in weak fields with a transition occurring over a very small voltage range. Peng and Jaffe proposed that these different responses were caused by different properties of the cell membrane in the two cases (i.e. germination towards positive or negative electrode) in allowing the Ca^{2+} to enter the future growth site. However, no suggestion was made as to why the differences in the membrane properties should occur.

The observations in one of our experiments (AG) of the translocation of the cytoplasmic content when a cap was formed, the change in the initiation sites of the action potentials from the O-end to the R-end and later the change in the properties of these action potentials (propagating → non-propagating) raise the question of whether all these effects are related. Our present work, however, could not provide any more evidence since the action potentials in the other ISS's which had formed caps were initiated predominantly at the R-ends long before caps were formed, and no other ISS showed any translocation of the cytoplasmic content.

6.2.3 Action Potential Propagation

Both propagating and non-propagating action potentials in the ISS's of *Actebularia* were observed. Propagation occurred as a result of the extension of the depolarized region over the length of the cell rather than the translocation of a narrow depolarized region.

The experimental results also indicated that the ability of an action potential to propagate could depend on the length of the ISS. In short segments less propagating action potentials occurred and in the shortest ISS in our experiments (AF) there were no propagating action potentials. This result seems to indicate that at least in a short ISS, propagation of the action potentials is not a necessary feature in the redevelopmental process. However, the model proposed by Zubarev and Rogatykh (1979, see chapter 1) in which action potentials were involved in morphogenesis and communication between the apex and the nucleus in longer cells is still a possibility.

6.3 Future Work

As indicated in section 6.2, a number of interesting features seem to emerge from the experiments. For example, the change of the initiation site of the action potential just before cap formation and the possibility that the site of development may depend on a different level (or type) of electrical activity. The observations of the stages of development in the experiments carried out so far were limited to observation through the stereomicroscope and hence only obvious developments such as tip growth could be detected.

The use of an optical scanner system in our type of experiments would enable the image of the developing ISS to be processed during the experiment. The system could be monitored by a computer which would collect the data of the images at a regular interval (probably ~1 hour). Therefore, the exact time of a tip growth, a cap formation, the rate of growth and their correlations with the electrical activities could be obtained.

In similar experiments carried out by Lertsithichai (1980), the results also indicated that spontaneous action potentials could initiate at both ends. Therefore, it was suggested that the points of the action potential initiations might be correlated with the region of growth rather than the exact form of growth (see also Goldsworthy, 1983). Although our results showed similar features, the fact that in one experiment (AF) none of the spontaneous action potentials initiated at the regenerating end seems to cast some doubt on this suggestion. However, to verify this, further experiments incorporating some imaging or other growth measurement are needed. The use of an imaging system would also enable us to observe the movement of the dark green patches during the mottled appearance

phase and elicit their correlation with the site of growth and/or electrical activities (if any).

Also in our experiments measurement of the potential gradient along the ISS was not possible due to the slow drift of the electrode potentials with time. Hence, we were unable to identify the site of the apex regeneration as the hyperpolarized or depolarized end. To obtain such measurement future work may include the use of the vibrating electrode technique (Jaffe and Nuccitelli, 1974) or the auto-zero electrode system (Williams, 1984) to avoid this problem. This would allow simultaneous measurements of the small overall potential gradient and of the action potentials. So far it has not been clearly established which of these electrical activities (or any particular combination) is more important to the development of the cell since suppression of either activity led to delays in the developmental process (Novak and Sironval, 1975; Rogatykh *et al.*, 1979). The use of the multi-extracellular recording system with a simultaneous steady gradient measurement could provide a lot of information on these two co-existing electrical activities. It could also reveal other electrical activities such as local transcellular current loops which may exist but were not able to be observed in the present work.

APPENDIX 1

DERIVATION OF EQUATIONS OF VOLTAGES AND CURRENTS IN CHAPTER 3

A1.1 EQUATIONS (3.5) AND (3.6)

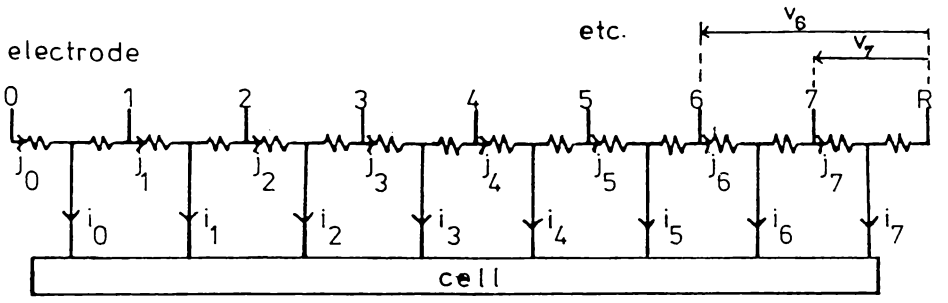

each resistor = $\frac{R_e}{2}$

From the above diagram we derive the following voltages

$$v_7 = v_R + j_7 \frac{R_e}{2} + (j_7 - i_7) \frac{R_e}{2}$$

Since $v_R = 0$ and $j_7 = i_7$ we have

$$v_7 = i_7 \frac{R_e}{2}$$

$$v_6 = v_7 + j_6 \frac{R_e}{2} + (j_6 - i_6) \frac{R_e}{2}$$

$$= i_7 \frac{R_e}{2} + (2j_6 - i_6) \frac{R_e}{2}$$

Since $j_6 = i_6 + i_7$ we have

$$v_6 = i_7 \frac{R_e}{2} + (2i_6 + 2i_7 - i_6) \frac{R_e}{2}$$

i.e. $$v_6 = (i_6 + 3i_7) \frac{R_e}{2}$$

Using the same method as above we obtain

$$v_5 = (i_5 + 3i_6 + 5i_7)\frac{R_e}{2}$$

$$v_4 = (i_4 + 3i_5 + 5i_6 + 7i_7)\frac{R_e}{2}$$

$$v_3 = (i_3 + 3i_4 + 5i_5 + 7i_6 + 9i_7)\frac{R_e}{2}$$

$$v_2 = (i_2 + 3i_3 + 5i_4 + 7i_5 + 9i_6 + 11i_7)\frac{R_e}{2}$$

$$v_1 = (i_1 + 3i_2 + 5i_3 + 7i_4 + 9i_5 + 11i_6 + 13i_7)\frac{R_e}{2}$$

$$v_0 = (i_0 + 3i_1 + 5i_2 + 7i_3 + 9i_4 + 11i_5 + 13i_6 + 15i_7)\frac{R_e}{2}$$

We can write the above equations in matrix form as

$$\begin{bmatrix} v_0 \\ v_1 \\ v_2 \\ v_3 \\ v_4 \\ v_5 \\ v_6 \\ v_7 \end{bmatrix} = \frac{R_e}{2} \begin{bmatrix} 1 & 3 & 5 & 7 & 9 & 11 & 13 & 15 \\ 0 & 1 & 3 & 5 & 7 & 9 & 11 & 13 \\ 0 & 0 & 1 & 3 & 5 & 7 & 9 & 11 \\ 0 & 0 & 0 & 1 & 3 & 5 & 7 & 9 \\ 0 & 0 & 0 & 0 & 1 & 3 & 5 & 7 \\ 0 & 0 & 0 & 0 & 0 & 1 & 3 & 5 \\ 0 & 0 & 0 & 0 & 0 & 0 & 1 & 3 \\ 0 & 0 & 0 & 0 & 0 & 0 & 0 & 1 \end{bmatrix} \begin{bmatrix} i_0 \\ i_1 \\ i_2 \\ i_3 \\ i_4 \\ i_5 \\ i_6 \\ i_7 \end{bmatrix}$$

i.e. $\underline{v} = A\,\underline{i}$

which is equation (3.5). From this equation the current $\underline{i}$ can be expressed as

$$\underline{i} = A^{-1}\,\underline{v}$$

which is equation (3.6) where A^{-1} is the inverse of matrix A

i.e. $$A^{-1} = \frac{2}{R_e}\begin{bmatrix} 1 & -3 & 4 & -4 & 4 & -4 & 4 & -4 \\ 0 & 1 & -3 & 4 & -4 & 4 & -4 & 4 \\ 0 & 0 & 1 & -3 & 4 & -4 & 4 & -4 \\ 0 & 0 & 0 & 1 & -3 & 4 & -4 & 4 \\ 0 & 0 & 0 & 0 & 1 & -3 & 4 & -4 \\ 0 & 0 & 0 & 0 & 0 & 1 & -3 & 4 \\ 0 & 0 & 0 & 0 & 0 & 0 & 1 & -3 \\ 0 & 0 & 0 & 0 & 0 & 0 & 0 & 1 \end{bmatrix}$$

A1.2 EQUATIONS (3.13) AND (3.14)

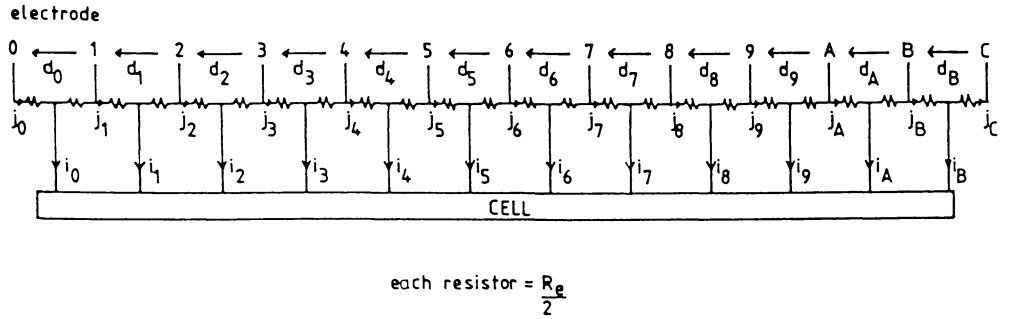

Consider the above diagram

$$d_B = (j_B + j_C)\frac{R_e}{2}$$

Since the cell ends midway between electrodes B and C, $j_C = 0$ and $j_B = i_B$. The above equation becomes

$$d_B = i_B \frac{R_e}{2}$$

$$d_A = (j_A + j_B)\frac{R_e}{2}$$

Since $j_A = i_A + j_B$ and $j_B = i_B$ we have

$$d_A = (i_A + i_B + i_B)\frac{R_e}{2}$$

i.e. $$d_A = (i_A + 2i_B)\frac{R_e}{2}$$

Similarly we obtain

$$d_9 = (i_9 + 2i_A + 2i_B)\frac{R_e}{2}$$

$$d_8 = (i_8 + 2i_9 + 2i_A + 2i_B)\frac{R_e}{2}$$

$$d_7 = (i_7 + 2i_8 + 2i_9 + 2i_A + 2i_B)\frac{R_e}{2}$$

$$d_6 = (i_6 + 2i_7 + 2i_8 + 2i_9 + 2i_A + 2i_B)\frac{R_e}{2}$$

$$d_5 = (i_5 + 2i_6 + 2i_7 + 2i_8 + 2i_9 + 2i_A + 2i_B)\frac{R_e}{2}$$

$$d_4 = (i_4 + 2i_5 + 2i_6 + 2i_7 + 2i_8 + 2i_9 + 2i_A + 2i_B)\frac{R_e}{2}$$

$$d_3 = (i_3 + 2i_4 + 2i_5 + 2i_6 + 2i_7 + 2i_8 + 2i_9 + 2i_A + 2i_B)\frac{R_e}{2}$$

$$d_2 = (i_2 + 2i_3 + 2i_4 + 2i_5 + 2i_6 + 2i_7 + 2i_8 + 2i_9 + 2i_A + 2i_B)\frac{R_e}{2}$$

$$d_1 = (i_1 + 2i_2 + 2i_3 + 2i_4 + 2i_5 + 2i_6 + 2i_7 + 2i_8 + 2i_9 + 2i_A + 2i_B)\frac{R_e}{2}$$

$$d_0 = (i_0 + 2i_1 + 2i_2 + 2i_3 + 2i_4 + 2i_5 + 2i_6 + 2i_7 + 2i_8 + 2i_9 + 2i_A + 2i_B)\frac{R_e}{2}$$

or in matrix form

$$\begin{bmatrix} d_0 \\ d_1 \\ d_2 \\ d_3 \\ d_4 \\ d_5 \\ d_6 \\ d_7 \\ d_8 \\ d_9 \\ d_A \\ d_B \end{bmatrix} = \frac{R_e}{2} \begin{bmatrix} 1 & 2 & 2 & 2 & 2 & 2 & 2 & 2 & 2 & 2 & 2 & 2 \\ 0 & 1 & 2 & 2 & 2 & 2 & 2 & 2 & 2 & 2 & 2 & 2 \\ 0 & 0 & 1 & 2 & 2 & 2 & 2 & 2 & 2 & 2 & 2 & 2 \\ 0 & 0 & 0 & 1 & 2 & 2 & 2 & 2 & 2 & 2 & 2 & 2 \\ 0 & 0 & 0 & 0 & 1 & 2 & 2 & 2 & 2 & 2 & 2 & 2 \\ 0 & 0 & 0 & 0 & 0 & 1 & 2 & 2 & 2 & 2 & 2 & 2 \\ 0 & 0 & 0 & 0 & 0 & 0 & 1 & 2 & 2 & 2 & 2 & 2 \\ 0 & 0 & 0 & 0 & 0 & 0 & 0 & 1 & 2 & 2 & 2 & 2 \\ 0 & 0 & 0 & 0 & 0 & 0 & 0 & 0 & 1 & 2 & 2 & 2 \\ 0 & 0 & 0 & 0 & 0 & 0 & 0 & 0 & 0 & 1 & 2 & 2 \\ 0 & 0 & 0 & 0 & 0 & 0 & 0 & 0 & 0 & 0 & 1 & 2 \\ 0 & 0 & 0 & 0 & 0 & 0 & 0 & 0 & 0 & 0 & 0 & 1 \end{bmatrix} \begin{bmatrix} i_0 \\ i_1 \\ i_2 \\ i_3 \\ i_4 \\ i_5 \\ i_6 \\ i_7 \\ i_8 \\ i_9 \\ i_A \\ i_B \end{bmatrix}$$

i.e. $\underline{d} = G\,\underline{i}$

which is equation (3.13). Therefore, we have

$$\underline{i} = G^{-1}\,\underline{d}$$

i.e. equation (3.14) where G^{-1} is the inverse of the matrix G

$$G^{-1} = \frac{2}{R_e}\begin{bmatrix} 1 & -2 & 2 & -2 & 2 & -2 & 2 & -2 & 2 & -2 & 2 & -2 \\ 0 & 1 & -2 & 2 & -2 & 2 & -2 & 2 & -2 & 2 & -2 & 2 \\ 0 & 0 & 1 & -2 & 2 & -2 & 2 & -2 & 2 & -2 & 2 & -2 \\ 0 & 0 & 0 & 1 & -2 & 2 & -2 & 2 & -2 & 2 & -2 & 2 \\ 0 & 0 & 0 & 0 & 1 & -2 & 2 & -2 & 2 & -2 & 2 & -2 \\ 0 & 0 & 0 & 0 & 0 & 1 & -2 & 2 & -2 & 2 & -2 & 2 \\ 0 & 0 & 0 & 0 & 0 & 0 & 1 & -2 & 2 & -2 & 2 & -2 \\ 0 & 0 & 0 & 0 & 0 & 0 & 0 & 1 & -2 & 2 & -2 & 2 \\ 0 & 0 & 0 & 0 & 0 & 0 & 0 & 0 & 1 & -2 & 2 & -2 \\ 0 & 0 & 0 & 0 & 0 & 0 & 0 & 0 & 0 & 1 & -2 & 2 \\ 0 & 0 & 0 & 0 & 0 & 0 & 0 & 0 & 0 & 0 & 1 & -2 \\ 0 & 0 & 0 & 0 & 0 & 0 & 0 & 0 & 0 & 0 & 0 & 1 \end{bmatrix}$$

A1.3 EQUATIONS (3.17) AND (3.18)

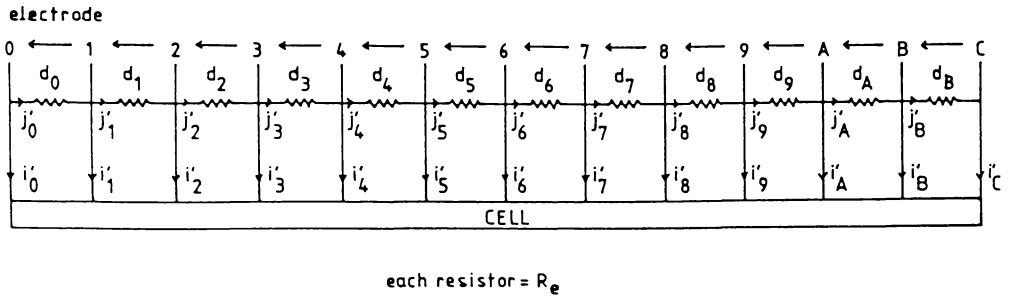

From the above diagram we derive the following differential voltages

$$d_0 = j_0' R_e$$

Since $j_0' = -i_0'$ we have

$$d_0 = -i_0' R_e$$

$$d_1 = j_1' R_e$$

$$= (j_0' - i_1') R_e$$

i.e. $$d_1 = (-i_0' - i_1') R_e$$

Similarly we have

$$d_2 = (-i_0' - i_1' - i_2') R_e$$

$$d_3 = (-i_0' - i_1' - i_2' - i_3') R_e$$

$$d_4 = (-i_0' - i_1' - i_2' - i_3' - i_4') R_e$$

$$d_5 = (-i_0' - i_1' - i_2' - i_3' - i_4' - i_5') R_e$$

$$d_6 = (-i_0' - i_1' - i_2' - i_3' - i_4' - i_5' - i_6') R_e$$

$$d_7 = (-i_0' - i_1' - i_2' - i_3' - i_4' - i_5' - i_6' - i_7') R_e$$

$$d_8 = (-i_0' - i_1' - i_2' - i_3' - i_4' - i_5' - i_6' - i_7' - i_8') R_e$$

$$d_9 = (-i_0' - i_1' - i_2' - i_3' - i_4' - i_5' - i_6' - i_7' - i_8' - i_9') R_e$$

$$d_A = (-i_0' - i_1' - i_2' - i_3' - i_4' - i_5' - i_6' - i_7' - i_8' - i_9' - i_A') R_e$$

$$d_B = (-i_0' - i_1' - i_2' - i_3' - i_4' - i_5' - i_6' - i_7' - i_8' - i_9' - i_A' - i_B') R_e$$

In matrix form

$$\begin{bmatrix} d_0 \\ d_1 \\ d_2 \\ d_3 \\ d_4 \\ d_5 \\ d_6 \\ d_7 \\ d_8 \\ d_9 \\ d_A \\ d_B \end{bmatrix} = R_e \begin{bmatrix} -1 & 0 & 0 & 0 & 0 & 0 & 0 & 0 & 0 & 0 & 0 & 0 \\ -1 & -1 & 0 & 0 & 0 & 0 & 0 & 0 & 0 & 0 & 0 & 0 \\ -1 & -1 & -1 & 0 & 0 & 0 & 0 & 0 & 0 & 0 & 0 & 0 \\ -1 & -1 & -1 & -1 & 0 & 0 & 0 & 0 & 0 & 0 & 0 & 0 \\ -1 & -1 & -1 & -1 & -1 & 0 & 0 & 0 & 0 & 0 & 0 & 0 \\ -1 & -1 & -1 & -1 & -1 & -1 & 0 & 0 & 0 & 0 & 0 & 0 \\ -1 & -1 & -1 & -1 & -1 & -1 & -1 & 0 & 0 & 0 & 0 & 0 \\ -1 & -1 & -1 & -1 & -1 & -1 & -1 & -1 & 0 & 0 & 0 & 0 \\ -1 & -1 & -1 & -1 & -1 & -1 & -1 & -1 & -1 & 0 & 0 & 0 \\ -1 & -1 & -1 & -1 & -1 & -1 & -1 & -1 & -1 & -1 & 0 & 0 \\ -1 & -1 & -1 & -1 & -1 & -1 & -1 & -1 & -1 & -1 & -1 & 0 \\ -1 & -1 & -1 & -1 & -1 & -1 & -1 & -1 & -1 & -1 & -1 & -1 \end{bmatrix} \begin{bmatrix} i_0' \\ i_1' \\ i_0' \\ i_3' \\ i_4' \\ i_5' \\ i_6' \\ i_7' \\ i_8' \\ i_9' \\ i_A' \\ i_B' \end{bmatrix}$$

i.e. $\underline{d} = G' \underline{i}'$

which is equation (3.17).

Hence $\underline{i}' = (G')^{-1}\,\underline{d}$

Where $(G')^{-1}$ is the inverse of matrix G'.

$$(G')^{-1} = \frac{1}{R_e}\begin{bmatrix} -1 & 0 & 0 & 0 & 0 & 0 & 0 & 0 & 0 & 0 & 0 & 0 \\ 1 & -1 & 0 & 0 & 0 & 0 & 0 & 0 & 0 & 0 & 0 & 0 \\ 0 & 1 & -1 & 0 & 0 & 0 & 0 & 0 & 0 & 0 & 0 & 0 \\ 0 & 0 & 1 & -1 & 0 & 0 & 0 & 0 & 0 & 0 & 0 & 0 \\ 0 & 0 & 0 & 1 & -1 & 0 & 0 & 0 & 0 & 0 & 0 & 0 \\ 0 & 0 & 0 & 0 & 1 & -1 & 0 & 0 & 0 & 0 & 0 & 0 \\ 0 & 0 & 0 & 0 & 0 & 1 & -1 & 0 & 0 & 0 & 0 & 0 \\ 0 & 0 & 0 & 0 & 0 & 0 & 1 & -1 & 0 & 0 & 0 & 0 \\ 0 & 0 & 0 & 0 & 0 & 0 & 0 & 1 & -1 & 0 & 0 & 0 \\ 0 & 0 & 0 & 0 & 0 & 0 & 0 & 0 & 1 & -1 & 0 & 0 \\ 0 & 0 & 0 & 0 & 0 & 0 & 0 & 0 & 0 & 1 & -1 & 0 \\ 0 & 0 & 0 & 0 & 0 & 0 & 0 & 0 & 0 & 0 & 1 & -1 \end{bmatrix}$$

To obtain i_C' we use the fact that the algebraic sum of transmembrane current is equal to zero i.e.

$$0 = i_0' + i_1' + i_2' + i_3' + i_4' + i_5' + i_6' + i_7' + i_8' + i_9' + i_A' + i_B' + i_C'$$

hence $$i_C' = -(i_0' + i_1' + i_2' + i_3' + i_4' + i_5' + i_6' + i_7' + i_8' + i_9' + i_A' + i_B')$$

using the above equations of $\underline{i}'$ in term of $\underline{d}$ we have

$$i_C' = -[(-d_0) + (d_0-d_1) + (d_1-d_2) + (d_2-d_3) + (d_3-d_4) + (d_4-d_5) + (d_5-d_6) + (d_6-d_7) + (d_7-d_8) + (d_8-d_9) + (d_9-d_A) + (d_A-d_B)] \frac{1}{R_e}$$

$$= -(-d_B) \frac{1}{R_e}$$

i.e. $$i_C' = \frac{d_B}{R_e}$$

Hence $\underline{i}' = (G')^{-1} \underline{d}$ and $i_C' = \frac{d_B}{R_e}$ which is equation (3.18).

APPENDIX 2

EXAMPLES OF PROPAGATION BEHAVIOUR OF SPONTANEOUS ACTION POTENTIALS ANALYSED BY USING DIFFERENTIAL VOLTAGE DISTRIBUTIONS

Each shows

(a) differential voltage waveforms

(b) the analysed depolarized regions (▨) at different points in time by using the differential voltage distributions to locate the depolarized regions boundaries

(from Thavarungkul, 1980).

A2.1

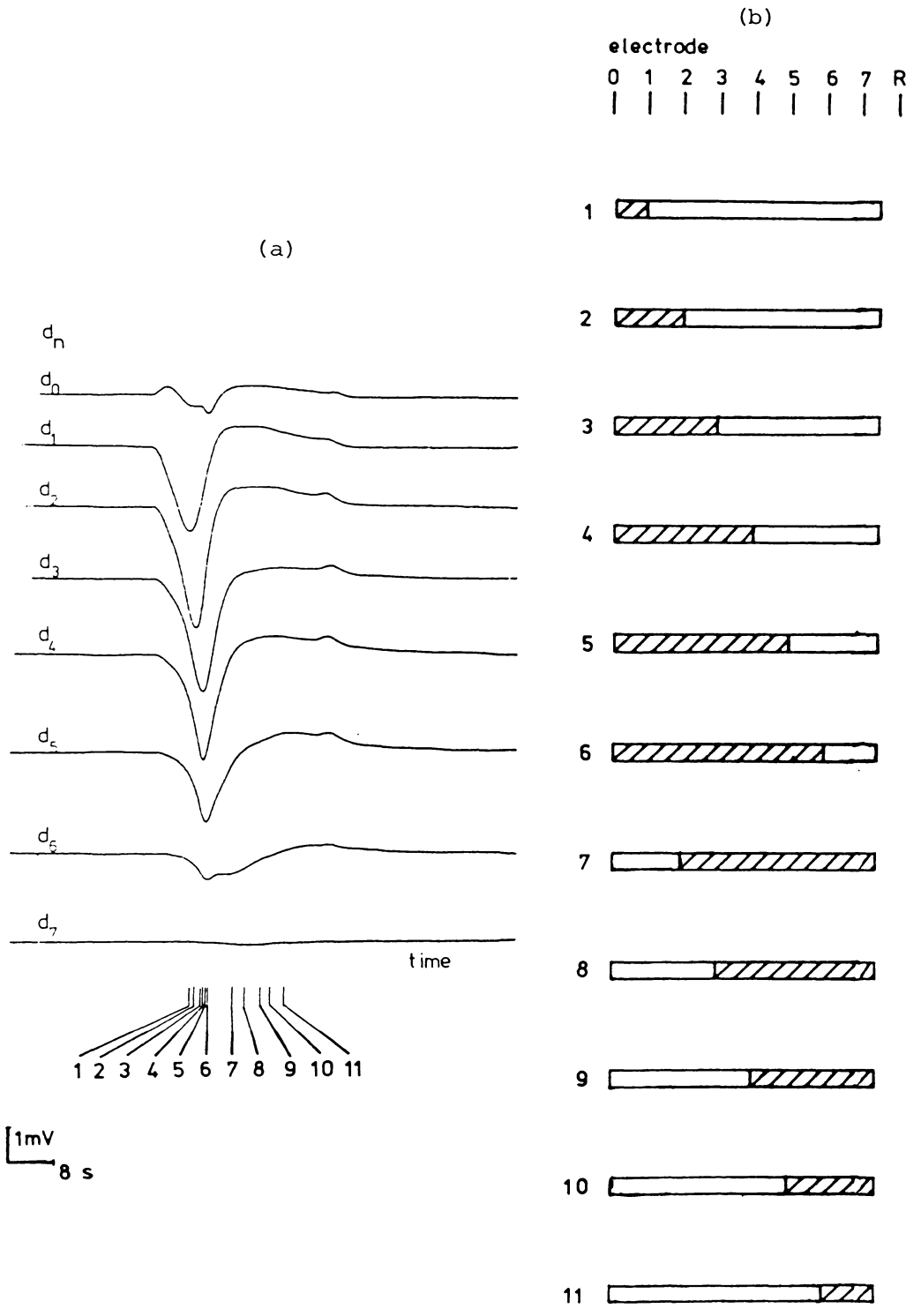
(a)
(b)
electrode
0 1 2 3 4 5 6 7 R
d_n
d_0
d_1
d_2
d_3
d_4
d_5
d_6
d_7
time
1 2 3 4 5 6 7 8 9 10 11
1mV
8 s
1
2
3
4
5
6
7
8
9
10
11

A2.2

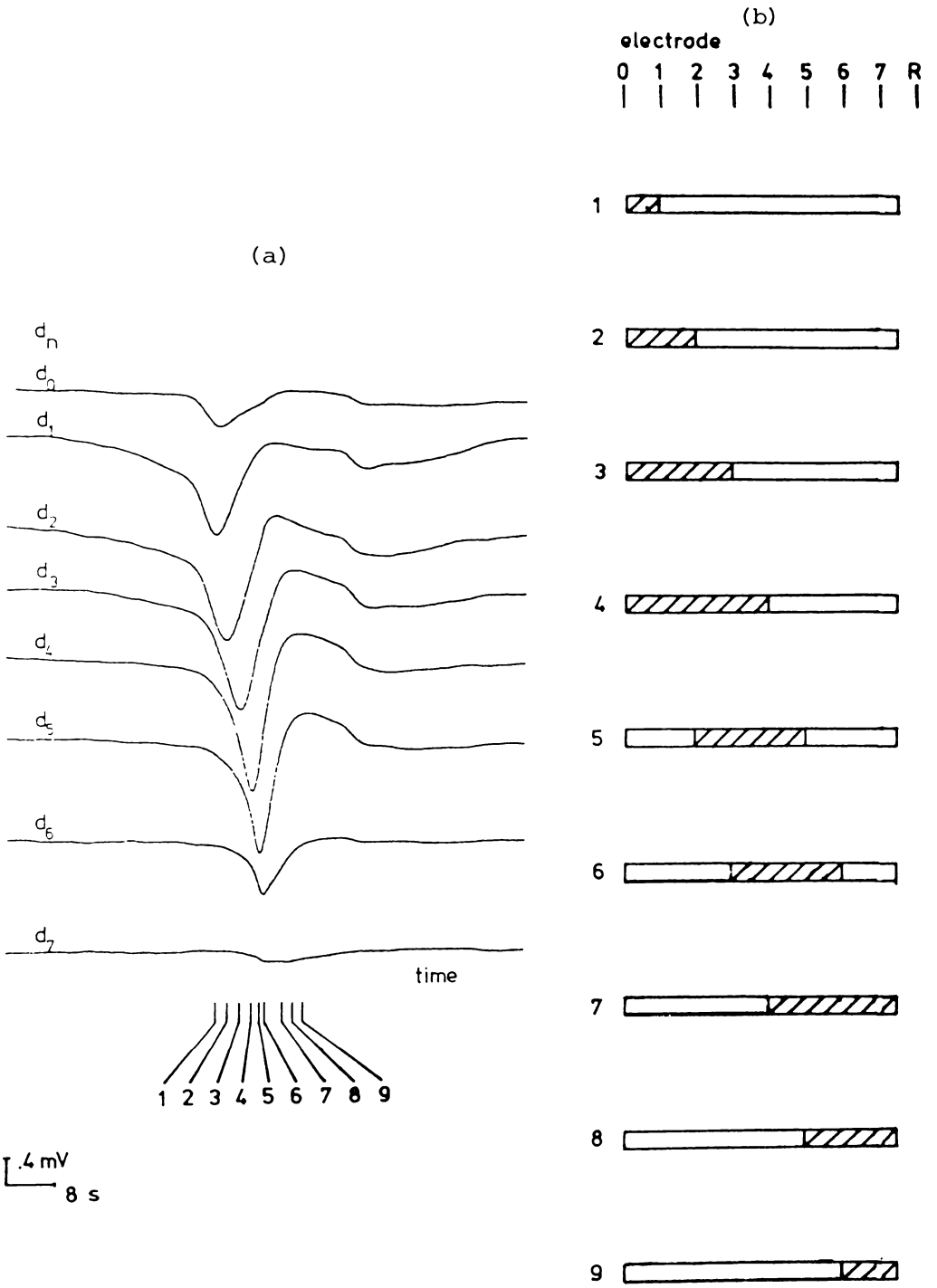
(a)
d_n
d_0
d_1
d_2
d_3
d_4
d_5
d_6
d_7
time
1 2 3 4 5 6 7 8 9
.4 mV
8 s
(b)
electrode
0 1 2 3 4 5 6 7 R
1
2
3
4
5
6
7
8
9

A2.3

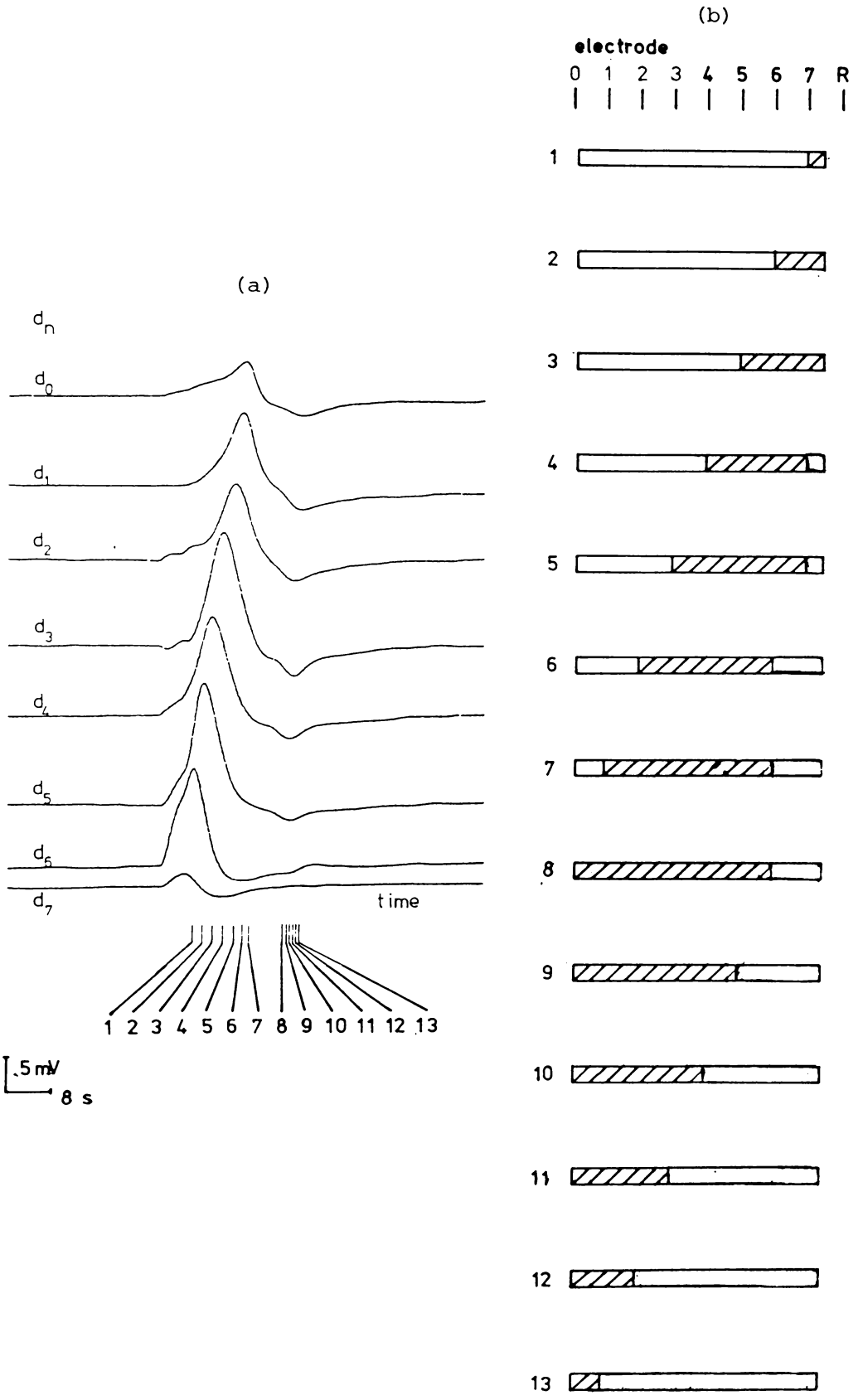
(a)
d_n
d_0
d_1
d_2
d_3
d_4
d_5
d_6
d_7
time
1 2 3 4 5 6 7 8 9 10 11 12 13
.5 mV
8 s
(b)
electrode
0 1 2 3 4 5 6 7 R
1
2
3
4
5
6
7
8
9
10
11
12
13

APPENDIX 3

COMPOSITION OF AE50 MEDIUM

AE50 medium consists of two main parts ASP2 medium and ERD SCHREIBER medium.

1. ASP2 Medium

Stock Solutions

Major Salts

NaCl	290	g
$MgSO_4.7H_2O$	80	g
KCl	9.6	g
$CaCl_2.6H_2O$	8.76	g
Distilled water	4	l

Autoclave at 15 PSI for 20 minutes

Tris

Tris (hydroxy methyl) amino methane

$NH_2.C\ (CH_2OH)_3$	40	g
Distilled water	1	l

Autoclave

Minor Salts

$NaNO_3$	5 g
K_2HPO_4	0.5 g
Distilled water	100 ml
Autoclave	

Metals

$FeCl_3.6H_2O$	0.77 g
$ZnCl_2$	0.0624 g
$MnCl_2.4H_2O$	0.86 g
$CoCl_2.6H_2O$	0.0024 g
$CuCl_2.2H_2O$	0.00064 g
H_3BO_3	6.84 g
Na_2EDTA	6.0 g
Distilled water	4 l
Autoclave	

Vitamins

Biotin	0.02 mg
Folic acid	0.04 mg
Vitamin B_{12}	0.04 mg
Thiamine	10.0 mg
Nicotinic acid	2.0 mg
Calcium pantothenate	2.0 mg
p-Amino benzoic acid	0.2 mg
Inositol	100.0 mg
Thymine	60.0 mg
Distilled water	100.0 ml
Filtered 0.2μm	

Preparatiion of ASP2 medium

a.	filtered distilled water	1400 ml
b.	add major salts	500 ml
c.	add tris	50 ml
d.	add 12 ml 1N HCl to adjust pH to	~7.8
e.	add metals	40 ml
f.	add minor salts	2 ml
g.	add vitamins	10 ml

2. ERD SCHREIBER Medium

Seawater - natural, .2μm filtered	2	l
Soil extract	100	ml
$NaNO_3$	0.4	g
Na_2HPO_4	0.0236	g

Mix ASP2 medium (exclude g) and ERD SCHREIBER medium, autoclave then add vitamins to produce AE50 medium.

Soil Extract

1. Mix soils with distilled water, ratio 1 : 2, shake well.
2. Autoclave at 15 PSI for 20 minutes.
3. Decant when it is cooled.
4. Leave for ~ 12-24 hours.
5. Decant and centrifuge at 5,000 rpm for 30 minutes.
6. Decant and filter through 0.2μm filter.
7. Autoclave for 15 minutes.

APPENDIX 4

COMMANDS EXECUTED BY THE TRANSIENT DATA DISPLAY PROGRAM-TDDP2E

PBUF - the process buffer - contains the experimental data copied directly from the floppy disc. Data generated as a result of the specified operations on this is written to OBUF - the output buffer- for outputting to printer or graphical display devices.

1. Load PBUF from floppy disc

L filename	Filename contains 6 characters. These include T (stands for transient) + 2 characters for the name of the experiment and 3 characters for the number of transient e.g.
LTAA002	load transient number 002 from experiment AA.

2. Processing with VDU (and printer) printout

TaaaaΔbbbb	Type all channel data (i.e. differential voltages) from sample number aaaa to bbbb inclusive. aaaa and bbbb are positive decimal in the range of 0-1023, with bbbb > aaaa.

N.B. Δ stands for a space.

X	Type maximum and minimum values and their positions, average of the first and last 20 percent of samples and peak to peak span for all channels (i.e. differential voltages).
ZX	Type maximum and minimum values, their positiions and peak to peak span for all differential signals (i.e. current solution by simplified equation).
VaaaaΔbbbb	Type average value of samples aaaa to bbbb inclusive for channel data currently in OBUF.
U	As in X, but only for channel data currently in OBUF.

3. Transfer of data from PBUF to OBUF and manipulation of OBUF data

R	Reset OBUF; all Y values set to 0 and X values (i.e. sample points) set in ascending sequence 0-1023.
Ah.(Sh.)	Adds (substracts) data from channel h (h-hexadecimal) to Y values in OBUF.
± ddddc	Adds or substracts decimal integer dddd to all c-values in OBUF, c = X or Y.
*aaaa/bbbb	Multiplies all c-values in OBUF by rational fraction aaaa/bbbb where both aaaa and bbbb are positive decimal integers.

Na	Normalises and shifts Y-values so that they are centred about Y = 0 and occupy 1/a of full scale (+2047 to -2048). a is a positive integer.
B	Shifts all Y-values so extrema are symetrical about Y = 0 baseline.
I	All Y values multiplied by -1 (any -2048 converted to -2047 before multiplication).

4. Graphical output - device d = C (CRT) or G (XY graph plotter).

Wd	Display all data in PBUF on device d (see above), automatically scaled and displaced (i.e. display all channels of differential voltage).
Zd	Display full set of differential signals of data on device d, automatically scaled and displaced (i.e. display current solution by simplified equation).
E	Erase CRT display.
C	CRT display of complete OBUF contents (single channel).
CaaaaΔbbbb	CRT display of points in OBUF from aaaa to bbbb inclusive.
D	X-Y graph plotter display of complete OBUF contents.

DaaaaΔbbbb	XY trace of points aaaa to bbbb inclusive.
PaaaaΔbbbb	As DaaaaΔbbbb but individual points plotted instead of single trace. (Take ~1 s/pt).
Qd	Plot 16 points on device d to define full, half and quarter scale values on both X and Y axes.
MxxxxΔ(-)yyyyd	Plot single point on device d with coordinate (xxxx,yyyy).

5. Annotation text and exit

#	Any character typed simple printed until next # encountered.

6. Transferring data to the VAX

O	Transfer data from PBUF to the VAX until the termination characters (9999) were encountered (operated together with a data-transfer program in the VAX).

REFERENCES

Aidley, D.J. (1978). *The Physiology of Excitable Cells.* 2nd ed. Cambridge, Cambridge University Press. 530p.

Alexeev, A.B.; M.I. Betina; S.L. Stvolinsky; A.A. Yazykov and T.N. Zubarev (1974). Evidence for a relationship between some ribonucleoprotein-complexes and the "morphogenetic substances" of *Acetabularia. Plant Science Letters* v. 3, p. 297-302.

Apostolova, R.D. and O.S. Ksenzhek (1977). Effect of ionic composition of the external medium on the intracellular potential of the alga *Acetabularia. Biophysics* v. 22, p. 89-95.

Babloyantz, A. and J. Hiernaux (1975). Models for cell differentiation and generation of polarity in diffusion-governed morphogenetic fields. *Bulletin of Mathematical Biology* v. 37, p. 637-657.

Baker, C.T.H. (1977). *The Numerical Treatment of Integral Equations.* Oxford, Clarendon Press. 1034p.

Barker, A.T.; B.H. Brown and I.L. Freeston (1979). Modeling of an active nerve fiber in a finite volume conductor and its application to the calculation of surface action potentials. *IEEE Transactions on Biomedical Engineering* v. BME-26(1), p. 53-56.

Benedek, G.B.and F.M.H. Villars (1979). *Physics with Illustrative Examples From Medicine and Biology. Volume 3: Electricity and Magnetism.* Reading, Massachusetts. Menlo Park, California, Addison-Wesley. 562p.

Bentrup, F.W. (1977). Electrical events during apex regeneration in *Acetabularia mediterranea.* In C.L.F. Woodcock. *Progress in Acetabularia Research.* New York, Academic Press. p. 249-254.

Bonotto, S.; P. Lurguin; L. Baugnet-Mahieu; R. Goutier; R. Kirchmann and J.R. Maisin (1972). Biology and radiobiology of anucleate *Acetabularia mediterranea*. In S. Bonotto; R. Goutier; R. Kirchmann and J.R. Maisin. *Biology and Radiobiology of Anucleate System II. Plant Cells*. New York, Academic Press. p.339-368.

Borgens, R.B.; J.W. Vanable, Jr. and L.F. Jaffe (1977a). Bioelectricity and regeneration. I. Initiation of frog limb regeneration by minute currents. *Journal of Experimental Zoology* v. 200, p. 403-416.

Borgens, R.B.; J.W. Vanable, Jr. and L.F. Jaffe (1977b). Bioelectricity and regeneration: Large currents leave the stumps of regenerating newt limbs. *Proceedings of the NationaL Academy of Sciences. U.S.A.* v. 74, p. 4528-4532.

Borghi, H.; S. Puiseux-Dao; M. Durand and A.C. Dazy (1983). Morphogenesis, bioelectrical polarity and intracellular streaming in a giant cell, *Acetabularia mediterranea*: Studies on their recovery after prolonged dark period. *Plant Science Letters* v. 31, p. 75-86.

Broda, H. and H.-G. Schweiger (1981). Long-term measurement of endogeneous diurnal oscillations of the electrical potential in an individual *Acetabularia* cell. *European Journal of Cell Biology* v. 26, p. 1-4.

Burden, R.L.; J.D. Faires and A.C. Reynolds (1978). *Numerical Analysis*. Boston, Prindle, Weber and Schmidt. 579p.

Chatfield, C. (1980). *The Analysis of Time Series: An Introduction*. 2nd ed. London, New York, Chapman and Hall. 268p.

Christ-Adler, M. and F.W. Bentrup (1976). Effect of K^+ and Cl^- ion gradients upon apex regeneration in *Acetabularia mediterranea*. *Planta* v. 129, p. 91-93.

Clark, J. and R. Plonsey (1966). A mathematical evaluation of the core conductor model. *Biophysical Journal* v. 6, p. 95-112.

Clark, J. and R. Plonsey (1968). The extracellular potential field of the single active nerve fiber in a volume conductor. *Biophysical Journal* v. 8, p. 842-864.

Clérin, P.; T. Vanden Driessche and J. Brachet (1975). Migration of cytoproteins into the nucleus of *Acetabularia*. In S. Puiseux-Dao. *Molecular Biology of Nucleocytoplasmic Relationships*. Amsterdam, Elsevier. p. 305-311.

Darby, M.I. (1980). Calculation of the fields near permanent magnets. In A.D. Boardman. *Physics Programs. Vol.2 Magnetism.* New York, John Wiley and Sons. p. 125-147.

Dazy, A.C.; H. Borghi and Y. Pichon (1980). Spontaneous bioelectrical activity in unicellular alga *Acetabularia mediterranea*. *Comptes Rendus Hebdomadaires des Seances de l'Academie des Sciences Serie D. Science Naturelles* v. 291, p. 637- 640.

Dazy, A.C.; S. Puiseux-Dao; M. Durand and A. Santa-Maria (1981). The effects of blue and red light on streaming recovery and RNA transport after dark treatment in *Acetabularia mediterranea*. *Protoplasma* v. 105, p. 354.

Ferris, C.D. (1974). *Introduction to Bioelectrodes*. New York, Plenum Press. 243p.

Fisher, K.A. and W. Stoeckenius (1983). Biomembrane models. In W. Hoppe; W. Lohmann; H. Markl and H. Ziegler. *Biophysics*. Berlin Heidelberg, Springer-Verlag. p. 413-425.

Freudling, C. and D. Gradmann (1979). Cable properties and compartmentation in *Acetabularia*. *Biochimica et Biophysica Acta* v. 552, p. 358-365.

Frömter, E. (1983). Transport of matter through biological membranes. In W. Hoppe; W. Lohmann; H. Markl and H. Ziegler. *Biophysics*. Berlin Heidelberg, Springer-Verlag. p. 465-502.

Gläsel, R.M. and K. Zetsche (1975). ^{36}Chloride fluxes of *Acetabularia*. *Protoplasma* v. 83, p. 175.

Goldsworthy, A. (1983). The evolution of plant action potentials. *Journal of Theoretical Biology* v. 103, p. 645-648.

Gomperts, B.D. (1977). *The Plasma Membrane: Models for Structure and Function*. London, Academic Press. 224p.

Goodwin, B.C. (1975). A membrane model for polar ordering and gradient formation. *Advances in Chemical Physics* v. 29, p. 269-280.

Goodwin, B.C. (1976). *Analytical Physiology of Cells and Developing Organisms*. London, Academic Press. 249p.

Goodwin, B.C. and S. Pateromichelakis (1979). The role of electrical fields, ions, and the cortex in the morphogenesis of *Acetabularia*. *Planta* v. 145, p. 427-435.

Goodwin, B.C.; J.L. Skelton and S.M. Kirk-Bell (1983). Control of regeneration and morphogenesis by divalent cations in *Acetabularia mediterranea*. *Planta* v. 157, p. 1-7.

Gradmann, D. (1975). Analog circuit of the *Acetabularia* membrane. *Journal of Membrane Biology* v. 25, p. 183-208.

Gradmann, D. (1976). "Metabolic" action potentials in *Acetabularia*. *Journal of Membrane Biology* v. 29, p. 23-45.

Gradmann, D. (1978). Green light (550 nm) inhibits electrogenic Cl^- pump in the *Acetabularia* membrane by permeability increase for the carrier ion. *Journal of Membrane Biology* v. 44, p. 1-24.

Gradmann, D. and F.W. Bentrup (1970). Light-induced membrane potential changes and rectification in *Acetabularia*. *Naturwissenschaften* v. 57, p. 46-47.

Gradmann, D. and G. Bokeloh (1975). Energy consumption of the electrogenic pump in *Acetabularia mediterranea*. *Protoplasma* v. 83, p. 172.

Gradmann, D. and W, Klemke (1974). Current-voltage relationship of the electrogenic pump in *Acetabularia mediterranea*. In U. Zimmermann and J. Dainty. *Membrane Transport in Plants*. Berlin-Heidelberg-New York, Springer-Verlag. p.131-138.

Gradmann D. and H. Mummert (1980). Plant action potentials. In R.M. Spanswick; W.J. Lucas and J. Dainty. *Plant Membrane Transport: Current Conceptual Issues*. Amsterdam, Elsevier/North-Holland Biomedical Press. p. 333-347.

Gradmann, D. and H. Mummert (1984). Mechanism of Cl^- efflux bursts in *Acetabularia*: Vesicle release *versus* permeability transients. *Journal of Membrane Biology* v. 78, p. 81-83.

Gradmann, D.; J. Tittor and V. Goldfarb (1982). Electrogenic Cl^- pump in *Acetabularia*. *Philosophical Transactions of the Royal Society of London. Series B. Biological Science* v. 299, p. 447-457.

Gradmann, D.; G. Wagner and R.M. Gläsel (1973). Chloride efflux during light-triggered action potentials in *Acetabularia mediterranea*. *Biochimica et Biophysica Acta* v. 323, p. 151-155.

Hämmerling, J. (1963). Nucleo-cytoplasmic interactions in *Acetabularia* and other cells. *Annual Review of Plant Physiology* v. 14, p. 65-92.

Hendry, B. (1981). *Membrane Physiology and Cell Excitation*. London, Croom Helm. 159p.

Hepler, P.K. and B.A. Palevitz (1974). Microtubules and microfilaments. *Annual Review of Plant Physiology* v. 25, p. 309-362.

Herth, W. (1978). Ionophore A23187 stops tip growth, but not cytoplasmic streaming, in pollen tubes of *Lilium longiflorum*. *Protoplasma* v. 96, p. 275-282.

Herth, W.; W.W. Franke and W.J. Vanderwoude (1972). Cytochalasin stops tip growth in plants. *Naturwissenschaften* v. 59, p. 38-39.

Hodges, T.K. (1976). ATPases associated with membranes of plant cells. In U. Lüttge and M.G. Pitman. *Encyclopedia of Plant Physiology, New Series, Volume 2, Transport in Plants II. Part A: Cells*. Berlin Heidelberg, Springer-Verlag. p. 260-283.

Hodgkin, A.L. and A.F. Huxley (1952a). Movement of sodium and potassium ions during nervous activity. *Cold Spring Harbor Symposia on Quantitative Biology* v. 17, p. 43-52.

Hodgkin, A.L. and A.F. Huxley (1952b). A quantitative description of membrane current and its application to conduction and excitation in nerve. *Journal of Physiology (London)* v. 117, p. 500-544.

Hodgkin, A.L. and B. Katz (1949). The effect of sodium ions on the electrical activity of the giant axon of the squid. *Journal of Physiology (London)* v. 108, p. 37-77.

Hodgkin, A.L. and R.D. Keynes (1955a). Active transport of cations in giant axons from *Sepia* and *Loligo*. *Journal of Physiology (London)* v. 128, p. 28-60.

Hodgkin, A.L. and R.D. Keynes (1955b). The potassium permeability of a giant nerve fibre. *Journal of Physiology (London)* v. 128, p. 61-88.

Hodgkin, A.L. and R.D. Keynes (1957). Movements of labelled calcium in squid giant axons. *Journal of Physiology (London)* v. 138, p. 253-281.

Hope, A.B. and N.A. Walker (1975). *The Physiology of Giant Algal Cells*. London, Cambridge University Press. 201p.

Jack, J.J.B.; D. Noble and R.W. Tsien (1975). *Electric Current Flow in Excitable Cells*. Oxford, Clarendon Press. 502p.

Jaffe, L.A.; M.H. Weisenseel and L.F. Jaffe (1975). Calcium accumulations within the growing tips of pollen tubes. *The Journal of Cell Biology* v. 67, p. 488-492.

Jaffe, L.F. (1966). Electrical currents through the developing *Fucus* egg. *Proceedings of the National Academy of Sciences. U.S.A.* v. 56, p. 1102-1109.

Jaffe, L.F. (1968). Localization in the developing *Fucus* egg and the general role of localizing currents. *Advances in Morphogenesis* v. 7, p.295-328.

Jaffe, L.F. (1969). On the centripetal course of development, the *Fucus* egg, and self-electrophoresis. *Developmental Biology. Supplement 3*, p. 83-111.

Jaffe, L.F. (1977). Electrophoresis along cell membranes. *Nature* v. 265, p. 600-602.

Jaffe, L.F. and R. Nuccitelli (1974). An ultrasensitive vibrating probe for measuring steady extracellular currents. *Journal of Cell Biology* v.63, p. 614-628.

Jaffe, L.F. and R. Nuccitelli (1977). Electrical controls of development. *Annual Review of Biophysics and Bioengineering* v. 6, p. 445-476.

Jaffe, L.F.; K.R. Robinson and R. Nuccitelli (1974). Local cation entry and self-electrophoresis as an intracellular localization mechanism. *Annals New York Academy of Sciences* v. 238, p. 372-389.

Jaffe, L.F.; K.R. Robinson and R. Nuccitelli (1975). Calcium currents and gradients as a localizing mechanism. In D. McMahon and F. Fox. *ICN-UCLA Symposium on Molecular and Cell Biology Vol. 2*. Menlo Park, California, W.A. Benjamin. p. 135-147.

Janz, G.J. and D.J.G. Ives (1968). Silver, silver chloride electrodes. *Annals New York Academy of Sciences* v. 148, p. 210-221.

Katz, B. (1966). *Nerve, Muscle, and Synapse*. New York, McGraw-Hill. 193p.

Keynes, R.D. (1951). The ionic movements during nervous activity. *Journal of Physiology (London)* v. 114, p. 119-150.

Keynes, R.D. (1963). Chloride in the squid giant axon. *Journal of Physiology (London)* v. 169, p. 690-705.

Kloppstech, K. and H.-G. Schweiger (1975). Nonribosomal ribonucleoprotein-particles in *Acetabularia mediterranea*. *Cytobiologie* v. 12, p. 1-12.

Knapp, E. (1931). Entwicklungsphysiologische untersuchungen an Fucaceen-eiern. *Planta* v. 14, p. 731-751.

Kof, E.M.; J. Hrib and V.I. Kefeli (1982). Analysis of specificities in the movement of cytoplasmic clusters in the cell of *Acetabularia mediterranea*. *Biologia Plantarum* v. 24, p. 410-414.

Koop, H.-U. (1977). Genetic aspects of *Acetabularia mediterranea*. In C.L.F. Woodcock. *Progress in Acetabularia Research*. New York, Academic Press. p. 7-18.

Koop, H.-U. (1981). Protoplasmic streaming in *Acetabularia*. *Protoplasma* v. 109, p. 143-157.

Koop, H.-U. and O. Kiermayer (1980a). Protoplasmic streaming in the giant unicellular green alga *Acetabularia mediterranea:* I. Formation of intracellular transport systems in the course of cell differentiation. *Protoplasma* v. 102, p. 147-166.

Koop, H.-U. and O. Kiermayer (1980b). Protoplasmic streaming in the giant unicellular green alga *Acetabularia mediterranea:* II. Differential sensitivity of movement systems to substances acting on microfilaments and microtubuli. *Protoplasma* v. 102, p. 295-306.

Kushmerick, M.J. and R.J. Podolsky (1969). Ionic mobility in muscle cells. *Science* v. 166, p. 1297-1298.

Lertsithichai, S. (1980). *Propagating Action Potentials and the Regeneration of Acetabularia mediterranea - A Pilot Study.* D.Phil. Thesis, University of Waikato. 203p.

Lorente de Nó, R. (1947). *A Study of Nerve Physiology.* New York, The Rockefeller Institute for Medical Research. Chapter XVI, p. 384-477.

Lüttke, A. (1983). Polarity of *Acetabularia mediterranea:* Stability in the anucleate state. *Annals of Botany* v. 52, p. 905-913.

Matthews, E.K.; R.J. Evans and P.M. Dean (1972). The ionogenic nature of the secretory-granule membrane. Electrokinetic properties of isolated chromaffin granules. *The Biochemical Journal* v. 130, p. 825-832.

Miller, G.F. (1974). Fredholm equations of the first kind. In L.M. Delves and J. Walsh. *Numerical Solution of Integral Equations.* Oxford, Clarendon Press. Chapter 13, p. 175-188.

Mummert, H. and D. Gradmann (1976). Voltage dependent potassium fluxes and the significance of action potentials in *Acetabularia. Biochimica et Biophysica Acta* v. 443, p. 443-450.

Mummert, H. and D. Gradmann (1980). Multi channel Cl^- pathways in *Acetabularia*. In R.M. Spanswick; W.J. Lucas and J. Dainty. *Plant Membrane Transport: Current Conceptual Issues*. Amsterdam, Elsevier/North-Holland Biomedical Press. p. 439-440.

Neumcke, B. (1983). Membrane potentials. In W. Hoppe; W. Lohmann; H. Markl and H. Ziegler. *Biophysics*. Berlin Heidelberg, Springer-Verlag. p. 457-460.

Novak, B. (1975). Periodical signals in the spatial differentiation of plant cells. *Advances in Chemical Physics* v. 29, p. 281-299.

Novak, B. and F.W. Bentrup (1972). An electrophysiological study of regeneration in *Acetabularia mediterranea*. *Planta* v. 108, p. 227-244.

Novak, B. and C. Sironval (1975). Inhibition of regeneration of *Acetabularia mediterranea* enucleated posterior stalk segments by electrical isolation. *Plant Science Letters* v. 5, p. 183-188.

Nuccitelli R. and L.F. Jaffe (1974). Spontaneous current pulses through developing fucoid eggs. *Proceedings of the National Academy of Sciences. U.S.A.* v. 71, p. 4855-4859.

Ohki, S. (1979). Membrane potential, surface potential and ionic permeability. *Physics Letters* v. 75A, p. 149-152.

Peng, H.B. and L.F. Jaffe (1976). Polarization of fucoid eggs by steady electrical fields. *Developmental Biology* v. 53, p. 277-284.

Phillips, D.L. (1962). A technique for the numerical solution of certain integral equations of the first kind. *Journal of the Association for Computing Machinery* v. 9, p. 84-97.

Pickard, B.G. (1973). Action potentials in higher plants. *The Botanical Review* v. 39, p. 172-201.

Poo, M.-m. and K.R. Robinson (1977). Electrophoresis of concanavalin-A receptors along embryonic muscle cell membrane. *Nature* v. 265, p. 602-605.

Puiseux-Dao, S. (1970). *Acetabularia and Cell Biology*. London, Logos Press. 162p.

Puiseux-Dao, S. (1979). Cytoplasmic streaming and cell morphogenesis in *Acetabularia*. In S. Bonotto; V. Kefeli and S. Puiseux-Dao. *Developmental Biology of Acetabularia*. Amsterdam, Elsevier/North-Holland Biomedical Press. p. 71-83.

Reed, P.W. and H.A. Lardy (1972). A23187: A divalent cation ionophore. *The Journal of Biological Chemistry* v. 247, p. 6970-6977.

Reiss, H.-D. and W. Herth (1978). Visualization of the Ca^{2+}-gradient in growing pollen tubes of *Lilium longiflorum* with chlorotetracycline fluorescence. *Protoplasma* v, 97, p. 373-377.

Reiss, H.-D. and W. Herth (1979a). Calcium ionophore A23187 affects locaized wall secretion in the tip region of pollen tubes of *Lilium longiflorum*. *Planta* v. 145, p. 225-232.

Reiss, H.-D. and W. Herth (1979b). Calcium gradients in tip growing plant cells visualized by chlorotetracycline fluorescence. *Planta* v. 146, p. 615-621.

Ribiere, G. (1967). Regularisation d'operateurs. *Revue Française d'Informatique et de Recherche Operationnelle* v. 1, p. 57-79.

Robertson, R.N. (1983). *The Lively Membranes*. Cambridge, Cambridge University Press. 206p.

Robinson, K.R. (1979). Electrical currents through full-grown and maturing *Xenopus* oocytes. *Proceedings of the National Academy of Sciences. U.S.A.* v. 76, p. 837-841.

Robinson, K.R. and R. Cone (1980). Polarization of fucoid eggs by a calcium ionophore gradient. *Science* v. 207, p. 77-78.

Robinson, K.R. and L.F. Jaffe (1975). Polarizing fucoid eggs drive a calcium current through themselves. *Science* v. 187, p. 70-72.

Rogatykh, N.P.; V.G. Melkumyan and T.N. Zubarev (1979). Action potential signals and cell morphogenesis in *Acetabularia*. In S. Bonotto; V. Kefeli and S. Puiseux-Dao. *Developmental Biology of Acetabularia*. Amsterdam, Elsevier/North-Holland Biomedical Press. p. 85-94.

Saddler, H.D.W. (1970a). The ionic relations of *Acetabularia mediterranea*. *Journal of Experimental Botany* v. 21, p. 345-359.

Saddler, H.D.W. (1970b). The membrane potential of *Acetabularia mediterranea*. *The Journal of General Physiology* v. 55, p. 802-821.

Saddler, H.D.W. (1970c). Fluxes of sodium and potassium in *Acetabularia mediterranea*. *Journal of Experimental Botany* v. 21, p.605-616.

Saddler, H.D.W. (1971). Spontaneous and induced changes in the membrane potential and resistance of *Acetabularia mediterranea*. *Journal of Membrane Biology* v. 5, p. 250-260.

Sandakhchiev, L.S.; L.I. Puchkova; A.V. Pikalov; N.B. Khristolubova and E.V. Kiseleva (1972). Subcellular localization of morphogenetic factors in anucleate *Acetabularia* at the stages of genetic information transfer and expression. In S. Bonotto; R. Goutier; R. Kirchmann and J.R. Maisin. *Biology and Radiobiology of Anucleate Systems II. Plant Cells*. New York, Academic Press. p. 297-320.

Schmid, R. and H.-U. Koop (1983). Properties of the chloroplast movement during the circadian chloroplast migration in *Acetabularia mediterranea*. *Zeitschrift fur Pflanzenphysiologie* v. 112, p. 351-357.

Schweiger, H.-G. (1966). Activity of ribonuclease in *Acetabularia*. *Planta* v. 68, p. 247-255.

Schweiger, H.G.; H. Bannwarth; S. Berger and K. Kloppstech (1975). *Acetabularia*, a cellular model for the study of nucleocytoplasmic interactions. In S. Puiseux-Dao. *Molecular Biology of Nucleocytoplasmic Relationships*. Amsterdam, Elsevier. p. 203-215.

Schweiger, H.-G. and M. Schweiger (1977). Circadian rhythms in unicellular organisms: An endeavor to explain the molecular mechanism. *International Review of Cytology* v. 51, p. 315-342.

Shephard, D.C. (1970). Axenic culture of *Acetabularia* in a synthetic medium. In D.M. Prescott. *Methods in Cell Physiology Vol.4*. New York, Academic Press. p. 49-69.

Singer, S.J. and G.L. Nicolson (1972). The fluid mosaic model of the structure of cell membranes. *Science* v. 175, p. 720-731.

Taylor, R.E. (1963). Cable theory. In W.L. Nastuk. *Physical Techniques in Biological Research Vol.6*. New York, Academic Press. p. 219-262.

Thavarungkul, P. (1980). A *Non-Invasive Technique for Measuring Action Potentials in Acetabularia mediterranea*. M.Sc. Thesis, University of Waikato. 124p.

Tihonov, A.N. (1963). On the solution of incorrectly posed problems and the method of regularization. *Soviet Mathematics: Doklady* v. 4, p. 1035-1038.

Tihonov, A.N. (1964). Solution of nonlinear integral equations of the first kind. *Soviet Mathematics: Doklady* v. 5, p. 835-838.

Turing, A.M. (1952). The chemical basis of morphogenesis. *Philosophical Transactions of the Royal Society. Series B* v. 237, p. 37-72.

Twomey, S. (1963). On the numerical solution of Fredholm integral equations of the first kind by the inversion of the linear system produced by quadrature. *Journal of the Association of Computing Machinery* v. 10, p. 97-101.

Twomey, S. (1965). The application of numerical filtering to the solution of integral equtions encountered in indirect sensing measurements. *Journal of the Franklin Institute* v. 279, p. 95-109.

Twomey, S. (1977). *Introduction to the Mathematics of Inversion in Remote Sensing and Indirect Measurements*. Amsterdam, Elsevier. 243p.

Vos, J.; K. Kuriyama and E. Roberts (1968). Electrophoretic mobilities of brain subcellular particles. *Brain Research* v. 9, p. 224-230.

Weisenseel, M.H. (1977). Changes in membrane properties and transcellular ion movements in developing plant cells. In E. Marrè and O. Ciferri. *Regulation of Cell Membrane Activities in Plants*. Amsterdam, Elsevier/North-Holland Biomedical Press. p. 267-274.

Weisenseel, M.H. (1979). Induction of polarity. In W. Haupt and M.E. Feinleib. *Encyclopedia of Plant Physiology. New Series Vol.7. Physiology of Movements*. Berlin Heidelberg, Springer-Verlag. p. 485-505.

Weisenseel, M.H. (1983). Control of differentiation and growth by endogeneous electric currents. In W. Hoppe; W. Lohmann; H. Markl and H. Ziegler. *Biophysics*. Berlin Heidelberg, Springer-Verlag. p. 460-465.

Weisenseel, M.H. and L.F. Jaffe (1972). Membrane potential and impedance of developing fucoid eggs. *Developmental Biology* v. 27, p.555-574.

Weisenseel, M.H. and L.F. Jaffe (1974). Return to normal of *Fucus* egg membrane after microelectrode impalement. *Experimental Cell Research* v. 89, p. 55-62.

Weisenseel, M.H.; R. Nuccitelli and L.F. Jaffe (1975). Large electrical currents traverse growing pollen tubes. *The Journal of Cell Biology* v. 66, p. 556-567.

Wendler, S.; U. Zimmermann and F.W. Bentrup (1983). Relationship between cell turgor pressure, electrical membrane potential, and chloride efflux in *Acetabularia mediterranea*. *Journal of Membrane Biology* v.72, p. 75-84.

Wendler, S.; U. Zimmermann and F.W. Bentrup (1984). *Reply to:* Mechanism of Cl^- efflux bursts in *Acetabularia*: Vesicle release *versus* permeability transients. *Journal of Membrane Biology* v. 78, p. 82-83.

Werz, G. (1970). Cytoplasmic control of cell wall formation in *Acetabularia*. *Current Topics in Microbiology and Immunology* v. 51, p. 27-62.

Wessells, N.K.; B.S. Spooner; J.F. Ash; M.O. Bradley; M.A. Luduena; E.L. Taylor; J.T. Wrenn and K.M. Yamada (1971). Microfilaments in cellular and developmental processes. *Science* v. 171, p. 135-143.

Williams, C. (1984). *Morphogenesis in Acetabularia*. M.Sc. Thesis, University of Waikato. 113p.

Wolpert, L. (1969). Positional information and the spatial pattern of cellular differentiation. *Journal of Theoretical Biology* v. 25, p. 1-47.

Wolpert, L. (1975). The development of pattern: Mechanisms based on positional information. *Advances in Chemical Physics* v. 29, p. 253-267.

Yasinovsky, V.G.; T.N. Zubarev; N.P. Rogatykh and I.V. Yanushevich (1979). Kinetics of synthesis and distribution of the morphogenetic substances in whole cells and in anucleate fragments of *Acetabularia mediterranea*. In S. Bonotto; V. Kefeli and S. Puiseux-Dao. *Developmental Biology of Acetabularia*. Amsterdam, Elsevier/North-Holland Biomedial Press. p. 65-70.

Zubarev, T.N. and N.P. Rogatykh (1979). Some remarks on the nucleo-cytoplasmic relationships in *Acetabularia*. In S. Bonotto; V. Kefeli and S. Puiseux-Dao. *Developmental Biology of Acetabularia*. Amsterdam. Elsevier/North-Holland Biomedical Press. p. 95-100.